PHENOTYPE, PATHOPHYSIOLOGY AND GENETICS OF TWO FORMS OF CONGENITAL MYOPATHY WITH MULTI-MINICORES

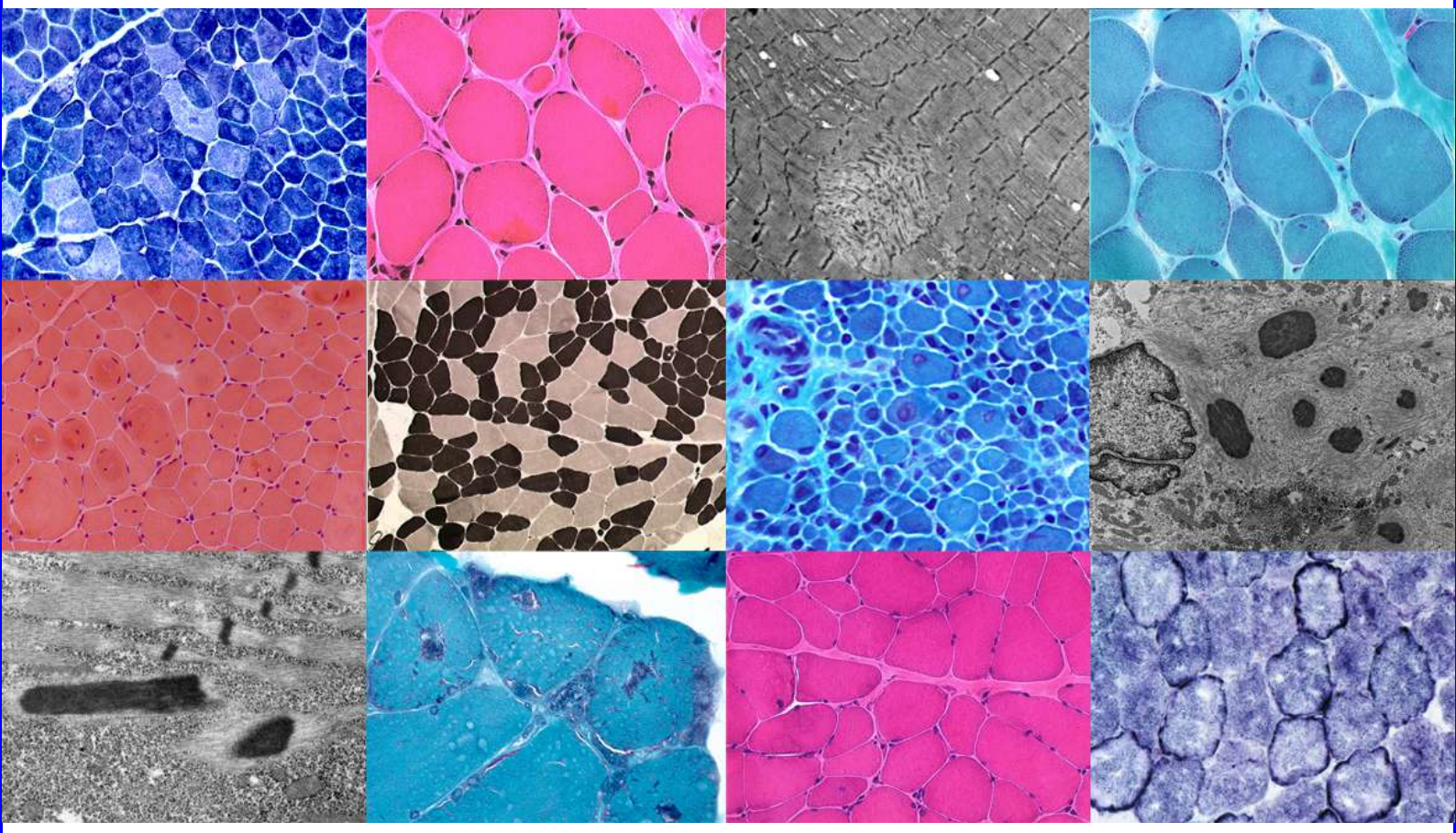

TESIS DOCTORAL

Rocío Nur Villar Quiles

2020

Phenotype, pathophysiology and genetics of two forms of congenital myopathy with multi-minicores

Estudio fenotípico, fisiopatológico y de correlaciones genotipo-fenotipo de dos formas de miopatía congénita con multi-minicores

Rocío Nur VILLAR QUILES

Directores:

Ana FERREIRO SIEIRO

María de la Luz CUADRADO PÉREZ

Tutor Académico:

Juan Antonio VARGAS NÚÑEZ

Universidad Autónoma de Madrid

Facultad de Medicina

2020

In examining disease, we gain wisdom about anatomy and physiology and biology. In examining the person with disease, we gain wisdom about life

Oliver Sacks

Acknowledgments

En primer lugar, querría agradecer a los pacientes y sus familias su participación en este estudio.

Quiero agradecer a mis directoras de tesis su apoyo y dedicación. En primer lugar, a Mª Luz Cuadrado, muchas gracias por haberme motivado para empezar a dar los primeros pasos en el mundo de la investigación durante la residencia y por haberme apoyado en proyectos posteriores, que me han conducido hasta este momento. A Ana Ferreiro, por haberme dado la oportunidad de integrarme en su equipo, formarme en el campo de la miología e introducirme en el universo de la investigación fundamental y de las miopatías congénitas, algo totalmente desconocido para mi hasta hace unos años. Muchas gracias también por los tés compartidos. Querría darle las gracias también al Dr Juan Antonio Vargas, tutor académico, por haber apoyado este proyecto.

Je tiens aussi à remercier Isabelle Duband-Goulet, qui s'est beaucoup investie pour m'apprendre les techniques expérimentales mais aussi le raisonnement scientifique avec beaucoup de patience et toujours avec un sourire. Sans Isabelle, ce projet ne serait pas si bien réussi qu'il ne l'est maintenant. Un grand merci aussi à tous les membres du labo « Myologie Fondamentale et translationnelle », qui m'ont aidé pendant ce temps et ont été toujours agréables et conviviales.

I would also like to thank all the co-investigators that have collaborated with me in the two main projects that conform this work.

Gracias también a Alicia, una gran amiga con la que he compartido mi día a día en el laboratorio y en el hospital estos últimos años, a pesar de la distancia.

Me siento muy afortunada también por tener unos padres que siempre me han apoyado y ayudado en todo lo que me he propuesto hacer, incluídos traslados internacionales. Infinitas gracias a mi madre, uno de mis mayores apoyos, por estar a mi lado de manera incondicional y haberme inculcado el valor de la perseverancia, entre otras cosas.

Por último, no hay palabras suficientes para agradecer todo lo que ha hecho Miguel durante estos años. Muchísimas gracias por haber estado a mi lado, motivarme y apoyarme en todos lo que me he propuesto hacer. Gracias por hacerme tan fácil el día a día y por tantos buenos momentos y risas compartidas. De manera más prosaica, tengo que agradecerte también toda tu « asistencia técnica » 24/24h. Sin ti, esto no hubiera sido posible. Te quiero.

Abstract

Congenital myopathies with multi-minicores are genetically and clinically heterogeneous early-onset conditions originally defined by the presence of multiple areas of sarcomeric disorganization and mitochondrial depletion.

This work is focused on Selenoprotein N-related myopathy (SEPN1-RM) and Activating Signal Cointegrator 1-related myopathy (ASC1-RM). It includes the retrospective clinical, histopathological and molecular analysis of the largest SEPN1-RM series so far, including 132 patients followed-up for several decades. Inferred prevalence from the present work is around 1 per million. The clinical phenotype was distinctive and recognizable, marked by severe axial muscle weakness, spinal rigidity and progressive scoliosis, contrasting with fairly preserved limb strength and ambulation. Previously-unreported ophthalmoparesis was observed in severe patients. All patients developed restrictive respiratory failure, most requiring assisted ventilation while still ambulant. SEPN1-RM histological spectrum included multi-minicores, the most common lesion, often associated with dystrophic features and occasionally with eosinophilic inclusions. This work unveils previously unknown factors underlying its histopathological variability: site of biopsy and age. 65 *SEPN1* mutations were identified, including 32 novel ones and the first pathogenic Copy Number Variation (CNV), with exon 1 being the main mutational hotspot. The first genotype-phenotype correlations presented here reveal that bi-allelic predicted null mutations are significantly associated with disease severity. SEPN1-RM is more severe and progressive than previously thought, leading to loss of ambulation in 10% cases, to systematic functional decline from the end of the third decade and to reduced life span even in mild cases. The main prognosis determinants are scoliosis and respiratory management, type of *SEPN1* mutation and body mass abnormalities.

ASC1-RM is a recently described congenital myopathy caused by recessive mutations in the *TRIP4* gene. So far, only three *TRIP4* nonsense mutations have been reported in four families presenting a very severe neonatal phenotype with hypotonia, lack of ambulation and potentially-lethal respiratory failure. This study reports five additional families with seven novel *TRIP4* mutations. The clinical phenotype was marked by early onset axial and proximal weakness, progressive scoliosis sometimes associated with rigid spine, dysmorphic facial features, frequent cutaneous involvement and variable respiratory failure correlated with disease severity. While the most severe patient never acquired head control and died at 8 months, the remaining five patients were able to walk unsupported at ages ranging from 9 to 62 years. Late-onset dilated cardiomyopathy was also part of the phenotype. The histopathological spectrum was also strikingly large, including multiminicores, rods, cytoplasmic bodies, caps or central nuclei, rimmed fibres and mild endomysial fibrosis. ASC-1 depletion in murine myoblasts and in patient-derived skin fibroblasts and muscles caused accelerated proliferation, altered expression of cell cycle proteins and/or shortening of the G0/G1 phase of the cell cycle leading to cell size reduction. Thus, ASC-1 seems to play a key role not only in late myogenic differentiation and myotube growth, as previously found, but also in early-stages of myogenesis as a novel cell cycle

regulator by modulating the expression and phosphorylation of cell-cycle regulatory proteins.

This work expands the clinical, histopathological and molecular spectrum of these two congenital myopathies with multi-minicores, having the potential to inform clinical practice and to improve diagnosis and management. Moreover, it represents a major breakthrough for clinical trial readiness in SEPN1-RM and highlights the importance of defects in transcriptional co-regulation by the ASC-1 complex as a novel pathophysiological mechanism in inherited muscle disease.

Resumen

Las miopatías congénitas con multi-minicores representan un grupo de enfermedades musculares de inicio temprano con un espectro clínico y genético heterogéneo, definidas originalmente por la presencia de múltiples áreas de desorganización sarcomérica y depleción mitocondrial.

El presente trabajo se ha centrado en las miopatías relacionadas con la selenoproteína N (SEPN1-RM) y con el co-integrador transcripcional ASCl-1 (ASC1-RM). Incluye el análisis retrospectivo de la mayor serie recopilada hasta la fecha de SEPN1-RM, con un total de 132 pacientes. A partir de nuestros datos, la prevalencia estimada para la SEPN1-RM es de 1 por millón. El fenotipo clínico se caracterizó por un déficit axial grave, rigidez espinal y escoliosis progresiva, lo que contrastaba con una relativa preservación de la fuerza apendicular y de la marcha. En pacientes graves, se ha observado asimismo la presencia de oftalmoparesia, no descrita previamente. Todos los pacientes acabaron presentando una insuficiencia respiratoria restrictiva que requirió ventilación no invasiva aun conservando la deambulación. La lesión histológica más frecuente fue la presencia de multi-minicores, a menudo acompañados de cambios distróficos y ocasionalmente de inclusiones eosinófilas. Este estudio desvela que tanto la edad como la localización de la biopsia son factores determinantes en la variabilidad histopatológica de. Se identificaron 65 mutationes del gen *SEPN1*, incluyendo 32 nuevas mutaciones y la primera variación en el número de copias (CNV). El exón 1 fue el principal *hotspot* mutacional. El análisis de las correlaciones entre genotipo y fenotipo reveló que las mutaciones nulas bialélicas se asociaban a una mayor gravedad. La SEPN1-RM es una enfermedad grave y progresiva, que comporta la pérdida de la marcha en un 10% de los casos, una degradación funcional desde el final de la tercera década y una disminución de la esperanza de vida incluso en casos con una afectación inicial leve. Los principales factores pronósticos son el manejo de la insuficiencia respiratoria y la escoliosis, el tipo de mutacion de *SEPN1* y las anomalías de la masa corporal.

La ASC1-RM es una entidad de reciente descripción, causada por mutaciones recesivas en el gen *TRIP4*. Hasta ahora, solo se han descrito cuatro familias portadoras de tres mutaciones sin sentido (*nonsense*), con un fenotipo neonatal grave consistente en hipotonía, falta de adquisición o pérdida precoz de la marcha e insuficiencia respiratoria grave, potencialmente letal. Este trabajo presenta cinco familias adicionales con siete nuevas mutaciones de *TRIP4*. El cuadro clínico se caracterizba por una debilidad axial y proximal temprana, escoliosis asociada ocasionalmente a rigidez espinal, rasgos dismórficos faciales, anomalías cutáneas e insuficiencia respiratoria de intensidad variable, relacionada con la gravedad de la afectación muscular. Aunque el paciente más grave nunca adquirió el control cefálico y falleció a los 8 meses, los restantes pacientes mantenían la deambulación con edades comprendidas entre los 9 y los 62 años. Entre las posibles manifestaciones fenotípicas, también se observó miocardiopatía dilatada de inicio tardío. El espectro histopatológico fue extraordinariamente amplio, incluyendo multi-minicores, bastones nemalínicos, cuerpos citoplasmáticos, lesiones de tipo cap, centralización nuclear, fibras ribeteadas (*rimmed fibres*) y fibrosis endomisial. La depleción de ASC-1 en mioblastos murinos y en fibroblastos y células musculares de pacientes provocó una

aceleración de la proliferación celular, una alteración en la expresión de las proteínas reguladoras del ciclo celular y/o un acortamiento de la fase G0/G1 del ciclo celular, asociado a una disminución de la superficie celular. ASC-1 parece jugar un papel no sólo en la diferenciación miogénica terminal y el crecimiento de los miotubos sino también en la miogénesis temprana como un nuevo regulador del ciclo celular.

El presente trabajo expande el espectro clínico, histopatológico y molecular de estas dos miopatías congénitas con multi-minicores, lo que puede contribuir a mejorar el diagnóstico y manejo de los pacientes en la práctica clínica. Asimismo, pretende contribuir al avance en la puesta a punto de ensayos clínicos en SEPN1-RM. Finalmente, pone en relieve la importancia de los defectos en la co-regulación transcripcional del complejo ASC-1 como un nuevo mecanismo fisiopatológico en las enfermedades musculares congénitas.

List of abbreviations

ACTA1: Actin alpha 1

AICD: Automated implantable cardioverter defibrillator

AKT/PI3K: Phosphatidylinositol 3-kinase pathway

ALS: Amyotrophic lateral sclerosis

AP-1: Activator protein 1

ASC-1: Activating signal cointegrator–1

ASC-1 RM: ASC-1 related myopathy

ASCC1: Activating signal cointegrator - 1 complex subunit 1

ASCC2: Activating signal cointegrator - 1 complex subunit 2

ASCC3: Activating signal cointegrator - 1 complex subunit 3

ASCH: Activating signal cointegrator-1 homology domain

ATP: Adenosine triphosphate

CBP: CREB-binding Protein

CDK: Cyclin-dependent kinases

CFTD: Congenital fibre type disproportion

CK: Creatin phosphokinase

CM: Congenital myopathy

CMD: Congenital muscular dystrophy

CNS: Central nervous system

COL6-RM: Collagen 6 related myopathies

Cox: Cyclo-oxygenase

CPAP: Continuous positive airway pressure

CT: Computed tomography

DCM: Dilated cardiomyopathy

DHPR: Dihydropyridine receptor

DM1-2: Myotonic dystrophy 1-2

DMD: Duchenne muscular dystrophy

DMEM: Dulbecco modified eagle media

DNA: Deoxyribonucleic acid

DNM2: Dynamin 2

EM: Electron microscopy

EMD: Emerin

ER: Oestrogen receptor

ExAC: Exome aggregation consortium

FACS: Fluorescence activated cell sorting

FHL1: Four and a half LIM domains 1

FVC: Forced vital capacity

FCS: Foetal calf serum

FSHD : Facioscapulohumeral muscular dystrophy

FXR1: Fragile X mental retardation syndrome-related protein 1

GAA: Alpha-glucosidase

gnomAD: Genome aggregation database

KD: Knocked-down

LMNA: Lamin A/C

LVEF: Left ventricle ejection fraction

MAPK: Mitogen-activated protein kinases

MEF2: Myocyte enhancer factor 2

MHC: Myosin heavy chain

MRC: Medical research council scale

MRI: Magnetic resonance imaging

MRF: Muscle regulatory factors

MYH2-7: Myosin heavy chain 2-7

MyoD: Myogenic differentiation protein 1

NADH: nicotinamide adenine dinucleotide

NCS: Nerve conduction studies

NFAT: Nuclear factor of Activated T-cells

NF-kappa-B: Nuclear factor kappa-B

NGS: Next generation sequencing

NT: non-transfected

PAS: periodic acid Schiff

PAX 3-7: Paired box protein 3-7

PBS: Phosphate buffered saline

PPARγ: Peroxisome proliferator-activated receptor γ

PYROXD1: Pyridine nucleotide-disulphide oxidoreductase domain 1

P/S: penicillin-streptomycin

Rb: Retinoblastoma protein

RNA: Ribonucleic acid

RXR: Retinoid X receptor

RYR1: Ryanodyne receptor 1

SDH: Succinate dehydrogenase

SDS-PAGE: Sodium Dodecyl Sulfate Polyacrylamide Gel Electrophoresis

SEPN1 or *SELENON*: Selenoprotein N gene

SEPN1 or SelN: Selenoprotein N

SEPN1-RM: SEPN1 Related Myopathy

SDH: Succinate dehydrogenase

siRNA: Small interfering RNA

SMA: Spinal muscular atrophy

SR: Sarcoplasmic reticulum

SRC-1: Steroid receptor coactivator-1

SRF: Serum response factor

TBP: TATA-box binding protein

TFIIA: Transcription factor IIA

TR: Thyroid Receptor

TRIP4: Thyroid hormone receptor interactor

TTN: Titin

TTNtv: Titin truncating variants

WES: whole exome sequencing

Table of Contents

Chapter 1:

INTRODUCTION

1.1 The muscular system

Muscle tissue is one of the primary tissues of the human body. According to their structure and function, muscles can be subdivided into smooth and striated muscles (Figure 1.1), the latter comprising cardiac and skeletal muscles which differ by their cellular organization but have similar contractile filament architecture.

All three muscle tissues are specialized tissues with a key property: excitability. They have specialized plasma membranes which can change their electrical states (depolarization and repolarization) to give rise to action potentials which will spread and eventually lead to muscle contraction. Cardiac muscle tissue is composed by a complex tridimensional branching network of cardiac muscle fibres, composed by cardiomyocites held together by specialized cell junctions called intercalated discs. Cardiomyocites have a single centrally located nucleus and their contraction is regulated by the autonomous nervous system. Smooth muscle is located in lymphatic and blood vessels walls as well as in the genitourinary and gastrointestinal tracts. It is composed by fusiform cells with a single elongated and centrally located nucleus.

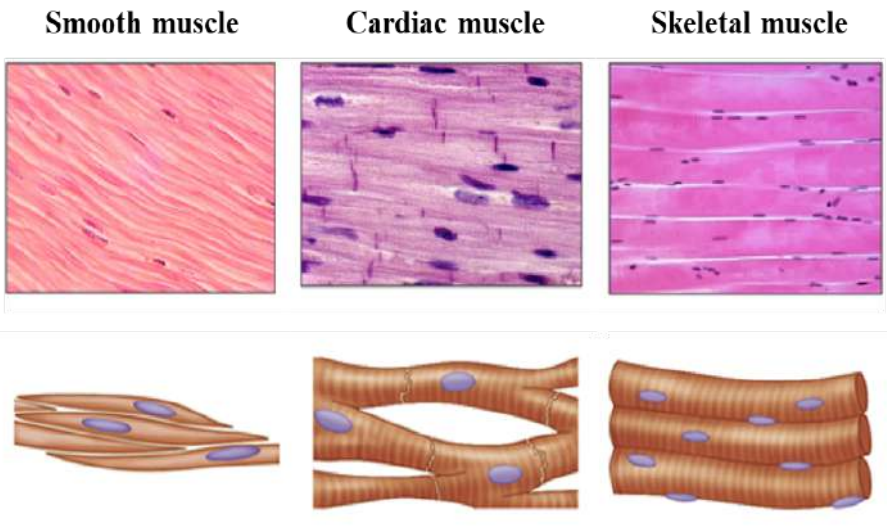

Figure 1.1: Classification of muscle tissues. Longitudinal histological sections (upper panel) and schematic representation of the cellular organisation in each type muscle (bottom panel). Figure adapted from © The McGraw Hills companies, Inc

1.2 The skeletal muscle structure

The skeletal muscles represent approximately 40% of total body weight and contain up to 75% of all body proteins (Frontera and Ochala, 2015). Their contraction is regulated by the voluntary nervous system. Motorneurons contact with the muscle fibres in the neuromuscular junction, one of the first chemical synapsis described (Dale *et al.*, 1936). Skeletal muscles contribute to multiple functions. They are responsible for the force generation needed for maintenance of the body posture, breathing, locomotion and other voluntary body movements. The main electrophysiological properties of the skeletal muscle tissue are: conductivity, excitability, contractility, extensibility and elasticity or distensibility. Skeletal muscle plays also an important role in metabolism. It contributes to basal energy metabolism, as it storages important substrates such as amino acids and carbohydrates, but also has high energy requirements during physical activity. Amino acid reserves in muscle can be used by other tissues such as brain or heart and amino acid release from muscle contributes to the maintenance of blood glycemia under starvation conditions. Finally, skeletal muscle is responsible for heat production, contributing to the maintenance of core temperature.

Skeletal muscle is composed by the assembly of muscle fibres (myofibres). The mature skeletal myofibres form by fusion of myoblasts to produce multinucleated myotubes which further mature into post-mitotic cells termed myofibres. Myofibres contain a highly organized cytoskeleton composed of aligned myofibres within the cytoplasm (sarcoplasm), whereas nuclei are located in a peripheral position under the cell membrane (sarcolemma). Quiescent cells localized between the sarcolemma and the basal lamina termed satellite cells represent the main pool of muscle progenitor cells contributing to muscle growth, repair and regeneration (Morgan and Partridge, 2003; Collins *et al.*, 2005).

Each individual myofibre is surrounded by a connective tissue layer termed endomysium (Figure 1.2). The assembly of 20 to 40 myofibres constitutes the muscle fascicule, enveloped by the perimysium. Finnaly, the whole muscle is surrounded by a connective tissue layer named epimysium, which also surrounds the nerve fibres and the blood vessels located within the muscle. The myotendinous junction links muscle fibres to collagen filaments which constitute the tendon, by which muscles are attached to bone's periosteum.

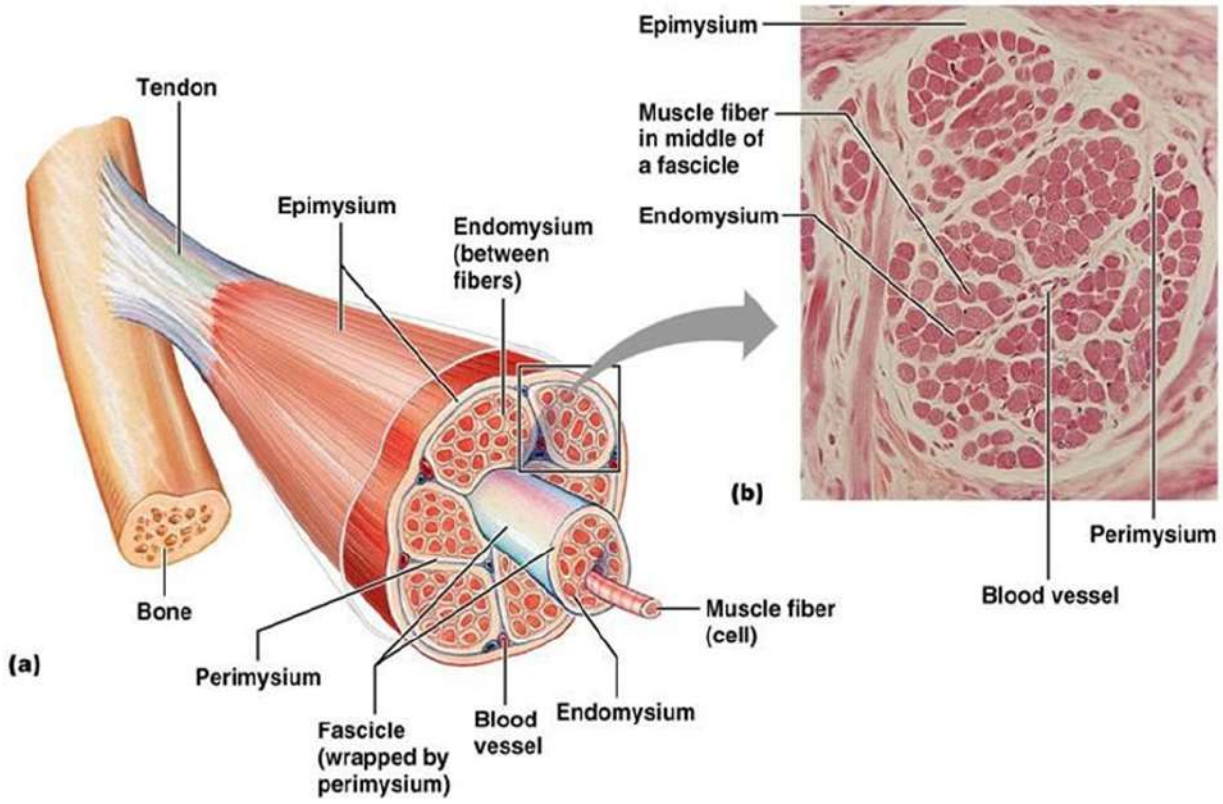

Figure 1.2: Skeletal muscle: (a) Schematic representation of skeletal muscle organization b) Transverse frozen section (Hematoxylin Eosin staining). Adapted from © 2006 Pearson Education, Inc.

1.3 Skeletal muscle contractile apparatus

Skeletal muscle is composed of a highly structured contractile network. The sarcomere is the basic functional contraction unit of the muscle fibre. It is a 2 µm maximal length symmetric structure formed by the assembly of thin and thick filaments. This confers the striated pattern observed in skeletal and cardiac muscles (Figure 1.3) with the alternation of dark and light bands visible by electron microscopy termed A-bands (Anisotropic) and I-bands (Isotropic) respectively.

Z-discs define the lateral borders of the sarcomere. The core of a Z-disc consists of actin filaments from adjacent sarcomeres which are crosslinked by-α actinin. Z-discs appear in the longitudinal view of electron microscopy as electron dense bands with varying sizes, ranging between 30 and 50 nm in fast muscle fibres and between 100 and 140 nm in slow muscle fibres. Although the Z disc along with its attached proteins are of major importance for mechanical stability of the sarcomere, Z disc has

also been implicated in signaling, mechanosensation and mechanotransduction (Luther, 2009; Knöll *et al.*, 2011).

The light zones surrounding each Z disc are the light or I-bands, made up of thin actin filaments. The dark or A-bands are formed by both types of filaments. It comprises myosin filaments crosslinked at the center by the M line. Thin actin-containing filaments are tethered at their barbed end at the Z-disc and interdigitate with the thick filaments in the A-band. Thus, within the A-band, two distinct structures can be found: H zone containing thick myosin filaments and the M line, situated in the middle of the H zone, where accessory proteins hold together the thick filaments.

Thin filaments are mainly composed by actin but also containing other proteins such as tropomyosin and troponin. Actin is a globular protein which combines with other actin globules to form two intertwined strands with a positive and negative end. On the other hand, thick filaments are composed by myosin. Myosin has two heavy chains, and two pairs of light chains. At the tail of the thick filament, the two heavy chains are intertwined in a helical formation. At the opposite end of the thick filament, each heavy chain is paired with two light chains giving rise to two heads. The myosin heads have an actin-binding site which helps them attach to the thin filaments.

Figure 1.3 (next page). Skeletal muscle contractile structure. Schematic representation of muscle fibres (upper panel, note striated pattern) and the sarcomere (middle panel), showing the antiparallel alignment of thin (blue) and thick (red) filaments. Note the presence of titin filaments (yellow) as a major component of the sarcomere. The lower figure shows a complete sarcomere bordered by two partial sarcomeres, in an electron microscope picture. The A-band is formed by the overlap of actin and myosin filaments. The I-band is formed by thin filaments anchored to the Z-disk, which forms the border between adjacent sarcomeres. Adapted from ©Pearson Education, Inc.

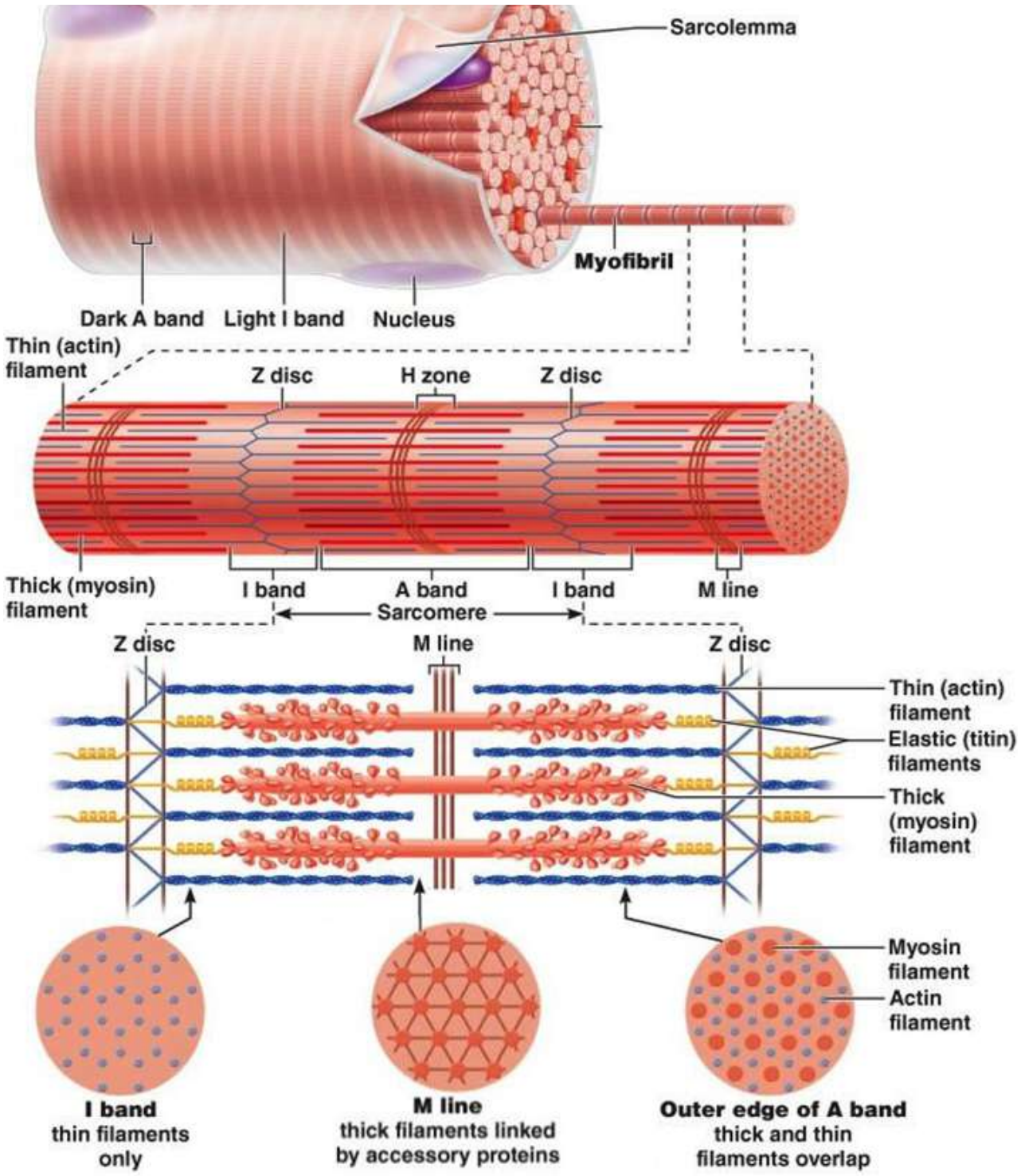
Sarcolemma
Myofibril
Dark A band
Light I band
Nucleus
Thin (actin) filament
Z disc
H zone
Z disc
Thick (myosin) filament
I band
A band
I band
M line
Sarcomere
Z disc
M line
Z disc
Thin (actin) filament
Elastic (titin) filaments
Thick (myosin) filament
Myosin filament
Actin filament
I band
thin filaments only
M line
thick filaments linked by accessory proteins
Outer edge of A band
thick and thin filaments overlap

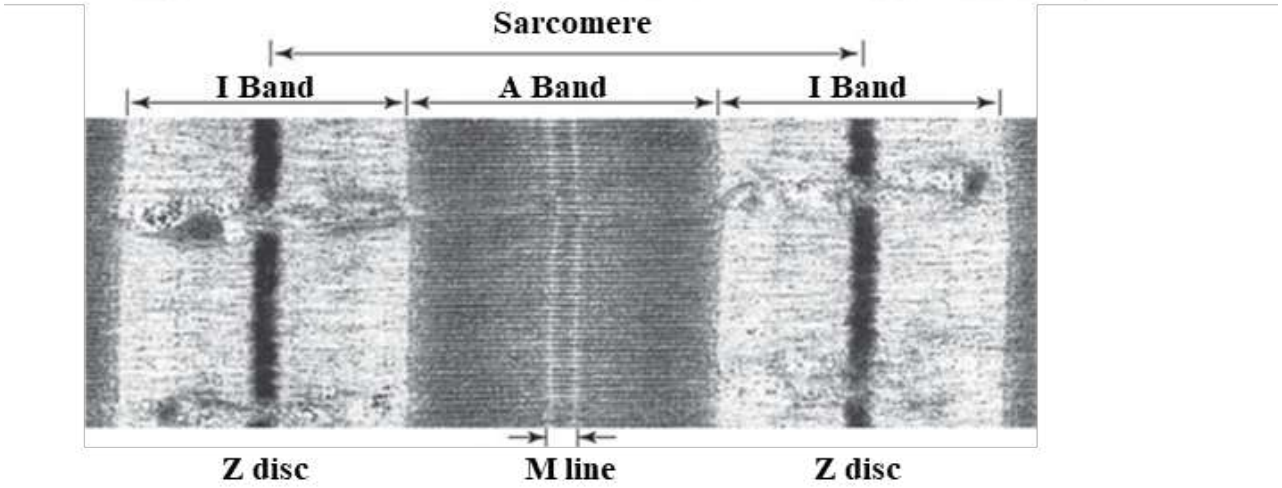
Sarcomere
I Band
A Band
I Band
Z disc
M line
Z disc

Besides actin and myosin filaments, many other proteins are embedded in the sarcomere and contribute to its integrity and mechanical stability during muscle contraction. As such, tropomodulin is a protein attached to the (+) or growing end of the actin filaments regulating thin filament length (Littlefield et al., 2001). Nebulin is a giant protein (800 kDa) associated to thin filaments which contributes to the structural link between sarcomeres and also plays a role in numerous cellular processes including regulation of actin filaments stabilization, muscle contraction, Z disc formation and myofibril organization and assembly (Pappas et al., 2008; Chu et al., 2016). Troponin and tropomyosin are also associated to thin actin filaments. Troponin is a heterotrimeric protein with three different subunits: troponin C which contains four calcium-binding EF hands, troponin I, the inhibitory subunit of the troponin complex, acting to inhibit actin-myosin interaction, and troponin T which anchors the troponin complex on tropomyosin. Tropomyosin blocks the binding sites for the myosin heads on the thin filaments, thus preventing contraction. When an action potential causes depolarization of the sarcolemma, it spreads via the transverse (T) tubules (invaginations of the cell membrane) and causes a conformation change in the dihydropyridine (DHP) receptors, resulting in the opening of the nearby ryanodin receptors on the sarcoplasmic reticulum, which release calcium to the sarcoplasm The troponin complex then binds to calcium trough troponin C leading to a conformational change shifting tropomysing and thus allowing the formation of actin-myosin cross bridges. The formation of these bridges will then lead, in an ATP dependent manner, to the antiparallel movement of the filaments, responsible for the shortening of the sarcomere and thus to muscle contraction.

The third major component of the sarcomere is the giant protein titin, the largest protein known so far. The complete sequence of the human titin gene *(TTN)* contains 363 exons, which together code for 38.138 residues (4200 kDa) (Bang *et al.*, 2001). The predominant isoform in skeletal muscle is N2A while isoform N2BA is the main isoform in the heart muscle(Savarese *et al.*, 2016). Titin is a 1µm elastic protein anchored to the Z disk and the M line. It binds numerous structural and functional proteins along the sarcomere (Chauveau *et al.*, 2014*b*). Through its N-terminal part it anchors to the Z disk and binds, among other, telethonin and actin. The I-band contains the titin PEVK domain with a major role in sarcomere elasticity and titin-actin binding (Linke and Fernandez, 2002). At the A-band, titin binds myosine and its partner myosin binding protein C (MyBP-C), the latter being involved in thin-thick filaments assembly and accessibility of myosin heads, thus participating in muscle contraction. At the M line the complex formed by titin and its partners myomesin, obscurin and obscurin-like plays an important role in sarcomeric elasticity and mechanical stabilization (Agarkova

and Perriard, 2005; Pernigo *et al.*, 2010). Thus, titin plays a major role as a scaffolding filament, contributing to myofilament assembly and global sarcomeric stability, providing passive tension and elasticity to myofibrilles. Moreover, it may also play a role in cell signaling and other yet to be known cellular processes (Linke, 2018).

1.4 Skeletal muscle fibre types

Skeletal muscles are made up by the combination of muscle fibres with different contraction speeds and force outputs. Muscles exclusively composed of fast or slow fibres are exceptional. The speed of fibre contraction is mainly determined by the isoform of the myosin heavy chain (MHC) expressed. Other important factors include the isoform of the calcium reuptake and release proteins expressed and the density of the sarcoplasmic reticulum (SR). Three major isoforms of MHC are expressed in human muscles: MHC I (slow myosin) and two fast isoforms MHC IIA and MHC IIX (also called MHC IID). ATPase activity at acid (4.6) and alkaline (9.4) pH allowed for the first time the distinction of two fibre types: slow (1) and fast (2) (Essén *et al.*, 1975) (Figure 1.4). In fact, the rate of ATP hydrolysis is the main determining factor of the speed of cross-bridge cycling and sarcomere shortening, hence of the speed of muscle contraction.

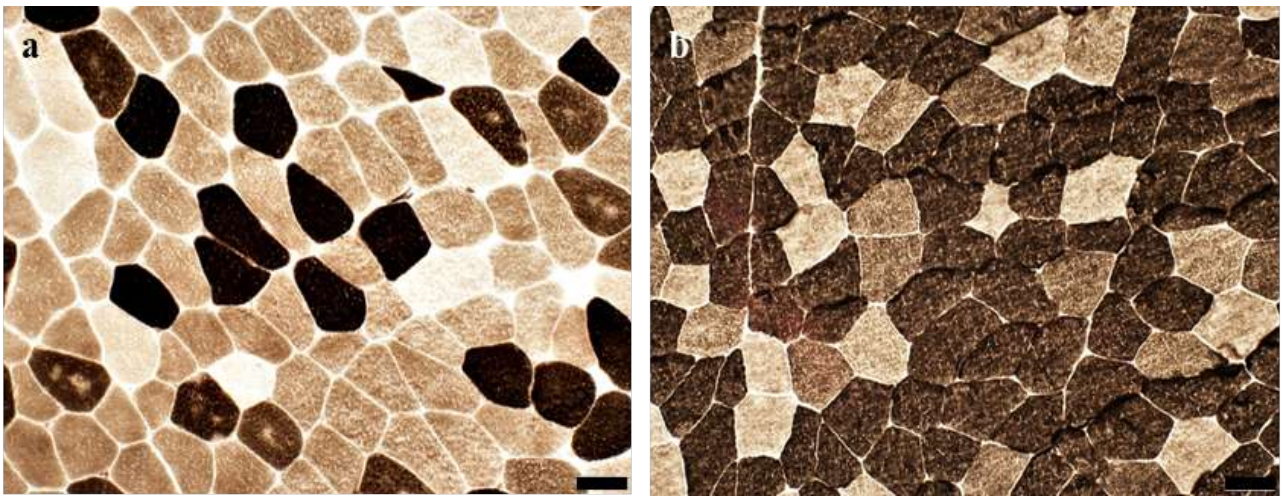

Figure 1.4. Muscle fibre type. (a) ATPase pH 4.6 stain: type 1 fibres look dark while type 2A look pale. Type 2B and 2C (immature) fibres exhibit an intermediate stain. (b): ATPase pH 9.4 stain: type 1 fibres appear pale while type 2 fibres are dark.

Fast and slow fibres can be further subdivided based on their metabolism: aerobic oxidative (requiring abundant mitochondria and lipid droplets) or anaerobic metabolism (richer in glycolytic enzyme and glycogen stores). Histochemical methods for analyzing mitochondrial activity combined with myosin ATPase activity allow to define three major muscle fibre types (Table 1.1).

Table 1.1. Main histochemical properties of muscle fibres according to fibre type.

Histochemical properties	Muscle fibre types		
	1	2A	2B
Myosin ATPase (pH 9.4)	Low (pale staining)	High (dark staining)	High (dark staining)
Myosin ATPase (pH 4.6)	High (dark staining)	Low (pale staining)	Medium (intermediate staining)
Oxidative enzymes (SDH, NADH dehydrogenase, Cox)	High	Medium	Low
Phosphorylase	Very low	High	High
Glycogen (PAS)	Low	High	Medium

Cox : Cyclo-oxygenase; NADH dehydrogenase : nicotinamide adenine dinucleotide, reduced; PAS : periodic acid Schiff; SDH, succinate dehydrogenase.

Type 1 are slow twitch oxidative fibres expressing MHC I which have strong myosin ATPase activity at low pH and a dense staining for mitochondrial enzymes NADH (nicotinamide adenine dinucleotide, reduced) dehydrogenase or SDH (succinate dehydrogenase). Their SR is less abundant, and they contain a slower isoform of the SR calcium ATPase compared to type 2 fibres. They contain myoglobin, which confers a red color, and have a rich capillary blood supply. For all these reasons, type 1 fibres are highly resistant to fatigue and are suitable for sustained aerobic contraction (Table 1.2). Conversely, type 2 or fast-twitch fibres, express fast isoforms of myosin and have a strong ATPase activity at alkaline pH. There are two main subtypes of type 2 fibres: 2A and 2B. Type 2A fibres expressing the MHC IIA isoform have a greater density of SR and express calcium handling proteins isoforms that allow a rapid calcium cycling. They are rich in mitochondria, glycolytic enzymes (e.g phosphorylase) and glycogen stores. Therefore, they have a relatively high resistance to fatigue under aerobic and anaerobic conditions. Type 2B fibres express the MHC IIX, the fastest myosin isoform,

have a dense SR with a fast isoform of SR calcium ATPase and have a mainly glycolytic metabolism. They are thus easily fatigable and are meant for intense, short anaerobic exercise.

Immature isoforms of myosin are expressed in muscle fibres prior to differentiation during development. These fibres, termed type 2C, show an intermediate staining for ATPase activity at acid and alkaline pH and can be found when there is fibre regeneration (e.g in muscular dystrophies). Different fibres within a muscle can express hybrid MYH thus leading to further fibre subtypes (1/2A, 2A/2X, 2X/2B), with an almost continuous range of ATP usage and muscle contraction speeds, from the fastest (type 2B) to the slowest (type 1) fibres.

Table 1.2. Main characteristics of the three muscle fibre types

Fibre Type	Type 1	Type 2A	Type 2B
Contraction time	Slow	Fast	Very fast
Size of motor neuron	Small	Large	Very large
Resistance to fatigue	High	Intermediate	Low
Activity	Aerobic	Long-term anaerobic	Short-term anaerobic
Force production	Low	High	Very high
Mitochondrial density	High	High	Low
Oxidative capacity	High	High	Low
Glycolytic capacity	Low	High	High
Major storage fuel	Triglycerides	Glycogen	Glycogen

The skeletal muscle fibres innervated by the same motor neuron's axonal terminals constitute a motor unit. Muscle fibres within the same motor unit have essentially the same histochemical and metabolic characteristics, hence the same mechanical properties. According mainly to the fatigue index and speed of contraction, motor units were initially classified as: type FF (fast twitch, fatigable), type FR (fast twitch, fatigue resistant) and type S (slow twitch, fatigue resistant). Some fast-twitch units exhibited intermediate fatigue resistance between those of FF and FR units and were termed F(int) or FI (Burke *et al.*, 1973, 1974). The mechanical classification into S, FR and FF motor units matched with the histochemically defined muscle fibre types 1, 2A and 2B, respectively. Intermediate units may result from hybrid combination of myosin isoforms. Type 1 fibres are embedded in smaller motor units (10 to 180 fibres per motor unit) compared to type 2 -fibres-motor units (composed by 300 to 800 fibres).

Human skeletal muscles are composed by varying proportion of different fibre types. Overall, type 1 fibres represent approximately 50% of muscle fibres while type 2A and type 2B represent 30% and 15% respectively. Nonetheless, muscles have distinct fibre proportions according to their localization and function. For instance, in the soleus muscle type 1 fibres can represent up to 80% of fibres while the triceps brachii has a predominance of type 2 fibres up to 60% (Ahmetov *et al.*, 2012). Moreover, these proportions may vary as muscle fibres are able to shift their metabolic and mechanic phenotypes under different conditions. As such, endurance exercise training can induce an increased proportion of type 1 fibres (Fluck, 2006) while sedentarism and muscle disuse leads to atrophy of all muscle fibre types but particularly of type 1 fibres along with a fibre-type shift from type 1 and 2A to type 2X fibres. Conversely, sarcopenia due to aging is characterized by a selective involvement of type 2 fibres (Talbot and Maves, 2016).

Under pathological conditions, muscle fibre type proportion can also be disturbed. In Duchenne muscular dystrophy (DMD) (Webster *et al.*, 1988) and facioscapulohumeral muscular dystrophy (FSHD) (Lassche *et al.*, 2013) type 2 fibres are preferentially affected. Strikingly, in myotonic dystrophies type 1 and 2 (DM1 and DM2) exhibit different fibre-type abnormalities: in DM1 there is type 1 fibre atrophy and high frequency of type 1 fibres with central nuclei while DM2 shows type 2 fibre atrophy and a higher frequency of type 2 fibres with central nuclei(Vihola *et al.*, 2003). Congenital myopathy due to mutations in the gene *MYH7* (Myosin heavy chain 7) consistently associates hypotrophy of type 1 fibres while mutations in fast *MYH2* lead to loss of type 2A fibres (Tajsharghi and Oldfors, 2013*a*). In congenital fibre type disproportion myopathy (CFTD), the main histologic abnormality is that type 1 fibres are consistently smaller than type 2 by at least 35-40% (Clarke, 2011). Finally, hypotrophic type 1 fibres and type 1 fibre predominance are common histological findings in congenital myopathies (Sewry and Wallgren-Pettersson, 2017) and may sometimes be the only histological abnormality found.

1.5 Skeletal myogenesis

Skeletal muscle originates from the paraxial mesoderm located at the posterior tip of the embryo. It can be subdivided into an immature posterior and a committed anterior region which will segment to form the somites. Within the somites, skeletal myogenesis is initiated with the generation of the

myogenic progenitors. These progenitors will proliferate and differentiate leading to mononucleated myoblasts which will fuse to form multinucleated myotubes and eventually give rise to the mature skeletal muscle (Chal and Pourquié, 2017) (Figure 1.5).

The first molecular markers of the myogenic progenitors are the transcription factors Paired Box protein 3 (PAX3) and 7 (PAX7), key regulators of early myogenesis. PAX3 and PAX7 activate other myogenic transcription factors such as the Muscle Regulatory Factors (MRFs)(Hernández-Hernández *et al.*, 2017). MRF family includes MyoD, Myf5, Myf6 (previously MRF4) and myogenin. While MyoD and Myf5 are the earliest factors involved in the determination of myogenic cells, myogenin is mainly involved in terminal myogenic differentiation(Hernández-Hernández *et al.*, 2017; Zammit, 2017). Myf6 is thought to be both a determination and a differentiation factor. Interestingly, although MyoD and Myf5 mark alternative lineages: the epaxial myotome, that will eventually give rise to trunk muscles, preferentially expresses Myf5 while the hypaxial myotome, at the origin of limb muscles, preferentially expresses MyoD.

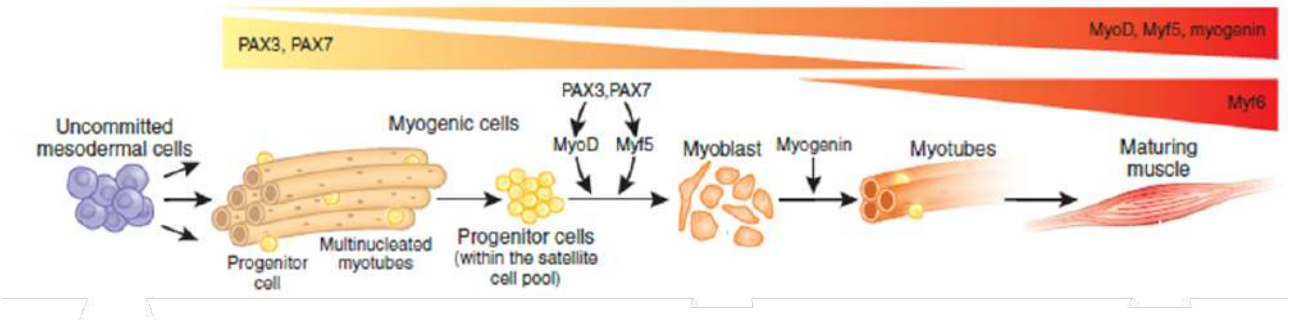

Figure 1.5. Schematic representation of skeletal myogenesis. Muscle determination from the mesoderm depends on myogenic transcription factors (i.e PAX3, PAX7, MyoD, Myf5, myogenin and Myf6). Postnatal muscle maintenance and regeneration depends on activation of quiescent muscle precursor cells (satellite cells) that proliferate, terminally differentiate and fuse to generate multinucleated myotubes. Myf5 and 6: Myogenic Factor 5 and 6; MyoD: Myogenic Differentiation protein 1; Pax3 and 7: Paired box protein Pax-3 and 7. Adapted from (Hettmer and Wagers, 2010)

Initially, MyoD and Myf5 promote expansion of the myogenic precursors. MyoD is also responsible for the initiation of the muscle differentiation process. Finally, myogenin and MyoD induce cell cycle arrest and promote terminal differentiation.

Terminal differentiation is characterized by irreversible loss of proliferative capacity and expression of muscle-specific proteins leading to the formation of mature muscle fibres. Both MyoD and myogenin are involved in terminal differentiation(Blais *et al.*, 2005). MyoD target genes include late muscular differentiation genes and cell-cycle exit proteins such as p21(Cao *et al.*, 2010). MyoD favours chromatin accessibility at muscle-specific loci but also facilitates DNA accessibility for myogenin promoting the transcriptional activation mediated by myogenin (Puri *et al.*, 1997; Blais *et al.*, 2005). Finally, myoblasts alignment and fusion lead to multinucleated myotubes which will form the myofibres of the mature muscle.

Once the mature muscle has been set, progenitor cells will enter quiescence. Postnatal muscle growth mostly results from individual fibre hypertrophy through the addition of novel myofibrils. Nonetheless, a subset of the Pax7+ progenitors will form the pool of adult muscle stem cells, the satellite cells. Adult skeletal myogenesis depends on the activation of satellite cells that have the potential to proliferate and differentiate into new fibres as well as to ensure the satellite cell pool self-renewal (Collins and Partridge, 2005; Collins *et al.*, 2005). Under quiescent conditions, satellite cells are Pax7+/MyoD-. When activated in response to muscle injury, MyoD is expressed and Pax7+/MyoD+ satellite cells are able to re-enter the cell cycle, proliferate and undergo differentiation eventually fusing to each other or to pre-existing myofibres to repair muscle damage. When satellite cells are commiting to differentiation, they become Pax7-/MyoD+.

1.6 Overview of the cell cycle in myogenesis

Cell proliferation and cell cycle exit are key steps in myogenesis (Chal and Pourquié, 2017). The eukaryotic cell cycle comprises the following phases: G0-G1 (the longest phase), S and G2 (which constitute the interphase) and the M phase (mitosis) (Figure 1.6).

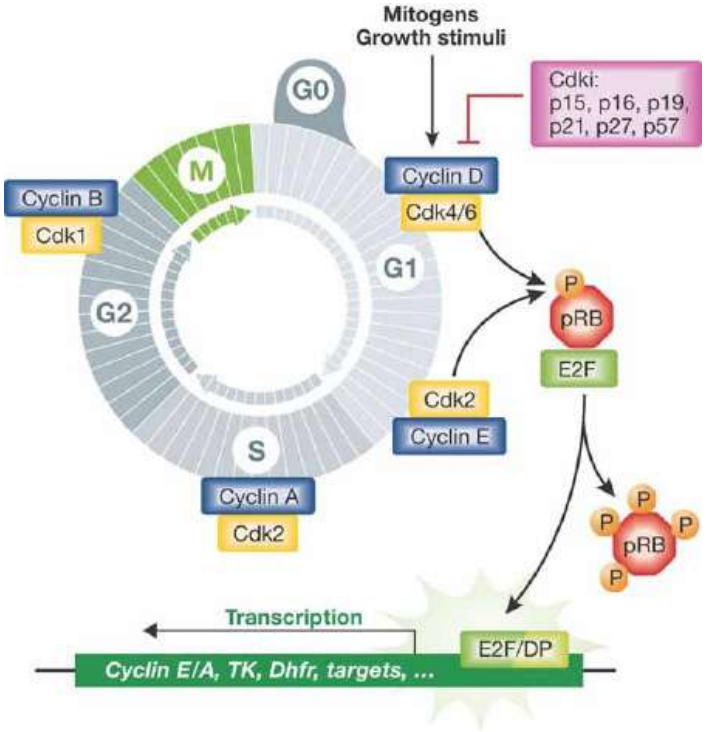

Figure 1.6. Schematic representation of the cell cycle regulation. CDK: cyclin dependent kinases; Cdki: cyclin dependent kinases inhibitor; E2F: E2F transcription factor; pRb: retinoblastoma protein; TK: thymidine kinase *(Aguilar and Fajas, 2010).*

In G1 phase, growth factors induce the expression of D-type cyclins (D1, D2, and D3) and activation of the cyclin dependent kinases (CDK) 4 and 6. The cyclin D-CDK4/6 complex phosphorylates the retinoblastoma protein (pRb) and weakens its interaction with the transcription factor E2F. As a consequence, it allows initial transcription of E2F dependent genes, involved in S-phase entry (i.e. cyclin E). Subsequent activation of CDK2-cyclin E leads to further phosphorylation and inactivation of pRb, release of E2F and full commitment to S-phase entry (Buttitta and Edgar, 2007; Aguilar and Fajas, 2010). pRb regulates not only cell cycle but also muscle-specific gene expression through its target E2F. It has been recently shown that in early G1, pRb is mono-phosphorylated at different specific sites. Those mono-phosphorylated forms may favor differential binding preferences to specific cellular targets including myogenic regulatory factors (Narasimha *et al.*, 2014).

In addition to the pRb-mediated control, another way to prevent the cells to enter the S-phase is the action of the CDK inhibitor proteins (CKIs) such as p21. They contribute to cell cycle exit and its expression is increased in differentiated cells. The main role of p21 in muscle cells is to down-regulate the CDK activities in order to maintain pRb in its hypo-phosphorylated form and to stop the

activity of transactivation of E2F, thus inhibiting the proliferation of myoblasts. Nonetheless, p21 is also involved in cyclin D1-CDK4 complex formation and stabilization, so it serves as a dual regulator of cell cycle progression depending on its concentration (LaBaer et al., 1997).

Other mechanisms of cell cycle control, such as the G2 checkpoint at the G2/M transition involving Cyclin B1/CDC2 and CHK1 and CHK2 kinases or the p53 post-translational modifications in response to chromatin changes, are beyond the scope of the present work.

Cell cycle exit is required for terminal differentiation. Along these lines, cyclins D, E or A overexpression inhibit MRF transcriptional activity, hence blocking terminal differentiation (Skapek *et al.*, 1996). MyoD also induces transcription of Rb and p21 leading to the postmitotic cell status (Halevy *et al.*, 1995) (Figure 1.7).

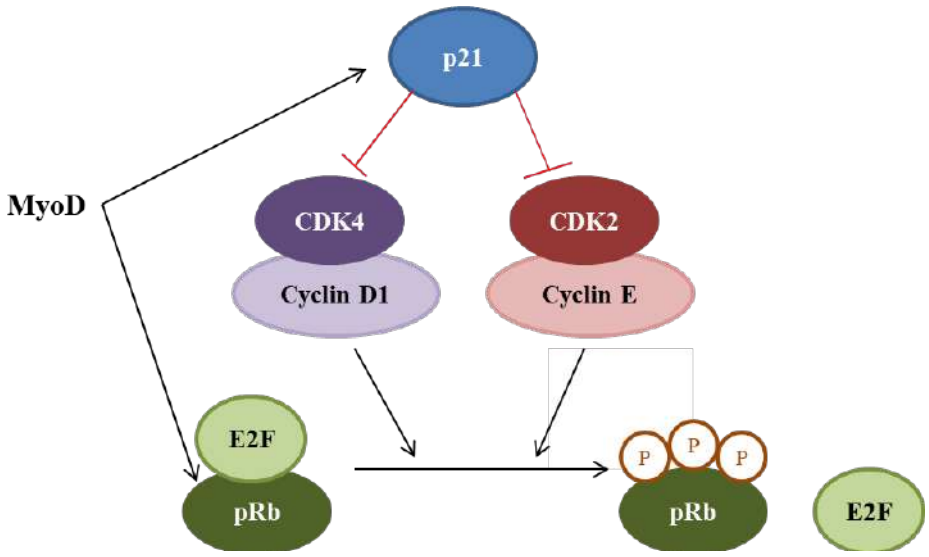

Figure 1.7. Impact of MyoD on cell cycle-related proteins. CDK 4-6: Cyclin-dependent Kinases 4 and 6; E2F: E2F transcription factor; MyoD: Myogenic Differentiation protein 1; p21: cyclin-dependent kinase inhibitor 1 or CDK-interacting protein 1; pRb: Retinoblastoma protein.

Myogenic transcription factors have distinct expression levels throughout the cell cycle (Kitzmann *et al.*, 1998). Myf5 levels are high in G0 and then drop in early G1 phase, rising againg at the end of G1; the levels remain stable through the M (mitosis) phase, at the end of which Myf5 will be phosphorylated and degraded. MyoD is mainly expressed in mid G1 phase and is degraded in late

G1 by a mechanism involving the CyclinE/CDK2 complex (Tintignac *et al.*, 2000). MyoD expression beyond the G1 phase blocks the G1/S transition (Sorrentino *et al.*, 1990).

1.7 Congenital myopathies

Congenital myopathies (CMs) are genetically and clinically heterogeneous inherited muscle disorders. CM are rare disorders, with an overall estimated prevalence of 1:25,000 (Amburgey *et al.*, 2011; Böhm *et al.*, 2013*b*). Previous point prevalence studies ranged from 1.4:100,000 of all age groups in northern England (Norwood *et al.*, 2009) to 5:100,000 in a Swedish paediatric population (Darin and Tulinius, 2000). CM prevalence is probably being underestimated due to underrecognition of mildly affected patients, sometimes being referred in adulthood, or cases with nonspecific histopathological findings.

CM usually present during the first years of life with delayed motor development, muscular weakness and hypotonia, and normally have a static or slowly progressive course (Böhm *et al.*, 2013*b*). They may be associated with orthopaedic and systemic involvement, which can be determinant for functional and vital prognosis (North *et al.*, 2017).

Traditionally, congenital myopathies have been classified on the basis of characteristic histopathological and ultrastructural features on muscle biopsy (Sewry and Wallgren-Pettersson, 2017; Phadke, 2019) (Figure 1.8). As such, the four major groups of CMs are (i) nemaline myopathies (characterized by rods, accumulations of Z-disk-derived material) and its variants, including cap myopathy, zebra body myopathy and core-rod myopathy (Malfatti and Romero, 2016), (ii) core myopathies including central core disease and multiminicore disease (marked by the presence of single or multiple areas lacking histochemical oxidative and glycolytic enzymatic activity) (Ferreiro *et al.*, 2000*a*, 2002*a*, *c*; Jungbluth *et al.*, 2011), (iii) centronuclear myopathies (Romero and Bitoun, 2011) and (iv) myopathies with congenital fibre type disproportion (CFTD), defined by the presence of type 1 fibre hypotrophy with mean diameter being uniformly smaller than type 2 fibres by more than 35-40% in the absence of other structural abnormalities and accompanied by clinical features compatible with a CM (Clarke, 2011). Other pathological features that can be associated to CMs include hyaline bodies (i.e. in myosin storage myopathy), necklace fibres, whorled fibres or radial sarcoplasmic strands. Nonetheless, there is considerable pathological overlap between this classically-described categories.

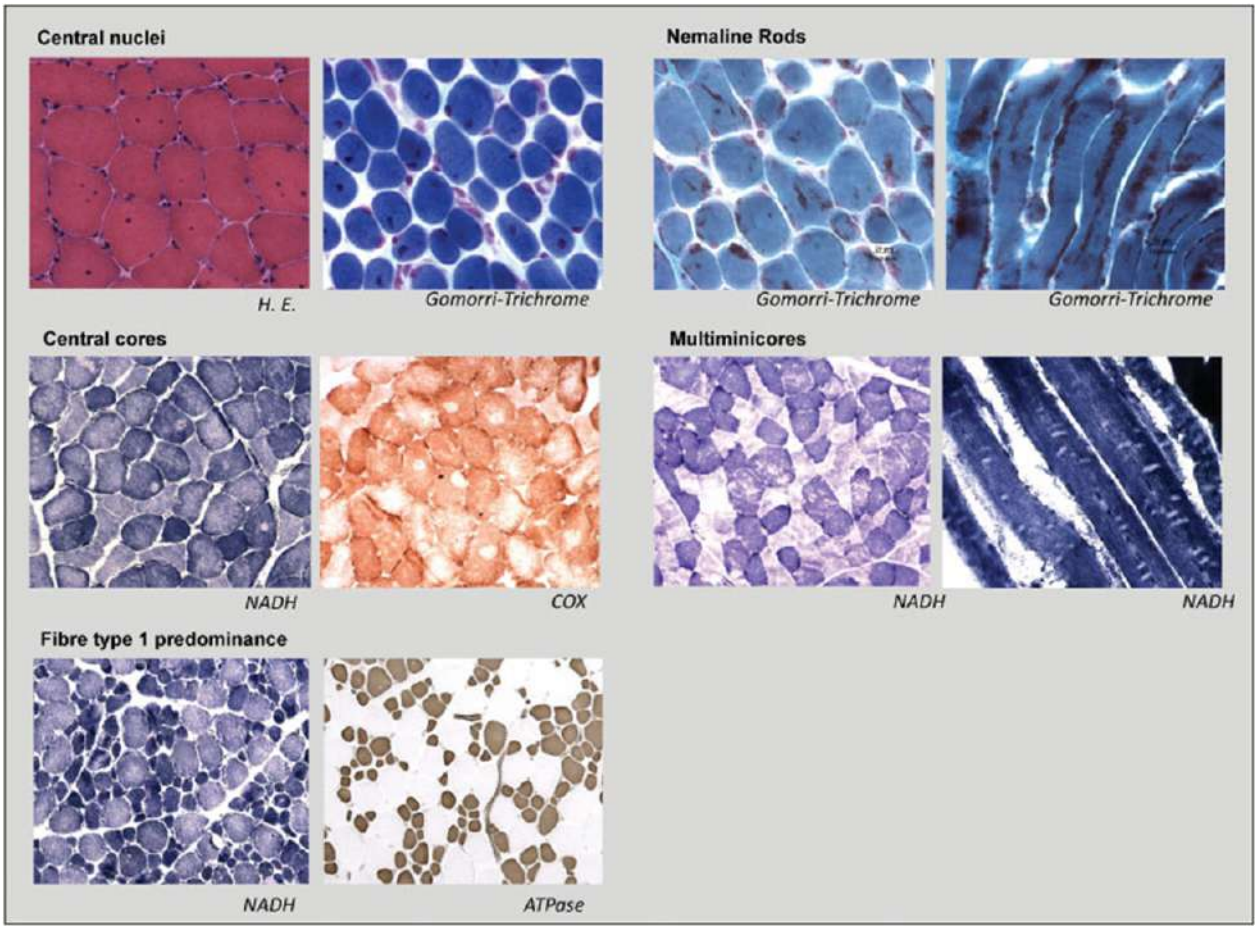

Figure 1.8. Main histopathological findings in CMs. From Schorling et al. (2017). COX: cyclooxygenase; H.E: Hematoxylin and eosin; NADH: nicotinamide adenine dinucleotide hydride.

Core myopathies are the most common subtype of CMs (Maggi *et al.*, 2013). Indeed, mutations of the ryanodine receptor 1 gene (*RYR1*) are the most frequently implicated in CMs, with a point prevalence of 1:90,000(Amburgey *et al.*, 2011). Moreover, in the Japanese population the carried frequency of *RYR1* mutations was estimated to be 1:2,000 individuals (Wu *et al.*, 2006). Nonetheless, an increasing number of mutations in the *TTN* gene are being recognized and may be involved in a substantial proportion of undiagnosed cases of congenital myopathies (Chauveau *et al.*, 2014*b*).

The increasing use of next generation sequence has allowed identification of the genetic cause underlying an increasing number of congenital myopathies. To date, more than 30 genes have been associated to CMs, with a remarkable genetic heterogeneity and pathological overlap, blurring the classically established boundaries (Kaplan and Hamroun, 2015; Schorling *et al.*, 2017; Gonorazky *et al.*, 2018) (Table 1.3). Indeed, most congenital myopathies can be caused by mutations in more than

one gene; for instance, nemaline myopathy can be caused by mutations in 12 known genetic loci: *NEB, TPM2, TPM3, CFL2, ACTA1, TNNT1, KBTBD13, KLHL40, KLHL41, MYO18B, MYPN* and *LMOD3* (Malfatti and Romero, 2016; Gonorazky *et al.*, 2018). Conversely, mutations in the same gene can cause different muscular diseases; for example mutations in *ACTA1* encoding α-actin can cause nemaline myopathy, CFTD, cap disease and zebra body myopathy (Laing *et al.*, 2004; Feng and Marston, 2009; Sewry *et al.*, 2015). In any case, despite the increasing knowledge of the genetics underlying congenital myopathies, up to a third of cases remains genetically unresolved (Maggi *et al.*, 2013).

The histopathological features in muscle biopsy may represent different manifestations within a pathological spectrum rather than define discrete pathological entities (Sewry and Wallgren-Pettersson, 2017). For instance, central nuclei are classically associated with mutations in BIN1, DNM2 or MTM1 (Romero and Bitoun, 2011; Jungbluth and Gautel, 2014) but they can also be found associated with mutations in *KBTBD13* (Olivé *et al.*, 2010), *CFL2* (Ockeloen *et al.*, 2012) or *TTN* (Ceyhan-Birsoy *et al.*, 2013), which are not classically considered as centronuclear myopathies. Furthermore, CMs with multiple structural abnormalities are increasingly being recognized. As such, core-rod myopathy has been described due to mutations in *RYR1*, *ACTA1* and *NEB*, and the combination of cores and central nuclei has been associated to mutations in *TTN, CCDC78, DNM2* and *SEPG* (Sewry and Wallgren-Pettersson, 2017; Jungbluth *et al.*, 2018). Along these lines, it is now widely accepted to classify these disorders based on the causative gene and refer to *ACTA1*-related myopathies, RYR1-related myopathies (RYR1-RM) or SEPN1-related myopathies which encompass a wide spectrum of clinical, histological and molecular phenotypes.

Moreover, novel entities lacking a single predominant histopathological abnormality and not fitting into the traditional pathological classification are increasingly recognized. For example, CACNA1S-related myopathy (Schartner *et al.*, 2017), due to recessive and dominant mutations in the voltage-dependent calcium channel subunit α1S, is characterized by marked neonatal hypotonia, prominent axial weakness and variable extraocular, bulbar and respiratory involvement. Muscle biopsies from these patients can show sarcoplasmic reticulum dilatations, internalized nuclei and myofibrillar disorganization resembling minicores. Hereditary myosin myopathies or myosinopathies due to mutations in *MYH2* and *MYH7* comprise congenital myopathies of variable onset and severity. MYH2-related myopathies are characterized by a significant reduction or absence of type 2A fibres

while muscle biopsies in MYH7-related myopathies may show accumulation of slow myosin (hyaline bodies). In both MYH2- and MYH7-related myopathies, cores, increased connective tissue, internal nuclei, rimmed vacuoles, and ring and lobulated fibres can also be found (Tajsharghi and Oldfors, 2013).

So far, no specific treatment is available for these conditions (Jungbluth *et al.*, 2017). Treatment is mainly supportive and should involve an interdisciplinary team to meet the individual needs of each patient (Wang *et al.*, 2010). Clinical trial readiness in CMs is hindered by the scarce data available concerning natural history of these conditions and the absence of reliable biomarkers and outcome measures to evaluate the impact of the potential treatments on the clinical phenotype and the course of the disease (Jungbluth and Muntoni, 2019). Potential therapeutic strategies include multiple and complementary strategies addressing the underlying pathomechanisms, such as gene therapy, enzyme replacement, upregulation of compensatory proteins, antiapoptotic drugs, muscle regulator proteins activators or antioxidants, among others (Jungbluth *et al.*, 2017; Jungbluth and Muntoni, 2019). Interestingly, while some of the potential therapies which are being developed target specific and distinct genetic entities, those focusing on enhancing excitation-contraction coupling or thin/thick filament interactions may be of benefit for a wider range of different CMs, or even other neuromuscular disorders.

Few clinical trials have been conducted so far in CMs. As such, there is an ongoing clinical trial for X-linked myotubular myopathy caused by mutations of the *MTM1* gene using an AAV gene therapy approach (Clinical trial identifier NCT03199469) (Amburgey *et al.*, 2017; Annoussamy *et al.*, 2019) and one trial evaluating the antioxidant N-acetylcystein (NAC) was completed for RYR-1 related myopathies (Clinical trial identifier NCT02362425). A small, pilot, clinical trial with NAC including 6 patients was also launched for SEPN1-related myopathies (Clinical trial identifier NCT02505087). Although the increasing knowledge of the pathomechanisms implicated have allowed the identification of promising therapeutic strategies and clinical trial development is accelerating, natural history data and tailored outcome measures are needed.

Table 1.3. Summary of the main genetically recognized CM.

	Gene	Locus	Protein	Main clinical features	Inheritance
Nemalin myopathies	*NEB*	2q23	Nebulin	Most common NM genetic cause (50%) Typical congenital NM but variable severity Characteristic facial involvement Scoliosis, neck weakness and pes cavus possible	AR
	ACTA1	1q42	Skeletal muscle α-actin	25% of NM Large spectrum ranging from severe congenital to adult onset NM Cardiac involvement possible but rare Often de novo mutations	AD, AR, de novo
	TPM3	1q21	A-tropomyosin slow	<5% of NM Variable phenotype May cause hypercontractile phenotype with generalized stiffness	AD, AR
	TPM2	9p13	B-tropomyosin	<1% of NM Typical congenital NM ± contractures, distal arthrogryposis Assymetric weakness possible Cardiomyopathy possible	AD
	TNNT1	19q13	Troponin T slow	Almost exclusively identified in Old Amish/Pennsylvania populations Early severe weakness, tremor, contractures Early death due to respiratory infections	AR
	CLF2	14q13	Cofilin	Rare. Typical congenial. No facial involvement	AR

	NEFL	8p21	Neurofilament protein	Rare. Associated to Charcot-Marie-Tood disease. Intrafamilial variation. Bulbar involvement possible	AD
	KBTBD13	15q22	Kelch repeat and BTB (POZ) domain containing 13	Rare. Childhood onset NM. Proximal muscle weakness Characteristic slow movements	AD
	KLHL40	3p21	Kelch-like family member 40	Rare. Almost exclusively in severe congenital NM. Contractures, fractures at birth. Respiratory failure, swallowing difficulties. Early death frequent	AR
	KLHL41	2q31	Kelch repeat and BTB (POZ) domain containing 10	Rare. One report of five unrelated children. Two patients with severe congenital NM, three with Intermediate congenital NM	AR
	LMOD3	3p14	Leiomodin 3	Predominantly "severe congenital" but also "Intermediate congenital" NM 21 patients in 14 families reported	AR
Core Myopathies	*RYR1*	19q13	Ryanodine receptor	Proximal weakness, facial involvement, frequent contractures and skeletal deformities Mild and moderate forms (mostly AD, onset in later childhood): rarely respiratory and bulbar involvement, contractures may be present, stable or slowly progressive course	AD, AR

				Congenital and severe forms (mostly AR): respiratory involvement, generalized weakness, congenital hip dislocation possible High risk for malignant hyperthermia	
	SEPN1 (SELENON)	1p36	Selenoprotein N	Early onset axial muscular weakness, scoliosis, rigid spine Early and severe respiratory insufficiency while still ambulant	AR
	ACTA1	1q42	Skeletal muscle α-actin	Rare Mild and nonprogressive weakness of proximal limb muscles	AD
	TTN	2q31	Titin	More commonly axial myopathy with contractures Stable weakness of lower limbs; pseudohypertrophy possible Severe and rapid progressive cardiomyopathy Respiratory failure possible	AR
Centronuclear myopathies	*MTM1*	Xq28	Myotubularin	Most common CNM Severe phenotype with neonatal weakness and respiratory insufficiency needing ventilator support Facial involvement with ptosis, sometimes ophthalmoplegia Characteristic macrosomy Mild dysmorphic features possible (long and thin face, pectus carinatum, thin fingers). Rare genital abnormalities (hypospadia, cryptorchidism)	X-linked

	DNM2	19p13	Dynamin 2	Inherited AD: childhood to adulthood onset. Facial involvement, external ophthalmoplegia, characteristic weakness of neck flexors. Characteristic pattern in MRI with distal leg involvement De novo: more severe phenotype with congenital onset	AD, de novo
	BIN1	2q14	Amphiphysin	Rare Intermediate phenotype with congenital onset. Ophthalmoplegia possible	AR
	RYR1	19q13	Rynodine receptor	See Core Myopathies	AR
	TTN	2q31	Titin	Rare Early onset Diffuse muscle weakness Respiratory difficulties possible No ophthalmoplegia	AR
Congenital fibre type disproportion	*TPM3*	1q21	α-Tropomyosin slow	Most common	AD
	RYR1	19q13	Rynodine receptor	Common	AR
	TPM2	9p13	β-tropomyosin	Rare	AD
	ACTA1	1q42	Skeletal muscle α-actin	Rare	AD
	SEPN1 (SELENON)	1p36	Selenoprotein N	May also associated insulin resistance	AR

Cap disease	*TPM2*	9p13	B-tropomyosin	See NM	AD
	TPM3	1q21	α-Tropomyosin slow	See NM	AD
	ACTA1	1q42	Skeletal muscle α-actin	Rare. Severe congenital weakness	AD
Zebra body myopathy	*ACTA1*	1q42	Skeletal muscle α-actin	See NM	UK
Core-rod myopathy	*NEB*	2q23	Nebulin	See NM	AR
	RYR1	19q13	Rynodine receptor	See Core mypathies	AR
	KBTBD13	15q22	Kelch repeat and BTB (POZ) domain containing 13	See NM	AD
Myosin storage myopathy	*MYH7*	14q11	Slow/ β cardiac myosin heavy chain	Broad spectrum from severe neonatal forms with contractures and respiratory failure to slowly progressive adult onset weakness. Pseudohypertrophy of calves and foot drop. Cardiac involvement possible	AD

AD: autosomal dominant; AR: autosomal recessive; NM: nemaline myopathy; UK: unknown

1.8 Diagnostic approach to congenital myopathies

The clinical diagnosis is challenging due to the extremely variable phenotypes and disease severity associated to CMs. Indeed, significant clinical heterogeneity exists even within the same family. A thorough anamnesis (including pregnancy, birth, motor development and family history) and neurological examination are of major importance. In addition to stable or slowly progressive early onset muscle weakness and hypotonia, other suggestive features include the presence of myopathic facies, ophthalmoplegia or bulbar involvement in some cases, hyporeflexia, muscle atrophy with a distinctive distribution as well as spinal rigidity, scoliosis or other orthopaedic complications. Extraocular muscle involvement or prominent ophthalmoplegia can be found in RYR1-related myopathy (RYR1-RM) but also in some forms of nemaline myopathy (i.e. those associated with mutations in *KLHL40* and *LMOD3*).

CMs are often accompanied by systemic involvement including respiratory failure, cardiac disease or malignant hyperthermia, among others (North, 2011; Gilbreath *et al.*, 2014; Davignon *et al.*, 2016*b*; Schorling *et al.*, 2017; Wang *et al.*, 2017). Respiratory and cardiac involvement can be severe, and its early recognition and management are crucial for the patients' vital and functional prognosis. Bulbar involvement and severe respiratory failure may necessitate invasive mechanical ventilation and gastrostomy feeding from birth in some cases. Malignant hyperthermia is also a potentially-lethal treatable condition associated with certain RYR1-mutations (Snoeck *et al.*, 2015). There is usually no involvement of the central nervous system (CNS) and intelligence is normally preserved. Patients with a prenatal onset of muscle weakness may have a history of reduced fetal movements and polyhydramnios; severe cases may present with congenital arthrogryposis multiplex as a consequence of fetal akinesia. Cases of prenatal onset may also present with craniofacial dysmorphism, pulmonary hypoplasia, hip dysplasia and profound generalized weakness.

The main diagnostic tools for CMs include serum creatin kinase (CK) levels, nerve conduction studies (NCS) and electromyogram (EMG), muscle imaging, muscle biopsy and genetic testing. Serum CK is normal or mildly elevated (less than three-four times the upper limit of normal) in most patients. Significantly raised CK levels are suggestive of an alternative diagnosis (e.g. congenital muscular dystrophies in the context of an early-onset muscle weakness and hypotonia or delayed motor development). Nerve conduction studies usually show normal motor and sensory responses while EMG may reveal the so-called myopathic pattern, characterized by early recruitment of small

polyphasic motor units. Neurophysiological studies (NCS and EMG) are useful to exclude alternative diagnoses such as congenital neuropathies, myotonic disorders and congenital myasthenic syndromes. Interestingly, decremental responses on repetitive stimulation or increased jitter can sometimes be found in CMs with associated neuromuscular junction defects, such as cap myopathy due to mutations in the *TPM2* gene, CFTD caused by *TPM3* mutations or centronuclear myopathies with *DNM2* or *MTM1* mutations (Rodríguez Cruz *et al.*, 2014).

Muscle imaging, mostly magnetic resonance imaging (MRI), is a remarkable non-invasive tool in the diagnostic workup of a CM, although sedation might be required in young children. The pattern of muscle involvement can be represented by heatmaps, which represent the "fingerprint" of every particular muscular disorder. Different algorithms have been proposed to distinguish among the different subtypes of CM, and increasing knowledge of these particular disease fingerprints for many CMs have contributed significantly to the diagnostic process (Wattjes *et al.*, 2010; Carlier and Quijano-Roy, 2019). Muscle MRI is also a useful tool to follow disease progression over time by using combined qualitative and quantitative analysis. Muscle ultrasound, performed by trained clinicians, can also be useful, especially as a screening tool in paediatric patients as it does not require sedation.

Accurate assessment of skeletal muscle biopsy with a standard panel of histological, histochemical and immunohistochemical stains (Dubowitz and Sewry, 2007) may reveal different architectural abnormalities characteristic of CMs. Moreover, muscle biopsy is also helpful to exclude alternative diagnoses such as the congenital muscular dystrophies or other muscular (i.e. myofibrillar myopathies) or neurogenic disorders. Electron microscopy (EM) is of major importance in the analysis and classification of the structural abnormalities that are seen with light microscopy.

Simultaneous analysis of multiple CM-associated genes through Next-generation sequencing (NGS) has become the preferred diagnostic approach in CM (Nigro and Piluso, 2012; Krahn *et al.*, 2018). A targeted exome sequencing strategy combined with muscle biopsy findings has recently been proposed to identify the genetic cause of potential CMs of unknown cause, including coverage of each exon of known CM genes (Böhm *et al.*, 2013*b*). Nonetheless, variants of uncertain significance (VUS) are a relatively common finding in large genes such as *TTN, NEB* or *RYR1*, even in healthy control populations, and can be challenging to interpret.

The differential diagnosis of early onset weakness and hypotonia is particularly large and includes other early-onset muscular diseases such as congenital myopathies, congenital muscular dystrophies and congenital myasthenic syndromes but also myofibrillar myopathies, spinal muscular atrophy, congenital neuropathies as well as other genetic and metabolic conditions (e.g. Prader-Willi syndrome or metabolic myopathies).

Interestingly, CMs can also manifest in adulthood, especially those related to mutations in *RYR1* (Snoeck *et al.*, 2015), *DNM2* (Echaniz-Laguna *et al.*, 2013), *ACTA1* (Zukosky *et al.*, 2015; Lehtokari *et al.*, 2018), *BIN1* (Böhm *et al.*, 2014), *MYH7* (Fiorillo *et al.*, 2016) and KBTBD13 (Garibaldi *et al.*, 2018). However, most adult patients retrospectively report nonspecific symptoms of earlier onset when specifically asked. Indeed, adults with CM commonly experience delays in diagnosis and misdiagnoses. In a recent series of 44 adults with CM, 18 of them had a clear paediatric onset of symptoms but were diagnosed in adulthood while others retrospectively reported poor athletic performance in childhood. The most frequent cause of diagnostic delays in these series was a failure to obtain any neurologic investigations for symptoms that were considered benign or attributed to non-neurologic conditions (Nicolau *et al.*, 2019). The most common misdiagnoses were non-neurologic conditions, such as rheumatologic and ortophaedic disorders. Remarkably, adult patients with CM typically report progressive weakness, which contrasts with the stable or slowly progressive course typical of CM in childhood and hinders the suspicion and proper investigation of a CM. Moreover, CK elevations are more common among adult-onset or adult-diagnosed CM patients, maybe linked to the higher proportion of RYR-related myopathies in this population. In addition, electrodiagnostic findings in chronic myopathic disorders can resemble a neurogenic process. Finally, muscle biopsies from adult patients often lack the characteristic histologic abnormalities associated with CMs, which contributes to misdiagnosis. Increasing awareness of these disorders among adult neurologists would be of major importance to diagnose and properly manage these patients.

1.9 Pathophysiological mechanisms implicated in congenital myopathies

The growing identification of the genetic basis and the study of genetic-pathologic correlations in CMs provide insight on their pathophysiological mechanisms (Ravenscroft *et al.*, 2015). This is of major importance for the development of shared potential therapeutic approaches for these so-far

untreatable diseases.

The main pathophysiologic pathways implicated so far are: (i) sarcolemmal and intracellular membrane remodeling and excitation-contraction coupling (Horstick *et al.*, 2013; Dowling *et al.*, 2014; Snoeck *et al.*, 2015; Jungbluth *et al.*, 2018); (ii) mitochondrial distribution and function (Pambianco *et al.*, 2016; Moulin and Ferreiro, 2017); (iii) myofibrillar force generation (Wallgren-Pettersson *et al.*, 2011; Tajsharghi and Oldfors, 2013); (iv) atrophy (Ravenscroft *et al.*, 2015), and (v) autophagy (Gibbs *et al.*, 2010; Joubert *et al.*, 2013) (Figure 1.9).

Membrane remodeling is involved in many relevant biological processes including exocytosis, intracellular transport, synaptic vesicle function, autophagy and membrane repair. Interestingly, *BIN1*, *DNM2, MTM1* and *MTMR14*, all of them underlying CMs with internalized nuclei, have been found to be involved in membrane remodelling (Cowling *et al.*, 2012). Excitation-contraction coupling depends on the integrity and proper functioning of highly specialized membranes, notably the components of the triad: T tubules and the voltage-sensing dihydropyridine receptors (DPHR) in the T tubule membrane, the sarcoplasmic reticulum and the ryanodin receptors (RYR1) in the SR membrane. Structural defects of the triad and abnormal localization of its components, namely DHPR and RYR1, have been demonstrated in myofibres from patients with centronuclear myopathies due to *MTM1*, *BIN1* and *CCDC78* mutations (Al-Qusairi *et al.*, 2009; Dowling *et al.*, 2009; Majczenko *et al.*, 2012).

Along these lines, autosomal dominant *RYR1* mutations causing different clinical phenotypes including malignant hyperthermia susceptibility, central-core disease, multi-minicore disease, congenital fibre-type disproportion and syndromic entities such as King-Denborough Syndrome (Snoeck *et al.*, 2015) are thought to lead to leaky RYR1 channel activity, channel instability or reduced calcium conductance (Wilmshurst *et al.*, 2010). Conversely, recessive mutations are thought to cause RYR1 channel mislocalization or quantitatively reduced RYR1 (Zhou *et al.*, 2013). Defects in sarcoplasmic reticulum function are also implicated in CMs associated to mutations in *NEB* (Witt *et al.*, 2006). Mutation of the SH3 and cystein-rich domain 3 gene (*STAC3*), encoding an excitation-contraction protein, were identified as the cause of native American myopathy, a recently described CM (Horstick *et al.*, 2013) while dominant mutations in the sarcoplasmic calcium sensor STIM1 have been recently found to cause a form of tubular aggregate myopathy (Böhm *et al.*, 2013*a*). Anomalies of the triad, altered calcium homeostasis and impaired excitation-contraction coupling are one of the main

pathomechanisms in a great number of CMs and may thus represent a relevant therapeutic target for many of them.

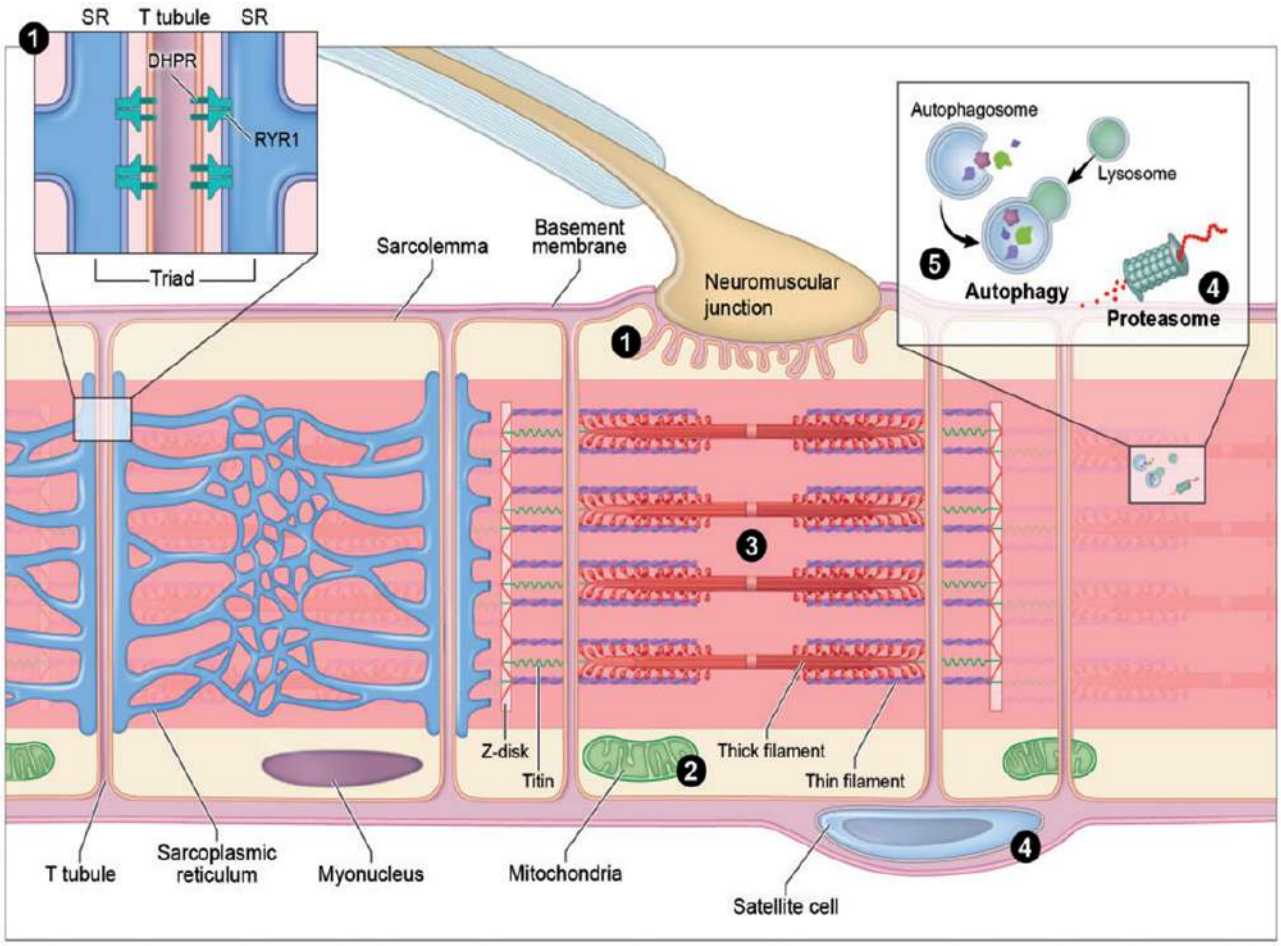

Figure 1.9. Schematic representation of a muscle cell and the cellular localization of the main pathophysiological mechanisms implicated in CM: (1) Sarcolemmal and intracellular membrane remodelling and excitation-contraction coupling; (2) mitochondrial distribution and function; (3) myofibrillar force generation; (4) atrophy; and (5) autophagy. DHPR: dihydropyridine receptor; SR: sarcoplasmic reticulum. Adapted from (Ravenscroft et al., 2015).

Neuromuscular junction defects have been found in animal models of *MTM1* (Dowling *et al.*, 2012*b*) and *DNM2* associated disease (Gibbs *et al.*, 2013). Moreover, electrophysiological recordings suggestive of impaired neuromuscular transmission have been found in *DNM2* mutant patients (Gibbs *et al.*, 2013). Finally, treatment with acetylcholinesterase (AChE) inhibitors improved the phenotype in some patients with *DNM2* mutations but also in some cases of RYR1-related myopathy

with associated fatigability and ptosis (Illingworth *et al.*, 2014).

Mitochondrial and energy metabolism abnormalities have been implicated as important disease pathomechanisms in core myopathies (Ravenscroft *et al.*, 2015). Indeed, cores are defined as areas devoid of mitochondria, and abnormal distribution, localization and/or ultrastructure of mitochondria has been found in these patients. Defective mitochondrial bioenergetics and mitochondrial-derived increased oxidative stress have been confirmed in a *ryr1* zebrafish model but also in *RYR1* mutated patients-derived myotubes, and were corrected with the antioxidant N-acetylcysteine (NAC) (Dowling *et al.*, 2012*a*). Pathophysiological mechanisms of SEPN1-related myopathy (SEPN1-RM) will be discussed below. Mitochondrial abnormalities and increased oxidative stress have also been found in centronuclear and nemaline myopathies due to mutations in *MTM1* (Dowling *et al.*, 2009), *TPM2* and *TPM3* (Davidson *et al.*, 2013). Along these lines, a randomized controlled trial of antioxidant therapy (N-acetylcysteine, NAC) for RYR1-RM (Todd *et al.*, 2020), including 33 participants, has confirmed preclinical reports of elevated oxidative stress (measured by 15-F2t isoprostane). Oral treatment with NAC for 6months was well-tolerated but the primary endpoint (urine 15-F2t isoprostane concentration) and the clinically meaningful co-primary endpoint 6-minute walk test (6MWT) distance did not significantly change. Importantly, they also observed stable disease course in ambulatory RYR1-RM patients and the treatment duration was 6 months. These two factors potentially hindered an accurate evaluation of the impact of NAC treatment on the long-term.

Other pathomechanisms involved in CMs are sarcomeric dysfunction and myofibrillar force generation defects which are the consequence of mutations in genes encoding thin filaments or proteins interacting with the latter such as *NEB, ACTA1, TPM2, TPM3* or *MYH7*, among others (Ottenheijm and Granzier, 2010; Ravenscroft *et al.*, 2015).

Finally, atrophy and autophagy are also important pathomechanisms involved in CM. The skeletal muscle bulk is determined by the balance of hypertrophy and atrophy and hence of protein synthesis and degradation pathways, the latter including atrophy and autophagy. Muscle atrophy is a common sign in CM patients, and type 1 fibre atrophy is a frequent histopathological finding in muscle biopsies. Interestingly, it has been shown that the sarcomeric contractile apparatus is directly involved in regulation of atrophy signaling (i.e. the M-line titin kinase domain is mechanosensitive and is known to recruit proteins involved in atrophy pathways such as MURF2). Mutations of genes encoding BTB-Kelch proteins (i.e. *KBTBD13*, *KLHL41*) , known to bind cullin 3 to form E3 ubiquitin ligases,

are an underlying genetic cause of nemaline myopathies, revealing the link between impairment of the ubiquitin-proteasome system and CMs (Ravenscroft *et al.*, 2015). Muscle atrophy and autophagy defects have also been found in *MTM1* animal models (Gibbs *et al.*, 2010; Romero-Suarez *et al.*, 2010). Finally, satellite cell defects implying defective skeletal muscle maintenance or regeneration have also been proposed as a disease mechanism in CM. As such, reduced satellite cells have been observed in *MTM1* (Buj-Bello *et al.*, 2002), *MEGF10* (Boyden *et al.*, 2012) and *SEPN1* (Castets *et al.*, 2012*b*) murine models. Moreover, satellite cell loss has also been found in SEPN1-RM patient muscles, suggesting that it may play a key role in maintenance of the skeletal muscle progenitor cells pool (Castets *et al.*, 2012).

.

1.10 Congenital myopathies with multi-minicores

Congenital myopathies with cores represent the most common subgroup of CMs, and traditionally comprised central-core and multi-minicore myopathies.

Cores are defined as areas of sarcomeric disorganization and mitochondrial depletion, which show reduced oxidative enzyme activity on oxidative stains (NADH-TR, SDH, COX) and various degrees of myofibrillar disorganization on EM. Cores or core-like lesions (with staining for oxidative enzymes showing absence of mitochondria but without the myofibrillar disorganization on EM observed in cores) can also be found in collagen VI myopathies (Bönnemann, 2011*b*), inflammatory myopathies (Vick, 1970), emetine myopathy (Duane and Engel, 1970), myasthenic syndromes (Dubowitz and Sewry, 2007), muscle atrophy of neurogenic origin (Schmitt and Volk, 1975), endocrinopathies (Mastaglia *et al.*, 1988), metabolic diseases (Pellissier *et al.*, 1979), ankylosing spondylitis (Kakulas *et al.*, 1987), glucocorticoid treatment in rats (Tice and Engel, 1967), tenotomy (Karpati *et al.*, 1972) or even in healthy young subjects (Meltzer *et al.*, 1976).

Minicores differ from cores by their nonselectivity for a particular fibre type and their smaller size. Unlike the cores typical of central-core myopathy, minicores affect both type 1 and type 2 fibres and are short in length, spanning only a few sarcomeres in the fibre longitudinal axis. Minicores are generally round, small, variable in size, multiple, randomly distributed and have poorly defined boundaries (Figure 1.10). They appear in oxydative stains as multiple small focal lesions with reduced or absent oxidative activity in a variable proportion of fibres. On EM, minicores appearance can range from

focal areas of Z-disc streaming and mitochondrial depletion to severe myofibrillar disorganization with complete loss of the sarcomeric architecture (Ferreiro *et al.*, 2000).

While central-core disease (CCD) is closely associated with dominant *RYR1* mutations, multi-minicore disease (MmD) is a strikingly heterogeneous condition (Ferreiro *et al.*, 2000). MmD was first reported as "multicore disease" in 1971 by Engel et al., as a congenital, benign and nonprogressive muscular condition in a family with two affected siblings (Engel *et al.*, 1971). After this initial description, a number of patients with heterogeneous clinical presentations were reported, including patients with variable respiratory or cardiac involvement, ophthalmoplegia and also severe forms leading to loss of ambulation and death due to respiratory failure. These cases were reported as "multicore myopathy", "multiminicore myopathy", "myopathy with multiple minicore", "pleocore disease" or "multi-minicore disease", amongst others (Mukoyama *et al.*, 1973; Bonnette *et al.*, 1974; Mukoyama, 1978; Ricoy *et al.*, 1980; Martin *et al.*, 1986).

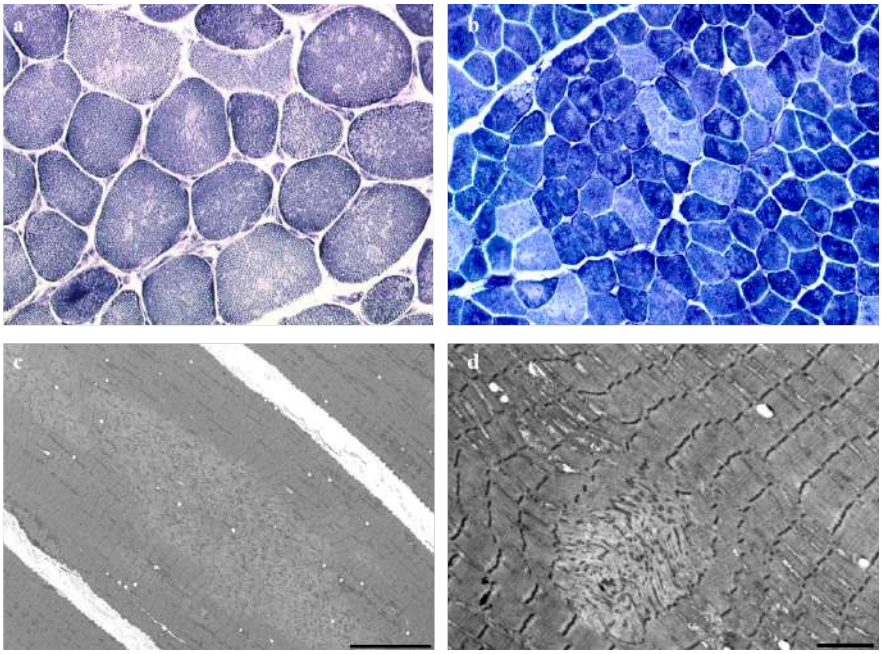

Figure 1.10. Minicore lesions. (a): NADH-TR (x20) stain show multiple focal areas lacking oxidative (Engel et al., 1971) activity. (b): ATPase 10.6 (x20) reveals involvement of both type 1 and 2 fibres. (c-d) Longitudinal sections on electron miscroscopy (EM) reveal different degrees of myofibrillar structure disorganization. Scale bars: c-10 µm, d-2 µm.

In order to define its phenotypic spectrum, MmD was initially divided into four subgroups (Ferreiro

et al., 2000): (i) the classical and more prevalent form, characterized by predominant axial weakness, scoliosis and life-threatening respiratory failure; (ii) the moderate form of MmD with hand involvement, where scoliosis and respiratory failure were mild or absent; (iii) a variant of the classical form with ophthalmoplegia, and (iv) MmD with antenatal onset and arthrogryposis. Genetic heterogeneity of MmD explained the wide clinical spectrum, as *RYR1* mutations were found to be responsible for the moderate MmD form with hand involvement and MmD with ophtalmoplegia (Ferreiro *et al.*, 2002*a*) while the other forms were attributed to recessive mutations in the *SEPN1* (*SELENON*) gene (Ferreiro *et al.*, 2002b). *SEPN1* mutations were subsequently associated with congenital fibre type disproportion (Clarke et al., 2006) and desmin-related myopathy with Mallory body-like inclusions (Ferreiro et al., 2004), a myopathy with protein aggregates. All these conditions, with common clinical and molecular features, are best understood as part of the spectrum of the same disorder, thereby called SEPN1-related myopathy (SEPN1-RM). Despite its heterogeneous pathological presentation, SEPN1-RM patients share a fairly homogeneous phenotype, characterized by early-onset prominent axial weakness, scoliosis, rigid spine and life-threatening respiratory failure strikingly disproportionate to the degree of limb muscular weakness (Ferreiro *et al.*, 2002*b*, 2004; Scoto *et al.*, 2011). SEPN1-RM clinical phenotype and pathophysiology will be further explained in chapter III. Patients with RYR1-RM have a distribution of weakness and wasting that resembles SEPN1-RM but have extraocular muscle involvement and usually lack severe respiratory failure (Snoeck *et al.*, 2015).

A number of genes have subsequently been associated with multi-minicores, such as *MYH7* (Cullup *et al.*, 2012; Fiorillo *et al.*, 2016), *TTN* (Oates *et al.*, 2018), *MEGF10* (Boyden *et al.*, 2012), *ACTN2* (Lornage *et al.*, 2019*a*), *FXR1* (Estañ *et al.*, 2019) or *PYROXD1* (Lornage *et al.*, 2019*b*). Autosomal dominant mutations in *ACTA1* have been also reported in two families with a mild and nonprogressive myopathy with both cores and minicores associated to an adult-onset hypertrophic cardiomyopathy and respiratory failure in one family (Kaindl *et al.*, 2004).

These genes are associated with different clinical phenotypes. Dominant mutations in the *MYH7* gene are associated with a wide clinical spectrum including an early-onset predominantly distal myopathy with minicores and variable cardiac involvement (i.e. hypertrophic cardiomyopathy)(Cullup *et al.*, 2012; Fiorillo *et al.*, 2016). *TTN*-related myopathies have a variable histological presentation including, among others, minicores, cap-like structures and centrally-located nuclei. Congenital titinopathies are characterized by neonatal or early-onset hypotonia and/or congenital contractures

associated with early-onset scoliosis and respiratory insufficiency and cardiac involvement in up to 50% of patients (Oates *et al.*, 2018). Nonsense and frameshift mutations in the *MEGF10* gene cause a severe congenital myopathy with minicores with severe respiratory failure and dysphagia (Boyden *et al.*, 2012). Recently, recessive mutations in the *FXR1* gene have been found to cause a congenital myopathy with multi-minicore in two unrelated families (Estañ *et al.*, 2019). In one of these families, the patients had a very severe, lethal phenotype marked by severe hypotonia, respiratory failure, tachycardia and congenital bone fractures while the probands of the second family had a congenital myopathy with neonatal hypotonia, delayed motor milestones and slowly progressive muscular weakness. Interestingly, dominant mutations in *ACTN2*, previously associated with cardiomyopathy, have been reported in two unrelated patients with an early-onset myopathy with respiratory involvement and minicores with jagged Z-lines (Lornage *et al.*, 2019*a*). Finally, recessive mutations in *PYROXD1*, encoding an oxidoreductase, have been recently reported to cause a congenital myopathy with progressive respiratory involvement, scoliosis, joint hypermobility and a histopathological presentation marked by internal nuclei and minicores (Lornage *et al.*, 2019*b*).

Moreover, minicores can be associated with other architectural or structural changes such as cores and rods (Vallat *et al.*, 1982), mitochondrial abnormalities (Pellegrini *et al.*, 1985) or centrally located nuclei (Chauveau *et al.*, 2014*a*; Oates *et al.*, 2018) as well as with dystrophic features (Ferreiro *et al.*, 2000; Davignon *et al.*, 2016).

The precise mechanism underlying minicore formation is not well understood. Although it was initially suggested that the minicore formation process began in the mitochondria (Engel *et al.*, 1971), this was not confirmed. Indeed, abnormal mitochondrial accumulation or localization and/or ultrastructural defects have been described in core myopathies (including CCD and MmD), centronuclear myopathies and nemaline myopathies and nemaline myopathy (Sanoudou *et al.*, 2006; Hnia *et al.*, 2011; Dowling *et al.*, 2012*a*). Nonetheless, it remains unclear whether the primary abnormality underlying minicore formation might be a mitochondrial lesion or rather a structural defect of sarcomeric components. It has been postulated that focal areas with loss of cross-striations might be caused by local stress within the muscle fibre (Swash and Schwartz, 1981). Furthermore, areas of Z-disk disintegration have also been observed in human muscular fibres damaged by eccentric contractions (Fridén *et al.*, 1984). Along these lines, minicores could arise as a secondary manifestation of a primary lesion causing a deficient resistance of the sarcomere to tension caused by repeated muscular contraction

which eventually lead to the sarcomeric disorganization (Ferreiro *et al.*, 2000). Thus, minicores could be a secondary manifestation of primary abnormalities of different origins. Indeed, the increasing knowledge of the genetic basis of myopathies with minicores could help clarify this point in the near future. Based on a murine model of RYR1-RM ($Ryr1^{I4895T/wt}$ (IT/+) mice, expressing a knockin mutation corresponding to the human I4898T excitation-contraction uncoupling mutation), it has been proposed that calcium leak or EC uncoupling resulting from RyR1 mutations could result in a heterogeneous contraction among myofibrils, eventually leading to focal and irreversible myofibrillar damage, which would, over time, enlarge to form minicores and cores (Zvaritch *et al.*, 2009). More recently, it has also been suggested that fragile X related protein (FXR1P) represses translation of specific mRNAs in muscle costamere structures. Thus, deregulated translation of specific mRNAs involved in Z-line organization may contribute to minicore formation in *FXR1*-related myopathy (Estañ *et al.*, 2019). Nonetheless, further studies are needed to elucidate the mechanism of minicore formation.

Chapter 2

HYPOTHESES AND OBJECTIVES

2.1 Hypotheses

1. Recessive mutations in the *SEPN1* (or *SELENON*) gene are associated with a congenital muscular phenotype but also with systemic and metabolic abnormalities, with a full phenotypic spectrum which has not been studied in-depth so far.
2. Selenoprotein N-related myopathy (SEPN1-RM) can be a severe, disabling condition with a more rapid disease progression than initially thought.
3. So-far unknown genotype-phenotype correlations and other severity determinants in SEPN1-RM could contribute to explain the phenotypic variability and the different degrees of disease severity observed in patients.
4. Recessive mutations in the *TRIP4* gene leading to the depletion of the transcriptional co-integrator ASC-1 are associated with a clinical and histological phenotype whose full spectrum is yet to be defined.
5. ASC-1 plays a key role in the pathophysiology of skeletal muscle, particularly as a regulator in the myogenic process. Cell-cycle regulation could be one of the mechanisms implicated in the role of ASC-1 on cell proliferation and myotube growth and thus could represent a key pathomechanism underlying ASC1-related myopathy (ASC1-RM).

2.2 Aims of the project

This project aims to delineate the phenotypical spectrum, potential genotype-phenotype correlations and natural history of two congenital myopathies with multi-minicores, SEPN1-related myopathy and ASC1-related myopathy. This will contribute to a better recognition, diagnosis and management of these patients in clinical practice as well as to the identification of potential biomarkers which could be of major importance for clinical trial readiness and the development of therapeutic approaches.

Moreover, the project aims to confirm the novel role of ASC-1 in human skeletal muscle and to contribute to elucidate the potential pathomechanisms involved.

The **specific aims** of the project are:

1- To characterize the clinical, histological and molecular spectrum of SEPN1-RM, and also to describe the natural history of the disease searching for potential biomarkers or prognostic factors

2- To investigate potential genotype-phenotype correlations in SEPN1-RM

3- To define the clinical and histological phenotype of ASC1-RM, as well as the genetic and molecular spectrum associated including the consequences of the mutations on protein expression in available patient samples

4- To investigate potential genotype-phenotype correlations in ASC1-RM

5- To explore the involvement of ASC-1 on skeletal muscle pathophysiology by investigating its role as a novel cell cycle regulator

2.3 Novelty and expected results

The main strength of this project lies in its novelty and its translational potential. Globally, the expected results of this project could contribute to the scientific progress in the biomedical field for the following reasons:

- ✓ A thorough phenotypical characterization as well as the description of the natural history of the disease would contribute to a better diagnosis, follow-up and management of the patients. It would also be of major importance to identify, prevent and manage potential disease complications, often responsible for disability, morbidity and mortality and having a great personal, family and socio-economic impact
- ✓ The project aims to identify potential biomarkers and prognostic factors which may be critical for clinical trial readiness in SEPN1-RM, a condition for which there is no specific treatment available so far
- ✓ Given the clinical and histological overlap between ASC1-RM and other early-onset

muscle diseases (i.e. other congenital myopathies and congenital muscular dystrophies), understanding ASC-1 role in the skeletal muscle pathophysiology could contribute to identify potential common pathological mechanisms involved in these conditions

Even though the project is focused on two rare congenital myopathies, it aims at contributing to the scientific progress in the neuromuscular field as well as to improve the management of these patients in clinical practice, often undiagnosed or not properly managed.

Chapter 3

SEPN-1 RELATED MYOPATHY

3.1 INTRODUCTION

Congenital myopathies (CMs) are heterogeneous inherited muscle disorders with an estimated prevalence of 1/25000 (Amburgey *et al.*, 2011) that may account for at least one tenth of all cases of neuromuscular disorders (Salih, 2012).

In 1998, a reportedly very rare form of congenital muscular dystrophy with early rigidity of the spine (rigid spine muscular dystrophy, RSMD1) was linked to chromosome 1p35-36 (Moghadaszadeh *et al.*, 1998). Shortly after that, the selenoprotein N gene (*SEPN1 or SELENON,* MIM*606210), localized in 1p36, was identified (Lescure et al., 1999). The previously described association between selenium deficiency and striated muscle dysfunction (Lamand, 1970; Brown *et al.*, 1986) pointed *SEPN1* as a positional candidate gene for RSMD1. Indeed, homozygous or compound heterozygous *SEPN1* mutations were rapidly found in most RSMD1 patients (Moghadaszadeh *et al.*, 2001), thus describing a selenoprotein implicated in a neuromuscular disorder for the first time. Surprisingly, mutations of the same gene, and often the same precise mutations, were subsequently associated with three additional early-onset muscle disorders: the classical form of multi-minicore disease (Ferreiro *et al.*, 2002*b*), rare cases of congenital fibre type disproportion (Clarke *et al.*, 2006) and desmin-related myopathy with Mallory body-like inclusions (Ferreiro *et al.*, 2004), a myopathy with protein aggregates. In spite of its strikingly heterogeneous histopathological presentation, patients shared a very homogeneous clinical phenotype, marked by severe axial weakness, early-onset scoliosis frequently associated with spinal rigidity and life-threatening respiratory insufficiency, but fairly preserved limb strength and ambulation (Schara *et al.*, 2008; Scoto *et al.*, 2011; Ardissone *et al.*, 2016). Indeed, after careful retrospective reassessment, it was shown that these four autosomal recessive muscle conditions shared so many clinical and molecular features that they were best understood as the same unique

disorder, thus termed SEPN1-related myopathy (SEPN1-RM) (Ferreiro et al., 2002b).

Selenoprotein N is a ubiquitous 65-kDa endoplasmic reticulum glycoprotein, whose mRNA is detected in most foetal and, at a lower level, adult tissues (Petit *et al.*, 2003). Since the identification of the first *SEPN1* mutations, basic and pathophysiological research has revealed that this protein with a putative enzymatic reductase activity plays a key role in mitochondrial bioenergetics, redox-based homeostasis (Arbogast and Ferreiro, 2010; Marino *et al.*, 2015) and human cell defense against oxidative stress (Arbogast *et al.*, 2009; Arbogast and Ferreiro, 2010; Rederstorff *et al.*, 2011; Moulin and Ferreiro, 2017*a*; Varone *et al.*, 2019). These pathways are drug-targetable, and indeed some compounds, such as N-acetylcysteine, have proven effective for rescuing the SEPN1-devoid cell phenotype *ex vivo* (Arbogast *et al.*, 2009). However, clinical trial readiness in SEPN1-RM is poor due to significant challenges which hinder therapeutic progress.

One of the main reasons is the scarcity of data on the phenotypical spectrum and natural history of SEPN1-RM patients, with only a few small series of cases having been reported so far (Ferreiro *et al.*, 2002*b*; Schara *et al.*, 2008; Scoto *et al.*, 2011) . There are no validated biomarkers and few quantitative data on disease severity, progression, or factors determining prognosis, including the impact of symptomatic (respiratory, orthopaedic) management. Disease evolution is considered to be stable or very slowly progressive, making it difficult to identify sensitive outcomes to measure impact of a potential therapy. Furthermore, the impact of age has never been analysed in a long follow-up series including older adults, and no phenotype-genotype correlations are known. Finally, while SEPN1-RM is considered an ultra-rare disease, the actual disease prevalence is unknown. This global situation has a negative impact on the diagnosis and management of patients and hampers planning of international clinical trials.

The present work represents the first large series of SEPN1-RM, including 132 patients with this rare disease recruited through an international multicentre collaboration. Retrospective clinical, morphological and molecular analyses have been collected, providing the first comprehensive natural history study including late adulthood. Quantitative parameters with diagnostic and management implications and phenotype-genotype correlations are also presented here, paving the way for clinical trial readiness.

3.2 MATERIALS AND METHODS

3.2.1 Patients

Between 2001 and 2017, 132 patients with *SEPN1* mutations were included in the study after informed consent according to local ethical committees. This series includes 63 French patients, identified through the main reference laboratories performing *SEPN1* screening as part of a national network. To estimate disease prevalence, other genetic diagnostic laboratories in France outside the reference network were also interrogated. A comprehensive list of the international collaborating centres where the patients were identified can be found in Annex 1.1. Thirty-one patients have been previously reported (Moghadaszadeh *et al.*, 2001; Ferreiro *et al.*, 2002*b*, 2004; Schara *et al.*, 2008).

Clinical data were systematically retrieved and retrospectively analysed according to a standardized form (Annex 2.1), except for 31 cases from which only genetic information was available. The following data were collected: age at onset and presenting symptoms, neurological examination and functional ability at the last visit, presence of contractures, rigid spine, scoliosis and spinal surgery, respiratory function (forced vital capacity [FVC], polysomnographic studies and age at the start of nocturnal non-invasive ventilation [NIV] and/or tracheostomy), cardiac assessment (transthoracic echocardiogram, electrocardiogram [ECG] and Holter ECG) and biometrical data (n=55 patients, Body Mass Index [BMI] (Garrow and Webster, 1985) and weight centile (Kuczmarski *et al.*, 2002)). The frequency of each finding was calculated over the number of patients from whom this data was available.

Standard blood test results including CK levels were collected from 76 patients. In a subset of 6 patients, detailed biochemical studies including serum selenium levels, serum and red blood cells glutathione peroxidase, lactate, pyruvate, thyroid hormones, and carnitine were performed. Electromyography and neuroimaging (brain magnetic resonance imaging [MRI] or computed tomography [CT] scan) were obtained in 24 and 27 patients, respectively.

3.2.2 Skeletal muscle biopsy

We reviewed 79 muscle biopsies and/or histopathological reports. Muscle biopsy site was known in 43 of these patients (45 biopsies), including deltoid (n= 22, 48.9%), quadriceps (n=17, 37.8%), biceps brachialis (n=2, 4.3%), gastrocnemius (n=2, 4.3%) and abdominal muscles (n=2, 4.3%). Muscle samples were frozen and processed for standard histological and histochemical studies and fixed for electron microscopy, as previously described(Ferreiro *et al.*, 2000*a*; Dubowitz and Sewry, 2007).

3.2.3 Genotyping

Genomic DNA was prepared from peripheral blood by routine procedures, and sequencing of the *SEPN1* gene was performed using Sanger sequencing, as previously described (Ferreiro *et al.*, 2002*b*), or Next Generation Sequencing-based gene panels [NGS] (Nigro and Piluso, 2012). If available, family members were Sanger sequenced for segregation studies.

The variants were reported according to Human Genome Variation Society recommendations (http://varnomen.hgvs.org/) using the complete *SELENON* transcript (NM_020451.2; NP_065184.2). Exons were numbered 1-13 according to the Locus Reference Genomic (LRG) schema. Genome Aggregation (gnomAD) (http://gnomad.broadinstitute.org/) and Clinvar (http://www.ncbi.nlm.nih.gov/clinvar/) databases were interrogated to identify previously-reported mutations and to determine the frequency of each mutation in the general population. Alamut-Batch-UI version 1.11® (Interactive Biosoftware, North Seattle, WA) was used to predict the impact of the different variants.

3.2.4 Statistical analysis

All data were analysed with the SPSS® Statistics version 22.0 (Armonk, NY: IBM Corp.). Results are expressed as mean ± standard deviation (SD) or median and interquartile range (IQR) depending on the normality of the distribution. Normality of data was evaluated using Shapiro-Wilk test. Differences were considered significant if p-value was <0.05. The Kaplan-Meier estimator was used to analyse ventilation-free probability.

3.3 RESULTS

The disease affected females and males in a similar proportion (50.8% and 49.2%, respectively). Patients were aged between 2 and 56 years (mean 18.06 ± 11.3 years) at last examination. Follow-up ranged from 8 months to 25 years.

The 132 patients belonged to 113 families, 29 of whom had several affected siblings. All pedigrees were compatible with an autosomal recessive transmission. Parental consanguinity was confirmed in 30 families and probable in three. Additionally, 14 families reported early deaths of 18 undiagnosed patient relatives (not included in our series because of scarce data and lack of genetic studies) at

ages ranging between 4 and 19 years, mainly due to respiratory failure and/or for unknown reasons during their sleep. Eight of them showed axial weakness and progressive scoliosis or rigid spine, four reportedly had clinical myopathic signs and one had a muscle biopsy showing a dystrophic pattern.

3.3.1 Clinical phenotype (Table 3.1)

Onset and first symptoms: an infantile myopathy, often under-recognized

The first symptoms were noticed before the age of 15 years in all patients, and within the first two years of life in 84.7% of cases (mean age 18.2± 29.8 months).

Delayed motor development was the most common presenting symptom (81.4%), in particular poor or delayed head control, which was the referral symptom in 57.7% and almost systematically retrieved by parents when retrospectively asked. Conversely, independent ambulation was acquired by all but one severely affected patient, often (59.3%) before the age of 18 months (mean 17.6± 4.9 months), hindering the diagnostic suspicion of a myopathy.

None of the patients presented with arthrogryposis or congenital contractures, excepting congenital torticollis in one patient. Information about pregnancy was retrieved in 29 patients. Most were normal, except for two pre-term deliveries, three cases of reduced foetal movements and two cases of intrauterine growth retardation.

Neonatal hypotonia was reported in a third of the patients. Other early signs were feeding difficulties and/or failure to thrive (17.5%) and early respiratory problems such as neonatal cyanosis and acute respiratory distress or recurrent respiratory infections (7.2%). Four patients were diagnosed because of early-onset scoliosis, hyperlordosis or rigid spine, and 16 were referred for unspecified muscular weakness and hypotonia, sometimes associated with abnormal gait, inability to run, difficulty climbing stairs or frequent falls.

One patient was diagnosed at the age of 31 years, following hypercapnic coma while bedridden aften an ischaemic stroke due to left carotid dissection. Chronic diaphragmatic and respiratory failure was unveiled and, retrospectively, mild axial and proximal weakness from early childhood.

	Number of cases (%)*
Age at first noticed signs (n=98)	
Birth to 6 months	46 (46.94%)
From 6 months to 1 year	25 (25.51%)
From 1 to 2 years	12 (12.24%)
From 2 to 8 years	12 (12.24%)
Older than 8 years	3 (3.06%)
First /Referral signs (n=97)	
Neonatal hypotonia	32 (32.99%)
Delayed motor milestones	79 (81.44%)
Poor head control (head lag)	56 (57.73%)
Delayed gait acquisition	31 (31.96%)
Abnormal gait, inability to run or frequent falls	34 (35.05%)
Non specified weakness/hypotonia	16 (16.49%)
Difficulty feeding/failure to thrive	17 (17.53%)
Early respiratory problems (e.g neonatal respiratory distress, recurrent respiratory infections)	7 (7.22%)
Scoliosis, hyperlordosis or rigid spine	4 (4.12%)
Hypercapnic coma	1 (1.03%)
Muscle weakness distribution (n=80)	
Predominantly axial+proximal	80 (100%)
Significant distal involvement	11 (13.75%)
Facial muscle weakness (n=60)	48 (80%)
High-arched palate (n=58)	36 (62.07%)
High-pitched/nasal voice (n=67)	52 (77.61%)
Mild ptosis (n=79)	6 (7.59%)
Ophthalmoparesis (n=79)	3 (3.79%)
Rigid spine (n=98)	86 (87.75%)
Scoliosis (n=101)	87 (86.14%)
Arthrodesis	32 (36,78%)
Thoracic deformities (n=57)	41 (71.93%)
Flat thorax	18 (31.58%)
Pectus excavatum	15 (26.32%)
Pectus carinatum	1 (1.75%)
Non specified	7 (12.28%)
Respiratory involvement (n=100)	94 (94%)
Not properly evaluated (< 6years)	6 (6%)
Age at detection (n=62)	
0-9 years	29 (46.77%)
10-15 years	27 (43.54%)
> 15 years	6 (9.67%)
FVC(%) (n=69)*	
FVC ≥65%	2 (2.89%)
FVC 50-65%	8 (11.59%)
FVC 30-50%	34 (49.28%)
FVC <30%	25 (36.23%)
Assisted ventilation	77 (81.91%)

	Number of cases (%)*
Cardiac abnormalities (n=76)*	12 (15.79%)
Cor pulmonale	4 (5.26%)
Increased RV systolic pressure	1 (1.32%)
Mitral valve prolapse	3 (3.95%)
Other valvular abnormalities	3 (3.95%)
Dilated cardiomyopathy	1 (1.32%)
Joint contractures/hyperlaxity (n=87)	56 (64.37%)
Only axial (spinal) contractures	10 (11.49%)
Mild-Moderate axial + limb contractures	37 (42.53%)
Severe axial+upper and lower limbs	9 (10.34%)
Mild distal hyperlaxity	21 (24.14%)
Distal hyperlaxity+Contractures	16 (18.39%)
Other clinical features:	
Foot deformities	14
Equinovarus foot	7
Flat feet	7
Hip dysplasia	2
Skin abnormalities	8
Trunk acne	3
Nevus flammeus	2
Follicular hyperkeratosis	1
Facial angyoma	1
Thoracic angyoma	1
Xerosis	1
Strabismus	4
Deglutition problems	15
Genitourinary involvement	6
Gastrointestinal involvement	3
Gastroesophageal reflux	1
Bulbar ulcer	1
Steatorrhoea	1
Mild learning difficulties	3
Dysarthria	3
Congenital torticollis	1
Progression of muscle weakness (n=77)	
Stable/Stationary	45 (58.44%)
Slowly progressive	32 (41.56%)
Rapidly progressive	2 (2.59%)
Wheel-chair bound patients	8
Deaths	6

Table 3.1 Summarized main clinical features reported by clinicians.

Patients of a wide age range (2-56 years) have been included. Younger patients may not have developed all the characteristic features yet. n= Number of patients from whom information about the clinical feature is available. The denominator for percentage calculations was the number of cases with available data for each item (*). FVC: Forced vital capacity. RV: right ventricle

The axial connection: a recognizable, homogeneous phenotype

All patients shared a remarkably consistent and recognizable phenotype, only varying in severity,

which was present from childhood but became more obvious around puberty.

In the first decade, the typical SEPN1-RM phenotype was marked by a particular facial appearance, long slender neck, flat retracted thorax, spinal rigidity and inner thigh amyotrophy in a patient with weak axial muscles but preserved ambulation. Most patients had a poor head control, were never able to lift their head from supine, and had to sit up from supine by rolling over and pushing on their arms, although this was rarely a spontaneous complaint. They were typically able to climb stairs and walk outdoors without support, limited mainly by fatigue. Sports performance was usually poor and, in some patients, cervical rigidity prevented them from rolling on the floor.

Upon examination, patients showed global amyotrophy involving preferentially neck and trunk muscles (particularly sternocleidomastoid, leading to a long slender neck appearance), as well as deltoids and the inner thigh compartment ('bracket-like thighs') (Figure 3.1). Most patients had a peculiar, typical facies, with tubular nose, prominent nasal sella, mid-segment hypotrophy, high-arched palate and low-set prominent ears, associated with facial weakness and a nasal high-pitched voice. Muscle weakness was severe in neck flexors and in abdominal muscles (power 0 to 3 according to the Medical Research Council [MRC] scale), with relatively well preserved neck extensors. Limb muscle weakness was usually milder and predominantly proximal (MRC: 3-4 in scapular girdle, 2-3 in psoas, glutei and adductor muscles). Remarkably, quadriceps strength was often normal or mildly reduced (MRC 4-5) and distal weakness was noticeable only in the most severe cases. Deep tendon reflexes were invariably diminished or absent.

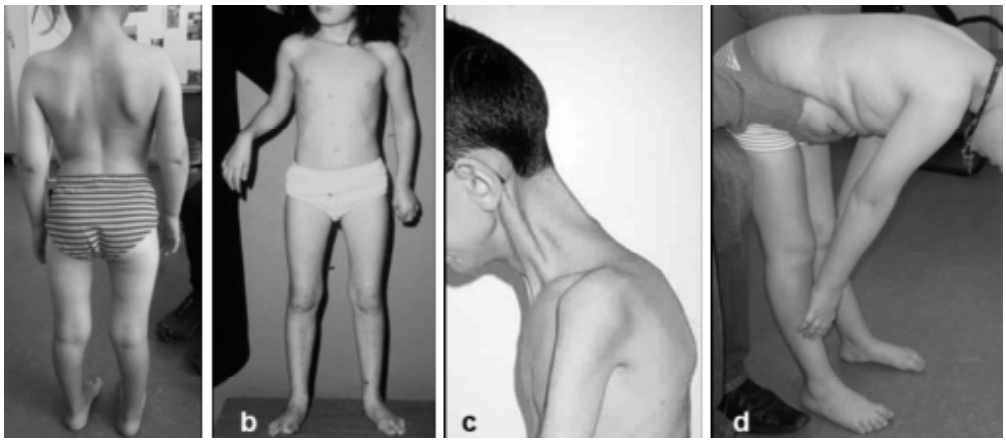

Figure 3.1. The clinical phenotype in early childhood was recognizable by predominantly axial weakness, deltoid and inner thigh amyotrophy ('bracket-like thighs') (a,b) and spinal rigidity identifiable upon specific examination (c,d). Axial rigidity was typically more prominent in the cervico-dorsal spine (c, d), with relative or full preservation of lumbar spine flexion (d).

Rigidity of the spine was present in 87.8% of patients and reported as early as in the first year of life. It appeared generally before the age of 10 years (mean 8.1±3.9 years), but was often overlooked unless specifically examined. Severe contractures of neck extensors and dorsal paraspinal muscles caused cervico-dorsal rigidity, although bending forward remained possible for some patients due to relative preservation of lumbar spine mobility. Loss of dorsal kyphosis and/or dorsal lordosis led to a flat thorax with reduced antero-posterior diameter. Pectoralis major and intercostal muscle retractions contributed to thoracic deformities and poor mobility.

Scoliosis appeared at the mean age of 8.9 ± 4.0 years (10.4 ±3.6 years in males, 7.9 ±3.9 years in females) and was present in 86.1% of all patients and in 93.8% of those older than 13 years. The SEPN1-RM scoliosis is peculiar and recognizable because of dorsal hyperlordosis (leading to scapular pseudo-protrusion) and an important lateral trunk shift contrasting with balanced hips. Shoulders were usually out of alignment with the hips axis, and this was associated with compensatory lateral neck deviation to the other side (Figure 3.2). Adapted bracing (particularly using the Garchois brace to avoid thorax compression) helped delaying surgery till the end of puberty, but did not prevent scoliosis progression. Arthrodesis (usually sequential, anterior and posterior) was performed in 32 post-pubertal patients at ages ranging from 10 to 17 years (mean age: 13.5±1.9 years).

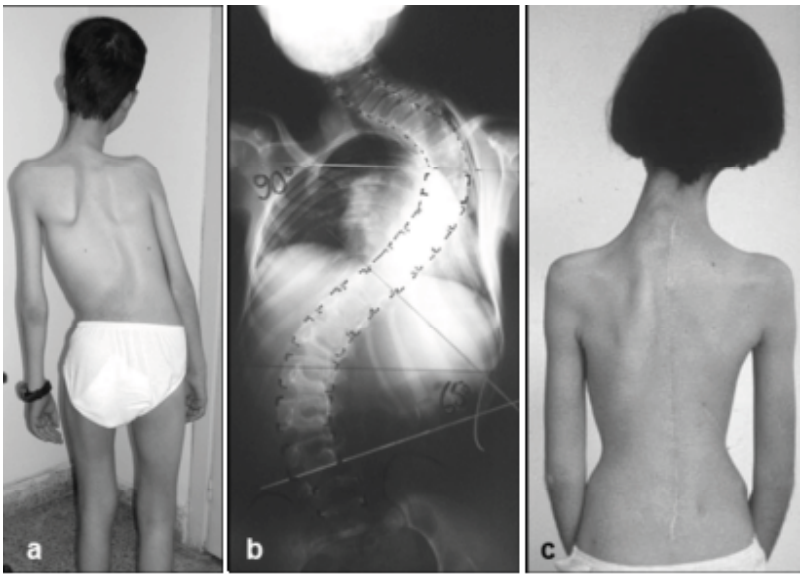

Figure 3.2. Typical scoliosis in SEPN1-RM. SEPN1-RM scoliosis is recognizable due to dorsal lordosis leading to pseudo-scapular winging, prominent lateral trunk deviation with compensatory contralateral neck shift and horizontally aligned hips (a). Severe progression despite bracing often required arthrodesis: (b) X-ray from a patient before arthrodesis; (c) same patient after spinal fusion.

The full phenotype usually manifested by the end of the first decade (Figure 3.3) with the development of scoliosis, the detection of respiratory failure, a further drop in weight curves and, in some cases, limb contractures, although all the former appeared earlier in severe cases.

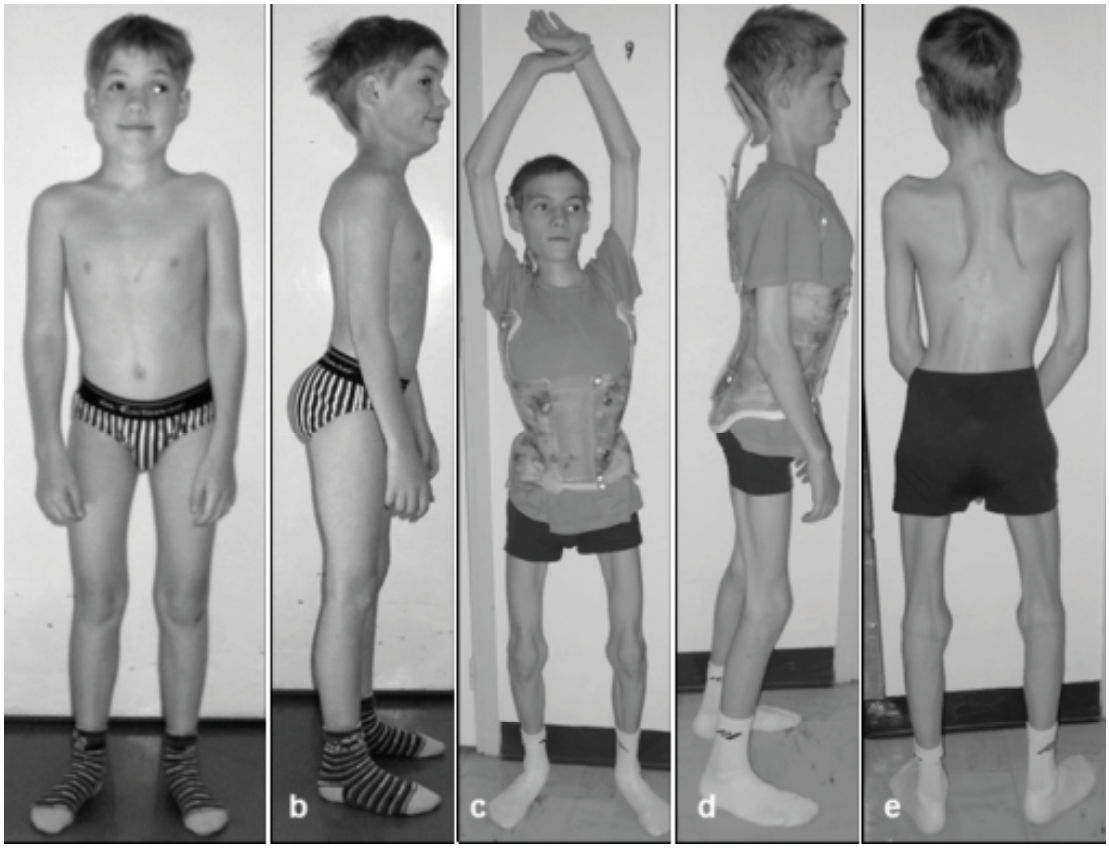

Figure 3.3. Typical moderate patient at ages 11 (a,b) and 14 years (c-e). Often subtle until late childhood, the full phenotype usually became apparent around puberty. Body weight decreased dramatically, leading in some cases to an apparent loss of subcutaneous adipose tissue (lower limbs in c, d) and a cachexia phenotype. Most patients developed scoliosis (e) which required adapted bracing to avoid thorax compression (Garchois brace, c,d).

Although birth weight was normal in most cases, typically body weight decreased drastically around puberty, leading to loss of subcutaneous adipose tissue and a cachexia-like appearance (Figure 3.3c-e). Most (72.7%) patients were under the 4th weight percentile, and the mean BMI in adults was 16.9± 4.0 (women 16.5±4.3, men 17.4±3.6, range 11.7 to 26.9; underweight<18.5, severe underweight<16). Remarkably, two patients were overweight and two were obese (above the 95th centile); these four patients showed abdominal fat accumulation and had severe forms of the disease with severe respiratory failure and early loss of ambulation in three of them.

Limb contractures

Limb joint contractures were reported in 64.4% of patients but were usually mild in children, involving the Achilles tendon (57.4%), hip flexors (50%), elbows (35.2%) or knees (31.5%). Only nine children showed a more contractile phenotype with severe axial and limb contractures. Contractures of finger flexors upon wrist extension or, less often, limitation of mouth opening appeared with age. Distal hyperlaxity was reported in 21 patients (associated with joint contractures in 16 of them), raising differential diagnosis with collagenopathies (Figure 3.4).

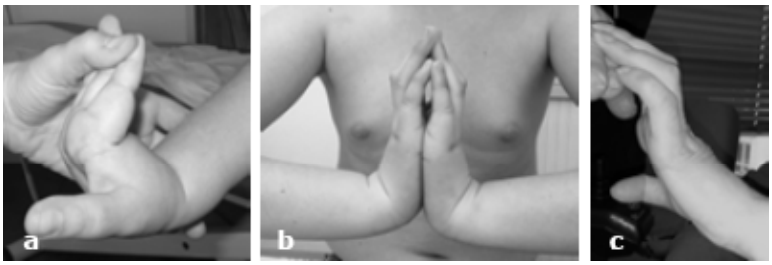

Figure 3.4. Hand hyperlaxity and finger flexor contractures. Moderate distal hyperlaxity was common in early childhood (a, 7 year-old patient) and often coexisted with finger flexor contractures visible upon wrist extension. The latter tended to appear from adolescence (b, 16 year-old patient) and became more prominent with age (c, 57 year-old patient).

Respiratory involvement

Respiratory involvement was strikingly disproportionate to the degree of limb weakness, most patients requiring assisted ventilation while ambulant. Both weakness of the respiratory and accessory respiratory muscles and thoracic deformities contributed to respiratory failure. Dorsal spine lordosis and rigidity led to severely reduced thorax anteroposterior diameter and sometimes to bronchial compression and subsequent atelectasis. As a consequence, restrictive, hypoxemic and hypercapnic respiratory failure was present in 93% of all patients (from the mean age of 10.06±6.10 years). FVC in the upright position was in most patients between 20 and 40% of predicted values (36.47±12.31 at the time of last survey) (Figure 3.5).

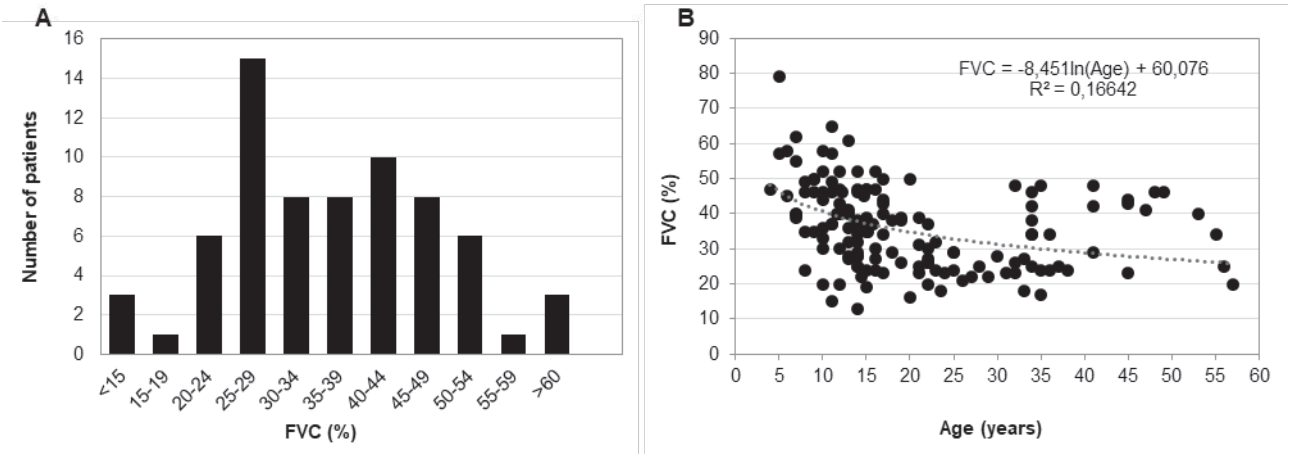

Figure 3.5. Respiratory involvement. (a) Distribution of FVC (% of predicted values) in 69 cases shows that most patients had FVC <39%, the most frequent range being between 25 and 29%. (b) Progression of FVC in 32 patients (ages 4 to 58 years) revealed decrease of FVC with age in years using a logarithmic regression (R^2 = 0,16642). Individual values are shown as grey dots. FVC: Forced Vital Capacity.

Diaphragmatic weakness (>10% decrease in supine from baseline sitting position) was reported in 30 patients, and several showed paradoxical abdominal breathing. Polysomnography detected nocturnal hypoventilation and frequent short apnea periods in 92.9% of patients from early ages, even in those with relatively preserved FVC and no daytime respiratory signs. The three youngest patients studied had polysomnographic values within normal range at 4 years (one patient) but abnormalities requiring ventilation at 5.5 years (two patients).

Taking together children and adults, 81.9% patients had assisted ventilation, from the mean age of 14.14±7.89 years (range 3-49 years). Most required nocturnal non-invasive volume ventilator with high pressure; 12 patients had a tracheotomy.

Use of compressive bracing (Milwaukee) led to hypercapnic coma in one patient. Four patients developed a *cor pulmonale* and one had an isolated increased right ventricular systolic pressure secondary to respiratory failure. Both abnormalities improved with instauration or adjustment of assisted ventilation.

Other features

Ophthalmoparesis with severe restriction of external eye movements was observed in three

overweight, severely affected patients. Mild limitation of superior vertical eye movements was found in most patients when specifically examined and tended to become more evident during evolution. Strabismus and mild ptosis were observed in four and six patients, respectively.

One patient with a family history of early-adulthood idiopathic cardiomyopathy developed dilated cardiomyopathy at the age of 42 years. None of the others had primary myocardial involvement. Fifteen patients developed swallowing difficulties; three had a gastrostomy. Gastrointestinal involvement and genitourinary disorders (vesical hyperactivity and mild urinary incontinence) were present in a minority of patients. Nonspecific skin abnormalities were reported in 9 patients. One patient suffered a cerebral venous thrombosis at age 38 and another had an ischaemic stroke due to left carotid dissection at age 31. There were no signs of intellectual disability or CNS involvement.

3.3.2 Ancillary tests

CK levels were normal or mildly elevated in 93.4% of patients (range 34- 453 U/L). Only five had CK levels elevated three times the upper limit of normal. In-vitro contracture testing (IVCT) for malignant hyperthermia susceptibility with halothane and caffeine was performed in deltoid muscles of two patients with negative results.

Electromyographic studies disclosed small amplitude, brief, polyphasic action potentials and normal nerve conduction studies.

Brain MRI or CT scan were normal aside from an arachnoid cyst in two patients and a Chiari malformation type 1 in one patient.

Detailed biochemical studies were performed in a pilot sample of six patients. No consistent alteration in serum selenium, lactate, pyruvate, thyroid hormones, vitamins A, B12, B6, D and folate were detected. Two patients with a mild phenotype showed mildly elevated serum glutathione peroxidase levels while one severe patient showed decreased values. Conversely, three patients had decreased erythrocyte glutathione peroxydase with normal serum levels. Free and total carnitine were assayed in four patients, and the free carnitine/total carnitine ratio was reduced in three of them.

To confirm the association between *SEPN1* defects and insulin resistance, follow-up data from eight patients in whom an oral glucose tolerance test (OGTT) had been performed were retrospectively evaluated (Table 3.2).

Table 3.2. Glucose metabolism in 8 SEPN1-RM patients.

Patient	**1**	**2**	**3**	**4**	**5**	**6**	**7**	**8**
Sex	M	F	F	F	M	F	M	M
Age (y)	38	22	52	47	28	17	34	43
***SELENON* mutation**	c.713dupA (p.N238Kfs*63) + c.1397G>A (p.R466Q)	c.713dupA (p.N238Kfs*63) homozygous	c.13_22dup (p.Q8Pfs*78) + c.883G>A (p.E295K)	c.13_22dup (p.Q8Pfs*78) homozygous	c.997_1000del (p.V333Pfs*6) homozygous	c.713dupA (p.N238Kfs*63) homozygous	c.1358G>C (p.W453S) + c.1397G>A (p.R466Q)	c.1A>G (p.M1V) + c.565C>T (p.R189*)
FPG (mmol/L)	<6 at 37y **6.7** at 38y	4.8	4.6	4.9	<6	<6	4.6	<6
OGTT	Normal at 37y	Increased 2h insulin concentration (61.2 mU/l)	Increased 1h and 2h plasma glucose (12.3 and 9.8 mmol/L). Increased 2h insulin (37.74 mU/L)	Increased 2h plasma glucose (9.9 mmol/L)	Normal	Normal	Normal	Normal
BMI (kg/m^2)	11.7	12.8	13.1	13	18	15.6	16.6	UK

BMI: Body Mass Index. Reference values: <18.5: underweight; 18.5-24.9: healthy weight; 25-29.9: overweight; >30: obese; F: female; FPG: Fasting plasma glucose. Reference range: 4-6 mmol/L; M: male; OGTT: Oral glucose tolerance test. Reference values: 1h post-load plasma insulin <80 mU/L, 2h post-load plasma insulin <14 mU/L, 1h and 2h post-load plasma glucose <10 mmol/L and <7.8 mmol/L respectively; UK: unknow

The results of the OGTT disclosed abnormal glucose metabolism in four of the eight patients, despite a very low BMI (<13.1). Patient 1 showed high level of fasting glycemia, without any increase in glycated hemoglobin. Patients 2-4 had normal basal glycemia but altered OGTT. Interestingly, Patient 1 evolved from normal fasting blood glucose and OGGT at age 37 to basal hyperglycemia one year later, stressing the need for regular controls of glucose metabolism during the follow-up of SEPN1-related myopathy patients. There was no correlation between abnormal glucose metabolism and patient age or the type of SEPN1 mutation (truncating, nonsense or missense). In contrast, insulin-resistance or prediabetes were observed only in patients with extremely low BMI values. These results confirm that paradoxical insulin resistance in very low BMI patients is part of the SEPN1-related myopathy phenotype.

Muscle imaging

A systematic review of whole-body MRI in SEPN1 myopathy has been published previously by a collaborating group(Hankiewicz et al., 2015) and includes five of the patients described in this study. There is a homogeneous and recognizable pattern with the most striking feature being the absence or severe atrophy of the semimembranosus muscle (Figure 3.6). This finding allows suspicion of the myopathy even in very young or mild patients. Other characteristic features are the atrophy of the sternocleidomastoid muscle and the axial predominance of signal abnormalities, with more severe changes in the paraspinal muscles (cervico-dorsal more than lumbar), the glutei (gluteus magnus) and the thigh (adductor magnus, sartorius and biceps femoris). The lower leg was less or latterly affected or showed fatty replacement in gastrocnemius, soleus and peroneal muscles. Upper limbs were relatively spared, the most affected muscle being biceps brachialis. Interestingly, subcutaneous tissue abnormalities were often observed, which showed either a diffuse or a regional localization (periscapular regions and forearms).

Figure 3.6. Typical radiological pattern in SEPN1-RM. Whole-body MRI from a 10-year-old patient with a severe form of SEPN1-RM. (A) Axial T1-TSE weighted sequences: neck, shoulder girdle, trunk and arms, pelvic girdle and forearms, and thigh and leg. (B) Frontal view reveals diffuse signal abnormalities. Black arrowhead (A) points to the anatomical place where the semimembranosus muscle (SM) should be visualized. Note severely atrophic sternocleidomastoid (SCM) contrasting with preserved levator scapulae (LS). Modified from (Hankiewicz et al., 2015b).

3.3.3 Histopathological phenotype

Multi-minicores were the most recurrent pathologic feature, which was present in 59.5% biopsies and represented the main lesion in 49.4%. Minicores were often associated with fibre size variation, type 1 fibre predominance and relative hypotrophy, internalized nuclei and mild dystrophic features, notably

mild increase in endomysial connective tissue (Figure 3.7 and Annexe 3). In 6.3% cases, minicores were associated with eosinophilic inclusions. Prominent dystrophic signs were present in 24.1% of samples, either isolated or associated with minicores or 'unspecific changes of internal structure' on oxidative stainings. In 25.3% of cases, biopsies disclosed non-specific myopathic findings, mainly fibre size variation, type 1 fibre predominance or internalized nuclei. Rare rimmed vacuoles were found in two patients. Interestingly, patients having non-specific biopsy abnormalities were younger than patients having more specific lesions (8.55±5.3 vs 13.89±11.7 years, p= 0.012).

Figure 3.7 (next page) Histopathological patterns. The relative frequency of the different histopathological patterns observed in this series (n=78) is represented in the graph. Foci of sarcomere disorganization and mitochondria depletion, spanning only a few sarcomeres on the longitudinal axis of the fibre (minicores), were observed in 60% of the biopsies (Ac-e, Bb,c). A: The most common pattern was typical of a congenital myopathy with minicores (Multi-minicore disease, MmD), including mild or no endomysial fibrosis (a), type 1 fibre predominance and relative hypotrophy (dark fibres, b) and multiple lighter zones devoid of SDH or NADH-enzymatic activity (c) corresponding to mitochondria depletion and sarcomere disorganization on EM (minicores) (d,e) B: Around 24% of biopsies showed a mild to moderate congenital muscular dystrophy pattern, associated with either abundant or scattered/inconspicuous minicores. Note prominent endomysial fibroadiposis but rare necrotic or regenerating fibres (a). C: Eosinophilic inclusions compatible with Mallory body-like inclusions (arrows, a-c) or rimmed vacuoles (arrowheads, d-e) were identified in some samples but typically involved a small percentage of fibres. Thus, they were easily overlooked unless specifically searched for. D: Two muscle samples taken from the same patient at 12 years of age revealed that histopathological changes were more severe in axial than in limb muscles, mirroring the clinical situation. Her deltoid muscle (a,b) showed minor myopathic changes, with mild fibre size variation and scattered internalized nuclei and minicores. In contrast, her abdominal muscles revealed major dystrophic changes with muscle fibre loss, fatty-adipose replacement, rimmed-vacuoles (c), rod-like inclusions (e), multi-minicores (d) and also well-delimited cores with a hyperoxidative perilesional rim (similar to those observed in Central Core Disease) (f). Transversal frozen sections stained with hematoxylin-eosin (HE) (A-a; B-a; C-b-d, reduced nicotinamide adenine dinucleotide (NADH) (A-c; B-c), ATPase 4.6 (A-b), Succinate dehydrogenase (SDH) (B-b), modified Gomori Trichrome (C-a,e); longitudinal electron microscopy (EM) sections (A-d,e). Scale bars: 50 µm except for A-d,e: 2 µm.

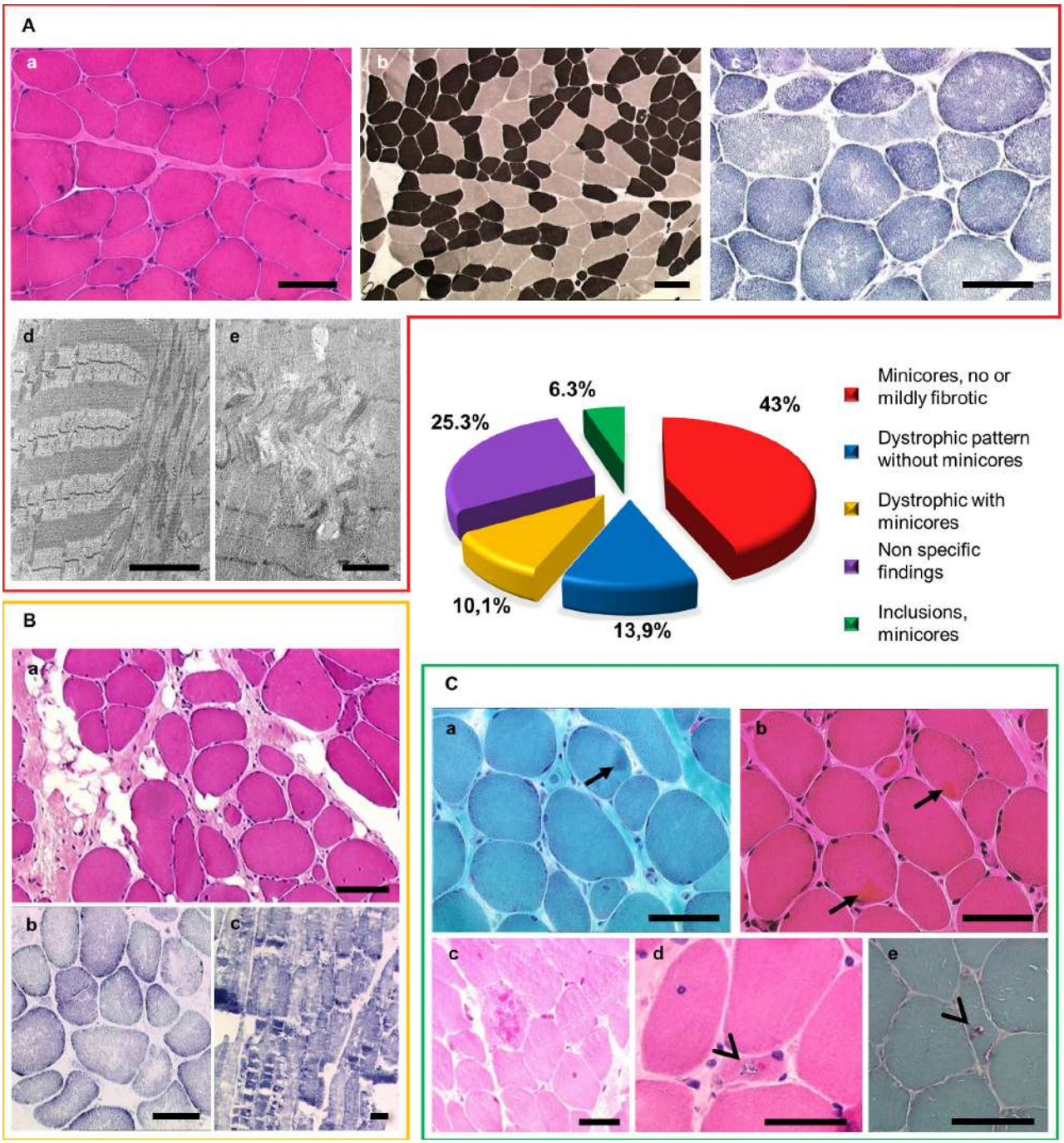

In patients who had biopsies from axial and limb muscles, we observed histological differences consistent with clinical weakness distribution. While minicores were found in both limb and axial muscles, the latter were usually more severely dystrophic and/or showed larger core lesions. Mallory bodies were exclusively found in quadriceps samples (Figure 3.8).

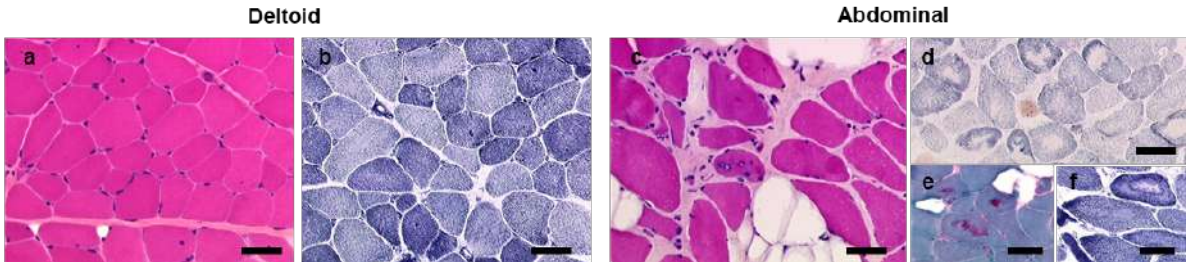

Figure 3.8. Different histological severity in axial versus limb muscles. Two muscle samples taken from the same patient at 12 years of age revealed that histopathological changes were more severe in axial than in limb muscles, mirroring the clinical situation. Her deltoid muscle (a,b) showed minor myopathic changes, with mild fibre size variation and scattered internalized nuclei and minicores. In contrast, her abdominal muscles revealed major dystrophic changes with muscle fibre loss, fatty-adipose replacement, rimmed-vacuoles (c), rod-like inclusions (e), multi-minicores (d) and also well-delimited cores with a hyperoxidative perilesional rim (similar to those observed in Central Core Disease) (f). Transversal frozen sections stained with hematoxylin-eosin (HE) (a,c), reduced nicotinamide adenine dinucleotide (NADH) (b,f), Succinate dehydrogenase (SDH) (d), modified Gomori Trichrome (e). Scale bars: 50 µm.

3.3.4 Natural history

Except for one severely affected patient, all cases acquired independent ambulation and had an improving motor function during infancy and childhood, compatible with motor maturation. After implementation of efficient ventilation and arthrodesis in their teens, most patients remained stable from more than one decade. This was followed, from the beginning of the fourth decade of life, by steady disease progression accelerated with aging (Figure 3.9).

This series includes the first cases beyond 35 years (n=9, age at last examination 35-56 years). Aging was associated with significant progression even in mild/moderately affected patients. Slow but steady increase of muscle weakness and fatigue from the beginning or the middle of the fourth decade led to reduced gait perimeter and motor performance of upper limbs with marked functional impact. Three mild patients lost ambulation at 33, 38 and 54 years of age; others required a wheelchair for long distances. Swallowing difficulties appeared during the course of the disease, and caused death in a 59-year-old patient due to choking. Another patient with a previous mild clinical course developed

severe tetraparesis, required a percutaneous endoscopic gastrostomy (PEG) and ventilation for 15 hours per day and died at 58 years of age due to general deterioration. The eldest patient is currently aged 55 years, ambulant and leads an active professional life with night-time ventilation, despite aggravation of his difficulties for climbing stairs from the end of the third decade. Interestingly, FVC in this age group were severely reduced but tended to remain stable (Figure 3.10). However, increasing diaphragmatic fatigue often led to decubitus intolerance over the years.

Loss of ambulation occurred in eight patients aged 8-54 years (median 21.5, IQR 19.75), three of them from the third decade of life. Six patients deceased during follow-up, three children and three adults, two of them due to sudden death and four due to respiratory failure. The only patient who never walked died at the age of 3 years while two patients died of respiratory failure at ages 5 and 16 years.

Five adult female patients successfully carried pregnancies to term and gave birth by cesarean section to healthy children. One of them suffered eclampsia with acute pulmonary oedema and required transient tracheostomy and one experienced significant worsening of motor abilities after delivery.

Figure 3.9. (next page) Disease course and variable severity. (a-h): Evolution in one severe patient. Note the particular facial appearance of SEPN1-RM patients at 6 years (tubular nose, prominent nasal sella, low-set ears and retrognathia) and frank ophthalmoplegia with restricted eye movements (a-b). Scoliosis developed around puberty (f). Progressive muscular weakness led to loss of ambulation before adulthood in the most severe patients (h). Note increase in subcutaneous tissue with trunk fat accumulation since early-childhood (d-g) contrasting with significant weight loss in adolescence (h). (i-n): Evolution of a typical SEPN1-RM patient from 15 to 39 years Note apparent disappearance of subcutaneous fatty tissue along with severe amyotrophy. Strikingly, most of the patients with good motor abilities were extremely underweight. Severe respiratory involvement required assisted ventilation while patients were still ambulant (j-n). Muscle weakness was stable or slowly progressive until the end of the third decade (l-n). (o-q): Evolution of one of the mildest patients in this series from age 43 to 57 years. Aging was associated with marked disease progression even in mild patients. Increasing muscle weakness and fatigue from the beginning of the fourth decade led to worsening of motor abilities with functional impact, reduction in gait perimeter and eventually loss of ambulation and tetraparesis at the end of the fifth decade (q).

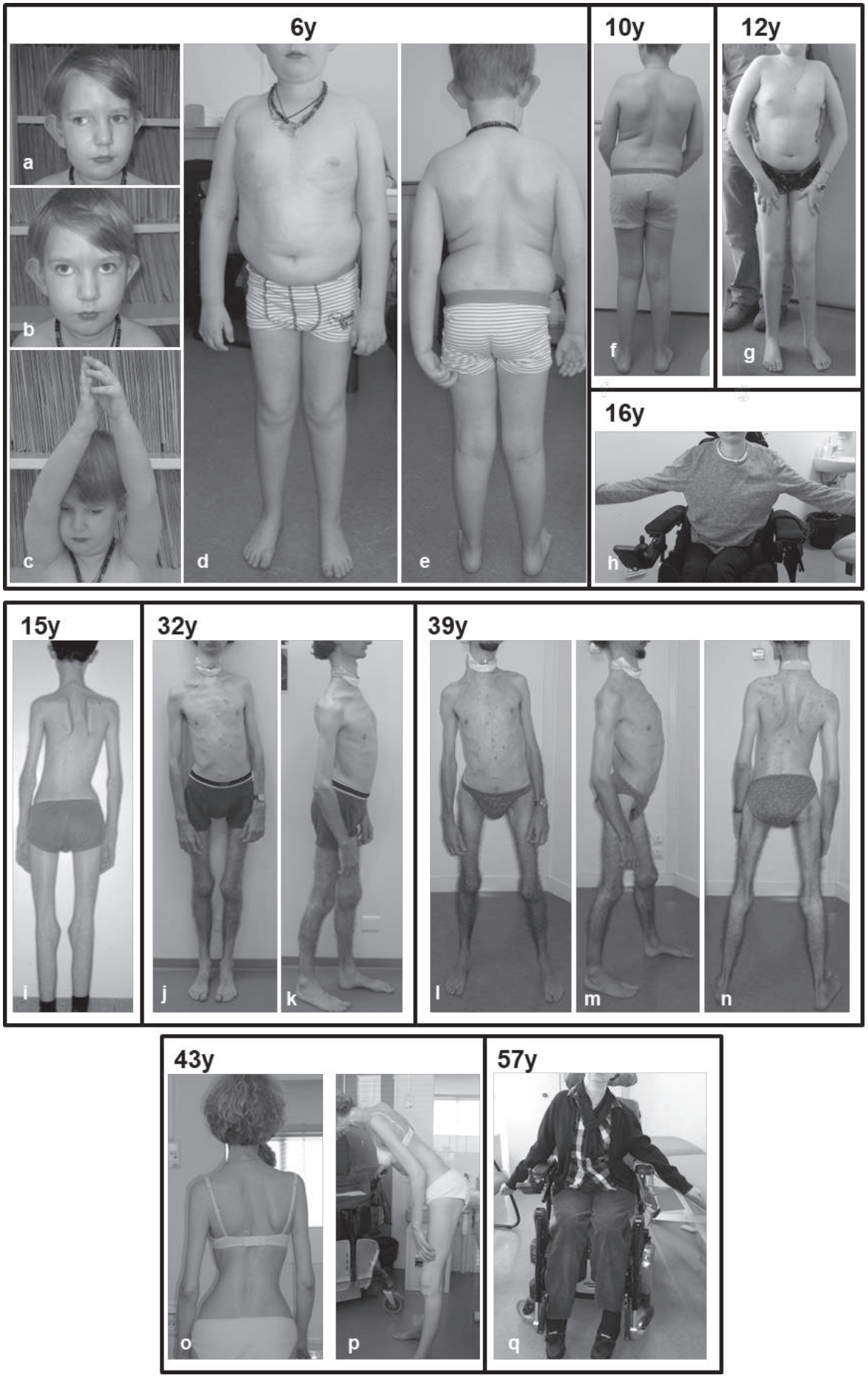

Figure 3.9. (Figure caption in previous page)

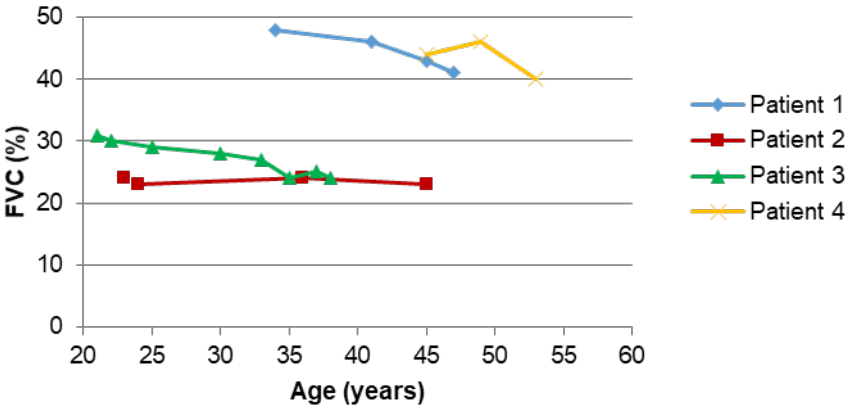

Fig 3.10. Evolution of Forced Vital Capacity (FVC, expressed in %) in four adult patients.

3.3.5 Potential predictive factors and disease severity determinants

The main predictive factor of the vital prognosis was respiratory failure. Kaplan-Meier curve showed that 50% of patients needed assisted ventilation within the first 13 years (Figure 3.11).

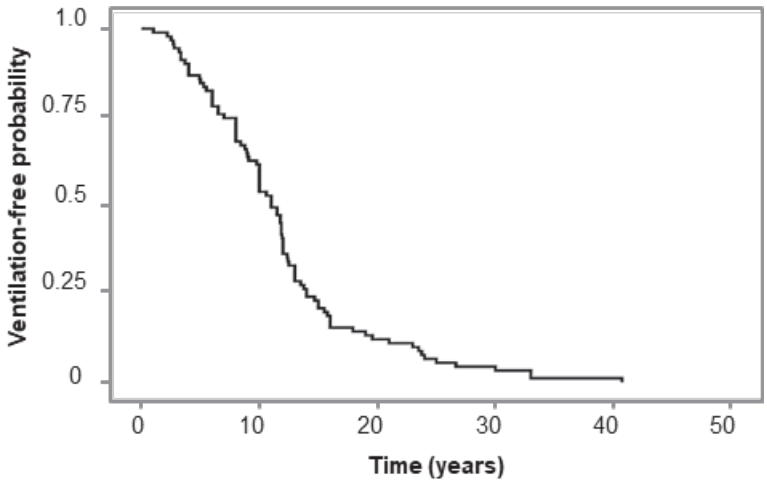

Fig 3.11. Kaplan-Meier curve showing ventilation-free probability related to age (years).

Around the end of the first decade was a critical period, when recognition and appropriate management of respiratory failure and scoliosis determined vital and functional prognosis. In depth analysis of a small subgroup of 11 patients demonstrated the impact of scoliosis and its management on FVC: spinal fusion led to a dramatic drop in FVC in the immediate post-operatory period which came back to preoperative values or higher within the first six months after surgery in those patients with intensive and regular postsurgical ventilatory management (Figure 3.12).

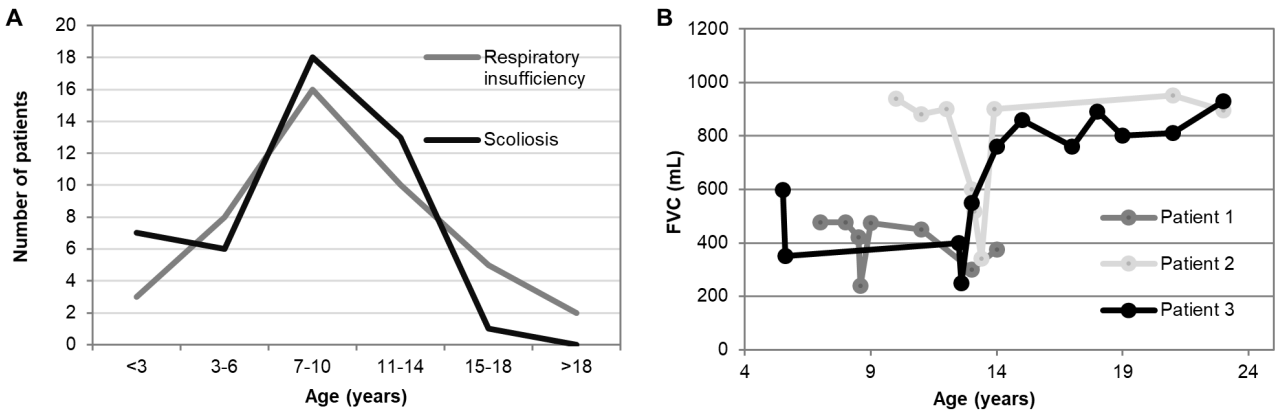

Figure 3.12. Scoliosis and respiratory involvement in SEPN1-RM. (A): Respiratory insufficiency (grey line) or scoliosis (black line) were first detected in most patients around the same age, most commonly between 7 and 10 years. (B) Follow-up of respiratory involvement before and after surgical correction of scoliosis in three patients. FVC typically dropped in the postsurgical period (arrows) and then came back to previous or even higher values with correct post-operatory management including ventilation.

This analysis also confirmed marked intra-individual variability (Figure 3.13), FVC values showing significant fluctuation possibly due to oscillating fatigue and/or intercurrent infections. Once arthrodesis was performed, spine biomechanics used to remain stable.

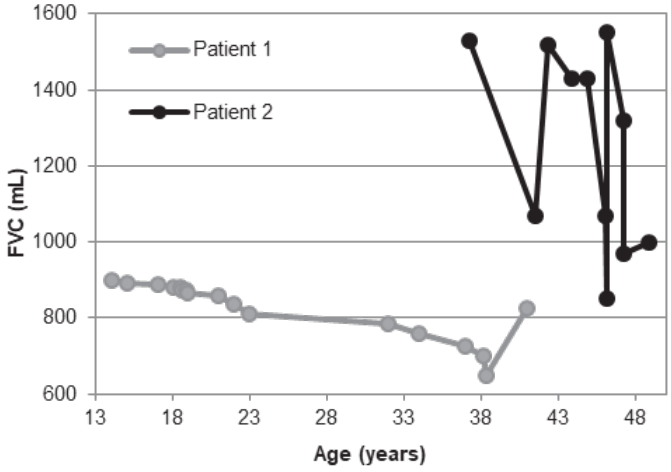

Figure 3.13. Progression of respiratory involvement in two mildly affected adult patients revealing extreme variability between patients with similar disease severity. Note also intra-patient variability in Forced Vital Capacity (FVC, expressed in mL) in Patient 2.

To assess severity and the potential determinants of disease progression, the following arbitrary severity criteria are proposed:

1) prominent neonatal hypotonia and/or persistent lack of head control

2) scoliosis and/or respiratory failure before the age of 10 years

3) progressive motor disability causing loss of ambulation before adulthood.

According to these, three groups according to disease severity were identified in a subgroup of 81 patients: 'severe' (n=23, 28.4%) when patients presented two or more criteria, 'moderate' (n=43, 53.1%) if only one criterion was present and 'mild' (n=15, 18.5%) if none of the criteria were fulfilled.

Mild/moderately affected patients corresponded to the previously described classical form of the disease. In severely affected patients, both scoliosis and severe respiratory failure developed earlier requiring assisted ventilation since childhood. A small subgroup of patients with a very severe phenotype had severe ophthalmoplegia, rapidly progressive muscular weakness leading to loss of ambulation before adulthood and severe tetraparesis in the third decade of life.

In clinical practice, an apparent association between body weight and disease severity has been observed. Strikingly, the most severely affected patients with early loss of ambulation and rapidly progressive respiratory failure showed an increase in subcutaneous tissue with a distribution resembling troncular obesity. Conversely, most of the patients with good motor abilities were extremely underweight, with apparent disappearance of subcutaneous fatty tissue leading to a cachexia-like appearance. In a subset of 47 patients (28 females, 19 males, aged 7-56 years, mean age 21.7 ± 11.1) with detailed anthropometrical and clinical data (Figure 3.14), we found a significant correlation between body weight category and disease severity (p=0.002). Remarkably, weight gain (usually through dietary supplements or enteral nutrition by PEG) led to poor functional performance in these patients.

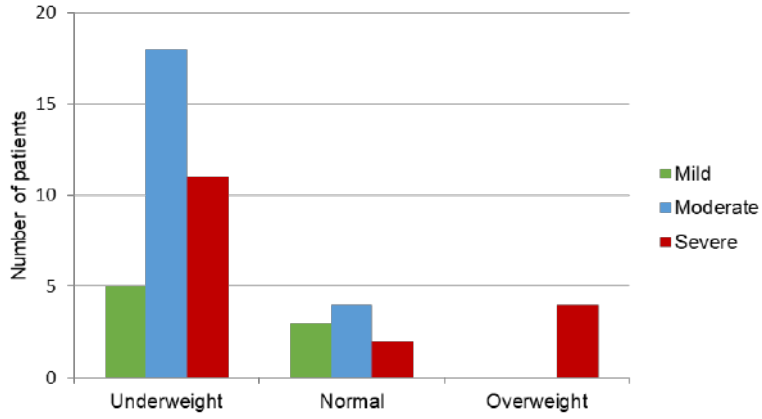

Figure 3.14. Distribution of disease severity according to body weight in a subset of 47 patients.

Moreover, the relationship between respiratory involvement (FVC) and body weight was also analysed in 45 of these patients. Overweight patients were found to have lower FVC values compared with underweight and normal-weight patients (Figure 3.15), although this was not statistically significant (p= 0.086).

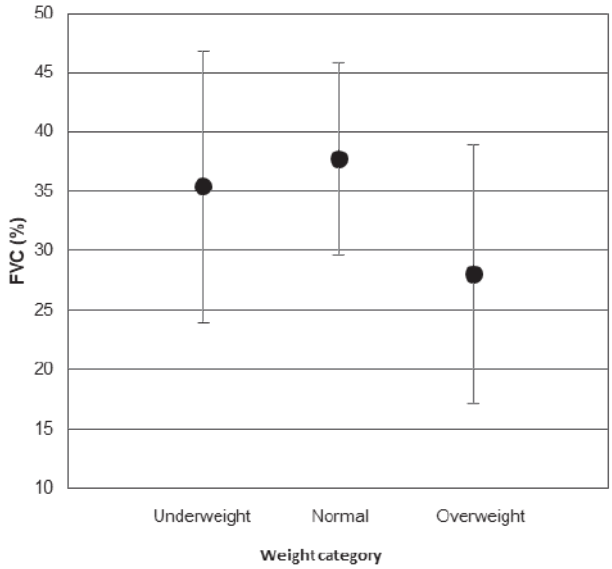

Figure 3.15. Forced Vital Capacity (FVC, expressed in %) according to body weight category in a subset of 45 patients.

3.3.6 Clinical genetics

Transmission of SEPN1-RM was invariably autosomal recessive. All parents were healthy heterozygous carriers and no *de novo* mutation was identified. Seventy-two patients were homozygous while 59 were found to be compound heterozygous.

Sixty-five variants (32 of them previously unreported) of the *SEPN1* Reference Coding Sequence (RCS) were identified (Figure 3.16 and Annexe 4), including missense mutations (n=23, 35.4%), duplications/insertions (n=14, 21.5%), deletions (n=13, 20%) and nonsense mutations (n=8, 12.3%). We also report the first Copy Number Variation (CNV) affecting the *SEPN1* gene, c.(872+1_873-1)_(1602+1_1603-1)del, a large likely out-of-frame deletion affecting exons 7 to 12. Twenty-nine variants were predicted to lead to truncated proteins (11 of them prone to nonsense-mediated decay [NMD]). Four variants led to loss of the start codon with subsequent loss of translation and thus absence of the protein, and were harbored by 29 patients (10 of them harbored two of these variants and were considered as complete null).

A cluster of mutations was found in exons 1, 6, 7 and 11. Exon 1 was the most frequently mutated (39.7% of patients) with the highest number of variants (28% of all the detected mutations). It harbored the most common variant, shared by 21 patients (from 15 families of different origins): a mutation of the starting codon (c.1A>G) that changes the initiator methionine codon to a valine causing a total loss of translation. No mutations were found in exon 3, which is spliced in the predominant transcript in humans (Petit *et al.*, 2003).

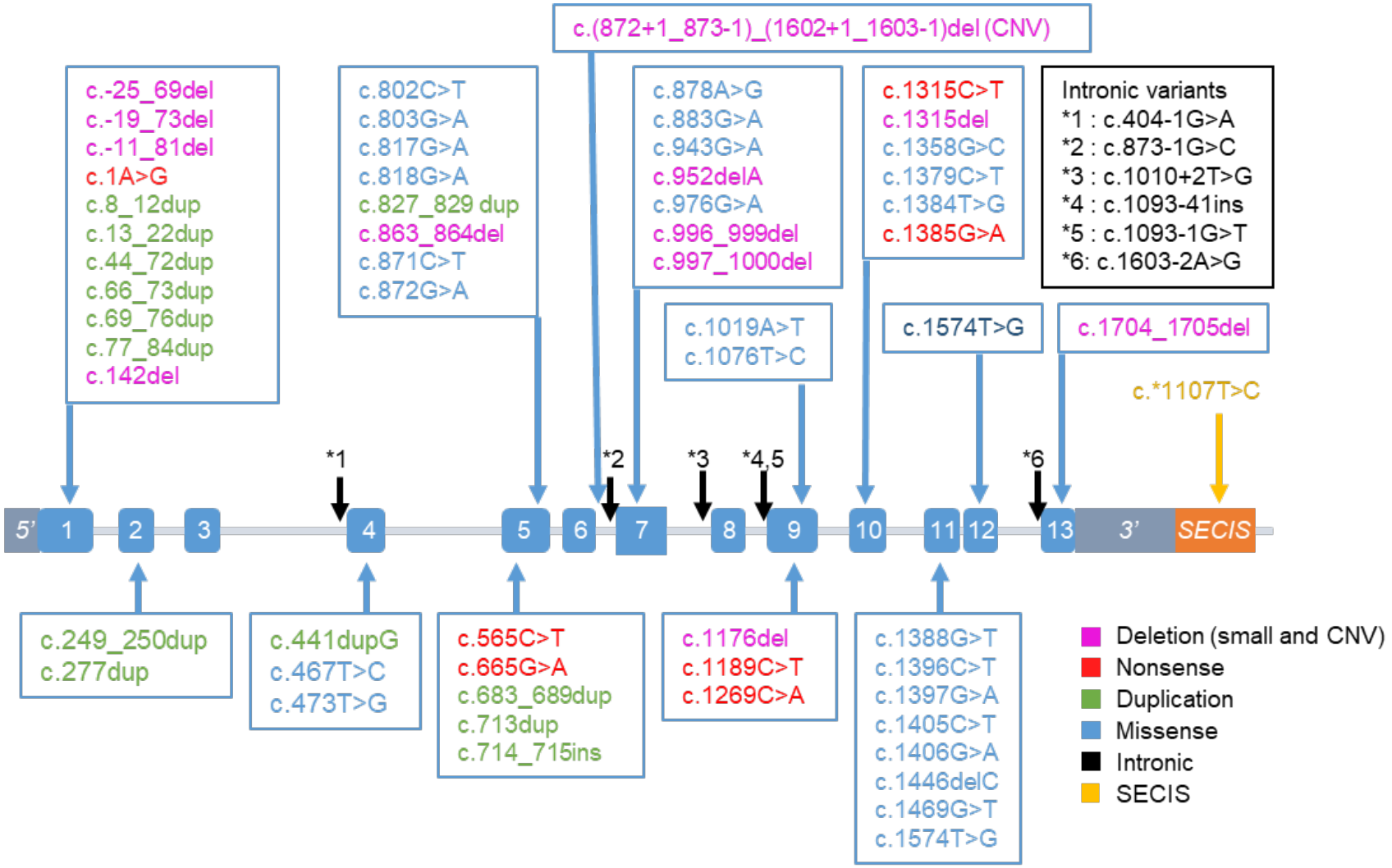

Figure 3.16. Schematic representation of the SEPN1 gene and localization of the identified mutations. Exons are depicted in light blue and SEPN1 3' UTR SECIS element in orange. Colour code for variants: pink-deletion; green-insertions/duplications; red-nonsense; blue-missense; black-intronic variants affecting splicing; orange-variants affecting SEPN1 3' UTR SECIS element.

Outside the RCS, six intronic variants affecting splicing and one single homozygous point mutation in the SEPN1 3′ UTR SECIS element, Sec codon redefinition element (SRE), were identified. This single-nucleotide modification abolishes the binding of the SECIS recognition factor SBP2, a central component of the selenocysteine insertion machinery, thereby preventing redefinition of the UGA Sec and leading to a premature stop codon(Lescure *et al*., 2009; Maiti *et al.*, 2009).

A geographic grouping for certain mutations was observed. Founder effects were found by haplotype analysis for the following mutations: c.817G>A (in Iran and Turkey), c.943G>A (in Northern Europe), c.713dupA (in Western Europe).

3.3.7 Genotype-phenotype correlations

Phenotype–genotype correlations are difficult to establish in a very rare disease due to low numbers of patients carrying the same mutation, and were unknown for SEPN1-RM. Analysis of this series revealed the first correlations between the genetic defects and the clinical severity, with no correlation between genotype and histopathological findings.

Some exon 1 variants (c.1A>G, c.13_22dup and c.-19_73del92nt) and the exon 6 c.818G>A mutation were most commonly found in patients with a severe phenotype, while other variants such as c.943G>A (exon7), c.1315C>T (exon 10) or c.1446delC (exon 11) were often found in milder cases.

Additionally, we found that exon 1 homozygous mutations predicting total loss of translation (c.-19_73del92nt and c.1A>G) were significantly associated with severity of the disease (p=0.003) and were carried by the most severe patients in this series. Moreover, homozygous or compound heterozygous patients carrying two variants located in any exon but predicting protein absence (by either loss of the start codon or NMD), exhibited more severe forms (p=0.017).

Indeed, there is a significant correlation between disease severity and the number of predicted viable alleles (0 for complete null patients, 1 for patients carrying one null mutation and another variant and 2 for patients carrying two variants predicting absence of the protein) (p=0.014).
Interestingly, mutations located in the putative catalytic site (SCUG sequence) located in exon 10 (Castets *et al.*, 2012*a*) were exclusively missense mutations carried by 23 patients (seven of them homozygous), most of them with moderate severity. Nonetheless, no significant correlation was found between disease severity and the involvement of the different domains (i.e. the putative catalytic site,

the transmembrane domain, the EF-hand domain or the Tyr Kinase phosphyraling site). Finally, no correlation between genotype and histopathological findings was found.

3.4 DISCUSSION

This study reports the largest SEPN1-RM series and the first one including paediatric and older adult patients followed-up for several decades, furthering our understanding of the phenotypical spectrum and natural history of the disease. Importantly, it also allows inferring information about SEPN1-RM prevalence. This series includes 63 French patients, identified through the main reference laboratories performing *SEPN1* screening as part of a national network. We also interrogated the other genetic diagnostic laboratories in France, which have identified 6 additional cases, thus very likely capturing virtually all the diagnosed patients in the country. A total number of 69 cases in France represents an estimated prevalence of 1.03 per million. This is consistent with a previous study of congenital muscular dystrophies in the UK (Sframeli *et al.*, 2017) and would correspond to 764 patients in Europe or 337 in the USA. Furthermore, a number of patients are initially misdiagnosed and patients with milder forms can be diagnosed in adulthood. This suggest that this disease, although ultra-rare, is under-recognized and thus the actual prevalence can be higher. Several reasons might explain this situation, including the peculiar distribution of muscle weakness, the absence of biomarkers, the variability of the histopathological presentation and gene screen pitfalls.

The clinical features are homogeneous and distinctive and include a particular facial appearance, long slender neck, flat retracted thorax, severe axial muscle weakness and rigid spine. Indeed, axial muscles (and particularly the diaphragm) are known to be particularly vulnerable to oxidative stress, which is a known consequence of SEPN1 depletion (Arbogast *et al.*, 2009). Neck and trunk weakness and rigidity are generally present from an early age but are often overlooked, since they are rarely a cause of spontaneous complaints in mild or moderate patients, and contrast with fairly preserved limb strength and walking ability. Moreover, the discordance between axial and limb muscle involvement often hinders the diagnosis of a muscle disorder until the full phenotype manifests around the end of the first decade with the development of scoliosis and restrictive respiratory failure, strikingly disproportionate to limb muscle involvement. These can be the most prominent problems, leading to referral to pulmonologists or orthopaedic surgery specialists for management rather than to muscle

clinics for diagnosis.

Interestingly, we show here that ophthalmoparesis can be part of the SEPN1-RM phenotype and correlates with disease severity, which can be useful for differential diagnosis (i.e., with titinopathies). The scoliosis and rigid spine pattern in SEPN1-RM was also characteristic. Spinal rigidity in SEPN1-RM, present since early stages of the disease and mainly affecting cervico-dorsal segments, is different from that observed in myopathies caused by mutations of *LMNA* (Quijano-Roy *et al.*, 2008), *EMD* (Kubo *et al.*, 1998), *FHL1* (Shalaby *et al.*, 2008), *COL6* (Bönnemann, 2011*a*), *RYR1* (Bharucha-Goebel *et al.*, 2013), *DNM2* (Quijano-Roy *et al.*, 2012), *TTN* (Chauveau *et al.*, 2014*a*; Oates *et al.*, 2018) or *GAA* (Fadic *et al.*, 1997; Laforêt *et al.*, 2010) (Figure 3.17).

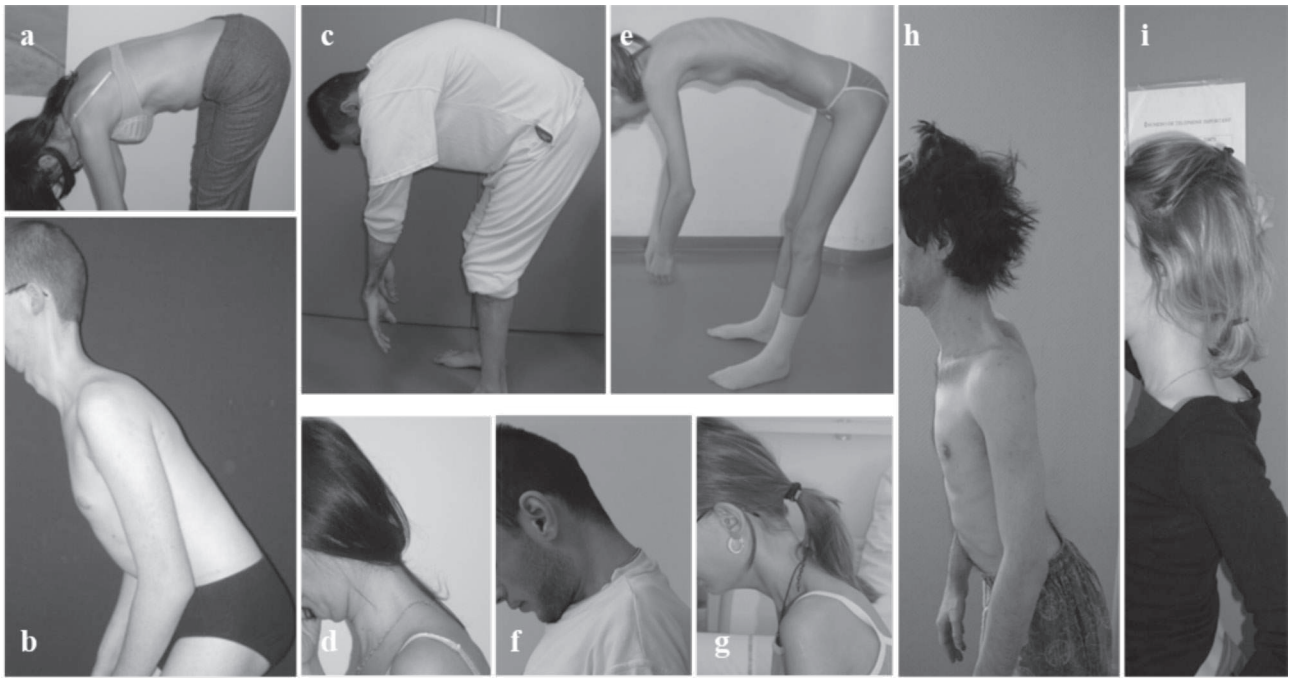

Figure 3.17. Differential diagnosis of Rigid spine. (a,b,d) Rigid spine in SEPN1-RM predominantly involves cervico-dorsal segments. Patients are able to bend forward due to relatively well preserved lumbar region (a). (c,f) Patients with COL6-related myopathies have rigid spine associated with prominent dorsal kyphosis. Prominent cervical rigidity can also be found (f). (e,g) Congenital muscular dystrophy due to LMNA mutations usually causes global spinal rigidity. Patients with Pompe disease (h) and RYR-1 related myopathies (i) can also present with rigid spine.

Along these lines, muscle imaging is a remarkable non-invasive tool for assessment and differential diagnosis in congenital muscular disorders (Quijano-Roy *et al.*, 2012; Tordjman *et al.*, 2018). SEPN1-RM is associated with a homogeneous and recognizable radiological pattern affecting axial muscles, severely wasted sternocleidomastoid muscle and absence or severe atrophy of semimembranosus with relative preservation of rectus femoris, long adductor and gracilis (Hankiewicz *et al.*, 2015). The dramatic involvement of semimembranous should raise suspicion of SEPN1-RM even in very young or mild patients. SEPN1-RM pattern differs from those of other early-onset muscular diseases. In particular, RYR1-related myopathies can also present with scoliosis and respiratory failure and may show very close radiological muscle findings in thighs, but in contrast there is a selective involvement of soleus muscle in lower leg and sternocleidomastoid is preserved, while other cranial muscles are affected (Jungbluth *et al*., 2004). Due to the involvement of muscles not only in lower extremities but also in upper extremities, cervico-axial and cranial regions, whole-body MRI (WBMRI) is recommended. Prominent axial weakness and dropped head may give rise to the suspicion of congenital muscular dystrophy due to LMNA mutations (Quijano-Roy *et al.,* 2008). Nonetheless, WBMRI from LMNA mutated patients reveals selective involvement of the vastii, shoulder and arm muscles with sparing of the forearm and head (Gómez-Andrés *et al.*, 2018). As previously mentioned, COL6-related myopathies (COL6-RM) may have also overlapping clinical features with SEPN1-RM, such as spinal rigidity, and radiological findings are of great help. Indeed, COL6-RM are associated with a characteristic MRI pattern with alternating bands of hypo- and hyperintensity within the muscle ("tigroid pattern") and have a predominant involvement of rectus femoris and vastus lateralis muscles (Mercuri *et al.*, 2003). Patients with centronuclear myopathies due to DNM2 mutations have also a predominant axial involvement and muscle MRI in these patients can reveal prominent wasting of the sternocleidomastoid, but a characteristic selective degeneration of masticator and deep forearm muscles allow differentiation of this condition (Susman *et al*., 2010). Finally, juvenile Pompe disease can present with rigid spine and typical MRI findings with selective involvement of the tongue and subscapularis muscle, with sparing of the sternocleidomastoid and absent or non-specific abnormalities in the lower limbs (Figueroa-Bonaparte *et al*., 2016; Tordjman *et al*., 2018). In conclusion, the homogeneous and recognizable SEPN1-RM radiological pattern (axial muscle involvement, severe wasting of sternocleidomastoid muscles and absence or dramatic atrophy of semimembranosus, with relative preservation of the rectus femoris, long adductor and gracilis) (Hankiewicz *et al*., 2015) can be useful for diagnosis even in very young or mild patients.

This series confirms that the SEPN1-RM histological spectrum is unusually large, and reveals some of its determinants. We found no correlation between the histopathological presentation and clinical severity. Most biopsies were typical of a CM, showing minicores, type 1 fibre predominance and a mild degree of endomysial fibrosis. Moderate dystrophic features or protein aggregates (Mallory body-like inclusions) were also found, although the latter typically affect a low percentage of fibres and were found only in quadriceps samples. Along these lines, we revealed a clear-cut discordance between severely dystrophic axial muscles and mildly myopathic limb muscles in the same patient. Thus, the site of biopsy can contribute to explain the strikingly large histopathological variability and the initial classification of SEPN1-RM patients as having four different diseases. Furthermore, younger ages correlated with less specific biopsy findings. Thus, unless life-support decisions are necessary, muscle biopsy might be best delayed until school-age to increase the diagnostic yield, and could be reserved for cases without a typical phenotype and/or when other tests have been inconclusive.

Regarding genetics, inheritance of the disease was autosomal recessive in all cases. The most common mutation identified in this series is a mutation of the starting codon (c.1A>G) that precludes protein translation. Interestingly, exon 1 emerged as major hotspot for *SEPN1* mutations. However, this GC-rich exon is poorly or not covered by NGS panels, which may contribute to underdiagnosis. Overall, the results presented here confirm that clinical characterization and recognition of the SEPN1-RM phenotype are essential and may be sufficient in most patients for indicating *SEPN1* genetic testing, which should systematically include Sanger-sequencing of exon 1.

A diagnostic algorithm is here proposed (Figure 3.18). If the typical phenotype is present, direct *SEPN1* gene sequencing should be performed. Muscle imaging could be helpful to guide genetic testing by NGS gene-panels, an efficient genetic diagnostic strategy in congenital muscular disorders (Nigro and Piluso, 2012; Krahn *et al.*, 2018).

Another important finding of this series is that SEPN1-RM is a more severe and progressive disease than previously thought. While motor abilities were reported to be stable, loss of ambulation occurred in 10% of the cases with full follow-up data. Muscle functional performances and respiratory function (in particular, diaphragmatic fatigue) declined systematically and progressively from the end of the third decade, even in mild cases. Mortality at young age was observed in three patients (including two severe cases that died at 3 and 5 years) and in 18 relatives, most of them never ventilated. But life span was reduced even in two mild cases with optimum respiratory support, the eldest patient being

currently 55 years-old.

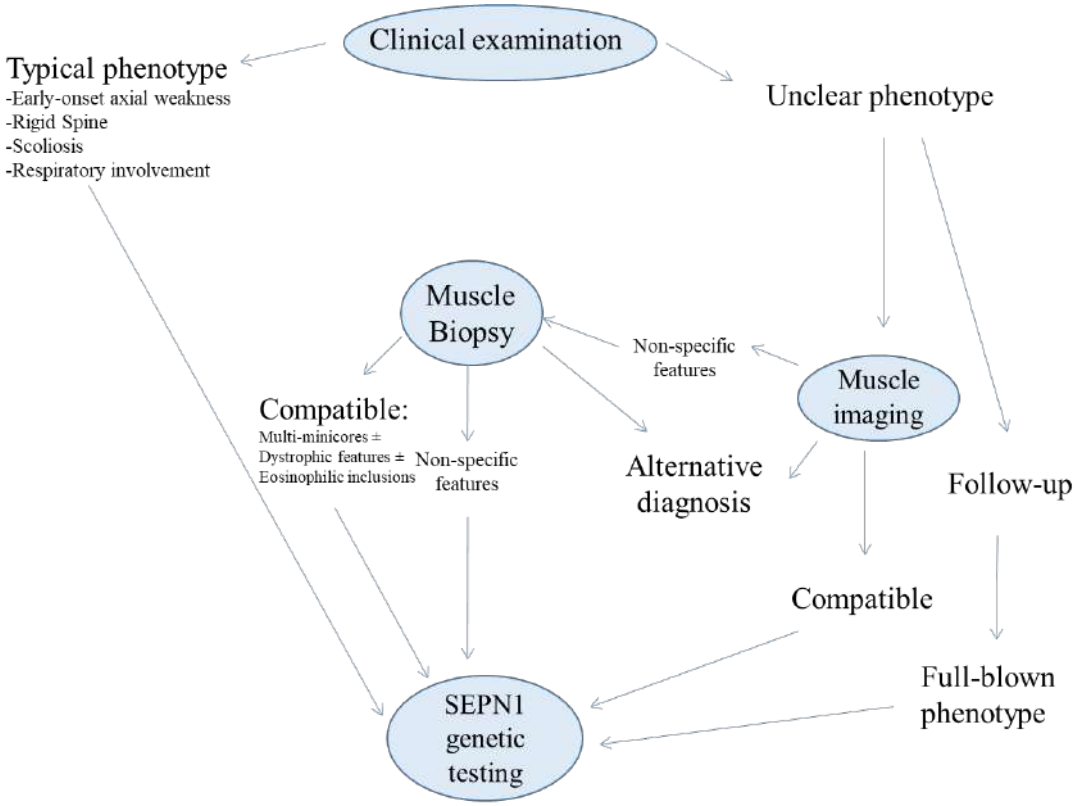

Figure 3.18. Proposed diagnostic algorithm in SEPN1-RM.

Management of the scoliosis and respiratory failure was a key determinant of prognosis. We reported that early non-invasive ventilation may initially stabilize the decline in respiratory muscle strength (Caggiano *et al.*, 2017). Our current data also reveal that scoliosis surgery had a positive impact on the respiratory function but induced a major drop in FVC in the immediate postsurgical period. Intensive or permanent ventilation at this decisive time was critical to restore or even improve FVC pre-surgery values.

Other factors associated with disease severity were the type of *SEPN1* gene defects and previously-unreported body mass abnormalities. Indeed, the analysis of this series allowed to establish the first phenotype-genotype correlations in SEPN1-RM. Some exon 1 variants were commonly found in patients with a severe phenotype, although the small number of patients harboring each individual variant and the different associated mutations in trans precluded statistical significance. However, biallelic null mutations significantly correlated with higher disease severity.

Unexpectedly, a statistically significant correlation between body weight and disease severity was also observed. Most patients with good motor abilities were extremely underweight. Indeed, extremely low body-weight can be very impressive and is often a cause of concern and referral as most of these patients experience a dramatic decrease in body weight around puberty leading to a cachectic phenotype. But there was a subgroup of patients with troncular obesity since childhood showing a homogeneous and rapid disease progression, leading to severe weakness (including non weight-bearing and extraocular muscles) and loss of ambulation before adulthood. This extramuscular phenotype is different from secondary weight gain in a wheelchair-bound patient and could be related to SEPN-RM pathophysiological mechanisms involving defective mitochondrial bioenergetics and lipid metabolism in muscle (Arbogast *et al.*, 2009; Arbogast and Ferreiro, 2010; Pozzer *et al.*, 2019; Varone *et al.*, 2019).

Furthermore, the present results also confirm the previously described association between SEPN1-RM and insulin resistance (Clarke *et al.*, 2006). Interestingly, insulin-resistance or prediabetes were found in extremely underweight patients, confirming that paradoxical insulin resistance is part of the SEPN1-RM phenotype. Skeletal muscle is the main contributor to post-prandial glucose uptake in the humans. Therefore, muscle defects leading to defective glucose availability may lead to glucose metabolism abnormalities (Varone *et al.*, 2019). Recently, we reported that SEPN1 depletion increased susceptibility to insulin resistance by triggering a chronic endoplasmic reticulum (ER) stress in skeletal muscle, providing a basis for abnormal glucose metabolism in SEPN1-RM (Clarke *et al.*, 2006; Varone *et al.*, 2019). Interestingly, SEPN1 deficiency triggers glucose intolerance in SEPN1-KO mice fed with a high-fat diet, even if they have a trend towards gaining less weight than their wild-type (WT) counterparts (Varone *et al.*, 2019). Thus, high caloric intake could trigger or aggravate glucose metabolism abnormalities and oxidative/ER stress. Together with the correlation between BMI and severity reported here and the complaints of functional aggravation after weight gain in mild/moderate patients, this suggests that hypercaloric diets/supplements should not be systematically administered on the basis of low weight alone, unless there are other clear indicators of malnutrition.

The results presented here have significant implications for the identification of outcomes, a keystone for clinical trials. In the last years, significant progress has been achieved in the identification of SEPN1-RM pathophysiological pathways which are targetable with existing drugs (Arbogast *et al.*,

2009; Arbogast and Ferreiro, 2010; Pozzer *et al.*, 2019; Varone *et al.*, 2019). While the phenotype in SEPN1-RM involves skeletal muscles exclusively, SEPN1 is a ubiquitous ER glycoprotein with putative enzymatic activity (Petit *et al.*, 2003) which plays a role in mitochondrial bioenergetics, oxidative stress and redox-based calcium homeostasis (Lassing *et al.*, 2007; Arbogast *et al.*, 2009; Arbogast and Ferreiro, 2010; Rederstorff *et al.*, 2011; Moulin and Ferreiro, 2017). Indeed, axial muscles such as the diaphragmare known to be particularly vulnerable to oxidative stress, which is consistent with the patients' phenotype. Interestingly, SEPN1 RM seems to share mechanisms withother muscle diseases, particularly redox homeostasis disturbances, which have been identified as a secondary pathophysiological mechanism in *RYR1*-, *COL6*-related myopathies and in Duchenne muscular dystrophy (Kim *et al.*, 2013; Moulin and Ferreiro, 2017). In fact, selenoprotein N-devoid myotubes also showed Ca^{2+} homeostasis abnormalities suggesting dysfunction of the redox-sensor Ca^{2+} channel ryanodine receptor type 1 (Jurynec *et al.*, 2008; Arbogast *et al.*, 2009).

The antioxidant N-acetylcystein (NAC) has been identified as an effective treatment *ex vivo* and has also proved to be effective in a murine model of SEPN1 knock-out (Arbogast *et al.*, 2009; Rederstorff *et al.*, 2011). NAC could act synergistically in different ways as a cysteine donor, reactive oxygen species (ROS) scavenger, glutathione precursor and also as an enhancer of glutathione peroxidase enzymatic activity (Atkuri *et al.*, 2007). Finally, it has been suggested that it may negatively regulate NF-kB expression (Li *et al.*, 2003). In view of the above, a small pilot clinical trial with oral NAC in SEPN1-RM was launched (ClinicalTrials.gov Identifier: NCT02505087) and results are currently being analysed by our team.

But multicentric, international phase II-III trials require overcoming bottlenecks which are highlighted by this study. One is the predominantly axial weakness, since there are few quantifiable validated measures of axial muscle power. This study also found an important intra-patient variability in FVC, potentially explained by fatigability of the diaphragm and other muscles, which could bias trial results. Another variability factor is heterogeneous orthopaedic and respiratory management, particularly around spinal surgery, which has a major functional impact. All the former, together with slow progression until the fourth decade, hinder the choice of outcome measures to evaluate treatment efficacy. The aim of this study was also to contribute here to overcome some of these bottlenecks by proposing a straightforward set of clinical criteria to classify patients according to disease severity, thus defining more homogeneous groups. Kaplan Meier curves quantifying ventilation-free probability

are provided here which could be useful to evaluate the impact of potential treatments. Moreover, the present results suggest that age stratification could be useful, given that limb strength is stable or slowly progressive in younger patients but steadily progressive after the fourth decade. In younger patients, the main measurable outcome could be the respiratory/diaphragmatic function, given that limb strength remains stable or slowly progressive in this age group.

Homogeneous management recommendations would be also particularly important in SEPN1-RM to reduce variability but also to improve vital prognosis. Based on the present data, systematic sleep studies should be performed in any child or adult with significant axial muscle weakness, even prior to genetic diagnosis and/or in the absence of day-time signs of respiratory failure or major FVC decrease. During follow-up, regular respiratory function tests are of major importance. Non-invasive ventilation should be initiated as soon as respiratory failure or signs of nocturnal hypoventilation are detected, and should be adjusted regularly (Wallgren-Pettersson *et al.*, 2004; Wang *et al.*, 2010) and sustained/intensified post-arthrodesis. SEPN1-RM follow-up should include yearly respiratory and cardiac function evaluations, given the possibility of pulmonary hypertension or secondary right-ventricle failure. Scoliosis monitoring would also be advisable every year, and can be intensified to every six months around the rapid growth spurt in adolescence due to the high probability of rapid evolution. Scoliosis management has also a positive impact on respiratory function. If surgical management is needed, it would be advisable to delay it until the end of the growth spurt, although this might change. Ventilation in the post-operative period is advised until FVC comes back to previous values. Finally, OGTT should be performed at least once during follow-up, particularly in adolescents and adults, and tailoring BMI control to the SEPN1-RM particularities. As previously mentioned, caloric supplements are not recommended in these patients since not only weight gain can lead to a poor functional performance but it can also trigger glucose metabolism abnormalities. Physical therapy is recommended in these patients and should be performed by trained staff.

The main limitation of our study is its retrospective character which may imply an overestimation of the prevalence of some clinical features. However, this is the largest series of SEPN1-RM patients so far, and it furthers our understanding of SEPN1-RM phenotype and natural history in children and adults, potentially contributing to improve diagnosis, management and follow-up and to increase disease awareness and recognition of its phenotypic specificities. The present results also pave the way for the design of prospective natural history studies and clinical trials in the near future.

Chapter 4.

ASC1-RELATED MYOPATHY CLINICAL ASPECTS

4.1 INTRODUCTION

Congenital myopathies (CMs) are genetically and clinically heterogeneous inherited disorders which usually present during the first years of life with delayed motor development, muscular weakness and hypotonia and have a stable or slowly progressive course. They are sometimes associated with systemic involvement (North, 2011; Schorling *et al.*, 2017; Wang *et al.*, 2017) and have no specific treatment (Jungbluth *et al.*, 2017). So far, more than 30 genes have been associated with CMs (Kaplan and Hamroun, 2015; Ravenscroft *et al.*, 2015), most of them encoding proteins involved in (i) skeletal muscle calcium homeostasis (Treves *et al.*, 2017); (ii) excitation-contraction coupling (Horstick *et al.*, 2013); (iii) membrane remodeling (Dowling *et al.*, 2014; Jungbluth and Gautel, 2014) or (iv) myofibrillar force generation (Wallgren-Pettersson *et al.*, 2011) or thin-thick filament assembly (Tajsharghi and Oldfors, 2013) and interactions (Jungbluth *et al.*, 2018). However, the genetic defect remains unknown in up to 25% CM patients (Böhm *et al.*, 2013*b*).

In 2016, Davignon et al described a novel form of CM caused by recessive mutations in the Thyroid Hormone Receptor Interactor 4 gene (*TRIP4,* MIM* 604501*),* located in the chromosome 15 (15q22.31; 67.5 kbp, 13 exons) and encoding the transcriptional co-activator Activating Signal Cointegrator–1 (ASC-1; 650 kDa, 581 aa) (Davignon *et al.*, 2016). In four patients from a large consanguineous family, they identified a recessive nonsense mutation situated in exon 7 (c.G950A, p.W297*) which introduced a premature termination codon (PTC) and resulted in *TRIP4* mRNA decay to around 10% of control levels and absence of detectable ASC-1 protein in patients' cells (Davignon *et al.*, 2016). This condition was termed ASC-1 Related Myopathy (ASC-1-RM), identifying transcriptional

regulation as a novel pathomechanism.

These patients presented with severe neonatal hypotonia, potentially lethal respiratory failure, predominantly axial weakness with early loss of ambulation, progressive scoliosis associated with rigid spine in two patients, joint hyperlaxity and skin abnormalities reminiscent of those observed in collagen VI-related myopathies (Bönnemann, 2011*a*). One of the patients deceased at 16 months due to respiratory failure. Muscle biopsies from these patients revealed the so-far unreported association of multiminicores, caps and dystrophic lesions (Davignon *et al.*, 2016).

This novel condition exhibited overlapping clinical and histopathological features with other early-onset muscle disorders such as cap myopathy, caused by mutations in the *TPM2, TPM3* or *ACTA1* genes, which encode contractile proteins (Sparrow *et al.*, 2003; Feng and Marston, 2009), SEPN1-related myopathy [SEPN1-RM] (Moghadaszadeh *et al.*, 2001; Ferreiro *et al.*, 2002*b*; Clarke *et al.*, 2006; Scoto *et al.*, 2011) or COL6-related myopathies [COL6-RM] (Bönnemann, 2011*a*).

The role of ASC-1 in neuromuscular diseases was confirmed by the simultaneous description of four families with recessive loss of function mutations in *TRIP4* (three families sharing two mutations: c.760C>T [p.Arg254*] and c.832C>T [p.Arg278*]) or in the gene *ASCC1* (one family carrying the variant c.157dupG [p.Glu53Glyfs19*] in homozygosis). *ASCC1* (10q22.1, MIM * 614215) encodes Activating signal cointegrator 1 complex subunit 1, part of the ASC-1 transcriptional cointegrator complex (Knierim *et al.*, 2016). Patients were reported as having a severe form of spinal muscular atrophy (SMA) and exhibited a phenotype marked by arthrogryposis multiplex, congenital respiratory distress and congenital bone fractures. Cardiac involvement was reported in two out of three families with *TRIP4* mutations. Interestingly, skeletal muscle biopsies from these patients showed major reduction of myofibre size, indicating that a primary muscle component in this second ASC-1 associated phenotype cannot be excluded.

Thereafter, no other patient with *TRIP4* mutations has been described. However, four additional families with *ASCC1* recessive nonsense or frameshift mutations have been recently reported (Oliveira *et al.*, 2017; Böhm *et al.*, 2018). Oliveira *et al*. reported a homozygous *ASCC1* frameshift mutation in a patient presenting with generalized hypotonia, congenital bone fractures, lack of spontaneous movements and poor respiratory effort who died within the first days of life (Oliveira *et al.*, 2017). The patient's muscle biopsy showed atrophic fibres with no further description. Moreover,

three additional families with *ASCC1* recessive nonsense or frameshift mutations have been recently reported (Böhm *et al.*, 2018). These novel patients presented a lethal phenotype with severe neonatal hypotonia, arthrogryposis, and congenital bone fractures. Interestingly, the muscle biopsies from these patients disclosed myopathic features (fibre size variability, intense oxidative rims beneath the sarcolemma, central or eccentric oxidative accumulations in the majority of the fibres as well as prominent myofibrillar disorganization and enlargement of the Z-bands on electron microscopy) and were not suggestive of motor neuron involvement (Böhm *et al.*, 2018). In summary, so far only four families with a total of three *TRIP4* mutations have been reported and the phenotypical spectrum associated with *TRIP4* mutations (including motor neuron versus primary muscle involvement) remains unclear.

4.2 MATERIALS AND METHODS

4.2.1 Patients and biological samples

Six patients with *TRIP4* mutations were recruited through an international collaboration between the following specialized neuromuscular and genetics units: I-Motion Neuromuscular Unit (Institute of Myology, AP-HP, Paris, France), The Manton Center for Orphan Disease Research-Division of Genetics and Genomics at Boston Children's Hospital (Harvard Medical School, Boston, USA), Department of Molecular Biology and Genetics- Biruni University (Istanbul, Turkey), Department of Paediatric Neurology- Neuromuscular Center (Queen Fabiola's Hospital, Brussels, Belgium), Neuromuscular Unit and Molecular Genetics Laboratory-Montpellier University hospital (France), Department of Translational Medicine and Neurogenetics, IGBMC (Université de Strasbourg, Illkirch, France), Molecular genetics unit- Grenoble University Hospital (France), Neuromuscular Unit-Division of Child Neurology (University Hospital Liege, Belgium) and Department of Pathology and Neuromuscular Unit (IDIBELL, Bellvitge University Hospital, Barcelona, Spain). The complete list can be found in Annexe 1.2.

Clinical data were systematically retrieved and retrospectively analysed according to a standardized form (Annexe 2.2). Electromyography and muscle imaging were available for four and two patients respectively. The original previously reported ASC1-RM family (Davignon et al., 2016) was also reassessed after 3 additional years of follow-up.

Diagnostic skeletal muscle biopsies were obtained from four patients, processed for standard histological and immunochemical studies and fixed for electron microscopy as previously described (Dubowitz and Sewry, 2007). Primary fibroblasts were obtained from skin biopsies (patients) or surgically discarded tissues (age-paired controls). Muscle tissue was obtained from diagnostic muscle biopsies in two patients and from surgically discarded tissue in one.

Informed consent for research participation and use of clinical data and photographs was obtained from all patients or their guardians according to local Ethic Committees. Muscle samples, skin biopsies and peripheral blood samples for DNA extraction were obtained after informed consent, in agreement with local Ethic Committees and the Declaration of Helsinki ('World Medical Association declaration of Helsinki: Ethical principles for medical research involving human subjects', 2013).

4.2.2 Genotyping

TRIP4 mutations were identified by whole exome sequencing (WES) for families B and D, as previously described (Böhm et al., 2018), or by next-generation sequencing-based myopathy genes panel for families A and E (Krahn et al., 2019). For family C, WES and data processing were performed with an Illumina exome capture (38 Mb target) and sequenced (150 bp paired reads) to cover >90% of targets at 20x and a mean target coverage of >100x. WES data was processed through a pipeline based on Picard and mapping done using the BWA aligner to the human genome build 38. Variants were called using Genome Analysis Toolkit (GATK) HaplotypeCaller package version 3.4.

TRIP4 mutations were Sanger confirmed in patients and relatives and reported according to Human Genome Variation Society recommendations (http://varnomen.hgvs.org).

Exome Aggregation Consortium (ExAC, http://exac.broadinstitute.org/) and Genome Aggregation (gnomAD, http://gnomad.broadinstitute.org/) databases were interrogated to identify previously-reported mutations and to determine the frequency of each mutation in the general population. Alamut® Visual (Interactive Biosoftware, North Seattle, WA) was used to predict the effect of the different variants.

4.2.3 Fibre type proportion and muscle fibre size evaluation

In collaboration with the Neuromuscular Morphology Unit/Myology Institute at Pitié-Salpêtrière Hospital in Paris (Dr Romero's team) we analysed three quadriceps biopsies from patients AIII.2 (age 4 years) and FII.1 (aged 6 years). Analysis was done in cross-sections of snap frozen muscle stained with ARPase at 9.40. Diameter was measured in µm. Measurements have been performed on two to three pictures at the magnification of x20 or x40. The image analysis was performed using CARPACCIO.cloud software.

4.2.4 Cell culture

Primary fibroblasts from patients and controls were grown at 37°C in a humidified atmosphere with 5% CO2. Cells were grown in Dulbecco Modified Eagle Media (DMEM) containing Glutamax (Gibco), foetal calf serum (FCS) 20% and penicillin-streptomycin (P/S) 1%.

4.2.5 Western Blot

Cells were washed twice with cold PBS and lysed with cold lysis buffer. After 20 min incubation on ice, cells were scraped and centrifuged at 15,000 g for 10 minutes at 4°C. The protein concentration of the supernatant was determined with the Bradford Protein Assay. Cell extracts (20 µg) were separated using 10% SDS-PAGE gel and transferred on nitrocellulose membranes using Bio-Rad Trans Turbo Transfer system. Nitrocellulose membranes (Biorad) were blocked for 2 hours in Tris buffered saline (TBS) containing 5% dry milk and probed with primary antibodies (Annexe 5) diluted in TBS–1% milk. Finally, membranes were incubated with secondary antibodies, goat anti-rabbit HRP conjugate (Thermo Scientific) for 1 hour in TBS–1% milk at room temperature (RT). Enhanced chemiluminescence (ECL, Bio-Rad) was used for detection of the signals. Quantification analysis was performed using Image J software.

4.3 RESULTS

4.3.1 Clinical findings

We identified six patients (2 females and 4 males) from five families with autosomal recessive *TRIP4* mutations (Figure 1). Age at last ascertainment ranged from 8 months to 63 years. All pedigrees were compatible with autosomal recessive transmission. Consanguinity was confirmed in three families (A,

C and E). Two patients had affected siblings with similar clinical features that have not been included in this series due to lack of genetic confirmation. Patient CIII.7 had two siblings with similar clinical features who deceased prematurely due to respiratory distress while patient DII.2 had an older brother with a similar phenotype who had been diagnosed with congenital myopathy with uniformity of type 1 fibres and died at the age of 5 years due to respiratory failure. There was no history of weakness or other neuromuscular abnormalities among the first-degree relatives of the other patients.

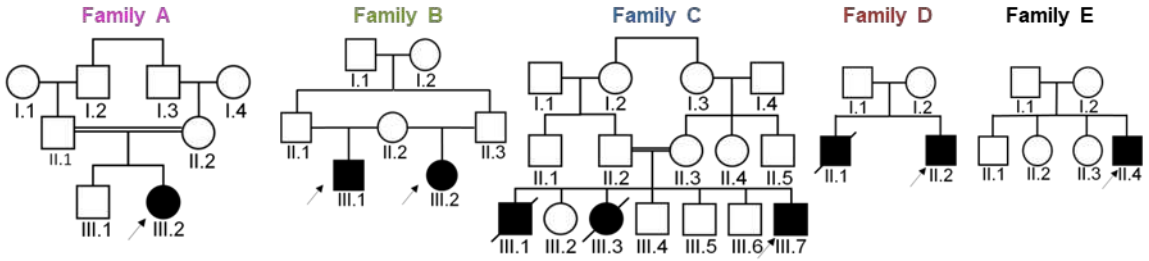

Figure 4.1. Pedigree of the novel identified families.

We also reassessed the three patients from the originally reported family (family F) (Davignon *et al.*, 2016) after 3 years of additional follow-up (Figure 4.2).

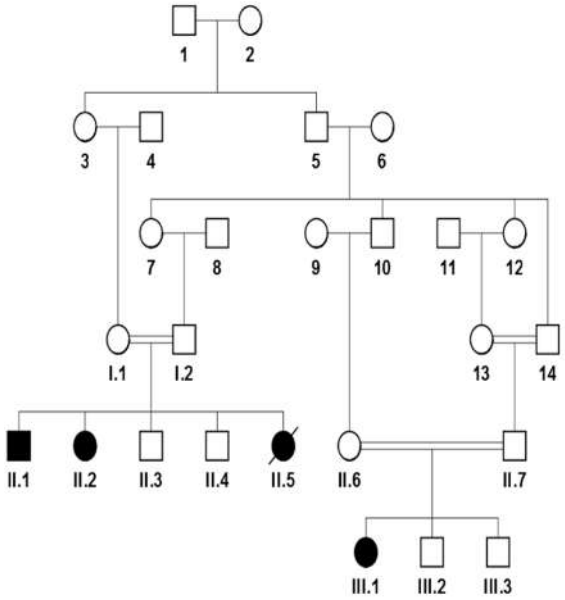

Figure 4.2. Pedigree of the original family reported (modified from Davignon et al., 2016)

Clinical features are summarized in Table 4.1. Overall, the clinical phenotype is marked by early onset proximal and axial weakness, scoliosis, skin involvement without major contractures and respiratory failure with variable severity, correlated with the degree of muscle weakness.

Table 4. 1. Summarized clinical findings.

Family	**A**	**B**		**C**	**D**	**E**	**F**			
Patient	III.2	III.1	III.2	III.7	II.2	II.4	II.1	II.2	II.5	III.1
Gender	F	M	F	M	M	M	M	F	F	F
TRIP4 **Pathogenic variant**	c.141_142delAT [p.Tyr48fs*3] homozygous	c.534C>G [p. His178Gln] + c.1544_1547delACTG [p.Asp515fs*34]		c.1065delC [p.Ile356fs*6] homozygous	c.55_56insCT [p.Gln19fs*47] + c.1197delA [p.Ser399fs*12]	Homozygous deletion of exons 8 and 9	c.890G>A [p.Trp297*] homozygous			
First signs	Hypotonia, DMM	DMM (gait acquisition)	DMM (gait acquisition), waddling gait, fatigability	NH, respiratory distress, feeding difficulties	NH, DMM	Difficulty running, poor sports performance (adolescence)	NH, neonatal respiratory distress, poor antigravity movements, feeding difficulties, DMM	NH, poor antigravity movements, DMM (gait acquisition at 4y)	Hydramnios, NH, poor antigravity movements, feeding difficulties, DMM	NH, feeding difficulties, respiratory difficulties, DMM
Best motor performance	Present age (9y): waddling gait, climb stairs, bipodal jump, starts to run	Present age (22y): waddling gait, climb stairs without aid	16y: waddling gait, climb stairs without aid	NA	Present age (35y): independent ambulation (short distances)	Adulthood: independent ambulation, climb stairs	14y: standing unsupported, walking a few steps indoors with a walker	7y: walking unsupported and raise from a chair with difficulties until 11y	8m: Poor head control and partial limb antigravity movements	10y: Partially rolls over, sits without support, crawls on her buttocks

Evolution of motor performance	Improving	Stable	Stable	NA	Stable	Stable	Improving until 14y, then slowly progressive. WCB at 15y	Improving until 7y, then slowly progressive. WCB at 11y	Stable. Deceased at 16m	Stable. WCB since early childhood
Scoliosis	Yes (early childhood)	Yes (early childhood)	Yes (early childhood)	No	Yes (early childhood) Arthrodesis (16y)	No	Yes (early childhood) Arthrodesis (15y)	Yes (early childhood) Arthrodesis (12y)	No	Yes (early childhood)
Rigid spine	No	No	Yes	No	Yes	Yes	Yes	Yes	No	No
Respiratory involvement	Respiratory infections since 7m. Restrictive RF since early-childhood. NIV since age 3y	Restrictive RF since childhood. Latest FVC 60% (22y)	Restrictive RF since childhood. Latest FVC 52% (18y).	From birth. Neonatal respiratory distress needing tracheostomy and ventilation. Died from RF at 8m	Restrictive RF. NIV since 18y. Latest FVC 35% (35y)	Latest FVC 80% (63y). Obstructive sleep apnea syndrome treated by CPAP	Restrictive RF since birth. NIV from 11m. Tracheotomy at 17m. Ventilated 23/24h since age 20y. Latest FVC 22% (15y)	Restrictive RF since early childhood. NIV from 11y. Latest FVC 27% (19y)	RF from birth. Intubation at 15m, deceased at 16m due to RF	Restrictive RF from birth. Tracheotomy at 10m.
Cardiac involvement	No	No	No	No	No	DCM (LVEF 25%) in the 5th decade	No	DCM in the 3rd decade	No	No
Joint contractures	Yes (Achilles)	No	No	No	Yes (elbows, achilles).	Yes (elbow, mild)	Yes (hips, ankles, mild)	Yes (hips, ankles, knees, moderate)	No	No
Joint hyperlaxity	No	No	No	No	Yes	No	Yes	Yes	Yes	Yes

Skin involvement	No	No	No	Yes (hyperelasticity)	Yes (FH, hyperelasticity)	Yes (xerosis, FH)	Yes (FH, hyperelasticity, xerosis)	Yes (FH, hyperelasticity, xerosis)	Yes (FH, hyperelasticity, xerosis)	Yes (FH, hyperelasticity, xerosis)
Dysmorphic features	Flat face, retrognathia	No	No	Flat face, prominent venous markings, tapering fingers	Elongated face, low-set ears, retrognathia. Flat thorax, pectus excavatum	Flat face, retrognathia. Flat thorax, pectus excavatum	Flat face, funnel thorax, pectus excavatum, valgus feet	Flat face, flat thorax, pectus excavatum, valgus feet	UK	Flat face, high-arched palate, flat thorax
Other features	Unnderweight (<P3). Learning and writing difficulties	Right-eye keratoconus	Underweight (<P4)	Severe ophthalmo-plegia	Underweight (<P3). Myopia	Mild ophthalmo-paresis. Myopia	Overweight, learning difficulties, delayed puberty, testicular ectopia	Overweight, LL lipodystrophy	UK	LL lipodystrophy, delayed language acquisition, learning difficulties

CPAP: Continuous Positive Airway Pressure; DCM: Dilated cardiomyopathy; DMM: Delayed motor milestones; F: female; FH: follicular hyperkeratosis; LL: lower limbs; LVEF: Left ventricular ejection fraction; M: male; m: months; NA: non-applicable; NH: neonatal hypotonia; NIV: non-invasive ventilation; RF: respiratory failure; UK: unknown; WCB: wheelchair-bound; y: years.

First symptoms and motor development

None of the patients presented with arthrogryposis or congenital contractures. There were no complications during pregnancy or labour, except for reduced foetal movements in the most severe patient (CIII.7).

First signs and symptoms appeared before adulthood in all cases. The most severe patient (CIII.7) presented at birth with severe neonatal hypotonia, poor antigravity limb movements, feeding difficulties, perinatal asphyxia and respiratory distress requiring assisted ventilation (Figure 4.3). He had dysmorphic features (flat face and tapering fingers) and dermatologic involvement (skin hyperelasticity, light colored skin and hair). He died at 8 months due to respiratory failure, never having acquired cephalic control.

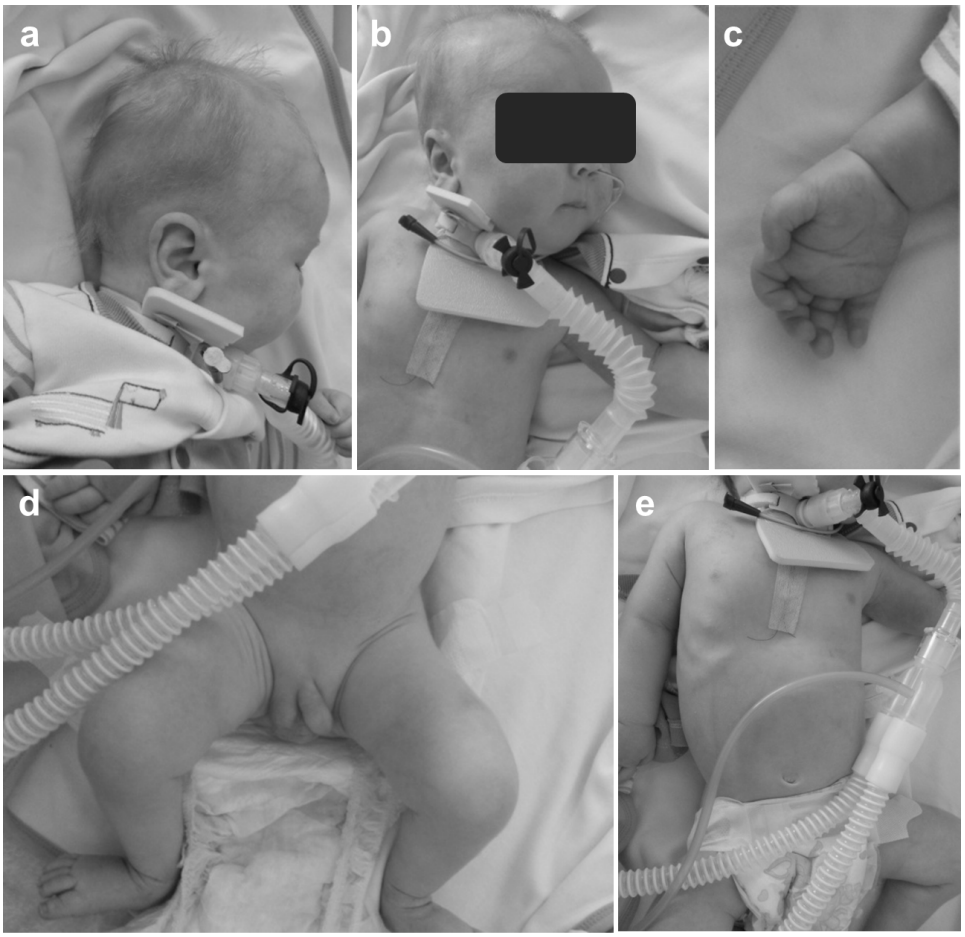

Figure 4.3. Clinical findings in patient CIII.7. Congenital presentation with neonatal hypotonia (d,e: frog position), poor limb movements and respiratory distress requiring tracheostomy and assisted ventilation (a,b). The patient had skin abnormalities, dysmorphic facial features (a, b: flat face, prominent venous markings) and tapering fingers (c).

Two patients (AIII.2 and DII.2) presented in the first year of life with neonatal hypotonia and delayed motor milestones. The two siblings from family B presented with delayed gait acquisition, waddling gait and fatigability. The mildest patient (EII.4) presented with difficulties for running and poor sports performance in adolescence (Figure 4.4).

The five surviving patients acquired independent ambulation, although only one did so before the age of 18 months.

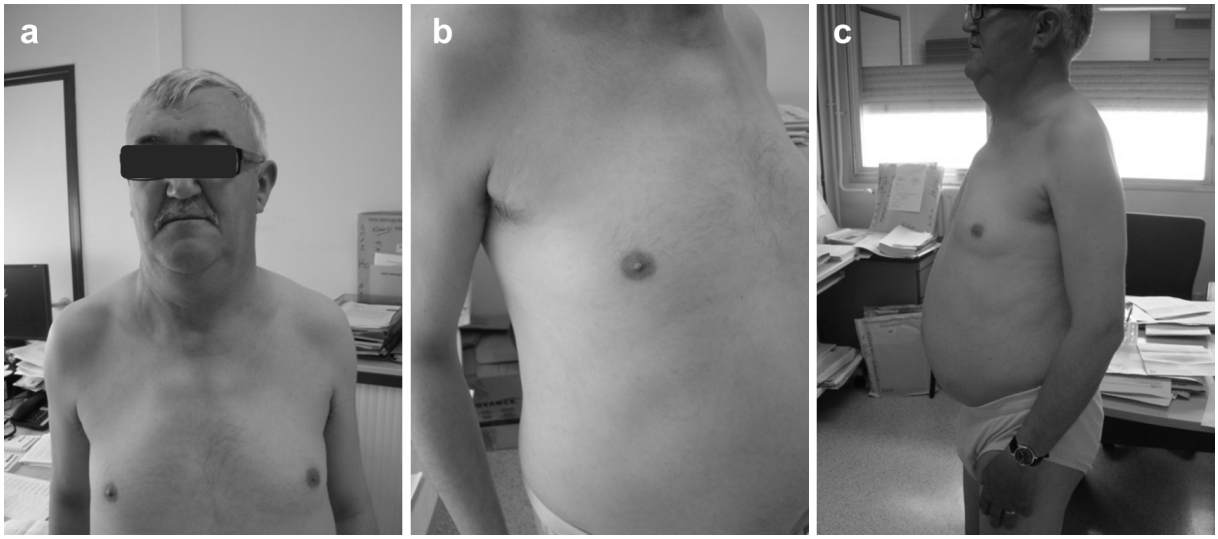

Figure 4.4. Clinical findings in the mildest patient in these series (DII.4), still ambulant at 63 years. The patient has proximal weakness and amyotrophy (a,c), pectus excavatum (b) and dysmorphic facial features (flat face, thick neck, retrognathia) (a,c).

Muscle weakness, muscle bulk and joint contractures

In all patients, muscle weakness and amyotrophy were predominantly axial and proximal (3-4/5 according to the Medical Research Council [MRC] scale) while distal limb strength was relatively well preserved. Only the most severe patient (CIII.7) had facial weakness.

Muscle weakness was stable or slowly progressive in all surviving patients. Excepting the three patients from the original family F, who never acquired independent ambulation, all adult patients could walk outdoors without support at ages 22-63 years. Three adult patients were still able to climb stairs with aid. Walking distance was limited by fatigue or dyspnea in most patients. The youngest patient in this series (AIII.2), currently 9 years old, was still improving her motor abilities and starting to run at the time of assessment.

Mild-to-moderate limb contractures, were present in five patients, mainly affecting the Achilles tendon and elbows. Prominent and generalized joint hyperlaxity was observed in five (Figure 4.5). Deep tendon reflexes were universally diminished or absent.

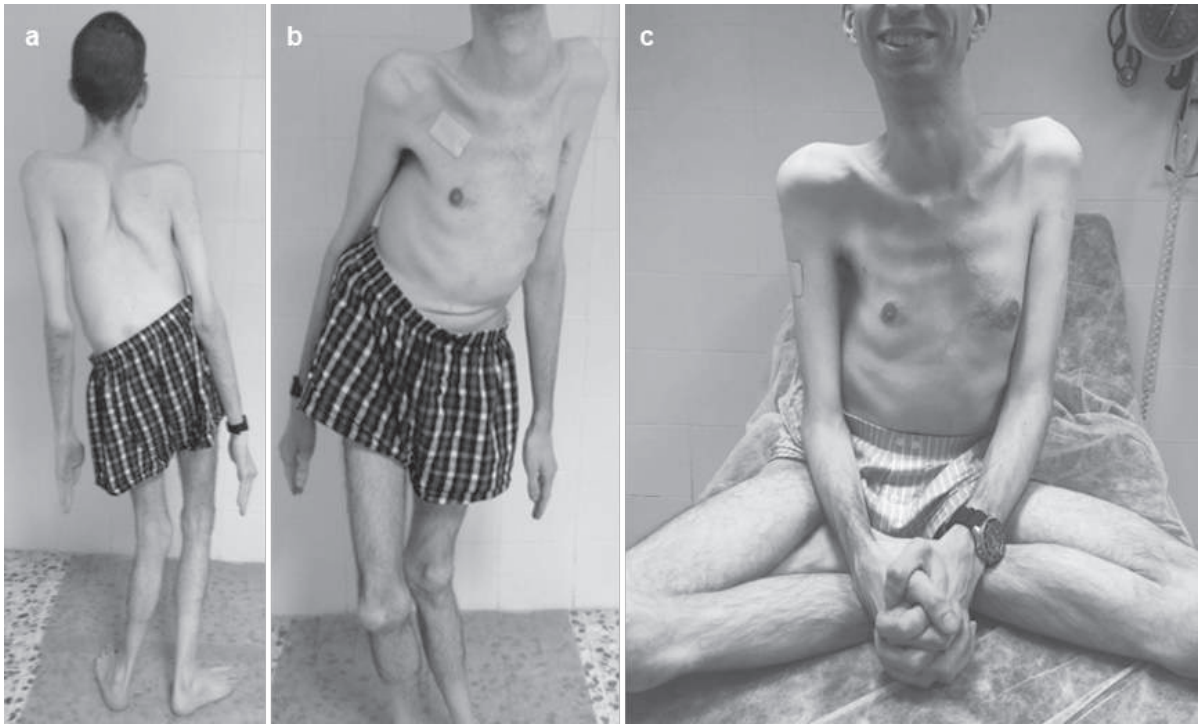

Figure 4.5. Clinical findings in patient DII.2, still ambulant at age 35 years. Note severe scoliosis with dorsal lordosis and unbalanced hips, thoracic deformities (pectus excavatum) and elbow contractures (a,b) contrasting with prominent joint hyperlaxity (c). Note also dysmorphic cranio-facial features (large, thick neck, temporal atrophy, retrognathism, low-set ears) (c).

Axial involvement and respiratory failure

With the exception of the mildest patient (D.II4), all the patients who survived into childhoodhad early-onset progressive scoliosis, which was associated with lateral trunk deviation and pelvic tilt in two cases (Figure 4.5a). One of them required arthrodesis at 16 years due to severe progressive scoliosis. Reassessment of family F revealed progressive scoliosis requiring arthrodesis at age 12 in the youngest patient (FIII.1). Scoliosis was associated with rigidity of the spine in a total of five patients. Thorax deformities (flat thorax and pectus excavatum) were present in five patients. Five patients had dysmorphic craniofacial features such as large and flat face or retrognathism, along with large and thick neck appearance (Figures 4.4a and 4.5c).

Respiratory failure was present in nine out of the ten patients since childhood. The most severe

patient suffered neonatal respiratory distress requiring tracheostomy and assisted ventilation. He died at age 8 months due to respiratory failure, and so did patient FII.5 at 16 months. Five patients needed chronic ventilation (nocturnal non-invasive in three cases, through a tracheostomy in two), while in the remaining two cases only respiratory physiotherapy was prescribed. The mildest patient, currently aged 63 years, had a FVC of 80% and was being treated by nasal continuous positive airway pressure (CPAP) due to sleep apnea/hypopnea syndrome. Polysomnography studies were very helpful during follow-up to survey respiratory function and to determine non-invasive ventilation settings to achieve optimal ventilatory support.

Cardiac involvement

None of the patients had congenital or early-onset cardiomyopathy. However, patient EII.4 developed rapidly progressive dilated cardiomyopathy (DCM) in the fifth decade leading to a severely reduced left ventricle ejection fraction (LVEF, 25%) requiring a preventive automated implantable cardioverter defibrillator (AICD). Interestingly, an early-stage DCM has been detected at the beginning of the third decade in one patient from the first family reported (FII.2). None of the other patients has developed cardiac abnormalities at ages 9-35 years. None of them had a family history of cardiac involvement.

Skin involvement

A total of seven patients had cutaneous involvement, mainly skin hyperelasticity, follicular hyperkeratosis and xerosis with scrath lesions (Figure 4.6). These findings were reminiscent of collagen VI- related myopathies except for the absence of keloid scars.

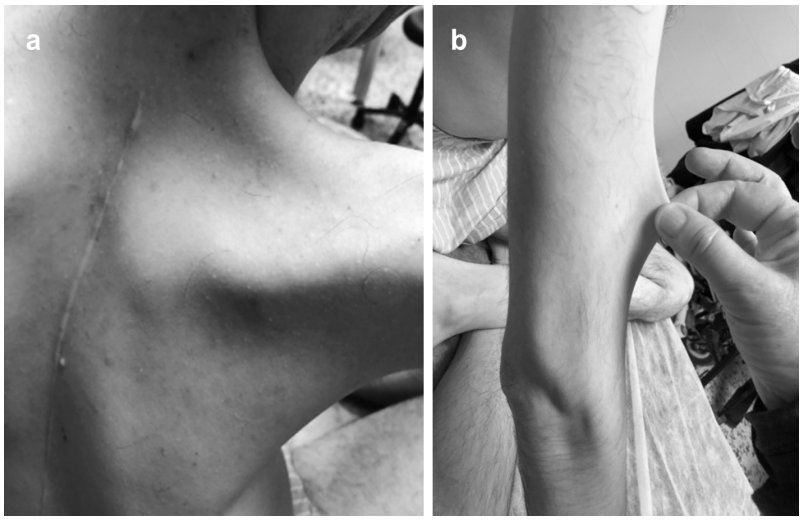

Figure 4.6: Cutaneous phenotype in patient DII.2: follicular hyperkeratosis, xerosis with scratch lesions and prominent scars (but no keloid scars) (a) along with marked skin hyperelasticity (b).

Other features

Oculomotor disturbances were noted in two patients: severe ophthalmoplegia in the most severe patient (CIII.7) and bilateral horizontal ophthalmoparesis in patient EII.4. None of them had ptosis. Only patient CIII.7 had feeding and swallowing difficulties.

Three of the novel patients were underweight (less than the 4th percentile) and one patient was overweight with abundant adipose tissue in the lower limbs. This last finding resembled those of the female patients from family F (Davignon *et al.*, 2016), who exhibited a peculiar aspect of the lower limbs with abundant adipose tissue giving a pseudo-infiltrative aspect.

None of the patients had intellectual disability nor symptoms or signs suggestive of CNS abnormalities.

4.3.2 ***Ancillary tests***

CK level was normal or mildly elevated (less than three times the normal value in all patients. Electromyographic studies performed in four of the novel patients and in two patients of family F revealed a myopathic pattern (short, small, polyphasic, high-pitch motor unit action potentials and early recruitment pattern) without denervation or abnormalities in nerve conduction studies. In three of the novel patients, repetitive stimulation was also performed with normal results.

Muscle imaging (MRI) of the lower limbs was performed in two patients (BIII.1 and EII.4). In both cases, there was a predominant involvement of the posterior compartment of the thigh, notably of glutei and adductor muscles, with relative preservation of gracilis, sartorius, and semitendinosus muscles (Figure 4.7). This pattern was similar to that previously observed in a patient from family F (Davignon *et al.*, 2016).

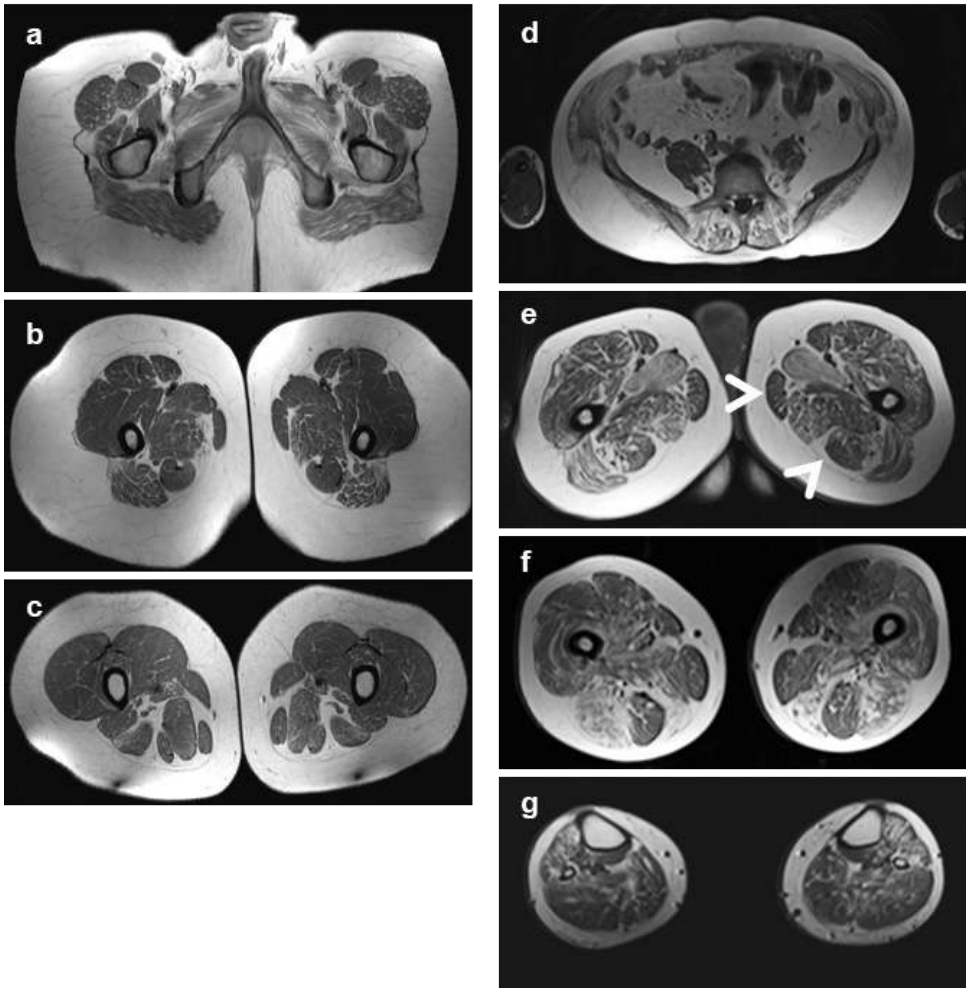

Figure 4.7. Muscle imaging in two patients revealed predominant involvement of posterior thigh compartment with relative preservation of the semitendinosus muscle. (a-c): Lower limb MRI from a mild patient (BIII.1), still ambulant at age 19 years. Axial T1-weighted images showed mild muscle atrophy and fatty infiltration of glutei, iliopsoas and posterior thigh muscles with major involvement of adductor longus and relative preservation of gracillis, sartorius and semitendinosus muscles (arrows). Note marked increase in subcutaneous adipose tissue. (d-g): Muscle MRI from patient EII.4 (aged 56 years), showed the same pattern, including fatty infiltration of paravertebral muscles (d) and the posterior thigh compartment, notably gluteus maximus, adductor longus and semimembranosus (e,f). Note relative preservation of semitendinosus. Leg muscles showed diffuse involvement (g).

4.3.3 Histopathological phenotype

Four patients underwent skeletal muscle biopsy (Table 4.2). One additional patient had a quadriceps biopsy in early childhood, reported as normal, but frozen sections could not be retrieved to review.

Table 4.2. Main histological findings in 5 patients.

Patient	Age at biopsy	Muscle sampled	Major findings
AIII.2	4 years	Quadriceps	IN, FSV, type 1 fibre predominance (95%) and hypotrophy, mild endomysial fibrosis, whorled fibres, multi-minicores
BIII.1	9 years	Quadriceps	Reported as normal
CIII.7	2 months	Quadriceps	Central nuclei, FSV, type 1 fibre predominance and hypotrophy, endomysial fibrosis
DII.2	27 years	Biceps brachii	IN, FSV, type 1 fibre predominance (99%), minicores, rimmed sarcolemma
EII.4	56 years	2 Quadriceps biopsies	IN, FSV, type 1 fibre predominance, lobulated fibres; minicores in one biopsy; caps, rods and cytoplasmic bodies in a second biopsy

IN: internalized nuclei. FSV: abnormally increased fibre size variation.

Samples from the remaining four biopsied novel patients showed congenital myopathy lesions, including increased fibre size variability, type 1 fibre predominance (and frequent hypotrophy) and internalized nuclei, along with variable changes in the muscle fibre architecture (Figure 8): three patients had minicores, often associated with other forms of sarcomere disorganization (cap lesions, rods and cytoplasmic bodies, whorled fibres).

Quadriceps biopsy from the most severe patient (CIII.7) showed fibres with centrally located nuclei interspersed with very small, rounded fibres without fascicular distribution or grouping, reminiscent of centronuclear/myotubular myopathy.

Lobulated fibres and rimmed sarcolemma (intense oxidative rims beneath the sarcolemma) (Figure 4.8) were occasionally observed. None of the biopsies disclosed fibre type grouping, angulated fibres or group atrophy suggestive of denervation.

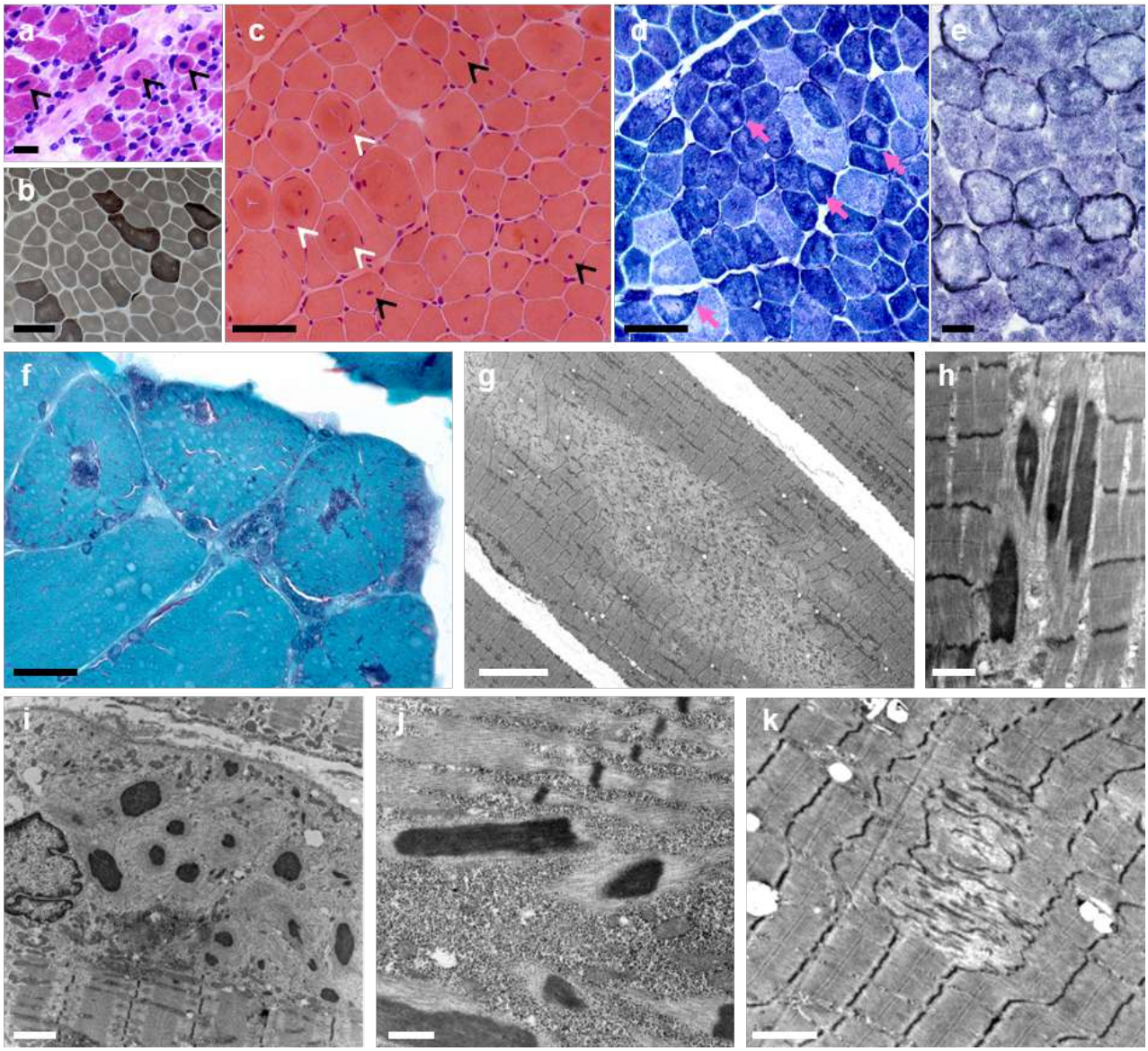

Figure 4.8. Histological spectrum. Skeletal muscle biopsies from patients CIII.7 (a), AIII.2 (b-d, g), EII.4 (f, h-j) and DII.2 (e, k). Muscle biopsy from the most severe patient (a) showed mildly increased endomysial connective tissue, a subpopulation of very small fibres and abundant fibres with apparently normal diameter but myotubular appearance (one central nucleus per transversal section, black arrowheads). In milder patients, dystrophic features were absent and the pattern was more typical of a congenital myopathy, including FSV (b,c), internalized nuclei, often central, (c, black arrowheads), whorled fibres (c, white arrowheads) and type 1 fibre predominance (b). Intense oxidative rims beneath the sarcolemma were found in one patient (e). There were multiple areas lacking oxidative activity (pink arrows in d) and showing mitochondrial depletion and sarcomere disorganization on EM (minicores) (g, k). Modified Gomori trichrome revealed purple stained lesions (f) which corresponded to electron-dense nemaline rods or cytoplasmic bodies on EM (h,j). Note subsarcolemmal myofibrillar disorganization compatible with a cap lesion on EM (i). Transversal

frozen sections, HE (a,c), ATPase pH 9.4 (b), NADH-TR (d,e), modified Gomori trichrome (f); EM (g-k). Scale bars= 25 µm (a), 50 µm (b-d), 25 µm (e,f), 10 µm (g), 1 µm (h), 2 µm (i,k), 500 nm (j). HE: Hematoxylin and eosin; EM: electron microscopy; FSV: Fiber size variation; NADH-TR: Nicotinamide adenine dinucleotide dehydrogenase-tetrazolium reductase.

Analysis of three muscle biopsies from two patients (AIII.2, FII.1) with an accurate evaluation of fibre proportion confirms type 1 fibre predominance in these patients (Table 4.3). Additionally, fibre type distribution was analysed in a biceps brachii biopsy from patient DII.2 at 27 years showing 99% of type 1 fibres, and in a quadriceps biopsy from patient FIII.1 at age 4 years revealing 83.71% of type 1 fibres. Accurate measurement of muscle fibre size was not possible due to technical problems in patients DII.2 and FIII.1.

Table 4.3. Evaluation of fibre type proportion and measurement of muscle fibre size in the biopsies of patients AIII.2 and FIII.1.

Patient	Muscle biopsied	Age (years)	Number of fibres analysed	% Type 1 Fibres	% Type 2 Fibres	Type 1 Mean Diameter (µm)	Type 2 Mean Diameter (µm)
AIII.2	Quadriceps	4	358	92,5	7,5	29,33 ±5.69	35,65±6.15
FII.1	Quadriceps	6	551	95,28	4,72	28,44±5.15	27,12±7.70

Results are expressed as mean ± standard deviation.

Nonetheless, muscle biopsies from patients AIII.2, FII.1 and FIII.1 were taken at early ages (4 and 6 years-old), which hinders a proper evaluation of fibre type proportion and especially of muscle fibre size, given the absence of normative values in the paediatric population. The Neuromuscular Morphology Unit at the Myology Institute (Pitié-Salpêtrière Hospital, Paris), headed by Dr Romero has performed an extensive analysis of 93 morphologically normal deltoid muscle biopsies from paediatric patients (aged 0-18 years) to establish normative values for muscle biopsy morphometry regarding fibre type distribution and muscle fibre size in this population (data not shown, confidential results). According to their results, there is type 1 fibre hypotrophy in both patients and, additionally,

there is type 2 fibre hypotrophy in patient FII.1. Analysis of quadriceps biopsies in a smaller paediatric population performed by the same group (data not shown, confidential results) also confirms these findings.

4.3.4 Genetics

Seven previously unreported mutations in *TRIP4* gene were found (Table 4.4). Transmission was autosomal recessive in all cases, and no *de novo* mutation was identified. Tested parents were healthy heterozygous carriers.

Three patients had homozygous mutations and three were compound heterozygous. Five mutations were frameshift, one missense and one patient had a homozygous deletion of exons 8 and 9 that was predicted to maintain the correct reading frame but to affect the ASCH domain.

Table 4.4. Summary of the mutations identified in the novel families.

Family	Family background	*TRIP4* Exon	cDNA change	Protein change	Variation Type	Predict effect	Allele Frequency (ExAC)	Mutation previously reported?
A	Tunisia	2	c.141_142delAT (homozygous)	p.Tyr48Cysfs*3	Deletion	Frameshift	Not present	Unreported
B	Burundi	4	c.534C>G	p. His178Gln	Substitution	Missense	0.00004942	rs200177653 (db SNP)
C	Turkey	11	c.1544_1547delACTG	p.Asp515Alafs*34	Deletion	Frameshift	Not present	Unreported
		8	c.1065delC (homozygous)	p.Ile356Leufs*6	Deletion	Frameshift	Not present	Unreported
D	Spain	1	c.55_56insCT	p.Gln19Profs*47	Insertion	Frameshift	Not present	Unreported
		9	c.1197delA	p.Ser399Serfs*12	Deletion	Frameshift	Not present	Unreported
E	France	8+9	Homozygous deletion exons 8 and 9		Deletion	In-frame deletion	Not present	Unreported

dbSNP: Single Nucleotide Polymorphism Database; ExAC: Exome Aggregation Consortium.

The different variants were located along the entire length of the protein. These included the first *TRIP4* missense variant, affecting a highly-conserved residue in the Zinc finger domain (c.534C>G, p. His178Gln). Four mutations affected the ASCH domain (c.1544_1547delACTG [p.Asp515Alafs*34],

c.1197delA [p.Ser399Serfs*12], c.1065delC [p.Ile356Leufs*6] and homozygous deletion of exons 8 and 9, respectively). Finally, two frameshift mutations (c.55_56insCT [p.Gln19fs*47] and c.141_142delAT [p.Tyr48fs*3]) were predicted to lead to truncated proteins without both functional domains (Figure 4.9).

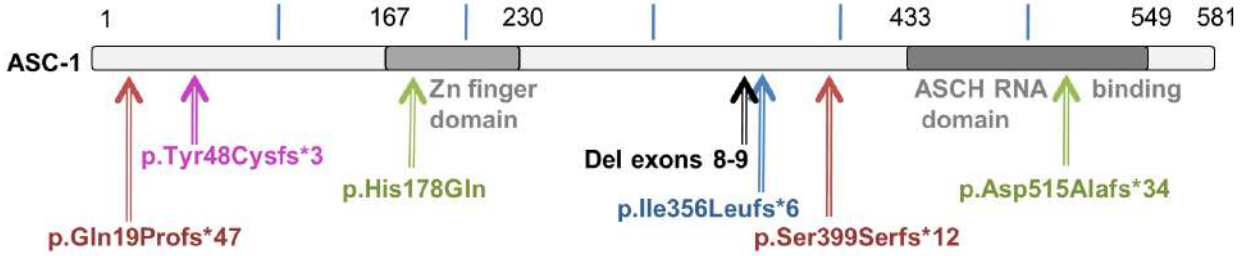

Figure 4.9. Schematic representation of the ASC-1 protein and localization of the patients' mutations. Colour code: pink, family A; green, family B; blue, family C; red, family D; black, family E.

Fibroblasts (family B) or muscle biopsies (families D, E and F) of five patients were analysed by Western blot. Compound heterozygosity for a missense and a truncating mutation affecting the two known functional domains of ASC-1 (family B) led to a reduced level of expression of the full-length protein (10-20% compared with control) (Figure 4.10a). Conversely, compound frameshift mutations (family D) or homozygous large deletions affecting the C-terminal part of the protein (family E) led to a total absence of full-length ASC-1 and no detectable truncated form (Figure 4.10b). ASC-1 expression in muscle from a patient from the first family reported (FII.1), harboring the recessive nonsense mutation c.G950A (NM_016213.4) or p.W297* (NP_057297.2)(Davignon *et al.*, 2016), was also analysed confirming its absence. Strikingly, both patients with severe (FII.1, DII.2) and milder forms (BIII.2, BIII.1, EII.4) had absence of detectable protein in muscle or fibroblasts.

None of the patients had mutations in other known neuromuscular genes except for the eldest patient (EII.4) in whom exome studies revealed a heterozygous variant of the titin gene (*TTN*) (c.6379_6380del, p.Tyr2127Leufs*8), also identified in one of his asymptomatic older sisters. This variant, predicted to lead to a truncated protein, was absent from ExAC and was not associated with any other *TTN* change (including missense variants) in the affected patient.

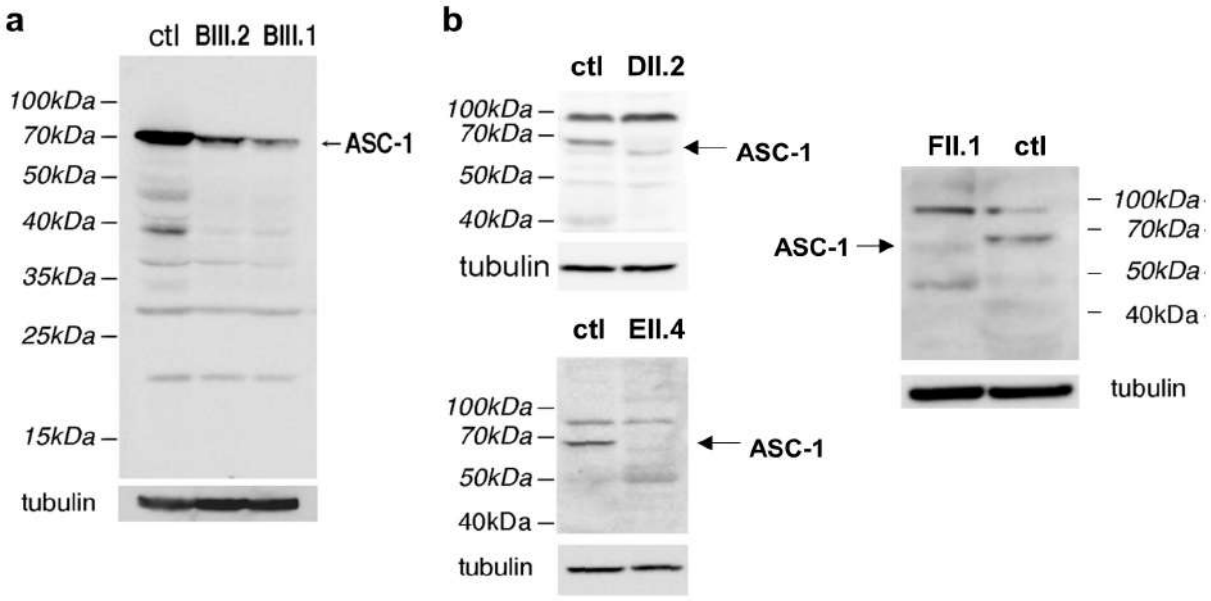

Figure 4.10. ASC-1 expression in patients' fibroblasts (a) and muscle tissue (b). Reduced expression of full-length ASC-1 (arrow) in fibroblasts from patients BIII.1 and BIII.2. (b) Full-length ASC-1 (arrows) was undetectable in muscle biopsies from patient DII.2, EII.4 and FII.1. ctl: Control fibroblasts (a), skeletal muscle control (b). Tubulin was used as a load marker.

4.4 DISCUSSION

Recessive mutations in the genes encoding different components of the ASC-1 complex are emerging as a novel cause of congenital neuromuscular disease, but its phenotypical spectrum remained to be defined. So far, four families have been described that harboured a total of three *TRIP4* mutations (encoding ASC-1), all with a severe neonatal phenotype (Davignon *et al.*, 2016; Knierim *et al.*, 2016). One of these families was reported as having a severe form of congenital myopathy while the three others were diagnosed of a form of prenatal spinal muscular atrophy marked by arthrogryposis multiplex congenital, respiratory distress and congenital bone fractures. In the present study, five additional families with seven novel *TRIP4* mutations are reported, expanding the phenotypical spectrum of the disease, beyond lethal congenital forms to mild ambulatory adult patients.

Overall, the clinical phenotype in these patients was characterized by early-onset axial and proximal weakness, progressive scoliosis -sometimes associated with rigid spine-, dysmorphic features, cutaneous involvement and respiratory failure of variable severity. No clinical, electromyographic or histological sign of motor neuron involvement was present in any of the patients reported here.

Unlike other congenital myopathies with minicores such as SEPN1-RM, in which patients need assisted ventilation while still ambulant (Ferreiro *et al.*, 2002b; Scoto *et al.*, 2011), in ASC1-RM the severity of respiratory involvement correlates with the degree of muscle weakness. Extraocular muscle involvement, previously unreported and present in two patients, might also be part of the phenotype and it is not correlated with disease severity.

The skin phenotype in ASC1-RM includes skin hyperlaxity, xerosis and follicular hyperkeratosis resembling COL6-RM (Bönnemann, 2011*a*), except for the absence of hypertrophic or keloid scars and absence of prominent joint contractures.

Disease course was stable in most patients. Remarkably, while the first patients identified never reached full ambulation (Davignon *et al.*, 2016), five of the novel patients reported here were able to walk without support, being limited mainly by respiratory failure and fatigability. In the mildest case the first referral signs were noticed in adolescence, and he remained able to climb stairs at the age of 63 years.

Interestingly, dilated cardiomyopathy was detected in two patients in the third and fifth decades. It has been previously shown that *TRIP4* expression is relatively high in murine cardiac muscle compared with limb muscles (Figure 4.11) (Davignon *et al.*, 2016).

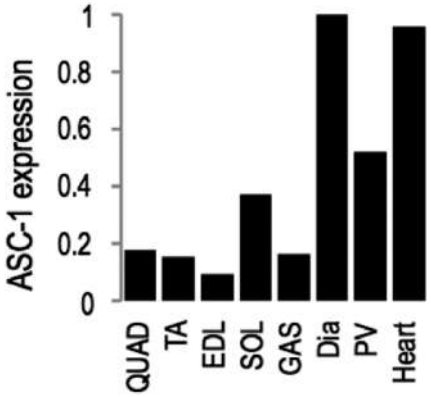

Figure 4.11. ASC-1 expression in adult murine striated muscles. Relative expression compared with GAPDH. Modified from (Davignon et al., 2016)

Moreover, neonatal cardiac involvement (i.e cardiomyopathy, secundum atrial septal defect or patent ductus arteriosus) was reported in two families with *TRIP4* mutations (Knierim *et al.*, 2016). The results of the present series confirm that cardiac disease is part of the clinical spectrum associated with *TRIP4* mutations, and reveal that the absence of congenital cardiac involvement at birth does not preclude the subsequent development of cardiomyopathy. Therefore, cardiac function should be periodically screened in patients with *TRIP4* defects, even if there are no signs of cardiomyopathy at

birth or in childhood.

Nonetheless, primary myocardial disease is not a typical feature in the CMs. When present in this context, it typically led to consider *TTN*- and *MYH7*-related myopathies (Tajsharghi and Oldfors, 2013; Oates *et al.*, 2018), more rarely *ACTA1*-related myopathy (North *et al.*, 2014). Dominant mutations in the *MYH7* gene are associated with hypertrophic or dilated cardiomyopathies and a wide range of skeletal muscle phenotypes from isolated hyperCKaemia and exertional myalgia to distal and scapuloperoneal myopathies, sometimes associated to scoliosis and rigid spine. Moreover, multi-minicores are part of the histopathological spectrum of *MYH7*-related myopathies (Cullup *et al.*, 2012). Dominant mutations of *ACTA1*, which are typically associated with nemaline, actin and intranuclear-rod myopathies, have been reported in a family with a congenital myopathy with adult onset hypertrophic cardiomyopathy and multi-minicore without rods or actin filament accumulations (Kaindl *et al.*, 2004).

Interestingly, the eldest of the ASC1-RM patients diagnosed with DCM carried a heterozygous truncating variant in the *TTN* gene (c.6379_6380del, p.Tyr2127Leufs*8). Heterozygous *TTN* truncating variants are fairly common in the general population, as they can be present in up to 1% of nominally healthy individuals (Franaszczyk *et al.*, 2017; Ware and Cook, 2017) and have never been demonstrated to cause congenital skeletal muscle disease by themselves. Indeed, congenital titinopathies are autosomal recessive retractile myopathies associated with the combination of either two truncating mutations or one truncating and one missense changes (Chauveau *et al.*, 2014*a*; Evilä *et al.*, 2014; Oates *et al.*, 2018; Savarese *et al.*, 2018). In this patient, no other *TTN* variant has been detected that could contribute to explain his muscular phenotype. Such *TTN* variant was also carried by an older sister with normal neurological and cardiological examinations. Moreover, his muscle MRI was comparable to that of the other patients with *TRIP4* mutations. For all these reasons, his skeletal muscle phenotype is most likely explained by the large homozygous *TRIP4* deletion leading to absence of full-length ASC-1. However, although his *TTN* variant has never been reported in DCM patients and does not affect the domains of the titin protein most commonly associated with cardiomyopathy (exon 49, A-band or distal I band) (Schafer *et al.*, 2017), a potential digenic contribution to his cardiac phenotype cannot be fully excluded at this point. In the other *TRIP4*-mutant patient with adult-onset DCM, linkage and exomic studies excluded pathogenic *TTN* changes (Davignon *et al.*, 2016).

The spectrum of muscle fibre architectural lesions associated to ASC1-RM is particularly large. Aside from the multiminicores, cap lesions and mild dystrophic lesions previously reported (Davignon *et al.*, 2016), nemaline and cytoplasmic bodies can also be found. This identifies *TRIP4* as a novel culprit gene for nemaline myopathy, as well as for other forms of congenital muscle disease (including cap disease, core, centronuclear or cytoplasmic-body myopathies and congenital muscular dystrophy), that should be included in the corresponding diagnostic gene panels. Furthermore, one biopsy showed rimmed fibres (with intense oxidative rims beneath the sarcolemma) comparable to those recently reported in patients with *ASCC1* mutations (Böhm *et al.*, 2018). Indeed, muscle biopsies from patients with *ASCC1* mutations also showed prominent myofibrillar disorganization and enlargement of the Z-bands. This suggests that the proteins encoded by *TRIP4* and *ASCC1* are implicated in a common pathophysiological pathway leading to multiple forms of myofibrillar disarray, and thus to an overlap of different histopathological congenital myopathy lesions.

Interestingly, accurate measurement of muscle fibre size in quadriceps biopsies from two patients revealed type 1 fibre hypotrophy in both, which is a relatively common finding in CMs, but additional type 2 fibre hypotrophy in one of them. Further studies are needed to clarify whether it may be a hypotrophy of both types of fibres, which could be related to the pathomechanisms involved in ASC1-RM and particularly to the potential role of ASC-1 in several stages of myogenesis (proliferation and muscle fibre growth).

Although complex, the histopathological pattern can be useful for the differential diagnosis of ASC1-RM. The joint hyperlaxity, mild to moderate joint contractures, spinal rigidity and skin phenotype observed in some of our patients can raise the differential diagnosis with COL6-RM (Bönnemann, 2011*b*), although *TRIP4* mutant patients had no hypertrophic or keloid scars. Moreover, minicore-like lesions may be occasionally found in patients with COL6-RM (Bönnemann, 2011*a*, *b*). Extraocular muscle involvement, previously unreported, may be part of the ASC1-RM spectrum but is typically absent in congenital titinopathies (Oates *et al.*, 2018). One of the patients with dilated cardiomyopathy had rigid spine and developed mild elbow contractures with age, features that overlap with Emery Dreifuss muscular dystrophy. However, the conduction defects and marked contractures typical of the latter were absent in ASC1-RM patients.

Muscle imaging is a valuable tool for assessment and differential diagnosis of early onset muscle disorders, since the pattern of muscle involvement can be represented by heatmaps which constitute

"fingerprints" of every particular condition (Quijano-Roy *et al.*, 2012). Muscle MRI of the lower limbs in three ASC1-RM patients revealed a consistent pattern with predominant involvement of the posterior compartment of the thigh and relative preservation of semitendinosus, gracilis and sartorius, associated in two cases with increased subcutaneous adipose tissue (Davignon *et al.*, 2016). This MRI pattern differed from the typical abnormalities associated with COL6-RM. Indeed, COL6-RM is associated with a characteristic fatty replacement starting around the fascias surrounding the muscle, typically affecting the rectus femoris and vastus lateralis muscles with the so-called "central shadow" (Mercuri *et al.*, 2005; Bönnemann, 2011*b*). ASC1-RM radiological pattern also differs from the ones described in other congenital myopathies with minicores. For instance, those related to *SEPN1* mutations have predominant axial involvement, with more severe changes in the paraspinal muscles, the gluteus magnus and the thigh (adductor magnus, sartorius and biceps femoris), and absence or severe atrophy of the semimembranosus muscle (Hankiewicz *et al.*, 2015). *RYR1* mutations mainly affect the gluteus maximus and posterior thigh, with relative preservation of rectus femoris, adductor longus and semitendinous (Jungbluth *et al.*, 2004). Finally, MRI changes associated with *TTN* mutations predominantly involve the gluteus minimus and medianus, semitendinous, sartorius and gracilis(Carlier and Quijano-Roy, 2019). Furthermore, the increase in subcutaneous adipose tissue in the lower limbs contrasts with the diffuse lipoatrophy observed in muscle MRI of some SEPN1-RM patients. Further studies, preferentially with full-body MRI, are needed to confirm the specificity of this ASC1-RM radiological pattern.

Inheritance of the disease was autosomal recessive in all cases. The seven novel *TRIP4* mutations were distributed along the entire length of the gene and include the first *TRIP4* missense mutation predicting an aminoacid change affecting the Zinc-finger domain, as well as five frameshift changes and one large deletion which are predicted to affect either one or both functional domains. Indeed, all of the latter predict a reduction or absence of full-length ASC-1 protein, which was experimentally confirmed in the three families from which biological material was available. Interestingly, ASC-1 was undetectable by Western blot both in the mildest and in the first severe cases reported, suggesting other severity modulators. Additionally, the patients reported as having severe SMA (Knierim *et al.*, 2016) carried *TRIP4* nonsense mutations resulting in exon skipping and upregulation of a shorter isoform which contained most of the functional domains of ASC-1, notably the Zinc-finger and ASCH domains. Although the muscle biopsies from these patients disclosed major reduction of myofibre size, suggesting a primary muscle component, it cannot be excluded that different molecular defects in the

TRIP4 gene might give rise to different phenotypical forms of disease. Along these lines, the present results suggest that the TRIP4 mutations leading to ASC-1 protein depletion may be associated with a primary striated muscle phenotype, while those leading to the expression of a truncated protein might be associated with motor neuron disease. Interestingly, a mechanistic role of the ASC-1 complex has been recently reported in other forms of motor neuron disease, as this complex has been proposed as a common link between amyotrophic lateral sclerosis (ALS) and SMA (Chi et al, 2018). A better understanding of the molecular mechanisms of ASC-1 related disease should help to fully clarify this point.

In conclusion, this work expands the clinical, histological and molecular spectrum of ASC1-RM, an emerging congenital myopathy, potentially contributing to a better recognition, diagnosis and management of these patients. The present results suggest that *TRIP4* mutations should be considered in any patient with histopathological features of a congenital myopathy and non-progressive muscular weakness without marked limb contractures, even in ambulant patients without clear neonatal signs, particularly if this phenotype includes respiratory insufficiency, cardiomyopathy or skin abnormalities. Moreover, the clinical and histological phenotypes associated with this disease stress the overlap between different congenital myopathies, which may share common pathophysiological pathways that need to be further explored. Finally, based on the identification of common histopathological lesions in *TRIP4*- and *ASCC1*-mutant patients, the term ‘ASC1-related myopathies’ could be coined to include pathologies associated with both genes and with potential defects of any other protein of the ASC-1 complex, whose relevance in muscle and/or motor neuron pathophysiology will likely increase in the future.

Chapter 5

ASC1-RELATED MYOPATHY PATHOPHYSIOLOGY

5.1 INTRODUCTION

Activating Signal Cointegrator–1 (ASC-1) is a transcriptional co-activator encoded by the *TRIP4* gene. It is a protein of 581 aminoacids (AA) and a molecular weight of 68 kDa (Kim *et al.*, 1999). ASC-1 is ubiquitously expressed in mammals. Indeed, in humans *TRIP4* mRNA expression has been detected in highest levels in the spleen, the thymus, the prostate, the testes, the ovaries, the gastrointestinal system, leukocytes, the heart and skeletal muscles. In mice, its expression has been found to be higher in the heart, the diaphragm and axial muscles (i.e. paravertebral muscles) compared with limb muscles (Davignon *et al.*, 2016).

Regarding its precise subcellular localization, it has been localized within the nucleus in HeLa cells (Kim *et al.*, 1999), rat fibroblasts (Kim *et al.*, 1999) and human fibroblasts(Knierim *et al.*, 2016). Nonetheless, recent studies have shown that ASC-1 can also be found in the cytoplasm in a melanoma cell line (Hao *et al.*, 2018), suggesting that its localization can be altered under pathological conditions.

Transcriptional co-regulators are emerging as the principal modulators of the functions of nuclear receptors and other transcription factors (Dasgupta *et al.*, 2014). They either bridge transcription factors and the basal transcriptional apparatus and/or remodel the chromatin structures (Jung *et al.*, 2002). Some of them are bi-functional proteins that can also participate in RNA splicing (Auboeuf *et al.*, 2002). The scarce available data suggest that ASC-1 may be a double-function protein with transcriptional activities but also with post-transcriptional properties in RNA processing events (Kim *et al.*, 1999; Iyer *et al.*, 2006).

ASC-1 (Figure 5.1) is known to interact with basal transcription factors (TBP, TFIIA), transcription

integrators (CBP, SRC-1) and nuclear receptors (TR, RXR, ER) *in vitro* through its highly conserved zinc finger domain (Kim *et al.*, 1999). In addition, ASC-1 contains a conserved C-terminal ASCH domain with putative RNA-binding activity that has been predicted *in silico* to coordinate pre-mRNA processing (Auboeuf *et al.*, 2002; Iyer *et al.*, 2006). All these data suggest the involvement of this co-activator in the proliferation-differentiation pathway.

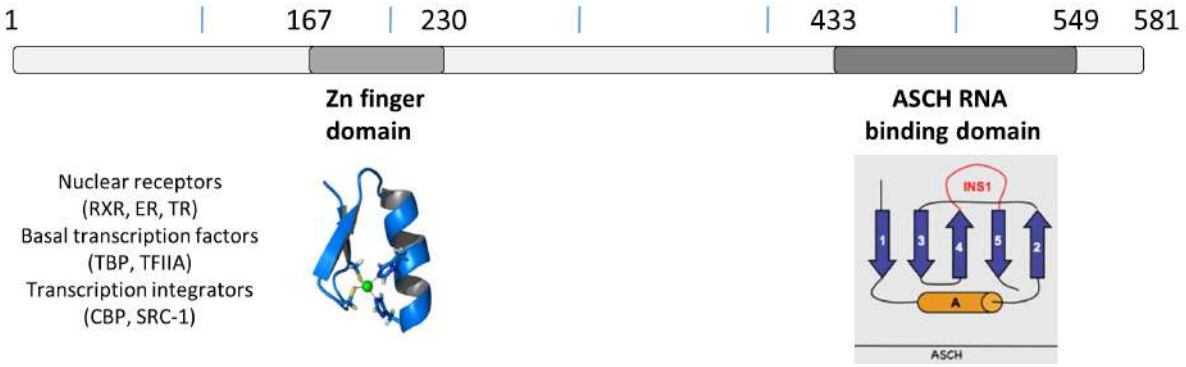

Figure 5.1. Schematic representation of the ASC-1 protein and its predicted domains. CBP: CREB-binding protein; ER: estrogen receptor; RXR: retinoid X receptor; SRC-1: steroid receptor coactivator-1; TBP: TATA-binding protein; TFIIA: transcription factor IIA; TR: thyroid hormone receptor

ASC-1 forms a co-integrator complex named ASC-1 complex (Figure 5.2), composed of the following subunits: (i) ASC-1 (MIM: 604501); (ii) ASCC1 (MIM 614215), which has an RNA binding KH domain fused to a 2H RNA-phosphoeserase; (iii) ASCC2 (MIM 614216), a 100 kDa subunit whose precise structure and function remains unknown, and (iv) ASCC3(MIM 614217), the largest subunit (200 kDa), an RNA helicase which shows paralogy to the small nuclear ribonucleoprotein 200 and is involved in RNA splicing (Jung *et al.*, 2002; Mazumder *et al.*, 2002).

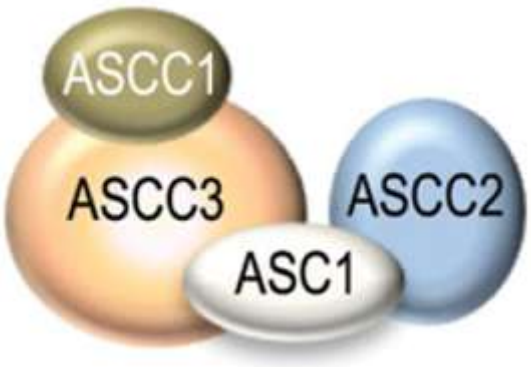

Figure 5.2. Activating signal cointegrator (ASC-1) complex.

Hence, ASC-1 complex is likely to be a ribonucleoprotein complex that participates in transcriptional coactivation and in RNA processing events. It acts as a co-activator through direct binding to transcription factors like AP-1, NF-kappa-B and Serum Response Factor (SRF), involved in cell fate-controlling pathways including proliferation and differentiation (Jung *et al.*, 2002). Interestingly, it has been also found that ASC-1 modulates the expression of PAI2 inhibitor (anti-apoptotic plasminogen activator inhibitor-2) in gastric cancer cells (Almeida-Vega *et al.*, 2009) and that it may be involved in mechanisms related with aging in *C. elegans* larvae (Cherkasova *et al.*, 2000). *TRIP4* has also been proposed as an Alzheimer's disease risk locus (Ruiz *et al.*, 2014). Moreover, a mechanistic role of the ASC-1 complex in motor nneuron disease has been reported lately, this complex being proposed as a common link between amyotrophic lateral sclerosis (ALS) and spinal muscular atrophy (SMA) (Chi *et al*, 2018).

Consistently with the patients' phenotype, ASC-1 levels are higher in axial than in limb murine muscles, and increase during differentiation from myoblasts to myotubes in C2C12 murine myogenic cells (Davignon *et al.*, 2016). Furthermore, depletion of ASC-1 in human cultured muscle cells and in *TRIP4* knocked-down C2C12 leads to a significant reduced myotube diameter (Davignon *et al.*, 2016). These data suggest that ASC-1 plays a pivotal role in late myogenesis, as its absence leads to defects in human myotube growth. Nevertheless, the pathophysiologic mechanisms involved in ASC-1 related muscle disease remain incompletely characterized, and the role of ASC-1 is largely unknown.

5.2 MATERIALS AND METHODS

5.2.1 Biological samples

Primary fibroblasts were obtained from skin biopsies of three patients with *TRIP4* mutations or surgically discarded tissues (age-paired controls). Two of the patients are the two siblings of family B (patients BIII.1, BIII.2) and the other one is a patient from the first family reported (Davignon *et al.*, 2016), termed family F in this study (FII.2). Muscle tissue was obtained from diagnostic muscle biopsies in two patients and from surgically discarded tissue in one (FIII.1). Patient muscles were biceps brachiallis (DII.2, biopsied at 27 years) and quadriceps (EII.4, 56 years). Control fibroblasts and muscles were obtained from a cell and tissue bank (Banque d'ADN et de Cellules du Généthon,

France; Myobank-AFM, France). Control muscles were ischiotibialis (Control 1, 38 years) and tibialis anterior (Control 2, 14 years).

Muscle samples and skin biopsies were obtained after informed consent from the patients or their guardians, in agreement with local Ethic Committees and the Declaration of Helsinki ('World Medical Association declaration of Helsinki: Ethical principles for medical research involving human subjects', 2013).

5.2.2 Cell culture

All cells were grown at 37°C in a humidified atmosphere with 5% CO2. Primary fibroblasts from patients and controls were grown in Dulbecco Modified Eagle Media (DMEM) containing Glutamax (Gibco), foetal calf serum (FCS) 20% and penicillin-streptomycin (P/S) 1%. Primary myoblasts from patients and controls were grown in F-10 Nutrient Mixture (Ham) containing L-Glutamine (Gibco), FCS 15%, P/S 1% and Chick Embryo Extract Ultrafiltrate (LifeSciences) 0.1%. The murine myoblast C2C12 cell line was grown in DMEM containing Glutamax (Gibco), FCS 10% and P/S1%.

5.2.3 Cell proliferation studies

For proliferation studies of primary fibroblasts, cells were seeded at a known concentration (40,000 cells per well) in 6-well plates and cultured for 4 days. Six wells were seeded for each sample. Numbers of cells per optical field (bright-field images, Zeiss Axio Observer A1 inverted microscope; three optical fields per well) were counted every 24 hours from 24 to 96 hours after seeding (Figure 5.3).

The proliferation rate of C2C12 cells was quantified in the absence or presence of ASC-1 24h after siRNA transfection by counting the number of cells per optical field from 24 to 72 hours (Figure 5.4). Four wells were seeded for each condition (NT: non-transfected; Scbl: scramble-transfected cells; siTrip4: cells transfected with the siRNA directed against *Trip4*) and three optical fields per well were counted.

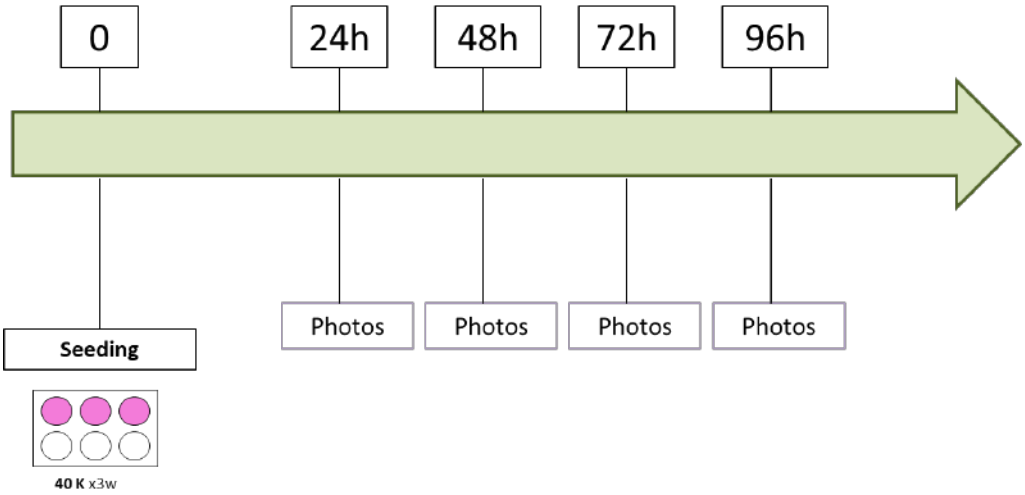

Figure 5.3. Schematic representation of primary fibroblasts proliferation studies

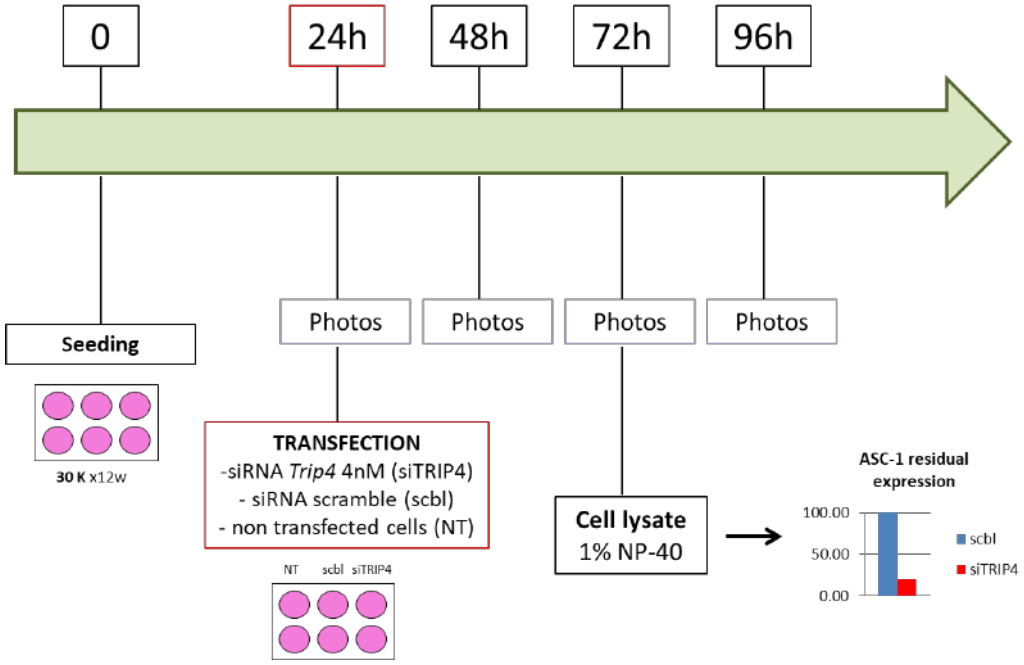

Figure 5.4. Schematic representation of C2C12 proliferation studies. NT: non-transfected; Scbl: scramble-transfected cells; siTrip4: cells transfected with the siRNA directed against Trip4.

5.2.4 Cell size measurements

C2C12 cultures were imaged on a Zeiss Axio Observer A1 inverted microscope at different times (24-48-72-96 hours) after seeding. Measurements (length and width) of cells were conducted on bright-field images with Image J (National Institute of Health, Bethesda, MS, USA). Three independent experiments were performed. Fibroblasts were imaged 24 hours after seeding and the surface was measured on bright-field images with ImageJ.

Primary fibroblasts were seeded in 6-well plates for 24 hours. Three bright-field optical fields (X10) per well were imaged to measure the cell surface. There were 6 well per condition (NT, Scbl, SiTrip4).

Surface measurement was performed using Image J (National Institute of Health, Bethesda, MS, USA). Measurement was performed only at one time point (24 hours after seeding). Point times beyond 24 hours were not useful due to the high overlap between cells which hindered an accurate measurement.

5.2.5 FACS Analysis

Fibroblasts and C2C12 cell cycle distributions were measured using Fluorescence Activated Cell Sorting (FACS). For fibroblasts, analysis was performed on control or patient cells in exponential cell growth. Two independent FACS analyses were conducted for each sample. Each patient was coupled with a control for each experiment.

Regarding C2C12, cells were seeded in a 6-well plate at densities of $6x10^4$ cells per well. Three conditions were stablished: non-transfected cells, cells transfected with si*Trip4* and cells transfected with scramble siRNA. Cells were harvested 48 hours after transfection and fixed in ice-cold 70% ethanol at -20°C overnight. Ethanol was removed and cells washed twice in Phosphate-Buffered Saline (PBS) before staining for 30 minutes at 37°C with 50µg/ml of propidium iodide in the presence of 0.1 or 1% triton and 100 or 50 µg/ml RNase A for fibroblasts or C2C12, respectively. Analysis was performed on 10^6 cells of each sample with a Cyan ADP analyser, and FlowJo software was used for data analysis.

5.2.6 Population doubling time and cell phase duration

The doubling time of primary fibroblasts or C2C12 was calculated using the website doubling-time.com/compute.php (Roth, A., 2006, Doubling time computing) and the formula

$$DoublingTime = \frac{\text{Duration} * \log(10)}{\log(\text{Final Concentration}) - \log(\text{Initial Concentration})}$$

Final and initial concentrations corresponded to numbers of cells counted during the exponential growth of cell cultures, i.e. number cell values at 48 and 24 hours respectively. The duration of each

cell phase was obtained by multiplying the doubling time corresponding to each cell sample by the percentage of cells recovered in G0/G1, S or G2M phases displayed by FACS analysis.

5.2.7 Transfection: siRNA and plasmid DNA

An *in vitro Trip4*KD model of C2C12 murine cell line had been previously developed and validated by our team (Figure 5.5). To silence the expression of *Trip4,* C2C12 were transfected with *Trip4*-specific siRNAs (siRNA1, 5'AGCACAAACUCAUCAAUAACUGUCT3'; siRNA2, 5'CGAUGAAUCAGAUUACUUUGCCAGT3') or scrambled negative control siRNA (Origene). Cells were seeded in a 6-well plate at a density of 4.5 x 10^4 cells per well and transfected 18 hours after seeding. Scramble and *Trip4* siRNA duplexes (8 pmol) were mixed with Lipofectamine RNAimax (Invitrogen) at a 1:2 volume ratio in serum-free medium (Opti-MEM) and added dropwise to each well. The final concentration of siRNAs was 4 nM. Maximal down-regulation (less than 20% residual expression) was achieved 48 hours post-transfection.

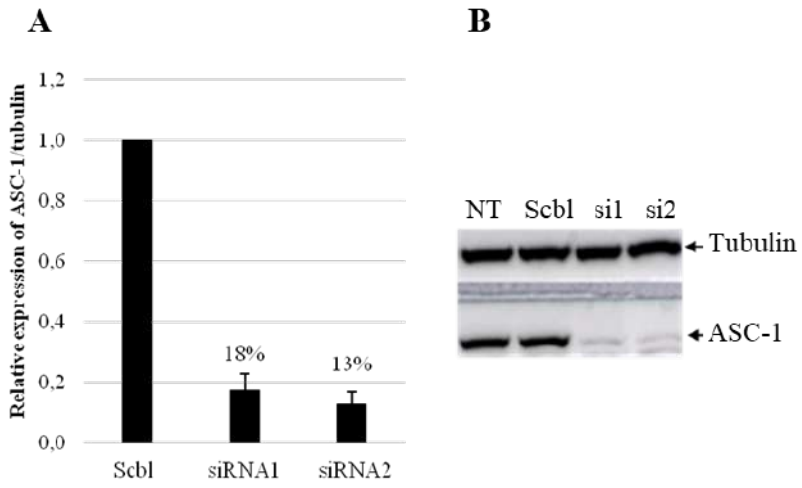

Figure 5.5. Trip4KD C2C12 model. A: Histogram representing the signal intensities of ASC-1 normalized to tubulin in cells treated with 4nM of siRNA 1 or 2 compared to the scramble control (Scbl). Signal intensity of the scramble control has been reported to 1. Values represent the mean ± SD of four different experiments performed to validate the model. B: Western blot analysis of the cell lysates from non transfected cells (NT) and cells treated with 4nM of siRNA1 (si1), siRNA2 (si2) or scramble (Scbl).

5.2.8 Rescue experiments

For rescue experiments, mammalian expression vectors (Promega) containing the ORF sequence of either the human *TRIP4* gene (pFN21AB7885) or the human *CELF1* gene (pFN21AB0039) fused with a HaloTag were used. Cells were seeded in a 6-well plate at a density of 7 x 10^4 cells per well and transfected 18 hours after seeding with a final concentration of scramble and *Trip4* siRNAs of 4Nm as described above. A second transfection was performed 24 hours later to overexpress the human *TRIP4* gene or the *CELF1* gene in the scramble or *Trip4* siRNA transfected or not transfected cells. Plasmids (1µg/well) and Lipofectamine 2000 reagent (5µl/well) were mixed in Opti-MEM according to manufacturer's instructions (Invitrogen) and added dropwise to the appropriate well. Cells were harvested 48 hours after the first transfection.

5.2.9 Western Blot

Transfected cells were washed twice with cold PBS and lysed with cold lysis buffer containing 25mM tris pH7.5, 150mM NaCl, 1.5mM MgCl2, 0.5mM EDTA, 1% NP-40, 1mM Dithiothreitol (DTT) and anti-protease and anti-phosphatase inhibitors (Roche). After 20 min incubation on ice, cells were scraped and centrifuged at 15 000g for 10 min at 4°C. The protein concentration of the supernatant was determined with the Bradford Protein Assay. Cell extracts (20 µg) were separated using 10% SDS-PAGE gel and transferred on nitrocellulose membranes using Bio-Rad Trans Turbo Transfer system. Nitrocellulose membranes (Biorad) were blocked for two hours in TBS (10 mM Tris pH 8.0, 150 mM NaCl, 0.05% Tween-20) containing 5% dry milk and probed with primary antibodies including anti-ASC-1 (ab70627; Abcam), anti-tubulin (T5168; Sigma), anti-p21 (sc-397; Santa-Cruz), anti-cyclin D3 (sc-6283; Santa-Cruz), anti-cyclin D1 (sc-450; Santa-Cruz or DCS-6; Millipore for muscle samples), anti-pRb (G3-245; BD Pharmingen), anti-MHCe (F1.652; DSHB) diluted in TBS–1% milk and anti-halotag (G9211; Promega) diluted in TBS–3% BSA. Finally, membranes were incubated with secondary antibodies, goat anti-rabbit HRP conjugate (31460; Thermo Scientific) and goat anti-mouse HRP conjugate (31430; Thermo Scientific) for 1 h in TBS–1% milk at RT. Enhanced chemiluminescence (ECL, Bio-Rad) was used for detection of the signals. Quantification analysis was carried out using Image J software.

5.2.11 Statistical analyses

Results are expressed as mean ± standard deviation unless otherwise stated. Normality of data was evaluated using Shapiro-Wilk test. Statistics student's t-test (two samples) or one-way ANOVA test (three or more groups) were used for comparison between groups as appropriate. For cell surface comparison, Kruskal-Wallis test was used since data did not fit to a normal distribution. When comparing temporal evolution, time was considered as cofactor in order to obtain the comparison at each sampling point. Differences were considered significant if p-value was <0.05. All data were analysed with the SPSS® Statistics version 22.0 (Armonk, NY: IBM Corp.).

5.3 RESULTS

5.3.1 Analysis of cultured primary fibroblasts

Proliferation studies

While amplifying primary fibroblasts from patient with novel *TRIP4* mutations for Western blot studies, a faster growth of patient cells compared to healthy controls was noticed. Thus, we compared the proliferative rate of patient skin fibroblasts from families B (BIII.1 and BIII.2) and F (FII.2) with four primary fibroblast cultures from age-paired controls.

The two siblings from family B harboured two recessive mutations: c.1544_1547delACTG [p.Asp515Alafs*34], a frameshift mutation localized in exon 11, and a missense mutation c.534C>G [p. His178Gln] on exon 4 affecting the Zinc finger domain (Figure 5.6).

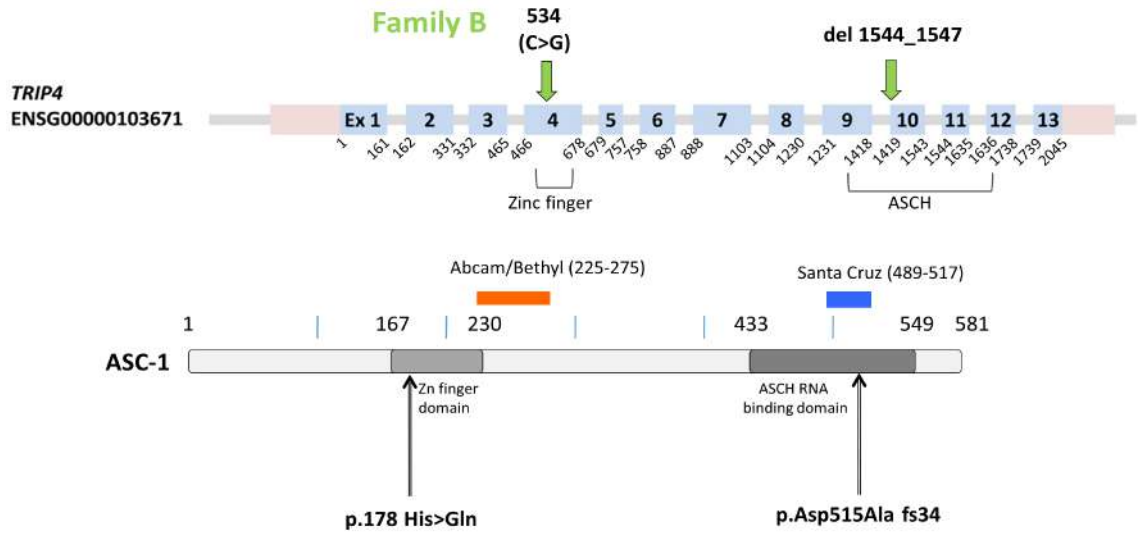

Figure 5.6. Schematic representation of the TRIP4 gene (upper panel) and ASC-1 protein (lower panel) with localization of the two mutations identified in family B.

ASC-1 expression in both patients was lower than 20% (Figure 5.7). Two different antibodies (Abcam and Santa Cruz) were used to assess ASC-1 residual expression, as they recognize two different epytopes (Figure 5.7). Interestingly, no truncated protein was detected.

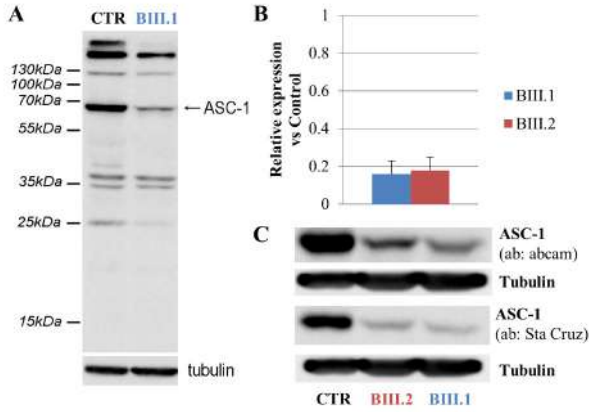

Figure 5.7. A, C: Detection of ASC-1 expression by Western Blot of fibroblasts lysates from patients BIII.1 and BIII.2 and control (CTR). B: Residual expression of ASC-1 (normalized to tubulin) in patient fibroblasts normalized to control expression.

Patient FII.2 carried a nonsense *TRIP4* variant localized on exon 7. The c.890G>A [p.Trp297*] mutation changes a highly conseved amino acid localized in a coiled coil domain and introduces a premature terminacion codon (PTC) leading to a predicted truncated ASC-1, devoid of its 284 most C-terminal amino acids. Nonetheless, this mutation resulted in *TRIP4* mRNA decay to around 10% of control levels and absence of detectable protein in patients cells (cultured fibroblasts, myoblasts and myotubes) (Davignon *et al.*, 2016) (Figure 5.8).

Figure 5.8 (next page): A: Family F pedigree. B: Schematic representation of ASC-1 protein and localization of the TRIP4 variant. C: Western blot of ASC-1 (antibody: abcam) in fibroblasts form patient II.1 and a healthy control (C) showing absence of ASC-1 expression in patient cells. In the control sample, there are two different bands including one at the full-length ASC-1 expected size (68 kDa) and a second 43 kDa band whose significance is unclear. D: Semi-quantitative electrophoresis gel showing reduced levels of the full-length TRIP4 cDNA (1.8 kbp) in fibroblasts from the heterozygous mother I.2 and severe transcript depletion both in fibroblasts and in primary cultured muscle cells from patients compared with control. (E): qRT-PCR on primary fibroblasts confirming major depletion of TRIP4 mRNA in patients (residual expression in II.2: 8.8%). Modified from Davignon et al., 2016.

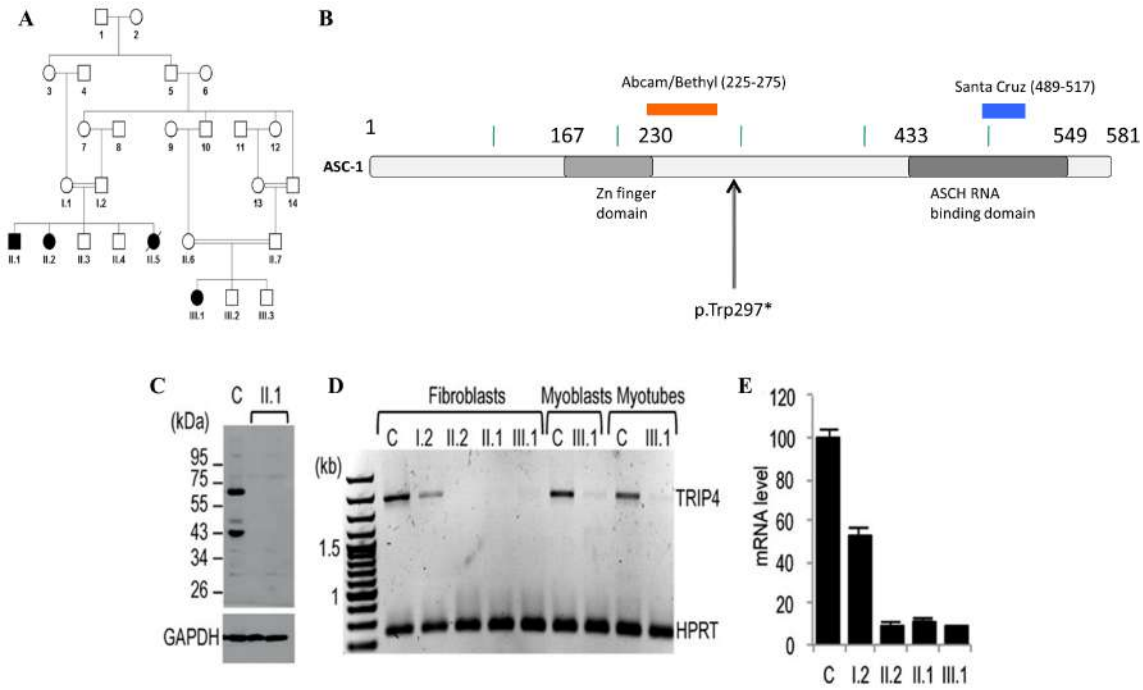

Figure 5.8. Figure caption in previous page.

To assess the proliferative potential of patient and control fibroblasts, brightfield pictures from cell cultures were taken every 24 hours to count the cells per optical field (figures 5.9 and 5.10).

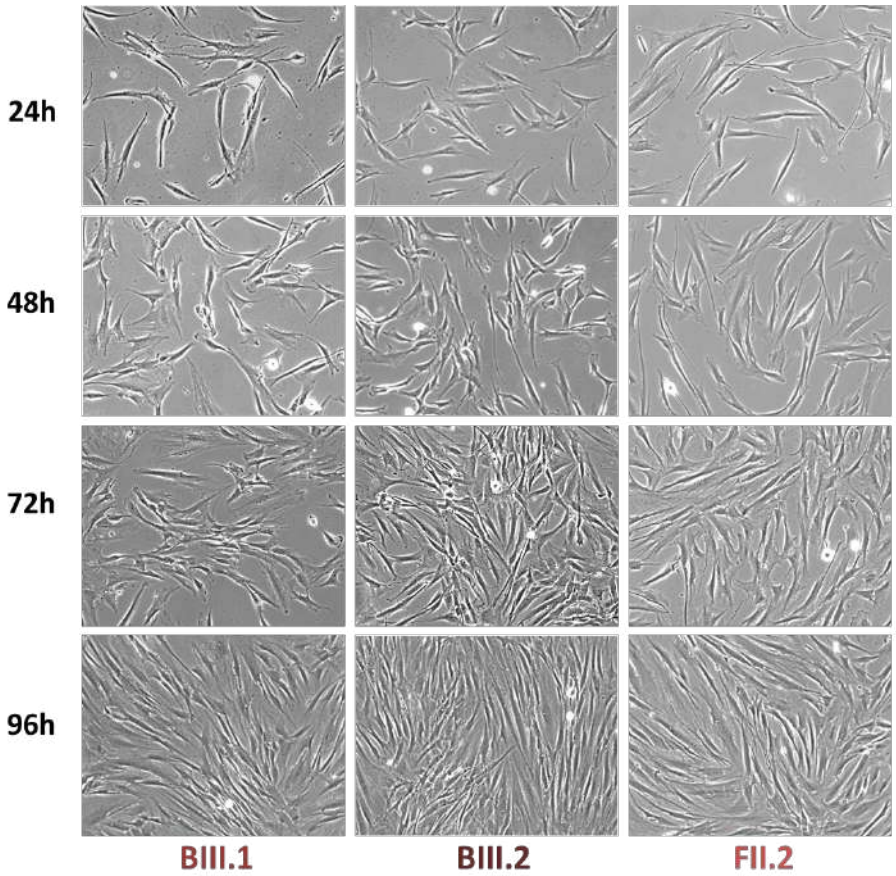

Figure 5.9. Bright-field pictures (X10) from three patient fibroblasts from 24 to 96 hours after seeding.

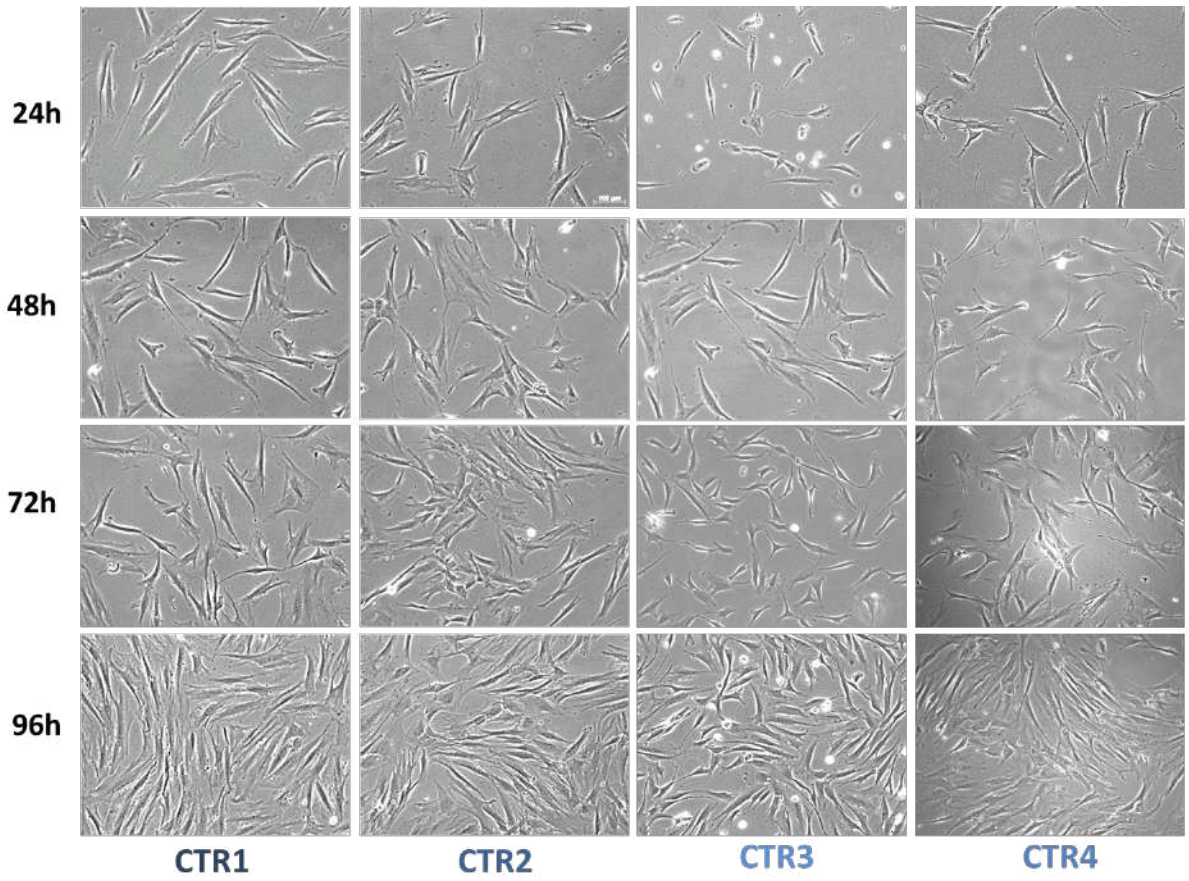

Figure 5.10. Bright-field pictures (X10) from four control fibroblasts from 24 to 96 hours after seeding.

Mean values at each point for each sample are summarized in Table 5.1 and represented in Figure 5.11. Both partial decrease (BIII.1-2) and complete absence (FII.2) of ASC-1 expression altered the proliferation capacities of patient fibroblasts.

Table 5.1. Number of cells per optical field at different time points.

Sample		BIII.1	BIII.2	FII.2	CTR1	CTR2	CTR3	CTR4
24h	Mean	39.56	47.56	40.5	29.83	28.44	29.94	28.44
	SD	4.69	5.63	5.82	4.71	4.23	5.56	3.85
48h	Mean	72.5	82.83	68.33	48.94	51.22	55.89	54.39
	SD	7.74	9.54	6.98	5.24	6.33	6.88	5.63
72h	Mean	118.44	138.67	113.28	72.28	80.83	86.17	82.22
	SD	8.31	17.49	4.51	12.09	8.72	10.35	8.45
96h	Mean	158.00	172.5	147.50	90.22	101.33	106.11	105.61
	SD	14.41	17.71	5.66	13.38	9.47	13.2	13.39

Three pictures per well and a total of 6 wells were used to calculate the mean number of cells at each point. CTR: control; SD: standard deviation.

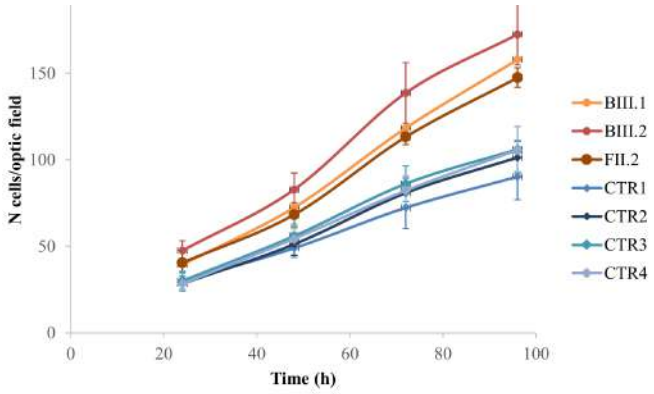

Figure 5.11. Proliferation curves of patient and control cultured fibroblasts. N: number; h: hours

Average patient and control number of cells at each point are represented in Figure 5.12. Differences between patient and control fibroblast proliferation curves are statistically significant (p= 0.001).

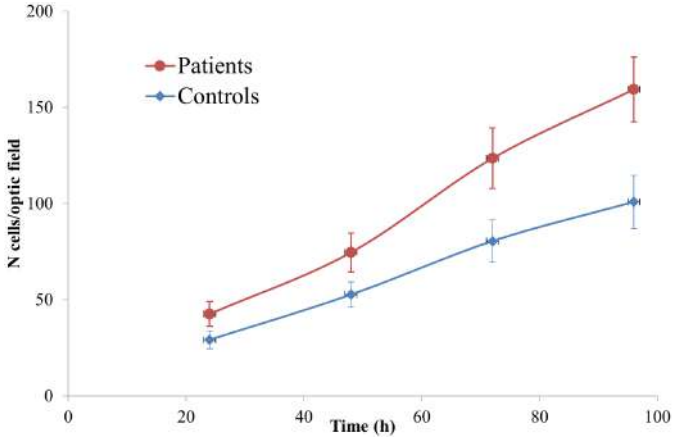

Figure 5.12. Curves representing the mean values of mean patient and control fibroblasts cells at each time point. h: hours; N: number.

Patient fibroblasts showed a significantly higher proliferation rate with lower mean doubling time compared with controls (p= 0.001) (Table 5.2), thus revealing a shorter cell cycle length.

Table 5.2. Doubling times of patient and control fibroblasts.

Doubling Times	well1	well2	well3	well4	well5	well6	Mean	SD
BIII.1	33.30h	30.55h	37.90h	37.19h	27.70h	39.38h	34.30 h	4.59
BIII.2	35.55h	39.53h	28.87h	29.02h	28.82h	34.04h	32.60 h	4.40
FII.2	33.19h	27.31h	33.66h	31.28h	36.67h	36.92h	33.17 h	3.20
						PATIENT	**33.38 h**	**0.80**
Doubling Times	**well1**	**well2**	**well3**	**well4**	**well5**	**well6**	**Mean**	**SD**
CTR1	34.07h	51.36h	56.59h	34.56h	46.46h	37.19h	43.37h	9.49
CTR2	33.68h	32.72h	40.18h	48.07h	48.89h	26.36h	38.30h	9.01
CTR3	33.94h	35.40h	41.63h	54.43h	41.83h	31.24h	39.70h	8.3
CTR4	49.81h	37.24h	48.68h	34.66h	34.17h	42.46h	41.17h	6.92
						CONTROL	**39.74 h**	**1.43**

CTR: Control; h: hours; SD: standard deviation

Cell cycle analysis by FACS

We analysed the cell cycle of non-synchronous fibroblast cultures from the two patients of family B (BIII.1 and BIII.2), patient FII.2 (Figure 5.13) and four controls (Figure 5.14).

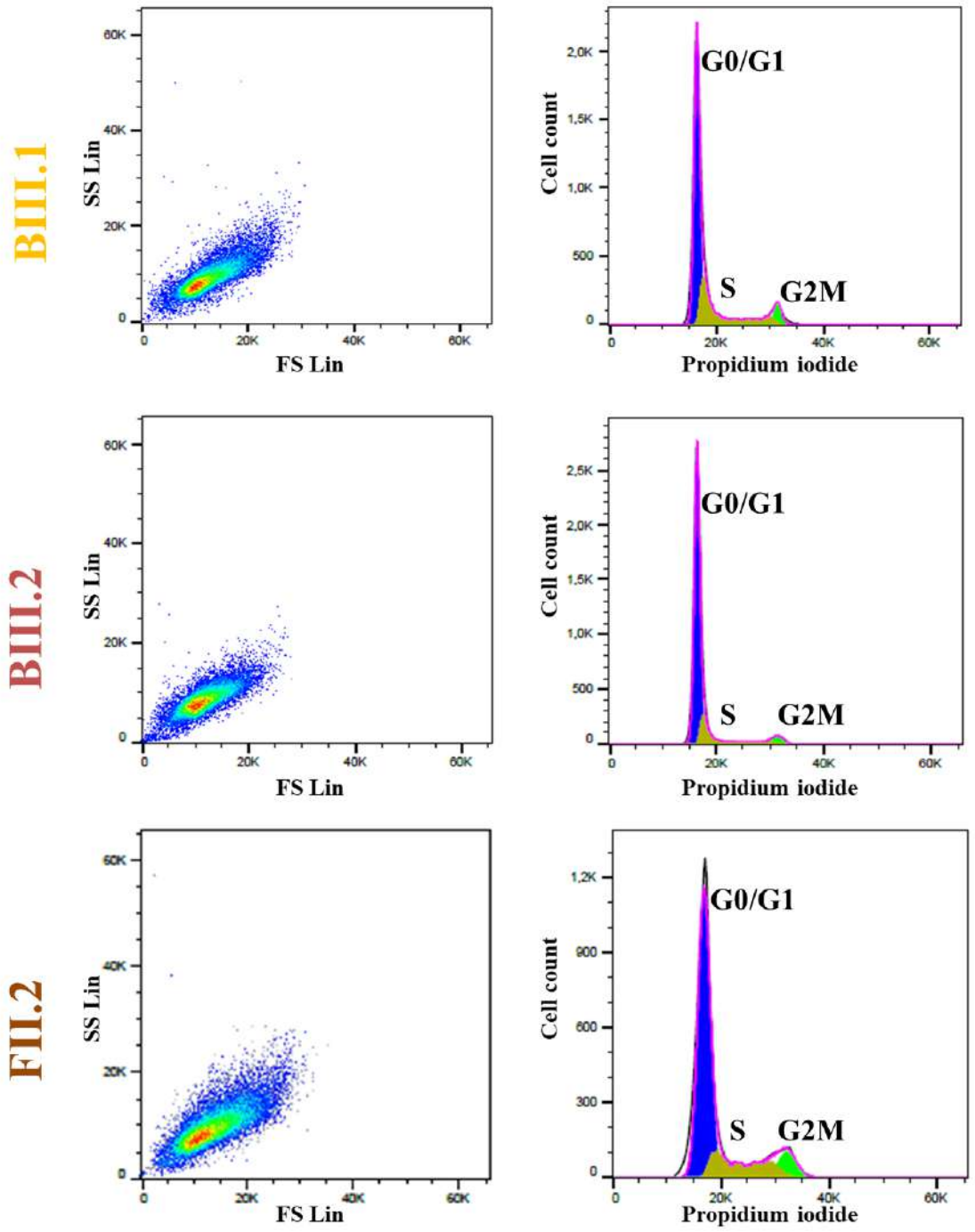

Figure 5.13. Cell cycle FACS analysis of the three patient fibroblasts samples. Dot-plots (left) represent the cell population of each sample. Histograms (right) show the distribution of the population according to each cell cycle phase. FACS: Fluorescence Activated Cell Sorting. FS Lin: Forward-scatter light intensity. SS Lin: Side-scatter light intensity.

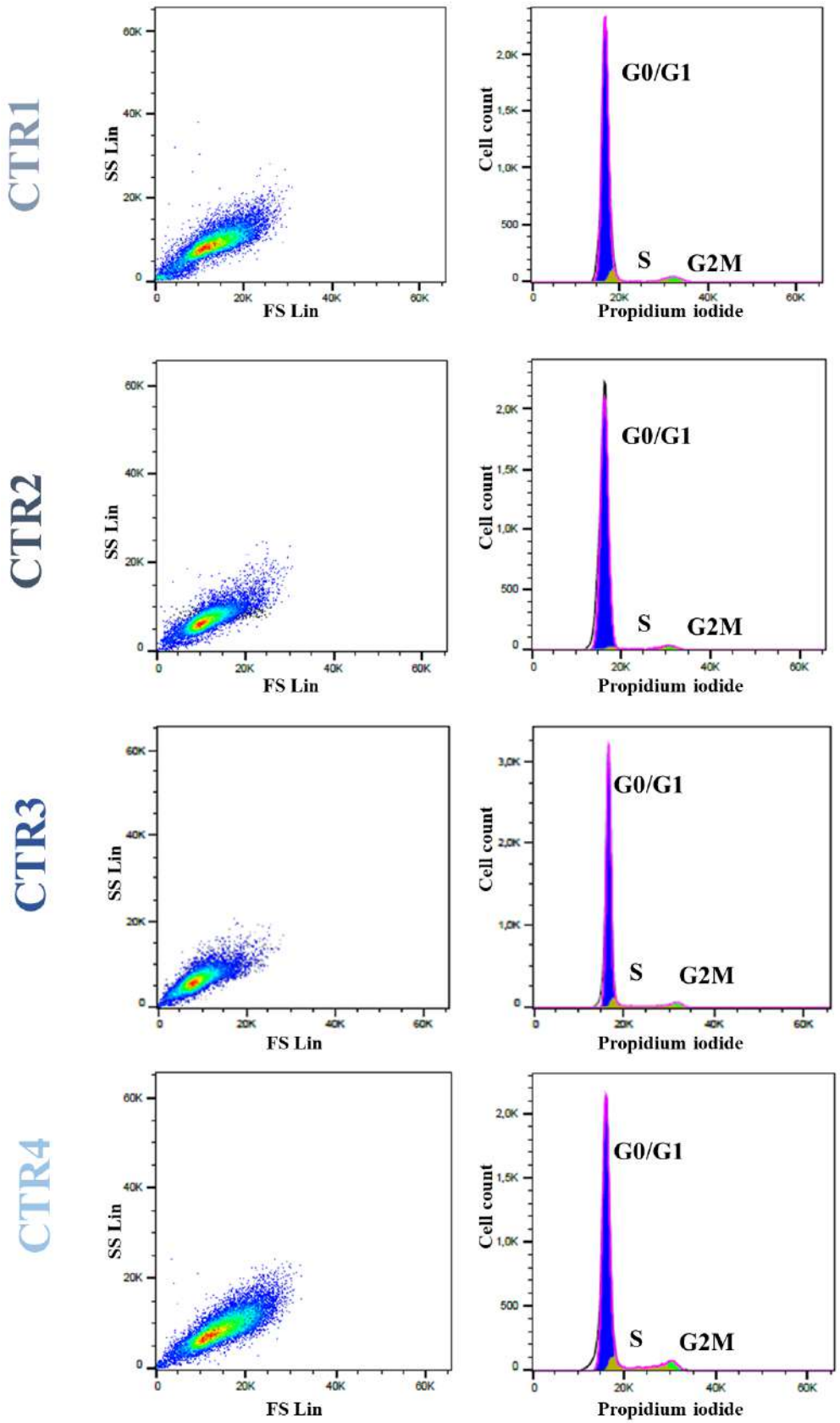

Figure 5.14. Cell cycle FACS analysis of the four control fibroblast samples. Dot-plots (left) represent the cell population of each sample. Histograms (right) show the distribution of the population according to each cell cycle phase. FACS: Fluorescence Activated Cell Sorting. FS Lin: Forward-scatter light intensity. SS Lin: Side-scatter light intensity.

The cell cycle profile in patient fibroblasts was significantly different from that of control fibroblasts (p= 0.01). Control fibroblasts were mainly in G0/G1 phase (more than 80% of the cells). Conversely, in patients there was a significant decrease in the number of cells in G0/G1 (p= 0.0027) with a parallel increase in the number of cells in S (p= 0.01) compared with controls (Figure 5.15).

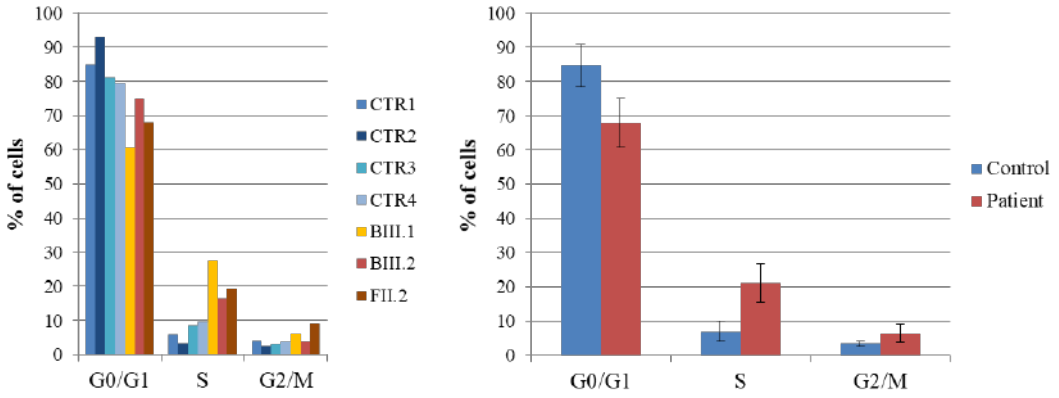

	Control fibroblasts		Patient fibroblasts	
	Mean	SD	Mean	SD
G0/G1 (%)	84.38	4.95	67.84	7.13
S (%)	7.08	2.4	21.54	5.66
G2/M (%)	3.45	0.76	5.87	2.22

Figure 5.15. Cell cycle distribution in patient and control fibroblasts. Percentage of cells of each sample for the different cell cycle phases (left) and mean control and patient percentages (right). SD: standard deviation.

Considering the cell cycle length determined for each sample, the duration of each cell cycle phase was calculated (Table 5.3).

Table 5.3. Duration of each cell cycle phase (expressed in hours) in control and patient fibroblasts.

Cycle phase	CTR1	CTR2	CTR3	CTR4	Mean Control	SD	BIII.1	BIII.2	FII.2	Mean Patient	SD
G0/G1	36.84	35.71	32.33	32.64	**34.38**	**1,93**	20.59	24.44	22.19	**22.41**	**1.57**
S	2.62	1.26	3.44	4.00	**2.83**	**1,02**	9.36	5.40	6.33	**7.03**	**1.69**
G2/M	1.79	0.95	1.19	1.60	**1.38**	**0,33**	2.14	1.25	2.94	**2.11**	**0.69**

CTR: control; SD: standard deviation

The temporal distribution of the cell cycle in patient fibroblasts was significantly different from that of control fibroblasts (p <0.0001). Moreover, the G0/G1 phase was significantly shortened in patient fibroblasts compared with control fibroblasts (p <0.0001), and the S phase was increased in parallel (p= 0.0318). (Figure 5.16 and 5.17).

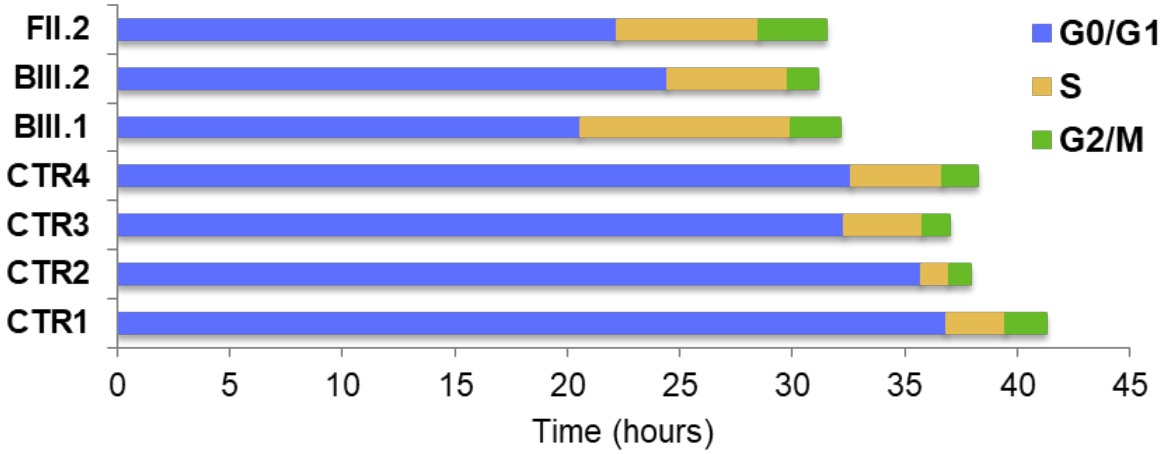

Figure 5.16. Graph showing the duration of each cell cycle phase in patient and control samples. CTR: control.

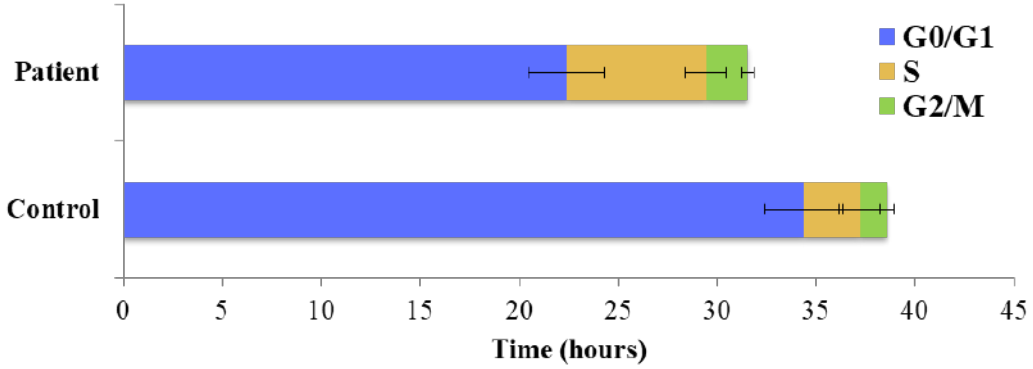

Figure 5.17. Mean values of patient and control fibroblasts cell cycle phase temporal distribution. There is a significant decrease in G0/G1 phase in patient fibroblasts versus control with a parallel increase in S phase duration.

Cell surface

Primary control and patient fibroblasts' surface was measured at 24 hours after seeding. Patient fibroblast showed an apparent thinner and longer aspect in bright-field images (Figure 5.18).

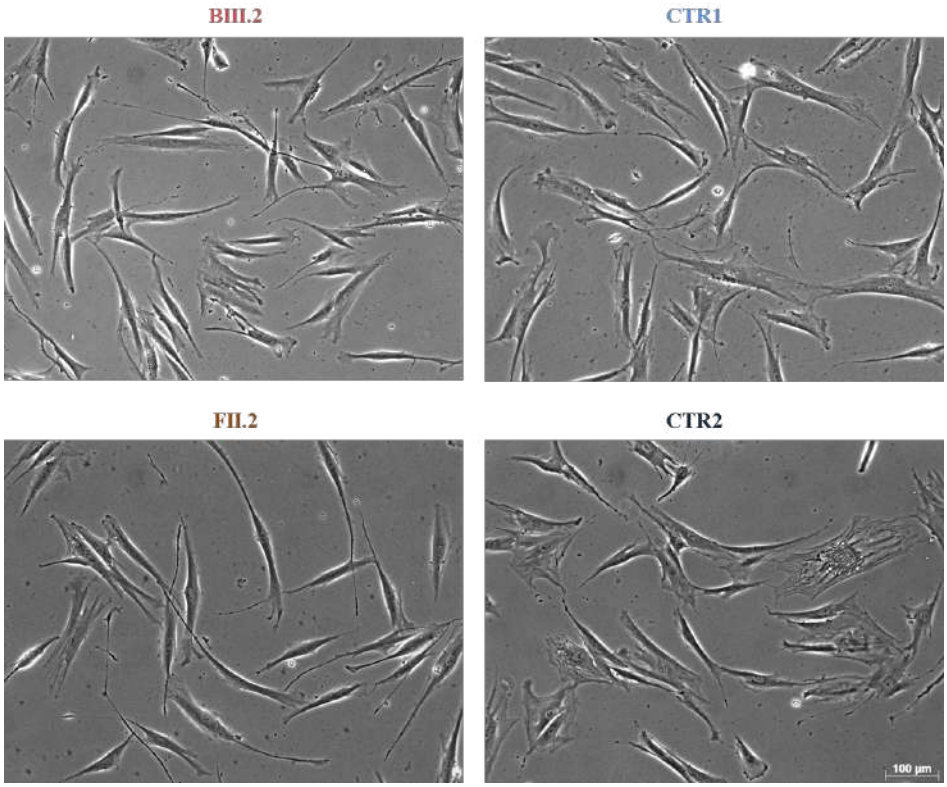

Figure 5.18. Bright-field images of cultured primary fibroblasts 24 hours after seeding

Control fibroblasts had a greater cell surface as compared with patient fibroblasts (p= 0.001) at 24 hours after seeding (Table 5.4 and Figure 5.19).

Table 5.4. Cell surface of primary fibroblasts (µm²).

	BIII.2	FII.2	Mean Patient	CTR1	CTR2	Mean Control
N	311	320	631	318	316	634
Mean	1563.98	1817.67	1692.64	2632.11	2692.69	2662.26
SD	586.99	678.96	646.85	936.76	877.49	906.83

CTR: control; N= cells analysed for each sample. SD: standard deviation.

Prominent cell overlap in culture hindered accurate cell surface measurement beyond 24 hours of culture.

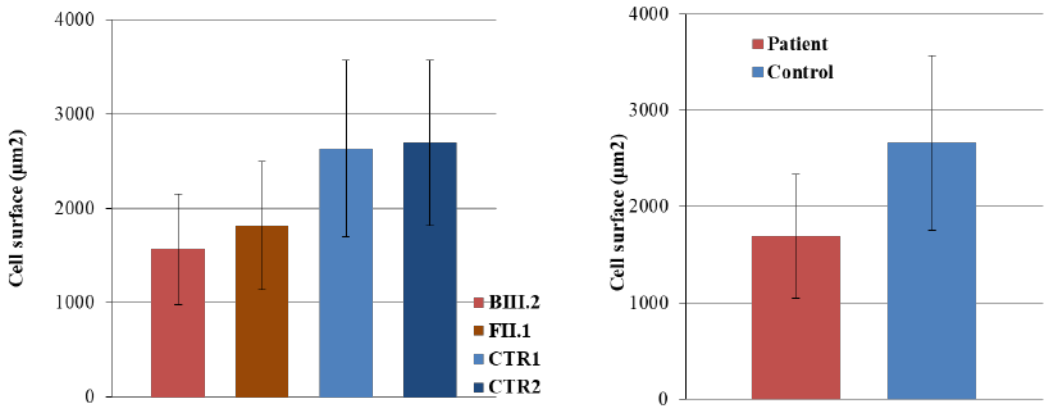

Figure 5.19. Graphs showing the mean cell surface (µm2) of each sample (left) and mean surface of patient and control fibroblasts (right).

5.3.2 C2C12 murine myogenic model

In order to further clarify the role of ASC-1 in myogenesis, the in vitro *Trip4*KD model of C2C12 murine cell line was studied. Three conditions were systematically analysed: cells transfected with the control siRNA (Scbl), cells transfected with the siRNA directed against *Trip4* (si*Trip4*) and non-transfected cells (NT). A strong reduction of more than 80% of the expression of ASC-1 was observed within 48 hours after transfection in all experiments.

Proliferation studies

Proliferation studies were conducted to analyse the proliferative potential of C2C12 cells both in the presence and in the absence of ASC-1 (Figure 5.20).

In the absence of Trip4 (siTrip4), there was a significant increase in the mean number of cells compared with scramble control (Scbl) at 48 and 72 hours after transfection (Table 5.5) (p= 0.01 at 48h and p= 0.001 at 72h).

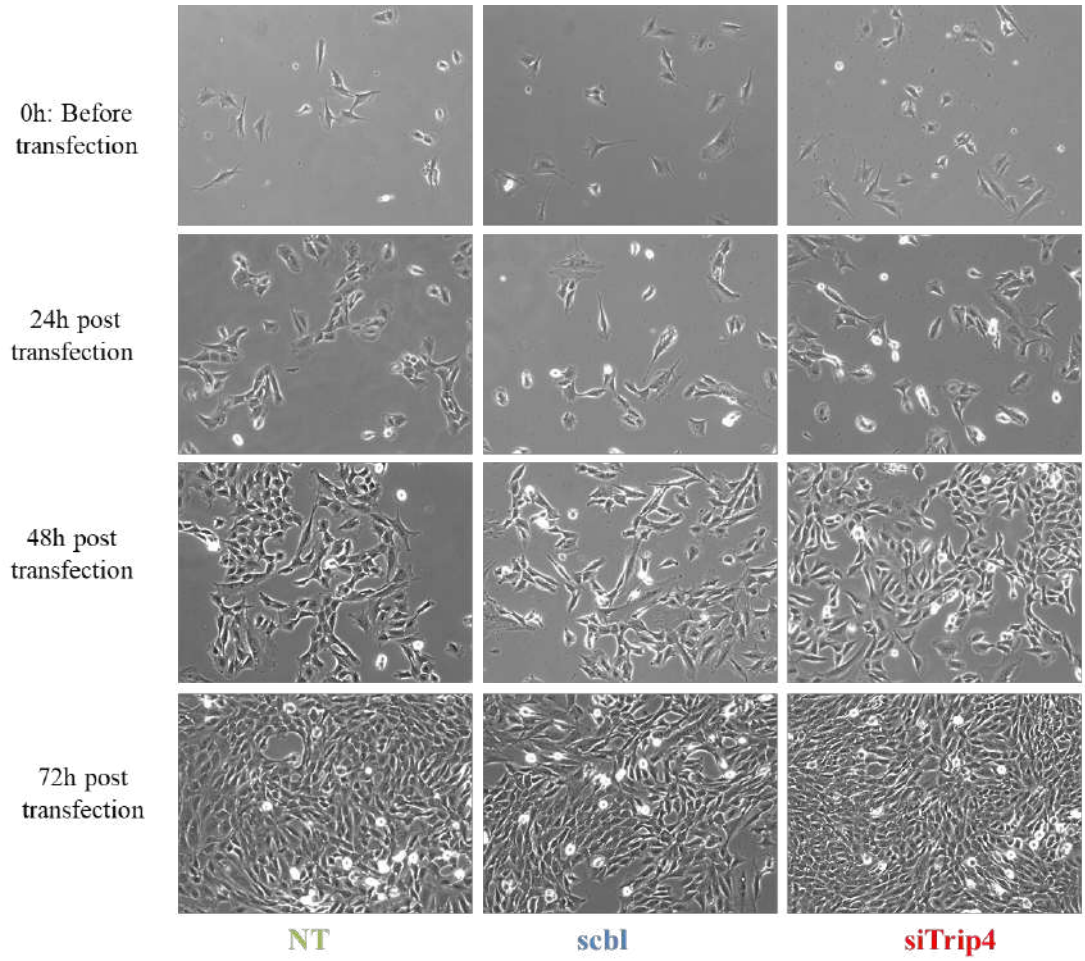

Figure 5.20. Proliferation studies in C2C12. Bright-field pictures of Trip4KD C2C12 (siTrip4) compared to non-treated (NT) or scramble (scbl) transfected controls from 24 to 72 hours post siRNA transfection

Table 5.5. Cell counting in C2C12 proliferation studies.

	Sample	NT	Scbl	siTrip4
0h	Mean	29.25	25.67	24.33
	SD	5.67	4.25	6.69
24h	Mean	82.5	68.58	80.08
	SD	20.75	15.81	23.83
48h	Mean	224.92	162.75	240.42
	SD	44.99	36.70	68.67
72h	Mean	580.11	399.11	621.89
	SD	99.84	38.15	60.49

Number of cells per optical field at different time points: 0h (before transfection) and 24-, 48- and 72h post transfection. Three pictures per well and a total of 4 wells were used to calculate the mean number of cells at each point. h: hours; *NT: non-transfected; Scbl: scramble-transfected cells; SD: standard deviation; siTrip4: cells transfected with the siRNA directed against Trip4.*

Overall, proliferation curves show a significantly increased proliferation of siTrip4 transfected cells compared to scramble transfected cells (p <0.001) (Table 5.5, Figure 5.21). No statistically significant differences were found between non-treated and *Trip4*KD cells.

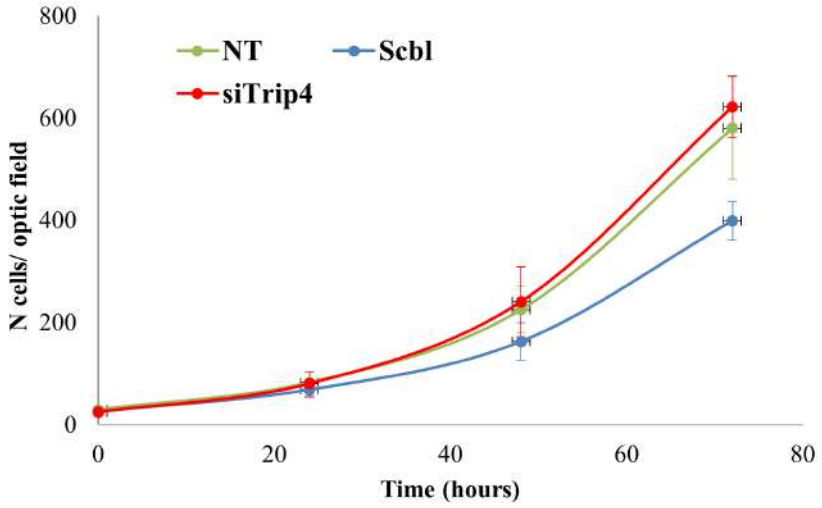

Figure 5.21. Proliferation curves of non transfected cells (NT), scramble control (Scbl) and Trip4KD (siTrip4). Overall, the proliferation curve of siTrip4 cells was higher than that from Scbl-transfected controls, maintaining values comparable to non-transfected cells. Values are the mean of four independent measurements for each time per condition.

Accordingly, *Trip4*KD C2C12 had the lowest doubling time, although differences did not reach statistical significance when compared to Scramble control (p=0.08) (Table 5.6).

Doubling time			
	NT	Scbl	siTrip4
W1	17.50	17.33	13.24
W2	14.82	18.94	17.35
W3	17.00	16.47	14.21
W4	17.06	27.58	15.84
Mean	**16.59**	**20.08**	**15.16**
SD	**1.04**	**4.41**	**1.57**

Table 5.6. Doubling time in C2C12. Doubling time per well (W) and calculated mean and SD (standard deviation) for each condition. Mean population doubling time was calculated for cells in exponential proliferation between 24 and 48h after transfection. NT: non-transfected; Scbl: scramble-transfected cells; SD: standard deviation; siTrip4: cells transfected with the siRNA directed against Trip4.

Cell cycle analysis (FACS)

Cell cycle was analysed by FACS in three non-synchronous cell populations (NT, Scbl and siTrip4) (Figure 5.22).

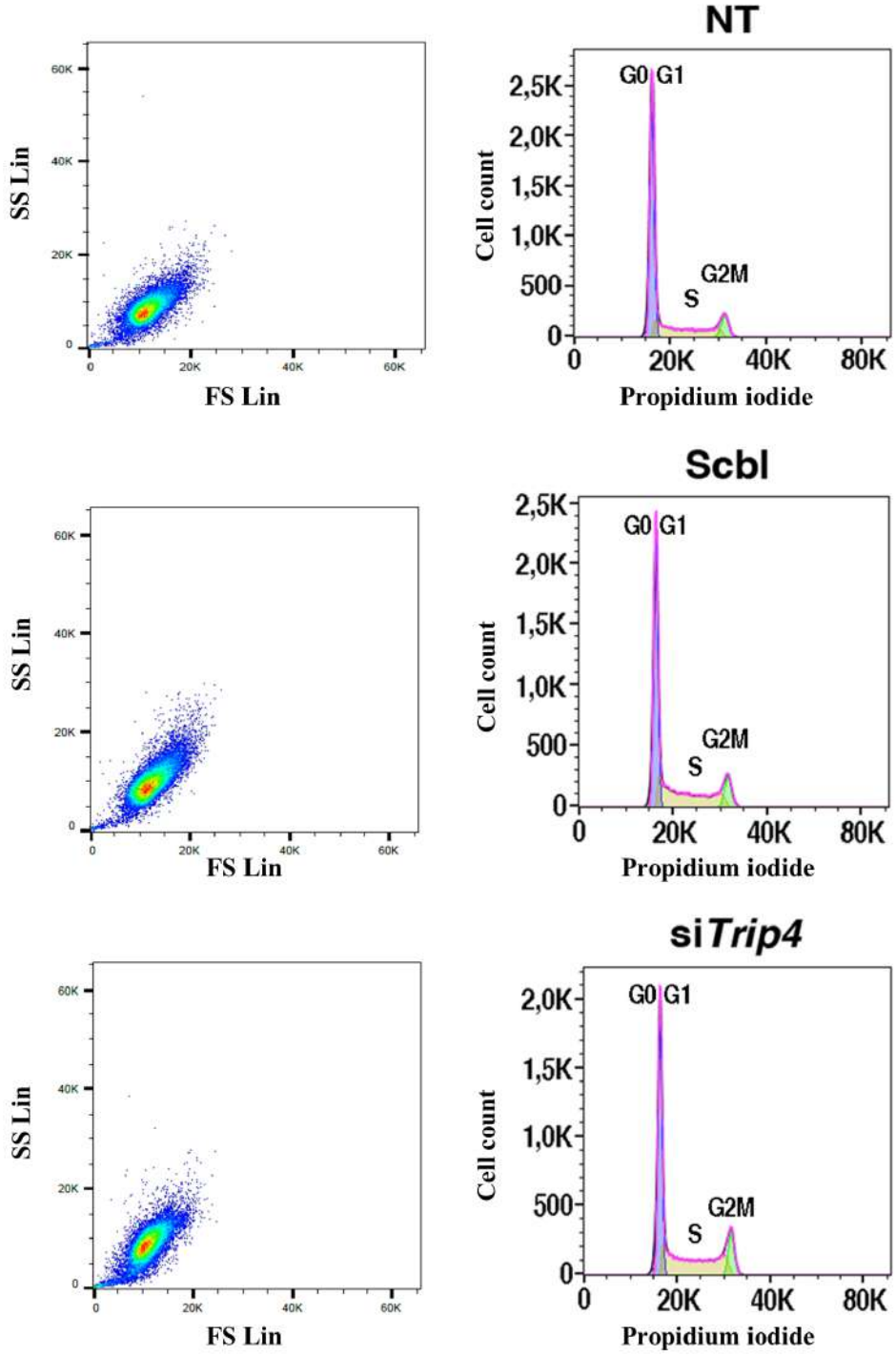

Figure 5.22. Cell cycle FACS analysis in C2C12. Analysis of the three conditions: non transfected (NT), scramble control (Scbl) and Trip4KD (siTrip4) C2C12 cells. Dot-plots (left) represent the cell population of each sample. Histograms (right) show the distribution of the population according to each cell cycle phase. FACS: Fluorescence Activated Cell Sorting. FS Lin: Forward-scatter light intensity. SS Lin: Side-scatter light intensity.

In three independent experiments, FACS studies showed a trend towards a decrease in the number of cells in G0/G1 phase and a parallel increase in cells in S phase for *Trip4* KD compared to Scbl and NT cells (Figure 5.23). Nonetheless, significant differences in the mean percentage of cells in each cell cycle phase were only found between SiTrip4 and NT (p= 0.01).

	NT		Scbl		SiTrip4	
	Mean	SD	Mean	SD	Mean	SD
G0/G1 (%)	60.13	4.71	54.30	6.18	51.07	3.35
S (%)	29.07	3.77	35.63	3.97	36.40	2.37
G2/M (%)	9.74	2.29	9.64	1.18	10.79	1.35

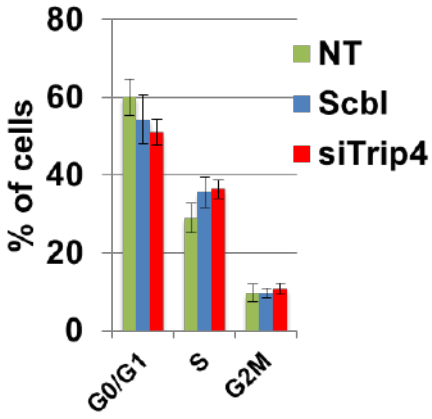

Figure 5.23. Cell cycle distribution in C2C12: mean percentage of cells in each cell cycle phase determined by FACS analysis. NT: non-transfected; Scbl: scramble-transfected cells; SD: standard deviation; siTrip4: cells transfected with the siRNA directed against Trip4.

Considering the cell cycle length determined for each sample, the duration of each cell cycle phase was estimated (Table 5.7).

Cell cycle phase duration (hours)		NT	Scbl	siTrip4
G0/G1	Mean	9.98	10.9	7.74
	SD	0.63	2.4	0.8
S	Mean	4.82	7.15	5.52
	SD	0.30	1.57	0.57
G2/M	Mean	1.61	1.94	1.64
	SD	0.10	0.43	0.17

Table 5.7. Cell cycle phase duration (hours). NT: non-transfected; Scbl: scramble-transfected cells; SD: standard deviation; siTrip4: cells transfected with the siRNA directed against Trip4.

Although the differences in cell cycle temporal distribution between *Trip4KD* cells and scramble-transfected cells were not statistically significant ($p = 0.06$), the duration of G0/G1 phase in *Trip4KD* cells was significantly decreased compared to Scbl ($p = 0.02$) (Figure 5.24).

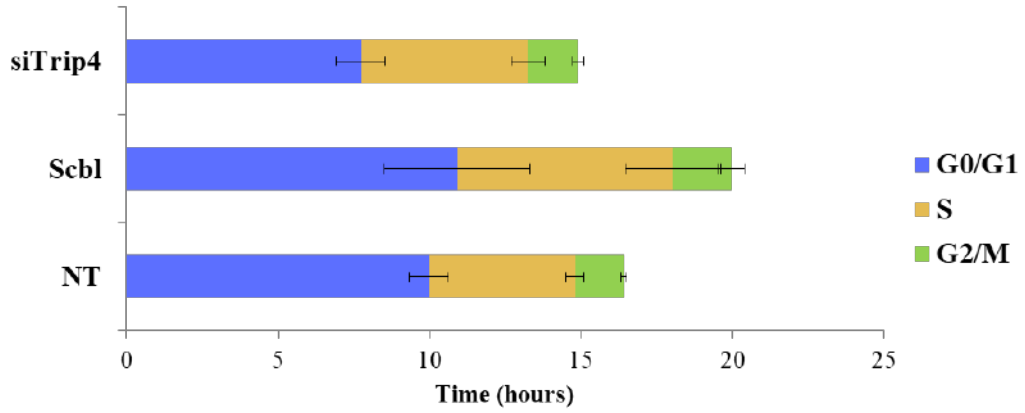

Figure 5.24 Temporal distribution of the cell cycle in C2C12. NT: non-transfected; Scbl: scramble-transfected cells; siTrip4: cells transfected with the siRNA directed against Trip4.

Furthermore, ASC-1 depleted cells (SiTrip4) exhibited a smaller cell surface (μm^2) compared to NT or Scbl cells after 24, 48 and 72h of culture ($p < 0.05$) (Figure 5.25).

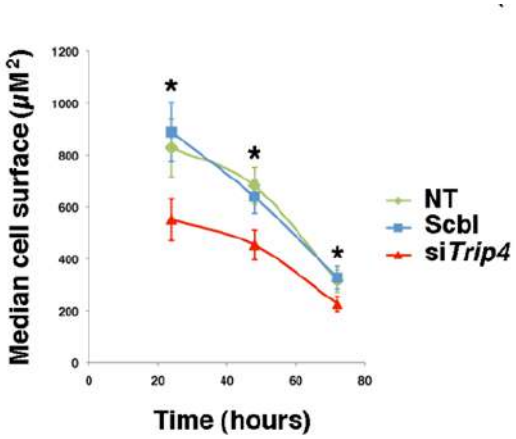

Figure 5.25. Median cell surface (µm2) in C2C12. ASC1 depleted cells (siTrip4) exhibited a smaller size (µm2) compared to non-treated (NT) or control siRNA (Scbl) after 24, 48 or 72h of culture, which is consistent with acceleration of the cell cycle.

5.3.3 Analysis of expression and phosphorylation of cell cycle exit regulators

Analysis of cell cycle regulators in muscle tissue

Analysis of the expression of cyclins D1, D3 and the cell cycle exit marker p21 in frozen muscle samples showed a decrease in cyclin D1 expression and an increase in cyclin D3 in three *TRIP4* mutant patients compared to control. Additionally, the level of p21 was decreased in the two older patients (Figure 5.26A-B). Embryonic myosin heavy chain was not detectable by Western blot (Figure 5.26C).

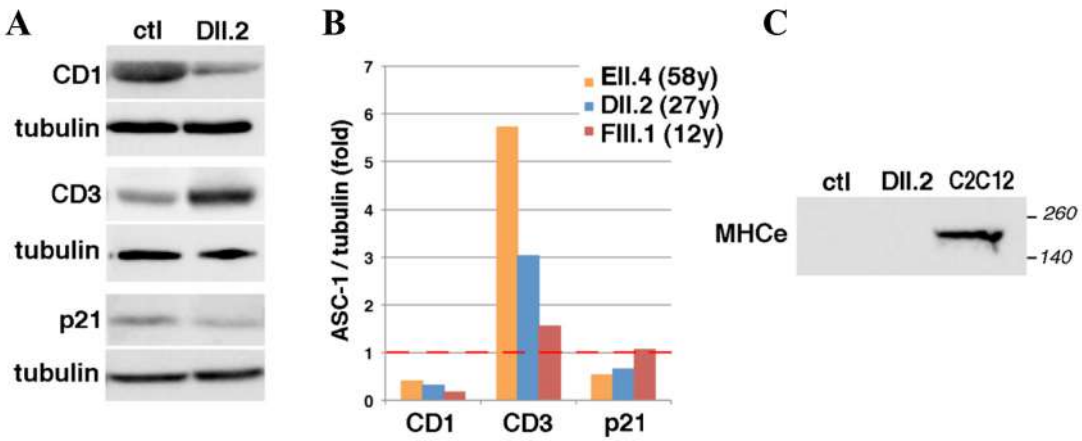

Figure 5.26. Altered expression of cell cycle related proteins in patient muscles. (A) Western blot of lysates from control (ctl) patient DII.2. (B): Graph showing the relative expression of cyclins D1 and D3 an p21 in patients DII.2, EII.4 and FIII.1 (control expression normalized to 1, dashed red line). (C): Absence of embryonic Myosin Heavy Chain (MHCe) in both patient DII.2 and control muscle samples excluded that this might be due to active muscle regeneration in patients. C2C12 was used as a positive control.

Analysis of cell cycle regulators in C2C12 murine myogenic cells

Cyclin D1, D3 and p21 expression was also quantified during myoblast proliferation in C2C12. *Trip4*KD C2C12 myoblasts showed a significant increase in cyclin D1 and p21 (p <0.05) (Figure 5.27). However, there were no significant abnormalities in cyclin D3 expression in *Trip4*KD C2C12 myoblasts (Figure 5.28).

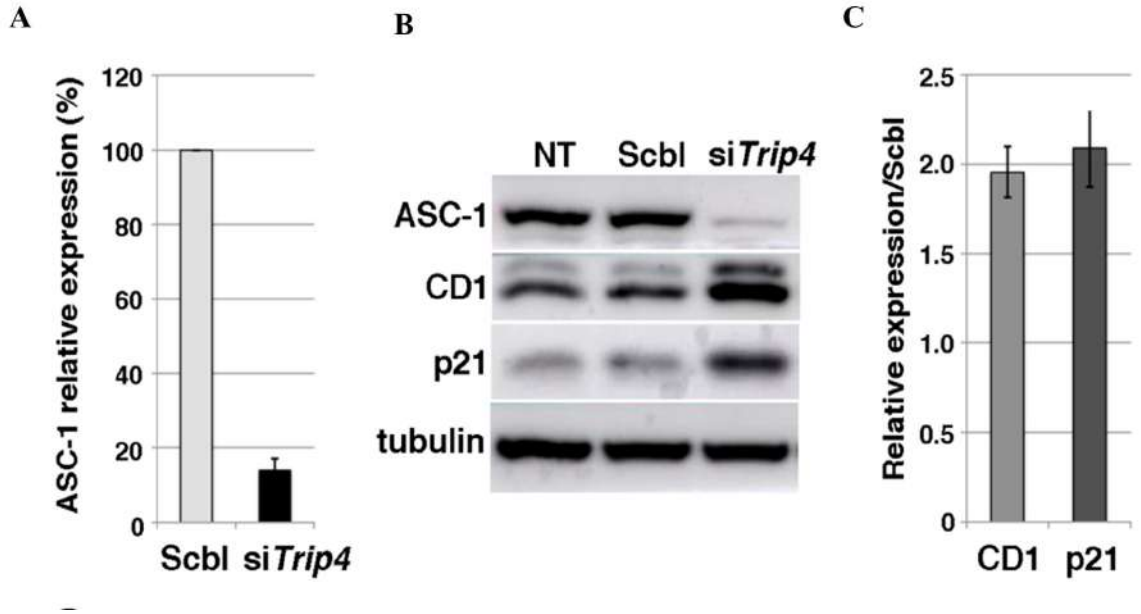

Figure 5.27. Increased CD1 and p21 expression in Trip4KD C2C12. (A): Relative expression of ASC-1 in Trip4KD C2C12 (siTrip4) compared is less than 20% compared with Scramble control (Scbl). Western blot analysis of cell cycle related proteins (B) shows an increased expression of CD1 and p21 in Trip4KD compared to non-transfected cells (NT) or cells transfected with siRNA control (Scbl) (C, expression normalized to Scbl transfected cells).

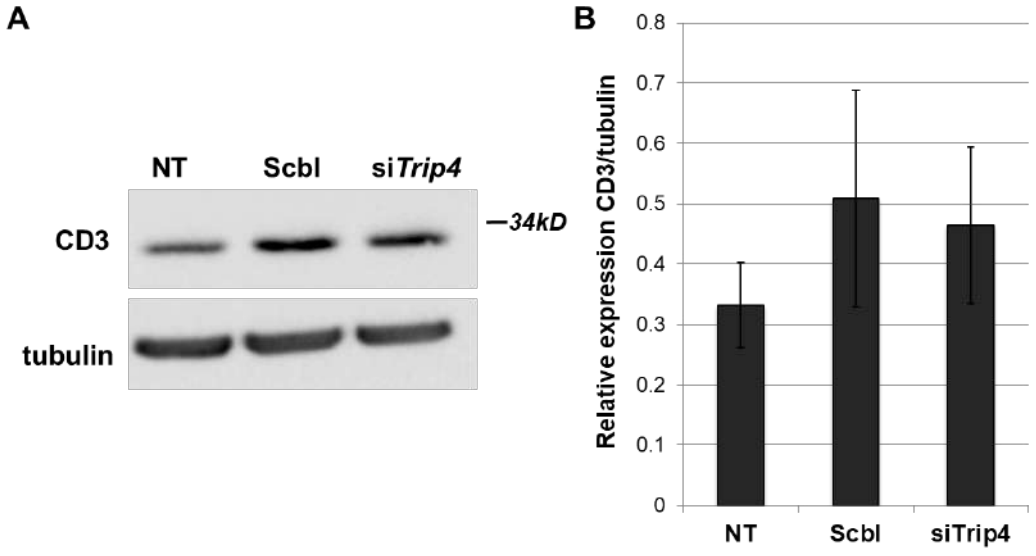

Figure 5.28. CD3 expression in C2C12. No significant changes were found between CD3 expression in Trip4KD C2C12 myoblasts (siTrip4) compared with Scramble control (Scbl) or non-treated cells (NT).

Increased expression of CD1 and p21 in *Trip4*KD was rescued by expression of human wild-type ASC-1 (hASC-1) (Figure 5.29).

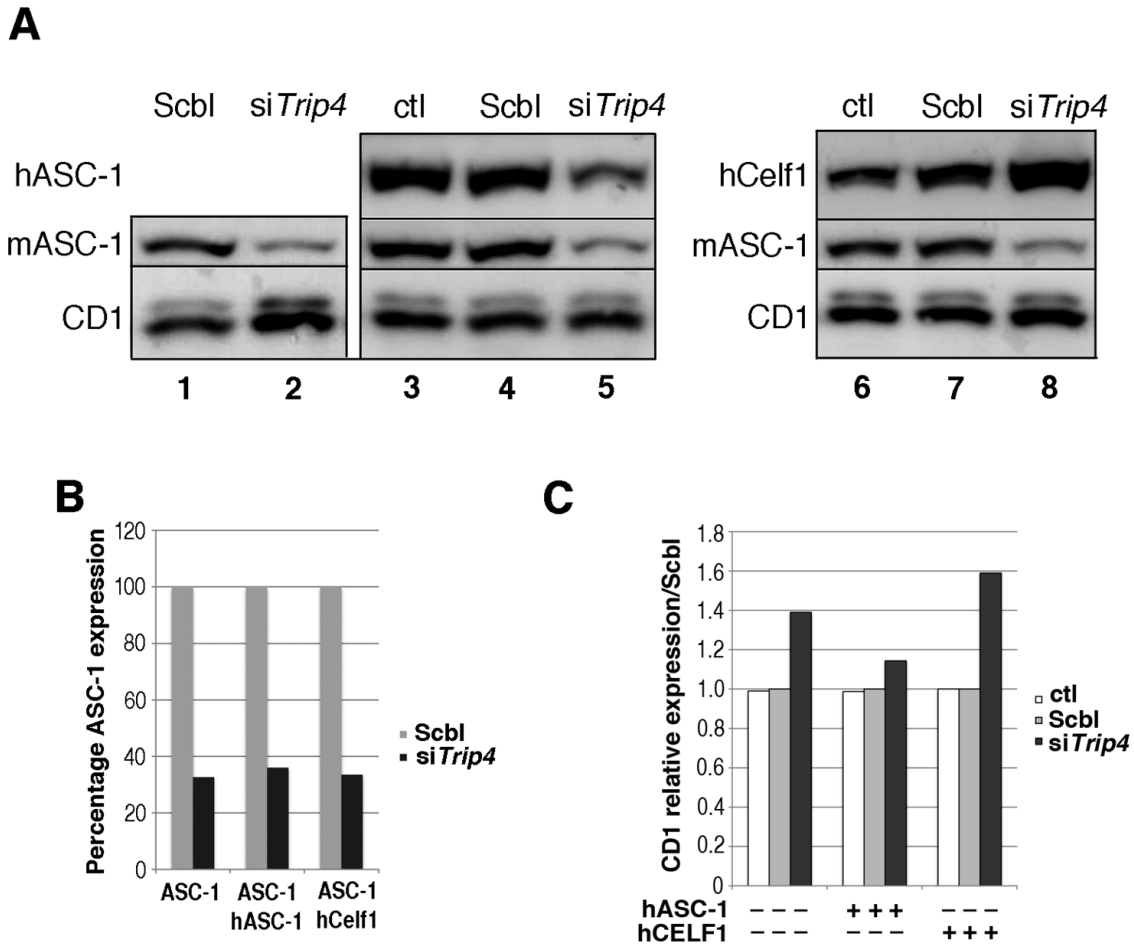

Figure 5.29: Rescue of the altered levels of cyclin D1 in Trip4KD C2C12. (A) Western blot analysis of protein extracts from Scbl (lanes 1, 4, 7), siTrip4 (lanes 2, 5, 8) or ctl cells (lanes 3 and 6) double-transfected with hASC-1 (lanes 3-5) or hCelf1 (lanes 6-8) expressing vectors 24h after endogenous ASC-1 silencing. ASC-1 (mASC-1, hASC-1), Celf1 (hCelf1) and cyclin D1 (CD1) were detected with the appropriate antibodies. (B) Residual expression of endogenous ASC-1 after Trip4 silencing in the presence or absence of hASC-1 or hCelf1 expressing vectors. (C) Quantification of the relative expression of CD1 (normalized for tubulin) in ctl, Scbl and siTrip4 cells in the presence or absence of hASC-1 or hCelf1 expressing vectors. The signal intensity of Scbl controls has been reported to 1. mASC-1= murine endogenous ASC-1; hASC-1 = human ectopic ASC-1; hCelf1 = human ectopic Celf1.

Moreover, in cell lysates from *Trip4*KD C2C12 we found an increase of the hyper-phosphorylated forms of Rb and the hyper-phosphorylated/total Rb ratio compared to controls (Figure 5.30).

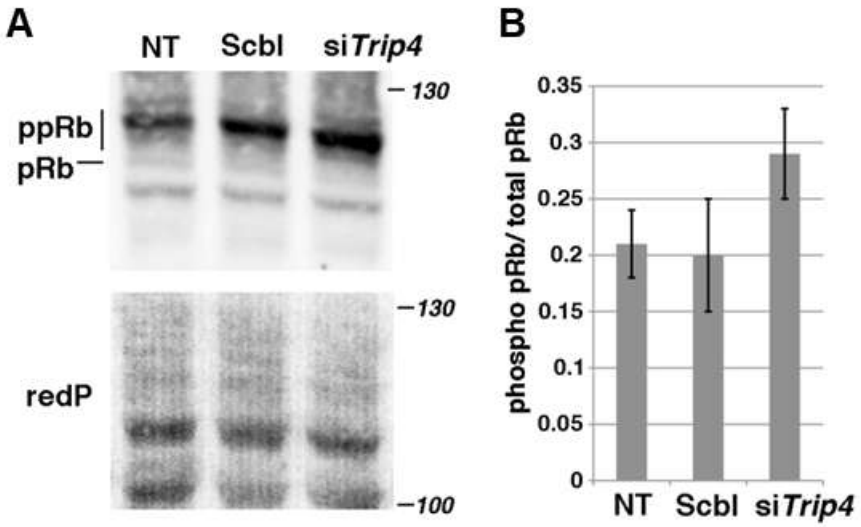

Figure 5.30. Analysis of Retinoblastoma protein (pRb) phosphorylation in C2C12. Western blot analysis of pRb phosphorylation state in NT, Scbl and siTrip4 cells revealed a fast migrating band corresponding to the hypo-phosphorylated form of Rb (pRb, 110 kDa) and slower migrating bands corresponding to hyper-phosphorylated forms of Rb (ppRb, 116kDa) (A). Red ponceau (redP) staining of the membrane showed similar loading in each condition. In all conditions, the hyper-phosphorylated forms of Rb were predominant compared to the hypo-phosphorylated form as expected for cycling cells. Although variability precluded reaching statistical significance, quantification of the ratio ppRb/ total pRb for each condition (N=4) showed an increase by nearly 50% of hyper-phosphorylated forms in siTrip4 cells (B) NT: non-transfected; Scbl: scramble-transfected cells; siTrip4: cells transfected with the siRNA directed against Trip4.

5.4 DISCUSSION

ASC-1 related disease is emerging as a novel cause of congenital neuromuscular disorders, but the role of ASC-1 and ASC-1 complex remains unclear. The present work identifies a pathophysiological pathway associated with ASC-1 defects which contributes to a better understanding of its so-far indefinite role and the potential pathomechanisms involved in the disease.

The results presented here show that, proliferation is accelerated in fibroblasts and myogenic cells in the absence of ASC-1, suggesting a role for this protein both in skin and muscle, which is consistent with the patient's phenotype involving muscular and cutaneous abnormalities (Davignon *et al.*, 2016). FACS studies showed a trend towards a decrease in the number of cells in G0/G1 phase and a parallel increase in cells in S phase for *Trip4* KD and patient fibroblasts compared with controls. A parallel increase in the number of cells in S phase in both Scbl and siTrip4 samples could be explained by the stress induced by transfection. Thus, the increased proliferation rate would mainly be due to shortening of the G0/G1 phase (quiescence/initiation of cell cycling).

Moreover, increased proliferation is associated with cell size reduction, suggesting that, in the context of cell cycle acceleration, cell growth is reduced. Although these data do not exclude a reduction of the number of quiescent cells, the shortening of the G1 duration has indeed been associated with cell size and growth reduction in yeast (Turner *et al.*, 2012) and in mammalian cells (Jiang *et al.*, 1993; Quelle *et al.*, 1993; Varsano *et al.*, 2017; Cadart *et al.*, 2018). This may contribute to explain the myotube growth defect, which was reported previously in ASC-1 depleted patients and C2C12 cells (Davignon *et al.*, 2016).

This cell cycle phenotype is associated with altered cyclin expression. In our murine C2C12 myogenic cell model, we found that ASC-1 depletion leads to an increase of cyclin D1 and p21, which are important regulators of the G0/G1 phase and of several downstream targets. Increased expression of CD1 and p21 in *Trip4*KD was rescued by expression of human wild-type ASC-1 (hASC-1), confirming that this molecular phenotype is not due to off-target effects of *Trip4* siRNA. Over-expression of D-type cyclins has been shown to shorten the G0/G1 phase and increase the number of cells entering S phase (Buttitta and Edgar, 2007). Furthermore, the high levels of p21 and cyclin D1 in the absence of ASC-1 suggest an increased formation of the cyclin D1 and cyclin-dependent kinases CDK4/6 complex, as this interaction relies on the stoichiometry between cyclin D1 and p21 (LaBaer *et al.*, 1997). This complex phosphorylates proteins such as the tumour suppressor retinoblastoma protein (pRb) (Ezhevsky *et al.*, 2001), a multi-functional protein best known for its role in controlling cell cycle. On the other hand, pRb interacts with cyclins and is a regulator of both the cell cycle and, through its target E2F, of muscle-specific gene expression (Ezhevsky *et al.*, 2001; Leshem and Halevy, 2002). In G1 phase, the complex cyclin D-CDK4/6 phosphorylates the pRb protein and weakens its interaction with the transcription factor E2F. As a consequence, it allows initial transcription of E2F dependent

genes including cyclin E and other cell cycle related proteins (Schafer, 1998; Poon, 2016). Subsequent activation of CDK2-cyclin E leads to further phosphorylation and inactivation of pRb, release of E2F and full commitment to S-phase entry (Figure 5.31). Differences in the pRb phosphorylation status may favour differential binding preferences to specific cellular targets including myogenic regulatory factors (Narasimha *et al.*, 2014). Hypophosphorylated pRb inhibits E2F transcription factor, required for S phase entry (Leshem and Halevy, 2002).

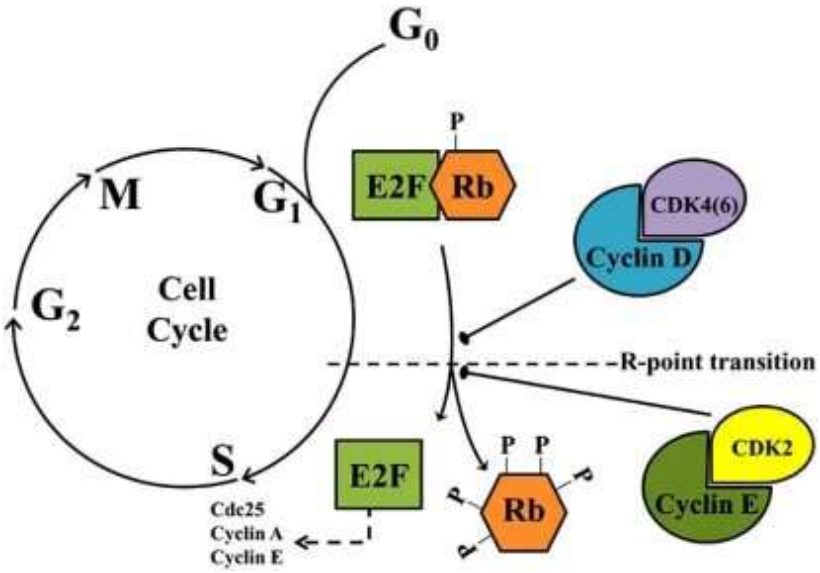

Figure 5.31. Overview of the pRb pathway in the cell-cycle. Sequential pRb phosphorylation by Cyclin D-Cdk 4/6 and Cyclin E-Cdk 2 kinase complexes induces conformational changes to the pRb structure and release of E2F, necessary for the expression of S-phases genes. Modified from Biggar and Storey, 2009. CDK: cyclin dependent kinases; E2F: transcription factor E2F; Rb: retinoblastoma protein.

It was hypothesized that abnormalities of Rb might be a key mechanism in the muscle phenotype associated with defects of ASC-1. In proliferating *Trip4* KD cells, there is a consistent tendency to the reduction of the hypophosphorylated forms of pRb in favour of hyperphosphorylation, which is consistent with loss of pRb-mediated inhibition of the G0/G1-S transition. This, associated with an increase in cyclin D1, can explain the rapid progression of *Trip4*KD cells from G1 to S phase.

Interestingly, pRb activity has been recently found to be also necessary for late muscle development, promoting myofibrillogenesis and muscle cell growth by activating transcription of myogenic and metabolic genes (Zappia *et al.*, 2019). The present results are consistent with the myofibrillar abnormalities observed in patients' muscles, suggesting that ASC-1 is critical for controlling both cell

cycle progression and myofibrillogenesis during myogenesis. Thus, defects on this pathway could also contribute to explain the various myofibrillar defects observed in ASC1-RM patients' biopsies. Further experiments are required to corroborate pRb abnormalities in ASC-1 deficiency and to clarify the latter point.

In frozen postmitotic muscles from patients with *TRIP4* mutations, altered cyclin expression has also been observed. Embryonic myosin heavy chain was not detectable by Western blot, suggesting that the cyclin changes in patient muscles are unlikely to be non-specifically due to muscle fibre regeneration and are probably directly associated with ASC1-related cell cycle defects in post-mitotic muscles. Along these lines, a variable but consistently increased amount of cyclin D3 was found. Cyclin D3 is a critical regulator of the proliferation/differentiation balance of myogenic progenitors in skeletal muscle (Cenciarelli *et al.*, 1999; De Santa *et al.*, 2007). Under non-pathological conditions, this protein is not expressed in adult muscle fibres, as it is more important for the establishment than for the maintenance of terminal myogenic differentiation (Bartkova *et al.*, 1998). It has been recently implicated in the regulation of muscle fibre-type specific gene expression, notably by regulating those genes encoding proteins involved in contractile and metabolic functions (Giannattasio *et al.*, 2018). Cyclin D3 increase in ASC-1 depleted patients' muscles suggests a dysregulation of its expression that could be attributed to inappropriate activation by MyoD or to improper stabilization by pRb (Cenciarelli *et al.*, 1999; De Santa *et al.*, 2007) thus leading to its reactivation in adult muscle in order to adapt to pathological conditions. Moreover, it has been reported in a model of C2C12 myogenic cells expressing a stabilized cyclin D3 mutant, that accumulation of cyclin D3 delay muscle gene expression by impairing pRb dephosphorylation (De Santa *et al.*, 2007). However, in the C2C12 *Trip4*-KD model reported here, no significant abnormalities in cyclin D3 expression were found.

Furthermore, cyclin D3 is also involved in adipogenesis through its interaction with the nuclear receptor PPARγ (Sarruf *et al.*, 2005). This could be related to the presence of excessive subcutaneous adipose tissue in lower limbs observed in some of the patients reported here and previously (Davignon *et al.*, 2016). In addition, cyclin D1 represses PPARγ function and inhibits adipocyte differentiation (Fu *et al.*, 2005). The drastic reduction of cyclin D1 in postnatal muscles from these novel *TRIP4* mutant patients might contribute to this adipose tissue phenotype through de-repression of PPARγ activity.

Interestingly, over-expression of ASC-1 has recently been reported in human cancers (Yoo *et al.*, 2014;

Hao *et al.*, 2018; Che *et al.*, 2019). It has been attributed a pro-tumourigenic role with proliferation promoting effect in cancer cells through activation of different signaling pathways involving NFκB, MAPK and AKT/PI3K or ERα, depending on the cancer cell type (Yoo *et al.*, 2014; Hao *et al.*, 2018; Che *et al.*, 2019). This further confirms the involvement of ASC-1 in the cell proliferation process. Nonetheless, the present results in C2C12 myogenic cells and in ASC1-RM patients' fibroblasts and muscle suggest a negative regulation of cell proliferation by ASC-1. In fact, as a transcriptional co-activator, ASC-1 is involved in the integration of environmental cues to relevant signaling pathways, which may be different in tumour cells compared to non-tumour cells. It can be assumed that the regulation of cell proliferation by ASC-1 relies on the nature, availability and functionality of cell type specific partners leading to different consequences on cell division and fate.

Finally, it has been found that recessive mutations in *ASCC1* and recessive *TRIP4* mutations (in particular those leading to a shorter ASC-1 isoform with preserved Zinc-finger and ASCH- domains) are associated to severe congenital neuromuscular disorders characterized by arthrogryposis multiplex congenita, bone fractures, severe hypotonia and respiratory involvement (Knierim *et al.*, 2016; Oliveira *et al.*, 2017; Böhm *et al.*, 2018). Given the similarity ot the histopathological findings observed in these patients and ASC1-RM patients (Böhm *et al.*, 2018; Villar-Quiles *et al.*, 2019), and the fact that in both conditions there are abnormalities in the components of the ASC-1 complex, the existence of common pathomechanism seems plausible. Whether in these patients a proliferation defect and myotube growth abnormalities are present remains to be elucidated.

It would also be relevant to study the impact of mutations in genes encoding different components of the ASC-1 complex in the expression of each component and, more importantly, in the integrity and function of the complex. In fact, different mutations could have a different impact on the ASC-1 complex and therefore could lead to different phenotypical expressions. Interestingly, preliminary results obtained during the development of this project showed that ASCC1 expression in patients' fibroblasts was not reduced compared with control fibroblasts (Figure 5.32).

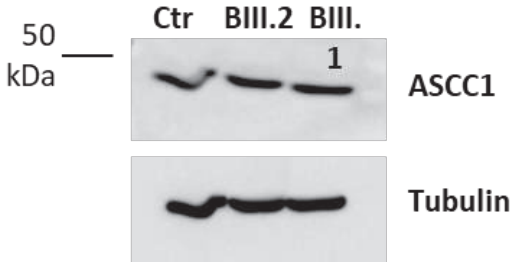

Figure 5.32. ASCC1 expression in patient (BIII.2 and BIII.1) and control (ctr) fibroblasts.

Further analysis using co-immunoprecipitation needs to be performed to assess whether the ASC-1 complex is still formed in the absence or depletion of ASC-1 or ASCC1. In case it is still intact, it would be necessary to investigate its function and performance under pathological conditions.

In conclusion, the present work contributes to disentangle potential pathophysiological mechanisms of ASC1-RM. As such, these results reveal that the transcriptional co-activator ASC-1 plays a key role not only in late stages of myogenic differentiation and myotube growth (Davignon *et al.*, 2016) but also as a novel cell-cycle regulator in several cell types, controlling cell proliferation via regulation of key cell-cycle proteins. Finally, this work further confirms the role of defects in transcriptional co-regulation as an emerging mechanism in inherited muscle disease.

Chapter 6

OVERALL DISCUSSION AND PERSPECTIVES

Congenital myopathies with multi-minicores represent a clinically and genetically heterogeneous group of early-onset muscular conditions, classically defined by the presence of multiple areas of sarcomeric disorganization and mitochondrial depletion which show reduced oxidative enzyme activity and various degrees of myofibrillar disorganization on electron microscopy (Ferreiro et al., 2000; Ferreiro and Fardeau, 2002).

The phenotypical spectrum of congenital myopathies with multi-minicores is quite large, ranging from very severe, lethal neonatal presentations to later-onset milder forms along with variable degrees of systemic involvement including cardiomyopathy, respiratory failure and orthopaedic complications. This is also in line with a remarkable genetic heterogeneity. A number of genes have been associated with multi-minicores including the well-known *RYR1* (Ferreiro et al., 2002a) and *SEPN1* (Moghadaszadeh et al., 2001; Ferreiro et al., 2002b) but also *MYH7* (Cullup et al., 2012), *TTN* (Chauveau et al., 2014; Oates et al., 2018), *MEGF10* (Boyden et al., 2012), *ACTN2* (Lornage et al., 2019a), *FXR1* (Estañ et al., 2019), *PYROXD1* (Lornage et al., 2019b), *ASCC1* (Böhm et al., 2018) or *TRIP4* (Davignon et al., 2016; Villar-Quiles et al., 2019).

The present work has focused on one of the first multi-minicore myopathies identified, Selenoprotein N-related myopathy (SEPN1-RM) and one of the most recently described, Activating signal cointegrator 1-related myopathy (ASC1-RM). Their histopathological presentation includes not only minicores, but also other muscle fibre architectural abnormalities which are typically associated with other forms of congenital myopathies (i.e. rods, caps, central nuclei). This study reveals the large clinical and histological spectrum associated with these two multi-minicore myopathies and supports the idea that there is a remarkable clinical and histopathological overlap between different congenital

muscle disorders. These findings blur the boundaries between distinct nosological entities and suggest the existence of common pathophysiological pathways.

6.1 SEPN1-Related Myopathy

SEPN1-RM is a potentially severe, life-threatening congenital myopathy with no specific treatment so far. The present work has allowed to estimate a disease prevalence which would be around 1 per million. Clinically, patients share a homogeneous and distinctive clinical phenotype, marked by severe axial weakness, early-onset scoliosis frequently associated with spinal rigidity and life-threatening respiratory insufficiency, but fairly preserved limb strength and ambulation. Ophthalmoparesis is also part of the SEPN1-RM phenotype and correlates with disease severity. SEPN1-RM is associated with a strikingly large histopathological spectrum, including minicores, type 1 fibres predominance, dystrophic features or protein aggregates. This heterogeneity may be partly explained by the site of biopsy, since axial muscles may exhibit more severe dystrophic findings while limb muscles may exhibit only mildly myopathic findings.

Importantly, while most congenital myopathies are considered to be stable or non-progressive conditions, the present work shows that SEPN1-RM is a more severe and progressive disease than previously thought. It may cause loss of ambulation in 10% of cases. Furthermore, it is associated with a rapid decline in functional performance and respiratory function from the end of the third decade, even in mild cases. Respiratory involvement is the main predictive factor of vital prognosis. Proper management of scoliosis and non-invasive ventilation improve respiratory and functional prognosis. Nonetheless, life span is reduced even in milder cases with optimum respiratory support.

The present work has revealed other severity determinants. As such, biallelic null mutations are significantly correlated with disease severity. Increased body weight is also associated with higher disease severity leading to severe weakness (including weakness of non-weight-bearing and extraocular muscles) and early loss of ambulation. The latter can be related to SEPN1-RM pathophysiological mechanisms involving defective mitochondrial bioenergetics and lipid metabolism in muscle (Arbogast et al., 2009; Arbogast and Ferreiro, 2010a; Pozzer et al., 2019; Varone et al., 2019). Paradoxical glucose metabolism abnormalities in SEPN1-RM patients (Clarke et al., 2006; Varone et al., 2019) have also been confirmed here and can be explained by chronic endoplasmic-reticulum

(ER) stress in skeletal muscle leading to an increased susceptibility to insulin resistance (Varone et al., 2019). Thus, high caloric intake leading to increased oxidative/ER stress in skeletal muscle can trigger or aggravate glucose metabolism abnormalities.

In the last years, significant progress has been achieved in the identification of SEPN1-RM pathophysiological pathways which are targetable with existing drugs (Arbogast et al., 2009; Arbogast and Ferreiro, 2010a; Pozzer et al., 2019; Varone et al., 2019). Interestingly, there seem to be common mechanisms between SEPN1-RM and other muscle diseases. The most salient one would be redox homeostasis disturbances, which have also been found in RYR1-related myopathies (Dowling et al., 2012), COL6-related myopathies (Bönnemann, 2011) and in Duchenne Muscular Dystrophy (Kim et al., 2013; Moulin and Ferreiro, 2017). Indeed, the antioxidant N-acetylcystein (NAC) was identified as an effective treatment *ex vivo*, which led to launching of a small pilot trial (ClinicalTrials.gov identifier: NCT02505087) whose results are pending.

Nonetheless, clinical trial readiness in SEPN1-RM remains poor because of the scarcity of quantitative data, lack of genotype-phenotype correlations and unawareness of the long-term disease evolution and its determinants. Multicentric, international phase II-III trials require overcoming bottlenecks which are highlighted by this study: (i) the predominantly axial weakness, since there are few quantifiable validated measures of axial muscle power; (ii) the intra-patient variability in forced vital capacity (FVC), potentially explained by diaphragm fatigability, which could bias trial results, and (iii) the heterogeneous orthopaedic and respiratory management, particularly around spinal surgery, which has a major functional impact. All the former, together with slow progression until the fourth decade, hinder the choice of outcome measures. Prospective natural history studies would be needed to confirm the results of the present work and to validate quantitative data on disease severity, progression and prognosis factors.

Furthermore, the definition of homogeneous groups according to disease severity, as proposed here, is important in clinical trial planning. Since respiratory involvement is the main vital prognostic factor, Kaplan Meier curves evaluating ventilation-free probability will also be useful to evaluate the impact of potential treatments. Age stratification would also be interesting, as limb strength is stable or slowly progressive in younger patients but steadily progressive after the fourth decade.

The setting up of homogeneous management recommendations for SEPN1-RM, taking into account

its peculiar features and disease course, would be of capital importance to reduce variability in clinical trials but, more importantly, to improve vital and functional prognosis. This work reveals the importance of systematic sleep studies, regular cardiac and respiratory surveillance, non-invasive ventilation and proper management of scoliosis. Surveillance of metabolic parameters, including glucose metabolism screening and tailored nutritional control, is also recommended.

Further fundamental research is needed to investigate potential quantitative biomarkers in patients' tissues, which would be of immense value in the identification of potential treatments but also for evaluating the effectiveness of candidate treatments *in vitro* and *ex vivo*. In the Basic and Translational Myology Laboratory (Paris), where this work was conducted, the investigation of quantitative biomarkers including redox and bioenergetics parameters in patient and control fibroblasts and myoblasts is currently ongoing. Moreover, the optimisation of high-throughput screening (HTS) methods allowing the screening of large compound libraries for activity against these biomarkers or biological targets via the use of miniaturized assays is also ongoing in our laboratory. This will allow large-scale data analysis in the search for new potential treatments and for the efficacy evaluation of previously identified candidate drugs on patient cells.

6.2 ASC1-Related myopathy

ASC1-RM is associated with an expanding clinical spectrum ranging from very severe forms, lethal in the neonatal period, to milder forms with preserved ambulation and no respiratory assistance in adulthood. The clinical phenotype is marked by early onset proximal and axial weakness, scoliosis, skin involvement without contractures and respiratory failure with variable severity, correlated with the degree of muscle weakness. This work has confirmed that adult-onset cardiomyopathy and extraocular muscle involvement are also part of the ASC1-RM phenotype and do not correlate with disease severity.

The present work has also revealed that the ASC1-RM histopathological spectrum is particularly large. Aside from the multi-minicores, internalized nuclei, cap lesions and mild dystrophic lesions reported (Davignon et al., 2016), nemaline and cytoplasmic bodies can also be found. *TRIP4* is a novel culprit gene for multi-minicore and nemaline myopathies, as well as for other forms of congenital muscle disease (including cap disease, core, centronuclear or cytoplasmic-body myopathies and congenital

muscular dystrophy). As such, *TRIP4* should be included in the corresponding diagnostic gene panels.

Here we present a pathophysiological pathway associated with ASC-1 defects, which contributes to elucidate its so-far undefined role. ASC-1 plays a key role not only in late stages of myogenic differentiation and myotube growth (Davignon et al., 2016), but also as a novel cell-cycle regulator in cell proliferation in both muscular cells and fibroblasts by modulating the expression and phosphorylation of cell-cycle regulatory proteins. The cell cycle phenotype implies altered levels of cyclins, which are involved in the G0/G1-S transition, as well as a consistent tendency to hyperphosphorylation of retinoblastoma protein (pRb), indicating the loss of pRb-mediated inhibition of the G0/G1-S transition. pRb activity is also necessary for late muscle development, promoting myofibrillogenesis and muscle cell growth (Zappia et al., 2019). Defects in this pathway could contribute to explain the various myofibrillar defects found in patients' biopsies. Further experiments are required to corroborate pRb abnormalities in ASC1-RM and to clarify this last point. As such, the first step would be the analysis of the pRb and its different phosphorylated states in primary cells from different tissues such as patient fibroblasts and myoblasts.

Importantly, ASC1-RM shows clinical and histopathological features that overlap with other early-onset muscle disorders, with which it may share common pathophysiological mechanisms. It remains to be explored whether cell-cycle regulation and the pRb pathway can also be implicated in those overlapping muscular disorders. This work has allowed to establish the experimental set up for cell cycle analysis in primary fibroblasts and C2C12. As a first step, it will be interesting to analyse pRb in *TTN*-related congenital myopathies, which show clinical and histopathological abnormalities common with ASC1-RM, such as minicores, caps or cytoplasmic bodies (Oates et al., 2018).

The implication of the ASC-1 complex in neuromuscular diseases was previously confirmed by the description of recessive mutations in *TRIP4* (three families sharing two mutations) or in *ASCC1* (one family) (Knierim et al., 2016). These patients were reported as having Spinal Muscular Atrophy (SMA) with arthrogryposis multiplex congenita, respiratory distress and congenital bone fractures. Four additional families with *ASCC1* recessive nonsense or frameshift mutations have been reported (Oliveira et al., 2017; Böhm et al., 2018) with a severe neonatal phenotype including arthrogryposis, bone fractures and respiratory failure. Muscle biopsies from the latter patients were not suggestive of motor neuron involvement but disclosed myopathic features (i.e. intense oxidative rims beneath the sarcolemma and scattered remnants of sarcomeres with enlarged Z-bands) (Böhm et al., 2018).

Interestingly, the *TRIP4*-mutated patients reported as having severe SMA (Knierim et al., 2016) carried *TRIP4* nonsense mutations resulting in exon skipping and upregulation of a shorter isoform containing most ASC-1 functional domains. Conversely, in ASC1-RM patients, ASC-1 was undetectable by Western blot both in the mildest patient reported here and in the first severe cases described (Davignon et al., 2016; Villar-Quiles et al., 2019). This suggests that *TRIP4* mutations leading to ASC-1 protein depletion would be associated with a primary striated muscle phenotype, while those leading to expression of a truncated protein might be associated with motor neuron disease. The identification of more families will allow to clarify the phenotypical analysis and the impact of the different mutations on ASC-1 expression and function. In collaboration with Dr Markus Schuelke (Charité Universitätsmedizin Berlin), our team at the Basic and Translational Myology Laboratory is going to conduct proliferation and cell-cycle analysis on fibroblasts and myoblasts from some of the first *TRIP4* and *ASCC1*-mutated patients with a prenatal SMA phenotype (Knierim et al., 2016). We are also conducting RNAseq studies on these samples, along with primary fibroblast and myoblast samples from our ASC1-RM patients, to elucidate the potential upregulated or downregulated pathways that may lead to different phenotypical expressions.

Furthermore, the ASC-1 complex has been recently identified as a link between Amyotrophic Lateral Sclerosis (ALS) and SMA (Chi et al., 2018). Interestingly, four ALS-causative proteins (FUS, EWSR1, TAF15 and MATR3) are required for association of the ASC-1 complex with the RNAP II/U1 snRNP machinery. Moreover, *TRIP4* KO in HeLa cells disrupts association between the ASC-1 complex and the latter ALS-causative proteins. Thus, it will be of much interest to further study these interactions in the presence of different *TRIP4* and *ASCC1* mutations associated with a pure myopathic (Davignon et al., 2016; Böhm et al., 2018; Villar-Quiles et al., 2019) or a SMA phenotype (Knierim et al., 2016).

On another note, rimmed fibres have been found in ASC1-RM, which are comparable to those recently reported in relation to *ASCC1* mutations (Böhm et al., 2018). This further highlight that *TRIP4* and *ASCC1* are implicated in a common pathophysiological pathway which leads to multiple forms of myofibrillar disarray, and thus to an overlap of histopathological CM lesions.

The term ‘ASC1-related myopathies’ might be coined to include pathologies associated with both genes and with potential defects of any other protein of the ASC-1 complex. Nonetheless, a better understanding of the molecular mechanisms of the ASC-1 complex is needed to clarify the different phenotypes observed. The interaction between ASC-1 and ASCC1 and the integrity and functionality

of the ASC-1 complex in the presence of *TRIP4* or *ASCC1* mutations remain to be further explored. To that effect, co-immunoprecipitation studies could be helpful to explore the integrity of the ASC-1 complex in the absence or depletion of one of its components and in the setting of different mutations. Cell-cycle studies in *Ascc1*-KD C2C12 and in primary fibroblasts and myoblasts from ASCC1-mutated patients will also be of much interest and are currently ongoing in our laboratory. Finally, ongoing RNAseq studies on primary fibroblasts, myoblasts and in *Ascc1*- and *Trip4*-KD C2C12 will also be of much help to explore potential common and divergent pathophysiological pathways involved in *TRIP4*- and *ASCC1*- related disease. The choice of multiple cell type analysis, including myoblasts cell line (C2C12), primary fibroblasts and primary myoblasts, will be relevant to study ASC1 and ASCC1 functions in different tissues. Tissue differences could contribute to explain the diversity of systemic abnormalities, for example skin lesions present in *TRIP4*- but not in *ASCC1*-mutated patients. Moreover, these studies could be a first step towards the identification of potential therapeutic targets.

CONCLUSIONS

1. Congenital myopathies with multi-minicores represent a clinically and genetically heterogeneous group of early-onset muscular conditions.
2. Selenoprotein N-related myopathy (SEPN1-RM) estimated prevalence would be around 1 per million. Patients share a distinctive clinical phenotype, marked by severe axial weakness, early-onset scoliosis frequently associated with spinal rigidity and life-threatening respiratory insufficiency but fairly preserved limb strength and ambulation. SEPN1-RM is a more severe and progressive disease than previously thought, causing loss of ambulation in 10% of cases.
3. Metabolic and body mass abnormalities are part of the SEPN1-RM phenotype. SEPN1 absence triggers a chronic reticular stress in skeletal muscle leading to an increased susceptibility to insulin resistance. Patients with increased body weight have a more severe form of the disease, suggesting that caloric supplements should not be routinely prescribed.
4. The age and site of the muscle biopsy can contribute to explain the strikingly heterogeneous histopathological presentation in SEPN1-RM.
5. Exon 1 is a hotspot for *SEPN1* mutations and should be thoroughly analysed upon clinical SEPN1-RM suspicion. The first genotype-phenotype correlations identified here reveal that biallelic null mutations are significantly associated with disease severity.
6. Age stratification and the severity criteria proposed here can be used for definition of homogeneous groups in clinical trials. Since respiratory involvement is the main vital prognostic factor, Kaplan Meier curves evaluating ventilation-free probability will also be useful to evaluate the impact of potential treatments.
7. The clinical spectrum of Activating Signal Cointegrator 1-related myopathy (ASC1-RM), caused by recessive mutations in the *TRIP4* gene, ranges from very severe forms, lethal

in the neonatal period to milder forms with preserved ambulation in adulthood. ASC1-RM should be considered in any patient with histopathological features of a congenital myopathy and non-progressive muscular weakness without marked limb contractures, even in ambulant patients without clear neonatal signs, particularly if this phenotype includes respiratory insufficiency, cardiomyopathy or skin abnormalities.

8. ASC1-RM histopathological spectrum is strikingly large, including multiminicores, rods, cytoplasmic bodies, caps or central nuclei, rimmed fibres and mild endomysial fibrosis. *TRIP4* represents a novel culprit gene for minicore myopathy but also for other forms of congenital muscle disease such as nemaline myopathy, cap disease, core, centronuclear or cytoplasmic-body myopathies and congenital muscular dystrophies, and should be included in the corresponding diagnostic gene panels.
9. ASC-1 plays a key role in late myogenic differentiation and myotube growth but also in early-stages of myogenesis. ASC-1 emerges as a novel cell cycle regulator with a key role in cell proliferation of muscular cells and fibroblasts by modulating the expression and phosphorylation of cell-cycle regulatory proteins. Defects on the retinoblastoma protein pathway could contribute to explain the myofibrillar defects observed.
10. ASC-1 RM shows clinical and histopathological features that overlap with other early-onset muscle disorders, with which it may share common pathophysiological mechanisms. It remains to be explored whether the pathomechanisms known to be involved in ASC1-RM can also be implicated in those overlapping conditions.
11. Based on the identification of common histopathological lesions in *TRIP4*- and *ASCC1*-mutant patients, the term ‘ASC1-related myopathies’ might be coined to include pathologies associated with both genes and with potential defects of any other protein of the ASC-1 complex.

CONCLUSIONES

1. Las miopatías congénitas con multi-minicores constituyen un grupo de enfermedades musculares de inicio temprano, muy heterogéneo desde el punto de vista clínico y genético.
2. La prevalencia estimada de la miopatía relacionada con la selenoproteína N (SEPN1-RM) es de 1 por millón. Los pacientes presentan un fenotipo clínico distintivo, que se caracteriza por afectación grave de la musculatura axial, escoliosis de aparición precoz asociada a rigidez espinal e insuficiencia respiratoria potencialmente letal, y una relativa preservación de la fuerza apendicular y de la marcha. La SEPN1-RM es una enfermedad más grave y progresiva de lo que se consideraba anteriormente, y llega a causar pérdida de la marcha en un 10% de los casos.
3. El fenotipo de la SEPN1-RM incluye alteraciones metabólicas. La ausencia de SEPN1 provoca un estrés crónico en el retículo endoplásmico del músculo esquelético, con una mayor susceptibilidad a la resistencia a la insulina. Los pacientes con un incremento del peso corporal presentan formas más graves de de la enfermedad, lo que sugiere que no se deben prescribir suplementos calóricos de manera sistemática.
4. Tanto la edad como el sitio del que se obtiene la biopsia muscular pueden contribuir a explicar la llamativa heterogeneidad de la presentación histopatológica de la SEPN1-RM.
5. El exón 1 del gen *SEPN1* es un punto de gran mutabilidad, y debe analizarse de forma específica ante la sospecha de SEPN1-RM. Las primeras correlaciones encontradas entre genotipo y fenotipo muestran que las mutaciones nulas bialélicas se asocian con una mayor gravedad de la enfermedad.
6. En este trabajo se propone una estraficación por edad y unos criterios de gravedad que podrían ser utilizados para definir grupos homogéneos de pacientes en futuros ensayos clínicos. Dado que el principal factor pronóstico es la afectación respiratoria, las curvas Kaplan Meier que analizan la probabilidad de requerir ventilación asistida podrían ser útiles en la evaluación del impacto de nuevas terapias.

7. El espectro clínico de la miopatía relacionada con el co-activador transcripcional ASC-1 (ASC1-RM), causada por mutaciones recesivas en *TRIP4*, abarca desde formas muy graves, letales en el período neonatal, hasta formas leves con preservación de la marcha en la edad adulta. Se debe considerar la posible presencia de ASC1-RM ante cualquier paciente con una biopsia muscular compatible con una miopatía congénita y una debilidad muscular no progresiva, sin contracturas prominentes, incluso en pacientes ambulatorios sin síntomas neonatales, especialmente si el fenotipo incluye insuficiencia respiratoria, miocardiopatía o lesiones cutáneas.
8. La presentación histopatológica de ASC1-RM es extraordinariamente diversa, e incluye multi-minicores, bastones nemalínicos, cuerpos citoplásmicos, lesiones de tipo cap, centralizaciones nucleares, fibras ribeteadas y fibrosis endomisial. *TRIP4* constituye un nuevo gen asociado a la miopatía con multi-minicores, pero también a otras enfermedades musculares congénitas como la miopatía nemalínica, las miopatías con caps, cores, cuerpos citoplasmáticos o centronucleares y las distrofias musculares congénitas. Este gen debe incluirse en en los correspondientes paneles de diagnóstico genético.
9. ASC-1 desempeña una función importante en la diferenciación miogénica terminal y en el crecimiento de los miotubos, así como en las primeras etapas de la miogénesis. ASC-1 es un nuevo regulador del ciclo celular con un papel clave en la proliferación de células musculares y fibroblastos a través de la modulación de la expresión y fosforilación de las proteínas reguladoras del ciclo celular. La alteración de la vía de la proteína de retinoblastoma podría contribuir a explicar las anomalías observadas en las biopsias musculares a nivel miofibrilar.
10. La ASC1-RM presenta características clínicas e histopatológicas que se solapan con las de otras enfermedades musculares congénitas, con las que podría compartir mecanismos fisiopatológicos. Se debería explorar si los mecanismos implicados en la ASC1-RM podrían estar asimismo involucrados en dichas entidades.
11. Dado que existen lesiones histopatológicas comunes en pacientes con mutaciones en *TRIP4* y *ASCC1*, se podría emplear el término 'miopatías relacionadas con ASC1' para incluir los cuadros clinicopatológicos asociados con ambos genes y con otras subunidades del complejo ASC-1.

REFERENCES

Agarkova I, Perriard J-C. The M-band: an elastic web that crosslinks thick filaments in the center of the sarcomere. Trends Cell Biol 2005; 15: 477–485.

Aguilar V, Fajas L. Cycling through metabolism. EMBO Mol Med 2010; 2: 338–348.

Ahmetov II, Vinogradova OL, Williams AG. Gene polymorphisms and fiber-type composition of human skeletal muscle. Int J Sport Nutr Exerc Metab 2012; 22: 292–303.

Al-Qusairi L, Weiss N, Toussaint A, Berbey C, Messaddeq N, Kretz C, et al. T-tubule disorganization and defective excitation-contraction coupling in muscle fibers lacking myotubularin lipid phosphatase. Proc Natl Acad Sci U S A 2009; 106: 18763–8.

Almeida-Vega S, Catlow K, Kenny S, Dimaline R, Varro A. Gastrin activates paracrine networks leading to induction of PAI-2 via MAZ and ASC-1. Am J Physiol Gastrointest Liver Physiol 2009; 296: G414-23.

Amburgey K, McNamara N, Bennett LR, McCormick ME, Acsadi G, Dowling JJ. Prevalence of congenital myopathies in a representative pediatric united states population. Ann Neurol 2011; 70: 662–665.

Amburgey K, Tsuchiya E, De Chastonay S, Glueck M, Alverez R, Nguyen CT, et al. A natural history study of X-linked myotubular myopathy. Neurology 2017; 89: 1355–1364.

Annoussamy M, Lilien C, Gidaro T, Gargaun E, Chê V, Schara U, et al. X-linked myotubular myopathy: A prospective international natural history study. Neurology 2019; 92: e1852–e1867.

Arbogast S, Beuvin M, Fraysse B, Zhou H, Muntoni F, Ferreiro A. Oxidative stress in SEPN1-related myopathy: from pathophysiology to treatment. Ann Neurol 2009; 65: 677–86.

Arbogast S, Ferreiro A. Selenoproteins and protection against oxidative stress: selenoprotein N as a novel player at the crossroads of redox signaling and calcium homeostasis. Antioxid Redox Signal 2010; 12: 893–904.

Ardissone A, Bragato C, Blasevich F, Maccagnano E, Salerno F, Gandioli C, et al. SEPN1-related myopathy in three patients: novel mutations and diagnostic clues. Eur J Pediatr 2016; 175: 1113–1118.

Atkuri KR, Mantovani JJ, Herzenberg LA, Herzenberg LA. N-Acetylcysteine--a safe antidote for cysteine/glutathione deficiency. Curr Opin Pharmacol 2007; 7: 355–9.

Auboeuf D, Hönig A, Berget SM, O'Malley BW. Coordinate regulation of transcription and splicing by steroid receptor coregulators. Science 2002; 298: 416–9.

Bang M-L, Centner T, Fornoff F, Geach AJ, Gotthardt M, McNabb M, et al. The Complete Gene Sequence of Titin, Expression of an Unusual ≈700-kDa Titin Isoform, and Its Interaction With Obscurin Identify a Novel Z-Line to I-Band Linking System. Circ Res 2001; 89: 1065–1072.

Bartkova J, Lukas J, Strauss M, Bartek J. Cyclin D3: requirement for G1/S transition and high abundance in quiescent tissues suggest a dual role in proliferation and differentiation. Oncogene 1998; 17: 1027–37.

Bharucha-Goebel DX, Santi M, Medne L, Zukosky K, Dastgir J, Shieh PB, et al. Severe congenital RYR1-associated myopathy: The expanding clinicopathologic and genetic spectrum. Neurology 2013; 80: 1584–1589.

Blais A, Tsikitis M, Acosta-Alvear D, Sharan R, Kluger Y, Dynlacht BD. An initial blueprint for myogenic differentiation. Genes Dev 2005; 19: 553–69.

Böhm J, Biancalana V, Malfatti E, Dondaine N, Koch C, Vasli N, et al. Adult-onset autosomal dominant centronuclear myopathy due to BIN1 mutations. Brain 2014; 137: 3160–3170.

Böhm J, Chevessier F, Maues De Paula A, Koch C, Attarian S, Feger C, et al. Constitutive activation of the calcium sensor STIM1 causes tubular-aggregate myopathy. Am J Hum Genet 2013; 92: 271–8.

Böhm J, Malfatti E, Oates E, Jones K, Brochier G, Boland A, et al. Novel *ASCC1* mutations causing prenatal-onset muscle weakness with arthrogryposis and congenital bone fractures. J Med Genet 2018: jmedgenet-2018-105390.

Böhm J, Vasli N, Malfatti E, Le Gras S, Feger C, Jost B, et al. An integrated diagnosis strategy for congenital myopathies. PLoS One 2013; 8: e67527.

Bönnemann CG. The collagen VI-related myopathies. In: Handbook of clinical neurology. 2011. p. 81–96

Bönnemann CG. The collagen VI-related myopathies: muscle meets its matrix. Nat Rev Neurol 2011; 7: 379–390.

Bonnette H, Roelofs R, Olson Wh. Multicore disease: Report of a case with onset in middle age. Neurology 1974; 24: 1039–1039.

Boyden SE, Mahoney LJ, Kawahara G, Myers JA, Mitsuhashi S, Estrella EA, et al. Mutations in the satellite cell gene *MEGF10* cause a recessive congenital myopathy with minicores. Neurogenetics 2012; 13: 115–24.

Brown MR, Cohen HJ, Lyons JM, Curtis TW, Thunberg B, Cochran WJ, et al. Proximal muscle weakness and selenium deficiency associated with long term parenteral nutrition. Am J Clin Nutr 1986; 43: 549–54.

Buj-Bello A, Laugel V, Messaddeq N, Zahreddine H, Laporte J, Pellissier J-F, et al. The lipid phosphatase myotubularin is essential for skeletal muscle maintenance but not for myogenesis in mice. Proc Natl Acad Sci 2002; 99: 15060–15065.

Burke RE, Levine DN, Salcman M, Tsairis P. Motor units in cat soleus muscle: physiological, histochemical and morphological characteristics. J Physiol 1974; 238: 503–514.

Burke RE, Levine DN, Tsairis P, Zajac FE. Physiological types and histochemical profiles in motor units of the cat gastrocnemius. J Physiol 1973; 234: 723–748.

Buttitta LA, Edgar BA. Mechanisms controlling cell cycle exit upon terminal differentiation. Curr Opin Cell Biol 2007; 19: 697–704.

Cadart C, Monnier S, Grilli J, Sáez PJ, Srivastava N, Attia R, et al. Size control in mammalian cells involves modulation of both growth rate and cell cycle duration. Nat Commun 2018; 9: 3275.

Caggiano S, Khirani S, Dabaj I, Cavassa E, Amaddeo A, Arroyo JO, et al. Diaphragmatic dysfunction in SEPN1-related myopathy. Neuromuscul Disord 2017; 27: 747–755.

Cao Y, Yao Z, Sarkar D, Lawrence M, Sanchez GJ, Parker MH, et al. Genome-wide MyoD Binding in

Skeletal Muscle Cells: A Potential for Broad Cellular Reprogramming. Dev Cell 2010; 18: 662–674.

Carlier R-Y, Quijano-Roy S. Myoimaging in Congenital Myopathies. Semin Pediatr Neurol 2019; 29: 30–43.

Castets P, Lescure A, Guicheney P, Allamand V. Selenoprotein N in skeletal muscle: From diseases to function. J Mol Med 2012; 90: 1095–1107.

Cenciarelli C, De Santa F, Puri PL, Mattei E, Ricci L, Bucci F, et al. Critical Role Played by Cyclin D3 in the MyoD-Mediated Arrest of Cell Cycle during Myoblast Differentiation. Mol Cell Biol 1999; 19: 5203–5217.

Ceyhan-Birsoy O, Agrawal PB, Hidalgo C, Schmitz-Abe K, DeChene ET, Swanson LC, et al. Recessive truncating titin gene, TTN, mutations presenting as centronuclear myopathy. Neurology 2013; 81: 1205–1214.

Chal J, Pourquié O. Making muscle: skeletal myogenesis *in vivo* and *in vitro*. Development 2017; 144: 2104–2122.

Chauveau C, Bonnemann CG, Julien C, Kho AL, Marks H, Talim B, et al. Recessive *TTN* truncating mutations define novel forms of core myopathy with heart disease. Hum Mol Genet 2014; 23: 980–991.

Chauveau C, Rowell J, Ferreiro A. A rising titan: *TTN* review and mutation update. Hum Mutat 2014; 35: 1046–59.

Che Y, Li Y, Zheng F, Zou K, Li Z, Chen M, et al. *TRIP4* promotes tumor growth and metastasis and regulates radiosensitivity of cervical cancer by activating MAPK, PI3K/AKT, and hTERT signaling. Cancer Lett 2019; 452: 1–13.

Cherkasova V, Ayyadevara S, Egilmez N, Shmookler Reis R. Diverse Caenorhabditis elegans genes that are upregulated in dauer larvae also show elevated transcript levels in long-lived, aged, or starved adults. J Mol Biol 2000; 300: 433–48.

Chu M, Gregorio CC, Pappas CT. Nebulin, a multi-functional giant. J Exp Biol 2016; 219: 146–152.

Clarke NF. Congenital Fiber-Type Disproportion. Semin Pediatr Neurol 2011; 18: 264–271.

Clarke NF, Kidson W, Quijano-Roy S, Estournet B, Ferreiro A, Guicheney P, et al. SEPN1: associated with congenital fiber-type disproportion and insulin resistance. Ann Neurol 2006; 59: 546–52.

Collins CA, Olsen I, Zammit PS, Heslop L, Petrie A, Partridge TA, et al. Stem Cell Function, Self-Renewal, and Behavioral Heterogeneity of Cells from the Adult Muscle Satellite Cell Niche. Cell 2005; 122: 289–301.

Collins CA, Partridge TA. Self-Renewal of the Adult Skeletal Muscle Satellite Cell. Cell Cycle 2005; 4: 1338–1341.

Cowling BS, Toussaint A, Muller J, Laporte J. Defective Membrane Remodeling in Neuromuscular Diseases: Insights from Animal Models. PLoS Genet 2012; 8: e1002595.

Cullup T, Lamont PJ, Cirak S, Damian MS, Wallefeld W, Gooding R, et al. Mutations in *MYH7* cause Multi-minicore Disease (MmD) with variable cardiac involvement. Neuromuscul Disord 2012; 22: 1096–104.

Dale HH, Feldberg W, Vogt M. Release of acetylcholine at voluntary motor nerve endings. J Physiol 1936; 86: 353–380.

Darin N, Tulinius M. Neuromuscular disorders in childhood: a descriptive epidemiological study from western Sweden. Neuromuscul Disord 2000; 10: 1–9.

Dasgupta S, Lonard DM, O'Malley BW. Nuclear receptor coactivators: master regulators of human health and disease. Annu Rev Med 2014; 65: 279–92.

Davidson AE, Siddiqui FM, Lopez MA, Lunt P, Carlson HA, Moore BE, et al. Novel deletion of lysine 7 expands the clinical, histopathological and genetic spectrum of TPM2-related myopathies. Brain 2013; 136: 508–21.

Davignon L, Chauveau C, Julien C, Dill C, Duband-Goulet I, Cabet E, et al. The transcription coactivator ASC-1 is a regulator of skeletal myogenesis, and its deficiency causes a novel form of congenital muscle disease. Hum Mol Genet 2016; 25: 1559–1573.

Dowling JJ, Arbogast S, Hur J, Nelson DD, McEvoy A, Waugh T, et al. Oxidative stress and successful antioxidant treatment in models of RYR1-related myopathy. Brain 2012; 135: 1115–1127.

Dowling JJ, Joubert R, Low SE, Durban AN, Messaddeq N, Li X, et al. Myotubular myopathy and the neuromuscular junction: a novel therapeutic approach from mouse models. Dis Model Mech 2012; 5: 852–859.

Dowling JJ, Lawlor MW, Dirksen RT. Triadopathies: an emerging class of skeletal muscle diseases. Neurotherapeutics 2014; 11: 773–85.

Dowling JJ, Vreede AP, Low SE, Gibbs EM, Kuwada JY, Bonnemann CG, et al. Loss of myotubularin function results in T-tubule disorganization in zebrafish and human myotubular myopathy. PLoS Genet 2009; 5: e1000372.

Duane DD, Engel AG. Emetine myopathy. Neurology 1970; 20: 733–9.

Dubowitz V, Sewry CA. Muscle Biopsy: a Practical Approach [Internet]. Philadelphia: Saunders Elsevier; 2007 https://www.ncbi.nlm.nih.gov/nlmcatalog/101294751

Echaniz-Laguna A, Biancalana V, Böhm J, Tranchant C, Mandel J-L, Laporte J. Adult centronuclear myopathies: A hospital-based study. Rev Neurol (Paris) 2013; 169: 625–631.

Engel AG, Gomez MR, Groover R V. Multicore disease. A recently recognized congenital myopathy associated with multifocal degeneration of muscle fibers. Mayo Clin Proc 1971; 46: 666–81.

Essén B, Jansson E, Henriksson J, Taylor AW, Saltin B. Metabolic Characteristics of Fibre Types in Human Skeletal Muscle. Acta Physiol Scand 1975; 95: 153–165.

Estañ MC, Fernández-Núñez E, Zaki MS, Esteban MI, Donkervoort S, Hawkins C, et al. Recessive mutations in muscle-specific isoforms of FXR1 cause congenital multi-minicore myopathy. Nat Commun 2019; 10: 797.

Evilä A, Vihola A, Sarparanta J, Raheem O, Palmio J, Sandell S, et al. Atypical phenotypes in titinopathies explained by second titin mutations. Ann Neurol 2014; 75: 230–40.

Ezhevsky SA, Ho A, Becker-Hapak M, Davis PK, Dowdy SF. Differential regulation of retinoblastoma tumor suppressor protein by G(1) cyclin-dependent kinase complexes in vivo. Mol Cell Biol 2001; 21: 4773–84.

Fadic R, Waclawik AJ, Brooks BR, Lotz BP. The rigid spine syndrome due to acid maltase deficiency. Muscle Nerve 1997; 20: 364–366.

Feng J-J, Marston S. Genotype–phenotype correlations in *ACTA1* mutations that cause congenital

myopathies. Neuromuscul Disord 2009; 19: 6–16.

Ferreiro A, Ceuterick-de Groote C, Marks JJ, Goemans N, Schreiber G, Hanefeld F, et al. Desmin-related myopathy with Mallory body-like inclusions is caused by mutations of the selenoprotein N gene. Ann Neurol 2004; 55: 676–86.

Ferreiro A, Estournet B, Chateau D, Romero NB, Laroche C, Odent S, et al. Multi-minicore disease--searching for boundaries: phenotype analysis of 38 cases. Ann Neurol 2000; 48: 745–57.

Ferreiro A, Monnier N, Romero NB, Leroy J-P, Bönnemann C, Haenggeli C-A, et al. A recessive form of central core disease, transiently presenting as multi-minicore disease, is associated with a homozygous mutation in the ryanodine receptor type 1 gene. Ann Neurol 2002; 51: 750–759.

Ferreiro A, Quijano-Roy S, Pichereau C, Moghadaszadeh B, Goemans N, Bönnemann C, et al. Mutations of the selenoprotein N gene, which is implicated in rigid spine muscular dystrophy, cause the classical phenotype of multiminicore disease: reassessing the nosology of early-onset myopathies. Am J Hum Genet 2002; 71: 739–49.

Figueroa-Bonaparte S, Segovia S, Llauger J, Belmonte I, Pedrosa I, Alejaldre A, et al. Muscle MRI Findings in Childhood/Adult Onset Pompe Disease Correlate with Muscle Function. PLoS One 2016; 11: e0163493.

Fiorillo C, Astrea G, Savarese M, Cassandrini D, Brisca G, Trucco F, et al. MYH7-related myopathies: clinical, histopathological and imaging findings in a cohort of Italian patients. Orphanet J Rare Dis 2016; 11: 91.

Fluck M. Functional, structural and molecular plasticity of mammalian skeletal muscle in response to exercise stimuli. J Exp Biol 2006; 209: 2239–2248.

Franaszczyk M, Chmielewski P, Truszkowska G, Stawinski P, Michalak E, Rydzanicz M, et al. Titin Truncating Variants in Dilated Cardiomyopathy – Prevalence and Genotype-Phenotype Correlations. PLoS One 2017; 12: e0169007.

Fridén J, Sjöström M, Ekblom B. Muscle fibre type characteristics in endurance trained and untrained individuals. Eur J Appl Physiol Occup Physiol 1984; 52: 266–71.

Frontera WR, Ochala J. Skeletal Muscle: A Brief Review of Structure and Function. Calcif Tissue Int 2015; 96: 183–195.

Fu M, Rao M, Bouras T, Wang C, Wu K, Zhang X, et al. Cyclin D1 Inhibits Peroxisome Proliferator-activated Receptor γ-mediated Adipogenesis through Histone Deacetylase Recruitment. J Biol Chem 2005; 280: 16934–16941.

Garibaldi M, Fattori F, Bortolotti CA, Brochier G, Labasse C, Verardo M, et al. Core-rod myopathy due to a novel mutation in BTB/POZ domain of *KBTBD13* manifesting as late onset LGMD. Acta Neuropathol Commun 2018; 6: 94.

Garrow JS, Webster J. Quetelet's index (W/H2) as a measure of fatness. Int J Obes 1985; 9: 147–53.

Giannattasio S, Giacovazzo G, Bonato A, Caruso C, Luvisetto S, Coccurello R, et al. Lack of cyclin D3 induces skeletal muscle fiber-type shifting, increased endurance performance and hypermetabolism. Sci Rep 2018; 8: 12792.

Gibbs EM, Clarke NF, Rose K, Oates EC, Webster R, Feldman EL, et al. Neuromuscular junction abnormalities in DNM2-related centronuclear myopathy. J Mol Med 2013; 91: 727–737.

Gibbs EM, Feldman EL, Dowling JJ. The role of MTMR14 in autophagy and in muscle disease. Autophagy 2010; 6: 819–820.

Gilbreath HR, Castro D, Iannaccone ST. Congenital myopathies and muscular dystrophies. Neurol Clin 2014; 32: 689–703, viii.

Gómez-Andrés D, Díaz-Manera J, Alejaldre A, Pulido-Valdeolivas I, González-Mera L, Olivé M, et al. Muscle imaging in laminopathies: Synthesis study identifies meaningful muscles for follow-up. Muscle Nerve 2018; 58: 812–817.

Gonorazky HD, Bönnemann CG, Dowling JJ. The genetics of congenital myopathies. In: Handbook of clinical neurology. 2018. p. 549–564

Halevy O, Novitch BG, Spicer DB, Skapek SX, Rhee J, Hannon GJ, et al. Correlation of terminal cell cycle arrest of skeletal muscle with induction of p21 by MyoD. Science 1995; 267: 1018–21.

Hankiewicz K, Carlier RY, Lazaro L, Linzoain J, Barnerias C, Gómez-Andrés D, et al. Whole-body muscle magnetic resonance imaging in SEPN1-related myopathy shows a homogeneous and recognizable pattern. Muscle and Nerve 2015; 52: 728–735.

Hao J, Xu H, Luo M, Yu W, Chen M, Liao Y, et al. The Tumor-Promoting Role of *TRIP4* in Melanoma Progression and its Involvement in Response to BRAF-Targeted Therapy. J Invest Dermatol 2018; 138: 159–170.

Hernández-Hernández JM, García-González EG, Brun CE, Rudnicki MA. The myogenic regulatory factors, determinants of muscle development, cell identity and regeneration. Semin Cell Dev Biol 2017; 72: 10–18.

Hnia K, Tronchère H, Tomczak KK, Amoasii L, Schultz P, Beggs AH, et al. Myotubularin controls desmin intermediate filament architecture and mitochondrial dynamics in human and mouse skeletal muscle. J Clin Invest 2011; 121: 70–85.

Horstick EJ, Linsley JW, Dowling JJ, Hauser MA, McDonald KK, Ashley-Koch A, et al. Stac3 is a component of the excitation–contraction coupling machinery and mutated in Native American myopathy. Nat Commun 2013; 4: 1952.

Illingworth MA, Main M, Pitt M, Feng L, Sewry CA, Gunny R, et al. RYR1-related congenital myopathy with fatigable weakness, responding to pyridostigimine. Neuromuscul Disord 2014; 24: 707–12.

Iyer LM, Burroughs AM, Aravind L. The ASCH superfamily: novel domains with a fold related to the PUA domain and a potential role in RNA metabolism. Bioinformatics 2006; 22: 257–63.

Jiang W, Kahn SM, Zhou P, Zhang YJ, Cacace AM, Infante AS, et al. Overexpression of cyclin D1 in rat fibroblasts causes abnormalities in growth control, cell cycle progression and gene expression. Oncogene 1993; 8: 3447–57.

Joubert R, Vignaud A, Le M, Moal C, Messaddeq N, Buj-Bello A. Site-specific Mtm1 mutagenesis by an AAV-Cre vector reveals that myotubularin is essential in adult muscle. Hum Mol Genet 2013; 22: 1856–1866.

Jung D-J, Sung H-S, Goo Y-W, Lee HM, Park OK, Jung S-Y, et al. Novel transcription coactivator complex containing activating signal cointegrator 1. Mol Cell Biol 2002; 22: 5203–11.

Jungbluth H, Davis MR, Müller C, Counsell S, Allsop J, Chattopadhyay A, et al. Magnetic resonance imaging of muscle in congenital myopathies associated with RYR1 mutations. Neuromuscul Disord

2004; 14: 785–790.

Jungbluth H, Gautel M. Pathogenic Mechanisms in Centronuclear Myopathies. Front Aging Neurosci 2014; 6: 339.

Jungbluth H, Muntoni F. Therapeutic Aspects in Congenital Myopathies. Semin Pediatr Neurol 2019; 29: 71–82.

Jungbluth H, Ochala J, Treves S, Gautel M. Current and future therapeutic approaches to the congenital myopathies. Semin Cell Dev Biol 2017; 64: 191–200.

Jungbluth H, Sewry CA, Muntoni F. Core Myopathies. Semin Pediatr Neurol 2011; 18: 239–249.

Jungbluth H, Treves S, Zorzato F, Sarkozy A, Ochala J, Sewry C, et al. Congenital myopathies: disorders of excitation-contraction coupling and muscle contraction. Nat Rev Neurol 2018; 14: 151–167.

Jurynec MJ, Xia R, Mackrill JJ, Gunther D, Crawford T, Flanigan KM, et al. Selenoprotein N is required for ryanodine receptor calcium release channel activity in human and zebrafish muscle. Proc Natl Acad Sci U S A 2008; 105: 12485–90.

Kaindl AM, Rüschendorf F, Krause S, Goebel H-H, Koehler K, Becker C, et al. Missense mutations of *ACTA1* cause dominant congenital myopathy with cores. J Med Genet 2004; 41: 842–8.

Kakulas BA, Morrison I, Owen ET, Kitridou R. Unusual paraspinal muscle lesions in ankylosing spondylitis. Clin Exp Neurol 1987; 23: 23–9.

Kaplan J-C, Hamroun D. The 2016 version of the gene table of monogenic neuromuscular disorders (nuclear genome). Neuromuscul Disord 2015; 25: 991–1020.

Karpati G, Carpenter S, Eisen AA. Experimental core-like lesions and nemaline rods. A correlative morphological and physiological study. Arch Neurol 1972; 27: 237–51.

Kim HJ, Yi JY, Sung HS, Moore DD, Jhun BH, Lee YC, et al. Activating signal cointegrator 1, a novel transcription coactivator of nuclear receptors, and its cytosolic localization under conditions of serum deprivation. Mol Cell Biol 1999; 19: 6323–32.

Kim HJ, Kwak H-B, Thompson L V., Lawler JM. Contribution of oxidative stress to pathology in diaphragm and limb muscles with Duchenne muscular dystrophy. J Muscle Res Cell Motil 2013; 34: 1–13.

Kitzmann M, Carnac G, Vandromme M, Primig M, Lamb NJC, Fernandez A. The Muscle Regulatory Factors MyoD and Myf-5 Undergo Distinct Cell Cycle–specific Expression in Muscle Cells. J Cell Biol 1998; 142: 1447–1459.

Knierim E, Hirata H, Wolf NI, Morales-Gonzalez S, Schottmann G, Tanaka Y, et al. Mutations in Subunits of the Activating Signal Cointegrator 1 Complex Are Associated with Prenatal Spinal Muscular Atrophy and Congenital Bone Fractures. Am J Hum Genet 2016; 98: 473–489.

Knöll R, Buyandelger B, Lab M. The sarcomeric Z-disc and Z-discopathies. J Biomed Biotechnol 2011; 2011: 569628.

Krahn M, Biancalana V, Cerino M, Perrin A, Michel-Calemard L, Nectoux J, et al. A National French consensus on gene lists for the diagnosis of myopathies using next-generation sequencing. Eur J Hum Genet 2018

Kubo S, Tsukahara T, Takemitsu M, Yoon KB, Utsumi H, Nonaka I, et al. Presence of emerinopathy

in cases of rigid spine syndrome. Neuromuscul Disord 1998; 8: 502–7.

Kuczmarski RJ, Ogden CL, Guo SS, Grummer-Strawn LM, Flegal KM, Mei Z, et al. 2000 CDC Growth Charts for the United States: methods and development. Vital Health Stat 11 2002: 1–190.

LaBaer J, Garrett MD, Stevenson LF, Slingerland JM, Sandhu C, Chou HS, et al. New functional activities for the p21 family of CDK inhibitors. Genes Dev 1997; 11: 847–862.

Laforêt P, Doppler V, Caillaud C, Laloui K, Claeys KG, Richard P, et al. Rigid spine syndrome revealing late-onset Pompe disease. Neuromuscul Disord 2010; 20: 128–130.

Laing NG, Clarke NF, Dye DE, Liyanage K, Walker KR, Kobayashi Y, et al. Actin mutations are one cause of congenital fibre type disproportion. Ann Neurol 2004; 56: 689–694.

Lamand M. [Biochemical lesions in calf myopathy by selenium deficiency]. C R Acad Sci Hebd Seances Acad Sci D 1970; 270: 417–20.

Lassche S, Stienen GJM, Irving TC, van der Maarel SM, Voermans NC, Padberg GW, et al. Sarcomeric dysfunction contributes to muscle weakness in facioscapulohumeral muscular dystrophy. Neurology 2013; 80: 733–737.

Lassing I, Schmitzberger F, Björnstedt M, Holmgren A, Nordlund P, Schutt CE, et al. Molecular and structural basis for redox regulation of beta-actin. J Mol Biol 2007; 370: 331–48.

Lehtokari V-L, Gardberg M, Pelin K, Wallgren-Pettersson C. Clinically variable nemaline myopathy in a three-generation family caused by mutation of the skeletal muscle alpha-actin gene. Neuromuscul Disord 2018; 28: 323–326.

Lescure A, Gautheret D, Carbon P, Krol A. Novel selenoproteins identified in silico and in vivo by using a conserved RNA structural motif. J Biol Chem 1999; 274: 38147–54.

Lescure A, Rederstorff M, Krol A, Guicheney P, Allamand V. Selenoprotein function and muscle disease. Biochim Biophys Acta - Gen Subj 2009; 1790: 1569–1574.

Leshem Y, Halevy O. Phosphorylation of pRb is required for HGF-induced muscle cell proliferation and is p27kip1-dependent. J Cell Physiol 2002; 191: 173–182.

Li Y-P, Chen Y, Li AS, Reid MB. Hydrogen peroxide stimulates ubiquitin-conjugating activity and expression of genes for specific E2 and E3 proteins in skeletal muscle myotubes. Am J Physiol Physiol 2003; 285: C806–C812.

Linke WA. Titin Gene and Protein Functions in Passive and Active Muscle. Annu Rev Physiol 2018; 80: 389–411.

Linke WA, Fernandez JM. Cardiac titin: molecular basis of elasticity and cellular contribution to elastic and viscous stiffness components in myocardium. J Muscle Res Cell Motil 2002; 23: 483–97.

Littlefield R, Almenar-Queralt A, Fowler VM. Actin dynamics at pointed ends regulates thin filament length in striated muscle. Nat Cell Biol 2001; 3: 544–551.

Lornage X, Romero NB, Grosgogeat CA, Malfatti E, Donkervoort S, Marchetti MM, et al. *ACTN2* mutations cause 'Multiple structured Core Disease' (MsCD). Acta Neuropathol 2019; 137: 501–519.

Lornage X, Schartner V, Balbueno I, Biancalana V, Willis T, Echaniz-Laguna A, et al. Clinical, histological, and genetic characterization of PYROXD1-related myopathy. Acta Neuropathol Commun 2019; 7: 138.

Luther PK. The vertebrate muscle Z-disc: sarcomere anchor for structure and signalling. J Muscle Res Cell Motil 2009; 30: 171–85.

Maggi L, Scoto M, Cirak S, Robb SA, Klein A, Lillis S, et al. Congenital myopathies – Clinical features and frequency of individual subtypes diagnosed over a 5-year period in the United Kingdom. Neuromuscul Disord 2013; 23: 195–205.

Maiti B, Arbogast S, Allamand V, Moyle MW, Anderson CB, Richard P, et al. A mutation in the *SEPN1* selenocysteine redefinition element (SRE) reduces selenocysteine incorporation and leads to *SEPN1* -related myopathy. Hum Mutat 2009; 30: 411–416.

Majczenko K, Davidson AE, Camelo-Piragua S, Agrawal PB, Manfready RA, Li X, et al. Dominant mutation of *CCDC78* in a unique congenital myopathy with prominent internal nuclei and atypical cores. Am J Hum Genet 2012; 91: 365–71.

Malfatti E, Romero NB. Nemaline myopathies: State of the art. Rev Neurol (Paris) 2016; 172: 614–619.

Marino M, Stoilova T, Giorgi C, Bachi A, Cattaneo A, Auricchio A, et al. SEPN1, an endoplasmic reticulum-localized selenoprotein linked to skeletal muscle pathology, counteracts hyperoxidation by means of redox-regulating SERCA2 pump activity. Hum Mol Genet 2015; 24: 1843–1855.

Martin JJ, Bruyland M, Busch HF, Farriaux JP, Krivosic I, Ceuterick C. Pleocore disease. Multi-minicore disease and focal loss of cross striations. Acta Neuropathol 1986; 72: 142–9.

Mastaglia Fl, Ojeda Vj, Sarnat Hb, Kakulas Ba. Myopathies Associated With Hypothyroidism: A Review Based Upon 13 Cases. Aust N Z J Med 1988; 18: 799–806.

Mazumder R, Iyer LM, Vasudevan S, Aravind L. Detection of novel members, structure-function analysis and evolutionary classification of the 2H phosphoesterase superfamily. Nucleic Acids Res 2002; 30: 5229–43.

Meltzer Hy, Kuncl Rw, Click J, Yang V. Incidence of Z band streaming and myofibrillar disruptions in skeletal muscle from healthy young people. Neurology 1976; 26: 853–853.

Mercuri E, Cini C, Pichiecchio A, Allsop J, Counsell S, Zolkipli Z, et al. Muscle magnetic resonance imaging in patients with congenital muscular dystrophy and Ullrich phenotype. Neuromuscul Disord 2003; 13: 554–8.

Mercuri E, Lampe A, Allsop J, Knight R, Pane M, Kinali M, et al. Muscle MRI in Ullrich congenital muscular dystrophy and Bethlem myopathy. Neuromuscul Disord 2005; 15: 303–310.

Moghadaszadeh B, Desguerre I, Topaloglu H, Muntoni F, Pavek S, Sewry C, et al. Identification of a new locus for a peculiar form of congenital muscular dystrophy with early rigidity of the spine, on chromosome 1p35-36. Am J Hum Genet 1998; 62: 1439–45.

Moghadaszadeh B, Petit N, Jaillard C, Brockington M, Quijano Roy S, Merlini L, et al. Mutations in *SEPN1* cause congenital muscular dystrophy with spinal rigidity and restrictive respiratory syndrome. Nat Genet 2001; 29: 17–8.

Morgan JE, Partridge TA. Muscle satellite cells. Int J Biochem Cell Biol 2003; 35: 1151–6.

Moulin M, Ferreiro A. Muscle redox disturbances and oxidative stress as pathomechanisms and therapeutic targets in early-onset myopathies. Semin Cell Dev Biol 2017; 64: 213–223.

Mukoyama M. [Central core disease and multicore disease]. Nihon Rinsho 1978; Suppl: 1748–9.

Mukoyama M, Matsuoka Y, Kato H, Sobue I. [Multicore disease]. Rinsho Shinkeigaku 1973; 13: 221–7.

Narasimha AM, Kaulich M, Shapiro GS, Choi YJ, Sicinski P, Dowdy SF. Cyclin D activates the Rb tumor suppressor by mono-phosphorylation. [Internet]. Elife 2014; 3[cited 2019 Jun 12] Available from: https://elifesciences.org/articles/02872

Nicolau S, Liewluck T, Tracy JA, Laughlin RS, Milone M. Congenital myopathies in the adult neuromuscular clinic. Neurol Genet 2019; 5: e341.

Nigro V, Piluso G. Next generation sequencing (NGS) strategies for the genetic testing of myopathies. Acta Myol myopathies cardiomyopathies Off J Mediterr Soc Myol 2012; 31: 196–200.

North KN. Clinical Approach to the Diagnosis of Congenital Myopathies. Semin Pediatr Neurol 2011; 18: 216–220.

North KN, Wang CH, Clarke N, Jungbluth H, Vainzof M, Dowling JJ, et al. Approach to the diagnosis of congenital myopathies. Neuromuscul Disord 2014; 24: 97–116.

Norwood FLM, Harling C, Chinnery PF, Eagle M, Bushby K, Straub V. Prevalence of genetic muscle disease in Northern England: in-depth analysis of a muscle clinic population. Brain 2009; 132: 3175–3186.

Oates EC, Jones KJ, Donkervoort S, Charlton A, Brammah S, Smith JE, et al. Congenital Titinopathy: Comprehensive characterization and pathogenic insights. Ann Neurol 2018; 83: 1105–1124.

Ockeloen CW, Gilhuis HJ, Pfundt R, Kamsteeg EJ, Agrawal PB, Beggs AH, et al. Congenital myopathy caused by a novel missense mutation in the CFL2 gene. Neuromuscul Disord 2012; 22: 632–9.

Olivé M, Goldfarb LG, Lee H-S, Odgerel Z, Blokhin A, Gonzalez-Mera L, et al. Nemaline myopathy type 6: Clinical and myopathological features. Muscle Nerve 2010; 42: 901–907.

Oliveira J, Martins M, Pinto Leite R, Sousa M, Santos R. The new neuromuscular disease related with defects in the ASC-1 complex: report of a second case confirms ASCC1 involvement. Clin Genet 2017; 92: 434–439.

Ottenheijm CAC, Granzier H. Lifting the Nebula: Novel Insights into Skeletal Muscle Contractility. Physiology 2010; 25: 304–310.

Pambianco S, Giovarelli M, Perrotta C, Zecchini S, Cervia D, Di Renzo I, et al. Reversal of Defective Mitochondrial Biogenesis in Limb-Girdle Muscular Dystrophy 2D by Independent Modulation of Histone and PGC-1α Acetylation. Cell Rep 2016; 17: 3010–3023.

Pappas CT, Bhattacharya N, Cooper JA, Gregorio CC. Nebulin interacts with CapZ and regulates thin filament architecture within the Z-disc. Mol Biol Cell 2008; 19: 1837–47.

Pellegrini G, Barbieri S, Moggio M, Cheldi A, Scarlato G, Minetti C. A Case of Congenital Neuromuscular Disease with Uniform Type I Fibers, Abnormal Mitochondrial Network and Jagged Z-Line. Neuropediatrics 1985; 16: 162–166.

Pellissier JF, de Barsy T, Faugere MC, Rebuffel P. Type III glycogenosis with multicore structures. Muscle Nerve 1979; 2: 124–32.

Pernigo S, Fukuzawa A, Bertz M, Holt M, Rief M, Steiner RA, et al. Structural insight into M-band assembly and mechanics from the titin-obscurin-like-1 complex. Proc Natl Acad Sci U S A 2010; 107: 2908–13.

Petit N, Lescure A, Rederstorff M, Krol A, Moghadaszadeh B, Wewer UM, et al. Selenoprotein N: an endoplasmic reticulum glycoprotein with an early developmental expression pattern. Hum Mol Genet 2003; 12: 1045–53.

Phadke R. Myopathology of Congenital Myopathies: Bridging the Old and the New. Semin Pediatr Neurol 2019; 29: 55–70.

Poon RYC. Cell Cycle Control: A System of Interlinking Oscillators. In: Methods in molecular biology (Clifton, N.J.). 2016. p. 3–19

Pozzer D, Varone E, Chernorudskiy A, Schiarea S, Missiroli S, Giorgi C, et al. A maladaptive ER stress response triggers dysfunction in highly active muscles of mice with SELENON loss. Redox Biol 2019; 20: 354–366.

Puri PL, Avantaggiati ML, Balsano C, Sang N, Graessmann A, Giordano A, et al. p300 is required for MyoD-dependent cell cycle arrest and muscle-specific gene transcription. EMBO J 1997; 16: 369–383.

Quelle DE, Ashmun RA, Shurtleff SA, Kato JY, Bar-Sagi D, Roussel MF, et al. Overexpression of mouse D-type cyclins accelerates G1 phase in rodent fibroblasts. Genes Dev 1993; 7: 1559–71.

Quijano-Roy S, Avila-Smirnow D, Carlier RY, WB-MRI muscle study group. Whole body muscle MRI protocol: Pattern recognition in early onset NM disorders. Neuromuscul Disord 2012; 22: S68–S84.

Quijano-Roy S, Mbieleu B, Bönnemann CG, Jeannet P-Y, Colomer J, Clarke NF, et al. De novo *LMNA* mutations cause a new form of congenital muscular dystrophy. Ann Neurol 2008; 64: 177–186.

Ravenscroft G, Laing NG, Bönnemann CG. Pathophysiological concepts in the congenital myopathies: blurring the boundaries, sharpening the focus. Brain 2015; 138: 246–68.

Rederstorff M, Castets P, Arbogast S, Lainé J, Vassilopoulos S, Beuvin M, et al. Increased Muscle Stress-Sensitivity Induced by Selenoprotein N Inactivation in Mouse: A Mammalian Model for SEPN1-Related Myopathy. PLoS One 2011; 6: e23094.

Ricoy JR, Cabello A, Goizueta G. Myopathy with multiple minicore--report of two siblings. J Neurol Sci 1980; 48: 81–92.

Rodríguez Cruz PM, Sewry C, Beeson D, Jayawant S, Squier W, McWilliam R, et al. Congenital myopathies with secondary neuromuscular transmission defects; a case report and review of the literature. Neuromuscul Disord 2014; 24: 1103–10.

Romero-Suarez S, Shen J, Brotto L, Hall T, Mo C, Valdivia HH, et al. Muscle-specific inositide phosphatase (MIP/MTMR14) is reduced with age and its loss accelerates skeletal muscle aging process by altering calcium homeostasis. Aging (Albany NY) 2010; 2: 504–13.

Romero NB, Bitoun M. Centronuclear Myopathies. Semin Pediatr Neurol 2011; 18: 250–256.

Ruiz A, Heilmann S, Becker T, Hernández I, Wagner H, Thelen M, et al. Follow-up of loci from the International Genomics of Alzheimer's Disease Project identifies TRIP4 as a novel susceptibility gene. Transl Psychiatry 2014; 4: e358–e358.

Salih MAM. Hereditary and Acquired Myopathies. In: Elzouki AY, Harfi HA, Nazer HM, Stapleton FB, Oh W, Whitley RJ, editor(s). Textbook of Clinical Pediatrics. Berlin, Heidelberg: Springer Berlin Heidelberg; 2012. p. 3503–3541

Sanoudou D, Corbett MA, Han M, Ghoddusi M, Nguyen MAT, Vlahovich N, et al. Skeletal muscle repair in a mouse model of nemaline myopathy. Hum Mol Genet 2006; 15: 2603–2612.

De Santa F, Albini S, Mezzaroma E, Baron L, Felsani A, Caruso M. pRb-dependent cyclin D3 protein stabilization is required for myogenic differentiation. Mol Cell Biol 2007; 27: 7248–65.

Sarruf DA, Iankova I, Abella A, Assou S, Miard S, Fajas L. Cyclin D3 promotes adipogenesis through activation of peroxisome proliferator-activated receptor gamma. Mol Cell Biol 2005; 25: 9985–95.

Savarese M, Maggi L, Vihola A, Jonson PH, Tasca G, Ruggiero L, et al. Interpreting Genetic Variants in Titin in Patients With Muscle Disorders. JAMA Neurol 2018; 75: 557.

Savarese M, Sarparanta J, Vihola A, Udd B, Hackman P. Increasing Role of Titin Mutations in Neuromuscular Disorders. J Neuromuscul Dis 2016; 3: 293–308.

Schafer KA. The Cell Cycle: A Review. Vet Pathol 1998; 35: 461–478.

Schafer S, de Marvao A, Adami E, Fiedler LR, Ng B, Khin E, et al. Titin-truncating variants affect heart function in disease cohorts and the general population. Nat Genet 2017; 49: 46–53.

Schara U, Kress W, Bönnemann CG, Breitbach-Faller N, Korenke CG, Schreiber G, et al. The phenotype and long-term follow-up in 11 patients with juvenile selenoprotein N1-related myopathy. Eur J Paediatr Neurol 2008; 12: 224–230.

Schartner V, Romero NB, Donkervoort S, Treves S, Munot P, Pierson TM, et al. Dihydropyridine receptor (DHPR, CACNA1S) congenital myopathy. Acta Neuropathol 2017; 133: 517–533.

Schmitt HP, Volk B. The relationship between target, targetoid, and targetoid/core fibers in severe neurogenic muscular atrophy. J Neurol 1975; 210: 167–181.

Schorling D, Kirschner J, Bönnemann C. Congenital Muscular Dystrophies and Myopathies: An Overview and Update. Neuropediatrics 2017; 48: 247–261.

Scoto M, Cirak S, Mein R, Feng L, Manzur AY, Robb S, et al. SEPN1-related myopathies: Clinical course in a large cohort of patients. Neurology 2011; 76: 2073–2078.

Sewry CA, Holton JL, Dick DJ, Muntoni F, Hanna MG. Zebra body myopathy is caused by a mutation in the skeletal muscle actin gene (*ACTA1*). Neuromuscul Disord 2015; 25: 388–391.

Sewry CA, Wallgren-Pettersson C. Myopathology in congenital myopathies. Neuropathol Appl Neurobiol 2017; 43: 5–23.

Sframeli M, Sarkozy A, Bertoli M, Astrea G, Hudson J, Scoto M, et al. Congenital muscular dystrophies in the UK population: Clinical and molecular spectrum of a large cohort diagnosed over a 12-year period. Neuromuscul Disord 2017; 27: 793–803.

Shalaby S, Hayashi YK, Goto K, Ogawa M, Nonaka I, Noguchi S, et al. Rigid spine syndrome caused by a novel mutation in four-and-a-half LIM domain 1 gene (FHL1). Neuromuscul Disord 2008; 18: 959–961.

Skapek SX, Rhee J, Kim PS, Novitch BG, Lassar AB. Cyclin-mediated inhibition of muscle gene expression via a mechanism that is independent of pRB hyperphosphorylation. Mol Cell Biol 1996; 16: 7043–53.

Snoeck M, van Engelen BGM, Küsters B, Lammens M, Meijer R, Molenaar JPF, et al. *RYR1* -related myopathies: a wide spectrum of phenotypes throughout life. Eur J Neurol 2015; 22: 1094–1112.

Sorrentino V, Pepperkok R, Davis RL, Ansorge W, Philipson L. Cell proliferation inhibited by MyoD1 independently of myogenic differentiation. Nature 1990; 345: 813–5.

Sparrow JC, Nowak KJ, Durling HJ, Beggs AH, Wallgren-Pettersson C, Romero N, et al. Muscle disease caused by mutations in the skeletal muscle alpha-actin gene (ACTA1). Neuromuscul Disord 2003; 13: 519–31.

Susman RD, Quijano-Roy S, Yang N, Webster R, Clarke NF, Dowling J, et al. Expanding the clinical, pathological and MRI phenotype of DNM2-related centronuclear myopathy. Neuromuscul Disord 2010; 20: 229–37.

Swash M, Schwartz MS. Familial multicore disease with focal loss of cross-striations and ophthalmoplegia. J Neurol Sci 1981; 52: 1–10.

Tajsharghi H, Oldfors A. Myosinopathies: pathology and mechanisms. Acta Neuropathol 2013; 125: 3–18.

Talbot J, Maves L. Skeletal muscle fiber type: using insights from muscle developmental biology to dissect targets for susceptibility and resistance to muscle disease. Wiley Interdiscip Rev Dev Biol 2016; 5: 518–534.

Tice LW, Engel AG. The effects of glucocorticoids on red and white muscles in the rat. Am J Pathol 1967; 50: 311–33.

Tintignac LA, Leibovitch MP, Kitzmann M, Fernandez A, Ducommun B, Meijer L, et al. Cyclin E–Cdk2 Phosphorylation Promotes Late G1-Phase Degradation of MyoD in Muscle Cells. Exp Cell Res 2000; 259: 300–307.

Todd JJ, Lawal TA, Witherspoon JW, Chrismer IC, Razaqyar MS, Punjabi M, et al. Randomized controlled trial of N-acetylcysteine therapy for RYR1 -related myopathies . Neurology 2020: 10.1212/WNL.0000000000008872.

Tordjman M, Dabaj I, Laforet P, Felter A, Ferreiro A, Biyoukar M, et al. Muscular MRI-based algorithm to differentiate inherited myopathies presenting with spinal rigidity. Eur Radiol 2018; 28: 5293–5303.

Treves S, Jungbluth H, Voermans N, Muntoni F, Zorzato F. Ca 2+ handling abnormalities in early-onset muscle diseases: Novel concepts and perspectives. Semin Cell Dev Biol 2017; 64: 201–212.

Turner JJ, Ewald JC, Skotheim JM. Cell Size Control in Yeast. Curr Biol 2012; 22: R350–R359.

Vallat JM, de Lumley L, Loubet A, Leboutet MJ, Corvisier N, Umdenstock R. Coexistence of minicores, cores, and rods in the same muscle biopsy. Acta Neuropathol 1982; 58: 229–232.

Varone E, Pozzer D, Di Modica S, Chernorudskiy A, Nogara L, Baraldo M, et al. *SELENON* (*SEPN1*) protects skeletal muscle from saturated fatty acid-induced ER stress and insulin resistance. Redox Biol 2019; 24: 101176.

Varsano G, Wang Y, Wu M. Probing Mammalian Cell Size Homeostasis by Channel-Assisted Cell Reshaping. Cell Rep 2017; 20: 397–410.

Vick NA. Polymyositis: fine structure of capillaries and subcellular organelles. Neurology 1970; 20: 406.

Vihola A, Bassez G, Meola G, Zhang S, Haapasalo H, Paetau A, et al. Histopathological differences of myotonic dystrophy type 1 (DM1) and PROMM/DM2. Neurology 2003; 60: 1854–1857.

Villar-Quiles RN, Catervi F, Cabet E, Juntas-Morales R, Genetti CA, Gidaro T, et al. ASC1 is a cell cycle regulator associated with severe and mild forms of myopathy. Ann Neurol 2019: ana.25660.

Wallgren-Pettersson C, Bushby K, Mellies U, Simonds A, ENMC. 117th ENMC workshop: ventilatory support in congenital neuromuscular disorders -- congenital myopathies, congenital muscular dystrophies, congenital myotonic dystrophy and SMA (II) 4-6 April 2003, Naarden, The Netherlands. Neuromuscul Disord 2004; 14: 56–69.

Wallgren-Pettersson C, Sewry CA, Nowak KJ, Laing NG. Nemaline Myopathies. Semin Pediatr Neurol 2011; 18: 230–238.

Wang CH, Bonnemann CG, Rutkowski A, Sejersen T, Bellini J, Battista V, et al. Consensus statement on standard of care for congenital muscular dystrophies. J Child Neurol 2010; 25: 1559–81.

Wang CH, Quijano-roy S, Deconinck N, Bertini E, Ferreiro A, Muntoni F, et al. Diagnostic approach to the congenital muscular dystrophies. HHS Public Access ,Neuromuscul Disord 2017; 24: 289–311.

Ware JS, Cook SA. Role of titin in cardiomyopathy: from DNA variants to patient stratification. Nat Rev Cardiol 2017; 15: 241–252.

Wattjes MP, Kley RA, Fischer D. Neuromuscular imaging in inherited muscle diseases. Eur Radiol 2010; 20: 2447–2460.

Webster C, Silberstein L, Hays AP, Blau HM. Fast muscle fibers are preferentially affected in Duchenne muscular dystrophy. Cell 1988; 52: 503–513.

Wilmshurst JM, Lillis S, Zhou H, Pillay K, Henderson H, Kress W, et al. *RYR1* mutations are a common cause of congenital myopathies with central nuclei. Ann Neurol 2010; 68: 717–26.

Witt CC, Burkart C, Labeit D, McNabb M, Wu Y, Granzier H, et al. Nebulin regulates thin filament length, contractility, and Z-disk structure in vivo. EMBO J 2006; 25: 3843–55.

Wu S, Ibarra MCA, Malicdan MC V, Murayama K, Ichihara Y, Kikuchi H, et al. Central core disease is due to *RYR1* mutations in more than 90% of patients. Brain 2006; 129: 1470–1480.

Yoo HM, Kang SH, Kim JY, Lee JE, Seong MW, Lee SW, et al. Modification of ASC1 by UFM1 is crucial for ERα transactivation and breast cancer development. Mol Cell 2014; 56: 261–274.

Zammit PS. Function of the myogenic regulatory factors Myf5, MyoD, Myogenin and MRF4 in skeletal muscle, satellite cells and regenerative myogenesis. Semin Cell Dev Biol 2017; 72: 19–32.

Zappia MP, Rogers A, Islam ABMMK, Frolov M V. Rbf Activates the Myogenic Transcriptional Program to Promote Skeletal Muscle Differentiation. Cell Rep 2019; 26: 702–719.e6.

Zhou H, Rokach O, Feng L, Munteanu I, Mamchaoui K, Wilmshurst JM, et al. RyR1 deficiency in congenital myopathies disrupts excitation-contraction coupling. Hum Mutat 2013; 34: 986–96.

Zukosky K, Meilleur K, Traynor BJ, Dastgir J, Medne L, Devoto M, et al. Association of a Novel *ACTA1* Mutation With a Dominant Progressive Scapuloperoneal Myopathy in an Extended Family. JAMA Neurol 2015; 72: 689.

Zvaritch E, Kraeva N, Bombardier E, McCloy RA, Depreux F, Holmyard D, et al. Ca2+ dysregulation in Ryr1(I4895T/wt) mice causes congenital myopathy with progressive formation of minicores, cores, and nemaline rods. Proc Natl Acad Sci U S A 2009; 106: 21813–8.

World Medical Association declaration of Helsinki: Ethical principles for medical research involving human subjects. JAMA - J Am Med Assoc 2013; 310: 2191–2194.

ANNEXES

Annexe 1: Collaborating Centres

Annexe 1.1: SEPN1-RM phenotypical study

- Neuromuscular Unit, Centre de référence des maladies neuromusculaires Nord-Est-Ile de France, Institut de Myologie, AP-HP, Paris, France
- Neuromuscular Unit, Department of Pediatric Neurology, Intensive Care and Rehabilitation, Raymond Poincaré University Hospital, AP-HP, Garches, France.
- Department of Pediatric Neurology, Necker Enfants Malades Hospital, Paris Descartes University, Paris, France.
- Centre de Référence des maladies neuromusculaires Nord/Est/Ile de France, Service de neuropédiatrie, Hôpital Trousseau, Paris, France
- Molecular genetics department, UF Cardiogénétique et Myogénétique Moléculaire et Cellulaire, GH Pitié-Salpêtrière, AP-HP, Paris, France
- Neuromuscular Unit, Hôpital Marin, Hendaye, France
- Paediatrics Department, Hôpital de Hautepierre, Strasbourg, France
- Department of Neurology, Centre Hospitalier Universitaire, Grenoble, France
- Department of Neuropediatrics, CHRU de Tours, Université François Rabelais de Tours, UMR INSERM U1253, Tours, France
- Department of Paediatric Neurology, Medinzinische Fakultät Carl Gustav Carus, Technische Universität Dresden, Dresden, Germany
- Department of Pediatric Neurology; Center for Chronically Sick Children; Institute of Cell Biology and Neurobiology, Charité - Universitätsmedizin Berlin, Berlin, Germany
- Department of Pediatric Neurology, Georg-August University Goettingen, Germany
- Department of Neurology, FriedrichBaur-Institut, Ludwig-Maximilians-University of Munich, Germany
- Department of Pediatric Neurology, Developmental Neurology and Social Pediatrics, University of Essen, Germany.
- Institute of Human Genetics, University of Würzburg, Würzburg, Germany
- Department of Pediatric Neurology, University of Tübingen, Germany
- Neuromuscular and Neurogenetic Disorders of Childhood Section, National Institute of Neurological Disorders and Stroke, National Institutes of Health, Bethesda, MD, 20814, USA.
- Department of Child Neurology, University Hospitals Leuven, Leuven, Belgium
- Departments of Neuroscience and Pathology, Institute Born Bunge and University of Antwerp, Antwerp, Belgium
- Department of Pediatric Genetics, Marmara University Hospital, Istanbul, Turkey
- Hacettepe University, School of Medicine, Department of Child Neurology, Ankara, Turkey
- Department of Neurology, Amsterdam University Medical Centre, Amsterdam Neuroscience, Amsterdam, Netherlands.
- Neuromuscular and Neurodegenerative Disorders Unit, Bambino Gesu' Children's Research Hospital, Rome, Italy
- Department of Biomedical and Neuromotor Sciences, University of Bologna, Italy
- Department of Neuropediatrics, University children`s hospital of Basel (UKBB), Basel, Switzerland
- Neuromuscular Unit, Neuropaediatrics Department, Institut de Recerca Hospital Universitari Sant Joan de Deu, Barcelona, Spain; Center for the Biomedical Research on Rare Diseases (CIBERER), ISCIII, Spain
- Paediatric Neurology Department, Clínica Las Condes, Santiago, Chile
- Division of Pediatric Neurology, Department of Pediatrics, College of Medicine, King Saud University, Riyadh, Saudi Arabia

Annexe 1.2: ASC1-RM phenotypical study

- Basic and Translational Myology Lab, UMR8251, Université de Paris/CNRS, Paris, France
- Neuromuscular Unit, CHU Montpellier/EA7402 Université de Montpellier, IURC, Institut Universitaire de Recherche Clinique, Montpellier, France
- The Manton Center for Orphan Disease Research, Division of Genetics and Genomics, Boston Children's Hospital, Harvard Medical School, Boston, MA 02115, USA
- I-Motion, Institute of Myology AP-HP, Paris, France
- Biruni University, Department of Molecular Biology and Genetics, Istanbul, Turkey
- Department of Paediatric Neurology, Reference Neuromuscular Center, Hôpital Universitaire des Enfants Reine Fabiola HUDERF, Université Libre de Bruxelles, ULB, Brussels, Belgium
- Center for Mendelian Genomics, The Broad Institute of MIT and Harvard, Cambridge, MA 02142, USA
- Department of Translational Medicine and Neurogenetics, IGBMC (Institut de Génétique et de Biologie Moléculaire et Cellulaire), Inserm U1258, CNRS UMR7104, Université de Strasbourg, Illkirch, France
- Laboratoire de Biochimie et Génétique Moléculaire, CHU Grenoble, France
- AP-HP, Reference Center for Neuromuscular Disorders, Pitié-Salpêtrière Hospital, Paris, France
- Neuromuscular Morphology Unit, Myology Institute, Pitié-Salpêtrière Hospital, Paris, France
- Division of Child Neurology, Centre de Référence des Maladies Neuromusculaires, Department of Pediatrics, University Hospital Liège & University of Liège, Belgium
- Molecular Genetics Laboratory, CHU Montpellier/INSERM U827, Institut Universitaire de Recherche Clinique, Montpellier, France
- Neuropathology Unit, Department of Pathology and Neuromuscular Unit, IDIBELL-Hospital Universitari de Bellvitge, Barcelona, Spain

Annexe 2: Standardized Clinical Forms

Annexe 2.1: *SEPN1-Related Myopathy*

Clinical data

Please, do not forget to join a pedigree as extensive and detailed as possible and a picture of the patient if available.

Name:

Date of birth:

Sex (F/ M)

Referring clinician (name and address):

Place of birth:

Parent's origin:

Parents consanguinity: yes no

If yes, degree:

Mother's miscarriages (P-M-A):

Other cases in the family (specify):

First symptom(s) remarked:

Age at first symptom:

Age at diagnostic:

Pregnancy (normal/abnormal: specify: polyhydramnios, reduced foetal movements, drugs...):

Labour (normal/abnormal: specify):

Neonatal manifestations: yes no

Neonatal hypotonia: yes no

Degree: mild moderate severe

Ventilatory assistance: yes no

Sustained for days/months

Congenital bone fractures:

Congenital joint contractures/arthrogryposis:

Others (suction/deglutition troubles, dysmorphic features...):

Delayed motor milestones: yes no

Cephalic control at months

Walks unsupported at months

Sits up at months

Gets up unaided at months

Best motor performance (age):

Cranial involvement: yes no

Detected at age:

Ptosis: yes no

Degree: mild moderate severe

High arched palate: yes no

Ophtalmoplegia: yes no

Degree: mild moderate severe

Occlusion troubles: yes no

Myopia: yes no

Degree: mild moderate severe

Spinal rigidity yes no Degree (mild, moderate, severe):

Distribution (cervical, dorsal, lumbar): Distance chin-sternum (cm):

Scoliosis yes no

Detected at age: Surgical correction yes no
At age:

Distribution: Complications:

Degree: mild moderate severe

Associated lordosis/kyphosis:

Thorax deformities (flat thorax, pectus excavatum..):

Joint contractures: yes no Since age: Distribution (cervical, hips...):

Degree: mild moderate severe

Joint hyperlaxity: yes no

Skin involvement (hyperelasticity, dryness, follicular hyperkeratosis..) :

Dysmorphic features:

Micro/retrognathia:

High-arched palate:

Other:

Muscle power (MRC 0-5 scale):

Neck flexors	/5
Neck extensors	/5
Trapezius	/5
Scapular fix (others)	/5
Pectoral muscles	/5
Deltoid	/5
Elbow flexors	/5
Elbow extensors	/5
Wrist flexors	/5
Wrist extensors	/5
Intrinsic hand muscles	/5

Spinal flexors	/5
Spinal extensors	/5
Glutaeus	/5
Psoas	/5
Adductors	/5
Knee extensors	/5
Knee flexors	/5
Tibialis ant	/5
Peronaeus	/5
Triceps suralis	/5
Toes flex/ext	/5

Tendon reflexes (0 to 4):

biceps:	0	1	2	3	4
triceps:	0	1	2	3	4
radial:	0	1	2	3	4
patellar:	0	1	2	3	4
achilean:	0	1	2	3	4

Muscle bulk:

normal amyotrophy □□ □ generalized □□ □ localised on (pseudo)hypertrophy □□

Gait: Autonomous Climbs a stair? Needs a support? Wheelchair-bound?

Limited gait perimetre?(m/km): Lost at age:

Respiratory involvement: yes no Detected at age:

Because of (dyspnoea, drowsiness...):

Vital capacity known? (age) yes no

sitting/standing: litres (% of predicted value)

supine position : litres (%)

Arterial gasometry performed? yes no PO2: PCO2:

Polysomnography performed?(age) yes no Normal Nocturnal desaturation

Ventilatory assistance? yes no / Transitory Sustained /from age:

Type: Hours/day:

Tracheotomy? yes no Since:

Cardiac involvement: yes no

Type: Cardiomyopathy □□ Rhythm disturbance Cardiac malformation Other

Degree: mild moderate severe

Tests performed: ECG □ □ Chest Rx □□ EchoCG □□ Cardiac catheterisation □□ Myocardial biopsy □□

Physical activity/Physiotherapy: None □□ Occasionally □□ Habitual Intense □□

Respiratory physiotherapy (BIRD)?: yes no

Weakness evolution: Stable □□ Improving □□ Slowly deteriorating □□ Quickly deteriorating

General evolution:

Other remarks (dysmorphic features? flat feet, etc):

Associated abnormalities (anaesthetic complications?):

Death: yes no At age: Cause:

Necropsy performed?: yes no

Paraclinical data

Serum creatine kinase level: Normal Elevated Actual level / normal value U/l
Age at test:

EMG findings:

Non performed □□ Normal □□ Abnormal Specify:

Age at examination: MCVs: SCVs:

Other ancillary tests (muscle CT, brain CT/MRI, etc):

Muscle biopsy(-ies): Date/age: Muscle biopsied:

Date/age: Muscle biopsied:

Muscle available? yes no

Only for the patient □□ yes no

For other family members: □□ yes no Specify who:

If yes, as: Paraffin blocks □□ EM specimen □□ Frozen tissue □□ Mounted □
Unmounted

Light microscopy findings:

Electronic microscopy findings:

Please also submit a copy of the full report and, if possible, some photographs of the biopsy. If several biopsies, please fill out one copy of this page for each one of them.

DNA samples

From the patient:

DNA samples:

Available □□□

Will be collected

Not available

Cell culture:

Available Type:

Will be collected □

Not available

From family members (please indicate who):

DNA samples:

Available □□□

Will be collected

Not available

Cell line:

Available Type:

Will be collected □

Not available

Stored at (Department, address):

Other samples from patient: Cardiac muscle Smooth muscle CNS Spinal cord Peripheral nerve □

Please join informed consent from the patient

Annexe 2.2: ASC1-Related Myopathy

Clinical data

Please, do not forget to join a pedigree as extensive and detailed as possible and a picture of the patient if available.

Name:

Date of birth:

Sex (F/ M)

Referring clinician (name and address):

Place of birth:

Parent's origin:

Parents consanguinity: yes no

If yes, degree:

Mother's miscarriages (P-M-A):

Other cases in the family (specify):

First symptom(s) remarked:

Age at first symptom:

Age at diagnostic:

Pregnancy (normal/abnormal: specify: polyhydramnios, reduced foetal movements, drugs...):

Labour (normal/abnormal: specify):

Neonatal manifestations: yes no

Neonatal hypotonia: yes no

Degree: mild moderate severe

Ventilatory assistance: yes no

Sustained for days/months

Congenital bone fractures:

Congenital joint contractures/arthrogryposis:

Others (suction/deglutition troubles, dysmorphic features...):

Delayed motor milestones: yes no

Cephalic control at months

Walks unsupported at months

Sits up at months

Gets up unaided at months

Best motor performance (age):

Cranial involvement: yes no

Detected at age:

Ptosis: yes no

Degree: mild moderate severe

High arched palate: yes no

Ophtalmoplegia: yes no

Degree: mild moderate severe

Occlusion troubles: yes no

Myopia: yes no

Degree: mild moderate severe

Spinal rigidity yes no Degree (mild, moderate, severe):

Distribution (cervical, dorsal, lumbar): Distance chin-sternum (cm):

Scoliosis yes no

Detected at age: Surgical correction yes no At age:

Distribution: Complications:

Degree: mild moderate severe

Associated lordosis/kyphosis:

Thorax deformities (flat thorax, pectus excavatum..):

Joint contractures: yes no Since age: Distribution (cervical, hips...):

Degree: mild moderate severe

Joint hyperlaxity: yes no

Skin involvement (hyperelasticity, dryness, follicular hyperkeratosis..) :

Dysmorphic features:

Micro/retrognathia:

High-arched palate:

Other:

Muscle power (MRC 0-5 scale):

Neck flexors /5

Neck extensors /5

Trapezius	/5
Scapular fix (others)	/5
Pectoral muscles	/5
Deltoid	/5
Elbow flexors	/5
Elbow extensors	/5
Wrist flexors	/5
Wrist extensors	/5
Intrinsic hand muscles	/5

Spinal flexors	/5
Spinal extensors	/5
Glutaeus	/5
Psoas	/5
Adductors	/5
Knee extensors	/5
Knee flexors	/5
Tibialis ant	/5
Peronaeus	/5
Triceps suralis	/5
Toes flex/ext	/5

Tendon reflexes (0 to 4):

biceps:	0	1	2	3	4
triceps:	0	1	2	3	4
radial:	0	1	2	3	4
patellar:	0	1	2	3	4
achilean:	0	1	2	3	4

Muscle bulk:

normal amyotrophy □□ □ generalized □□ □ localised on (pseudo)hypertrophy □□

Gait: Autonomous Climbs a stair? Needs a support? Wheelchair-

bound?

Limited gait perimetre?(m/km): Lost at age:

Respiratory involvement: yes no Detected at age:

Because of (dyspnoea, drowsiness...):

Vital capacity known? (age) yes no

sitting/standing: litres (% of predicted value)

supine position : litres (%)

Arterial gasometry performed? yes no PO2: PCO2:

Polysomnography performed?(age) yes no Normal Nocturnal desaturation

Ventilatory assistance? yes no / Transitory Sustained /from age:

Type: Hours/day:

Tracheotomy? yes no Since:

Cardiac involvement: yes no

Type: Cardiomyopathy □□ Rhythm disturbance Cardiac malformation Other

Degree: mild moderate severe

Tests performed: ECG □ □ Chest Rx □□ EchoCG □□ Cardiac catheterisation □□ Myocardial biopsy □□

Physical activity/Physiotherapy: None □□ Occasionally □□ Habitual Intense □□

Respiratory physiotherapy (BIRD)?: yes no

Weakness evolution: Stable □□ Improving □□ Slowly deteriorating □□ Quickly deteriorating

General evolution:

Other remarks (dysmorphic features? flat feet, etc):

Associated abnormalities (anaesthetic complications?):

Death: yes no At age: Cause:

Necropsy performed?: yes no

Paraclinical data

Serum creatine kinase level: Normal Elevated Actual level / normal value U/l
Age at test:

EMG findings:

Non performed □□ Normal □□ Abnormal Specify:

Age at examination: MCVs: SCVs:

Other ancillary tests (muscle CT, brain CT/MRI, etc):

Muscle biopsy(-ies): Date/age: Muscle biopsied:

Date/age: Muscle biopsied:

Muscle available? yes no

Only for the patient □□ yes no

For other family members: □□ yes no Specify who:

If yes, as: Paraffin blocks □□ EM specimen □□ Frozen tissue □□ Mounted □ Unmounted

Light microscopy findings:

Electronic microscopy findings:

Please also submit a copy of the full report and, if possible, some photographs of the biopsy. If several biopsies, please fill out one copy of this page for each one of them.

DNA samples

From the patient:

DNA samples:

Available □□□

Will be collected

Not available

Cell culture:

Available Type:

Will be collected □

Not available

From family members (please indicate who):

DNA samples:

Available □□□

Will be collected

Not available

Cell line:

Available Type:

Will be collected □

Not available

Stored at (Department, address):

Other samples from patient: Cardiac muscle Smooth muscle CNS Spinal cord Peripheral nerve □

Please join the informed consent for being included in the present study and publication of clinical data and photographs

Annexe 3: Summarized histopathological findings in 79 SEPN1-RM patients.

Patient	Age at Bx, Site	Major findings
002	6y, Quadriceps	FSV, type 1 fibre predominance, mild fibrosis, eosinophilic inclusions, MMC
003	2y, Quadriceps	FSV, type 1 fibre predominance, eosinophilic inclusions, MMC
005	5y, Deltoid 6y, Quadriceps	FSV, type 1 fibre predominance, IN, mild fibrosis, MMC
006	13y, Deltoid	FSV, type 1 fibre predominance and hypotrophy, IN, endomysial fibrosis, scattered MMC
008	15y, NA	FSV, type 1 fibre predominance, MMC
009	3y, Quadriceps	MMC
010	35y, Deltoid	FSV, IN, endomysial fibrosis, scattered regenerating fibres, adipose replacement
012	22y, Quadriceps	FSV, IN, type 1 fibre predominance, endomysial fibrosis, scattered necrotic and regenerating fibres
013	10y, Deltoid	FSV, endomysial fibrosis, scattered necrotic and regenerating fibres
015	2y, Deltoid	FSV, endomysial fibrosis, scattered regenerating fibres
018	10y, NA	FSV, type 1 fibre predominance, mild endomysial fibrosis, IN, eosinophilic inclusions, MMC
021	12y, Deltoid 12y, Abdominal	Deltoid: FSV, IN, mild fibrosis, MMC Abdominal: prominent fibrosis, adipose replacement, eosinophilic inclusions, rimmed vacuoles, MMC, CC
022	8y, Abdominal	FSV, yype 1 fibre predominance, mild fibrosis, scattered regenerating fibres, inconspicuous MMC
024	11y, Deltoid	FSV, type 1 fibre predominance, IN, mild fibrosis, MMC
026	9y, Deltoid	Type 1 fibre predominance
027	14y, Deltoid	Prominent fibrosis, necrotic and regenerating fibres
029	11y, Deltoid	Type 1 fibre predominance, FSV, endomysial fibrosis, regenerating fibres
031	12y, NA	Type 1 fibre predominance, FSV, MMC
032	5y, NA	FSV, MMC
042	20y, Quadriceps	FSV, type 1 fibre predominance, mild fibrosis, eosinophilic inclusions, MMC
043	23y, Quadriceps	FSV, type 1 fibre predominance, mild fibrosis, eosinophilic inclusions, MMC
044	15y, Biceps brachii	MMC
045	6y, NA	MMC, CC
046	7y, NA	FSV, type 1 fibre predominance
047	16y, Deltoid	Endomysial fibrosis, scattered necrotic and regenerating fibres
049	10y, NA	FSV, type 1 fibre predominance
050	10y, Gastrocnemius	FSV, type 1 fibre predominance, IN, mild endomysial fibrosis, MMC
051	5y, Deltoid	FSV, type 1 fibre predominance, IN, MMC, lobulated fibres

052	6y, NA	FSV, prominent endomysial fibrosis, scattered regenerating fibres
056	13y, Quadriceps	FSV, type 1 fibre predominance
054	14y, NA	FSV, IN
055	17y, NA	MMC
056	10y, NA	FSV, prominent endomysial fibrosis
057	5y, Quadriceps	MMC
062	2y, NA	MMC
063	7y, Quadriceps	FSV, IN, MMC
065	1y, Deltoid	FSV, type 1 fibre predominance, IN, MMC
067	37y, Deltoid	FSV, type 1 fibre predominance, MMC
070	11y, NA	FSV, type 1 fibre predominance
071	6y, NA	FSV, type 1 fibre predominance and hypotrophy
072	15y, Deltoid	FSV, type 1 fibre predominance, IN, mild endomysial fibrosis, MMC
073	10y, NA	Type 1 fibre predominance
074	4y, Quadriceps	FSV, type 1 fibre predominance
075	8y, Quadriceps	FSV, IN, endomysial fibrosis, scattered necrotic and regenerating fibres
079	6y, NA	MMC
082	16y, NA	FSV, type 1 fibre predominance, coiled fibres
083	40y, NA	MMC
084	43y, Quadriceps	FSV, type 1 fibre predominance, endomysial fibrosis, MMC
086	27y, Quadriceps	FSV, endomysial fibrosis, IN, scattered regenerating fibres, MMC
088	44y, Deltoid	FSV, type 1 fibre predominance, endomysial fibrosis, scattered necrotic and regenerating fibres, MMC
089	11y, NA	MMC
090	17y, Quadriceps 18y, Deltoid	Quadriceps: FSV, type 1 fibre predominance Deltoid: FSV, type 1 fibre predominance, MMC
091	5y, NA	FSV, type 1 fibre predominance, MMC
092	40y, Deltoid	FSV, prominent endomysial fibrosis, adipose replacement
095	9y, NA	FSV, type 1 fibre predominance, IN
096	11y, NA	MMC
097	6y, NA	FSV, type 1 fibre predominance
098	6y, Deltoid	FSV, type 1 fibre predominance, IN mild endomysial fibrosis, MMC
101	13y, Quadriceps	FSV, type 1 fibre predominance

102	4y, Gastrocnemius	FSV, MMC
103	35y, NA	Prominent endomysial fibrosis, IN
105	12y, Biceps brachii	FSV, type 1 fibre predominance, IN
107	5y, NA	FSV, type 1 fibre predominance, MMC
108	8y, Deltoid	FSV, type 1 fibre predominance, mild fibrosis, IN, rimmed vacuoles, MMC
109	2y, Deltoid	FSV, type 1 fibre predominance, MMC
110	5y, NA	MMC
111	6y, Quadriceps	FSV, type 1 fibre predominance
112	24y, Deltoid	FSV, type 1 fibre predominance, IN, mild endomysial fibrosis, MMC
113	13y, NA	FSV, type 1 fibre predominance, IN, mild endomysial fibrosis, MMC
119	9y, NA	MMC
121	3y, NA	FSV, IN
122	7y, NA	FSV, type 1 fibre predominance
123	3y, NA	FSV
124	4y, NA	FSV, type 1 fibre predominance, MMC
125	2y, NA	FSV
129	14y	FSV, type 1 fibre predominance, IN, MMC
131	33y, Deltoid	FSV, mild endomysial fibrosis, MMC

y: years; NA: not available; FSV: fibre size variation; IN: internalized nuclei; MMC: multi-minicores; CC: central-cores

Annexe 4: Comprehensive summary of mutation data.

Variant (cDNA change)	Genomic position	Location	Variant Type	Coding Effect	Protein change	Allele Frequency (gnomAD)	rsID	ClinVarID	N
c.-25_69del	Chr1(GRCh38):g.25800209_25800302del	exon 1	deletion	start loss					1
c.-19_73del	Chr1(GRCh38):g.25800220_25800311del	exon 1	deletion	start loss		0.000041		RCV000413324.1 RCV000501710.1	10
c.-11_81del	Chr1(GRCh38):g.25800220_25800311del	exon 1	deletion	start loss		0.000041		RCV000413324.1 RCV000501710.1	1
c.1A>G	Chr1(GRCh38):g.25800231A>G	exon 1	substitution	start loss		0.000041	rs121908184	RCV000482307.1 RCV000004748.2	20
c.8_17dup	Chr1(GRCh38):g.25800242_25800243ins GGGCCCGGCC	exon 1	insertion	frameshift	p.Arg5Glyfs*81				1
c.13_22dup	Chr1(GRCh38):g.25800243_25800252dup	exon 1	duplication	frameshift	p.Gln8Profs*78	0.000121	rs970951421	RCV000173501.1	11
c.8_12dup	Chr1(GRCh38):g.25800248_25800252dup	exon 1	duplication	frameshift	p.Gln8Argfs*60				1
c.44_72dup	Chr1(GRCh38):g.25800274_25800302dup	exon 1	duplication	frameshift	p.Arg25Alafs*51		rs797044620	RCV000173498.1	2
c.66_73dup	Chr1(GRCh38):g.25800299_25800306dup	exon 1	duplication	frameshift	p.Arg26Hisfs*43	0.00004	rs911937146		1
1c.69_76dup	Chr1(GRCh38):g.25800299_25800306dup	exon 1	duplication	frameshift	p.Arg26Hisfs*43	0.00004	rs911937146		1
c.77_84dup	Chr1(GRCh38):g.25800307_25800314dup	exon 1	duplication	frameshift	p.Arg29Alafs*40				2
c.142delG	Chr1(GRCh38):g.25800372del	exon 1	deletion	frameshift	p.Val48Serfs*18				1
c.249_250dup	Chr1(GRCh38):g.25801108_25801109dup	exon 2	duplication	frameshift	p.Asp84Glyfs*17	0.000004		RCV000627410.1	1
c.277dup	Chr1(GRCh38):g.25801138dup	exon 2	duplication	frameshift	p.Pro94Thrfs*4				1
c.441dupG	Chr1(GRCh38):g.25805179dup	exon 4	duplication	frameshift	p.Pro148Alafs*3				2
c.467T>C	Chr1(GRCh38):g.25805205T>C	exon 4	substitution	missense	p.Leu156Pro				1
c.473T>G	Chr1(GRCh38):g.25805211T>C	exon 4	substitution	missense	p.Ile158Thr	0.000008			1
c.565C>T	Chr1(GRCh38):g.25808607C>T	exon 5	substitution	stop gain	p.Arg189*	0.000008	rs775713184		1
c.665G>A	Chr1(GRCh38):g.25808707G>A	exon 5	substitution	stop gain	p.Trp222*			RCV000545759.1	1
c.683_689dup	Chr1(GRCh38):g.25808725_25808731dup	exon 5	duplication	frameshift	p.Met230Ilefs*73			RCV000481356.1	9
c.713dup	Chr1(GRCh38):g.25808755dup	exon 5	duplication	frameshift	p.Asn238Lysfs*63	0.00017	rs750857935	RCV000277917.2 RCV000004751.4 RCV000178976.1	15
c.714_715ins	Chr1(GRCh38):g.25808756_25808757insA	exon 5	insertion	frameshift	p.Arg239Thrfs*62				1
c.802C>T	Chr1(GRCh38):g.25809080C>T	exon 6	substitution	missense	p.Arg268Cys	0.000008	rs368074297		1

c.803G>A	Chr1(GRCh38):g.25809081G>A	exon 6	substitution	missense	p.Arg268His				1
c.817G>A	Chr1(GRCh38):g.25809095G>A	exon 6	substitution	missense	p.Gly273Arg				5
c.818G>A	Chr1(GRCh38):g.25809096G>A	exon 6	substitution	missense	p.Gly273Glu		rs121908182	RCV000004746.3	8
c.827_829dup	Chr1(GRCh38):g.25809105_25809107dup	exon 6	duplication	in-frame	p.Ala276Cys277ins Ser	0.000008	rs797045950	RCV000192616.1 RCV000599220.1	1
c.863_864del	Chr1(GRCh38):g.25809141_25809142del	exon 6	deletion	frameshift	p.Val288Aspfs*12				2
c.871C>T	Chr1(GRCh38):g.25809149C>T	exon 6	substitution	missense	p.Arg291Trp	0.000008	rs757446463		1
c.872G>A	Chr1(GRCh38):g.25809150G>A	exon 6	substitution	missense	p.Arg291Gln	0.000012	rs199564797	RCV000358099.1	5
c.(872+1_873-1) _(1602+1_1603-1)del	Chr(GRCh38):g.(25809151-25809682)_ (25814179-25815547)	intron 6 _intron 12	deletion (CNV)	Unknown	p.?				1
c.878A>G	Chr1(GRCh38):g.25809688A>G	exon 7	substitution	missense	p.His293Arg	0.000008	rs776738184	RCV000349806.1	5
c.883G>A	Chr1(GRCh38):g.25809693G>A	exon 7	substitution	missense	p.Glu295Lys		rs978886878	RCV000592718.1	2
c.943G>A	Chr1(GRCh38):g.25809753G>A	exon 7	substitution	missense	p.Gly315Ser	0.000191	rs121908188	RCV000681664.1 RCV000004753.11 RCV000004754.9 RCV000082020.7	17
c.952del	Chr1(GRCh38):g.25809761del	exon 7	deletion	frameshift	p.Ile318Serfs*22				1
c.976G>A	Chr1(GRCh38):g.25809786G>A	exon 7	substitution	missense	p.Val326Ile	0.00002	rs764032922		1
c.996_999del	Chr1(GRCh38):g.25809805_25809808del	exon 7	deletion	frameshift	p.Phe332Cysfs*7				1
c.997_1000del	Chr1(GRCh38):g.25809807_25809810del	exon 7	deletion	frameshift	p.Val333Profs*6	0.000012	rs886041686	RCV000299743.1	2
c.1019A>T	Chr1(GRCh38):g.25811462A>T	exon 8	substitution	missense	p.Asn340Ile		rs749911126		2
c.1076T>C	Chr1(GRCh38):g.25811519T>C	exon 8	substitution	missense	p.Ile359Thr				1
c.1176del	Chr1(GRCh38):g.25811773del	exon 9	deletion	frameshift	p.Ser392fs*1				1
c.1189C>T	Chr1(GRCh38):g.25811787C>T	exon 9	substitution	stop gain	p.Gln397*				1
c.1269C>A	Chr1(GRCh38):g.25811867C>A	exon 9	substitution	stop gain	p.Tyr423*				1
c.1315del	Chr1(GRCh38):g.25812720del	exon 10	deletion	frameshift	p.Arg439Glufs*55				1
c.1315C>T	Chr1(GRCh38):g.25812720C>T	exon 10	substitution	stop gain	p.Arg439*	0.000029	rs377215510	RCV000082011.5 RCV000173886.2	4
c.1358G>C	Chr1(GRCh38):g.25812763G>C	exon 10	substitution	missense	p.Trp453Ser	0.000004	rs121908186	RCV000004750.4	2
c.1379C>T	Chr1(GRCh38):g.25812784C>T	exon 10	substitution	missense	p.Ser460Phe	0.000008	rs767530943		1
c.1384T>G	Chr1(GRCh38):g.25812789T>G	exon 10	substitution	stop loss	p.Sec462Gly		rs121908187	RCV000004752.3	2

c.1385G>A	Chr1(GRCh38):g.25812790G>A	exon 10	substitution	synonymous	p.Sec462=		rs587776597	RCV000004747.3	1
c.1388G>T	Chr1(GRCh38):g.25813881G>T	exon 11	substitution	missense	p.Gly463Val				1
c.1396C>T	Chr1(GRCh38):g.25813889C>T	exon 11	substitution	missense	p.Arg466Trp	0.000011	rs752156505		1
c.1397G>A	Chr1(GRCh38):g.25813890G>A	exon 11	substitution	missense	p.Arg466Gln	0.000054	rs121908185	RCV000413832.3 RCV000004749.6	15
c.1405C>T	Chr1(GRCh38):g.25813898C>T	exon 11	substitution	missense	p.Arg469Trp	0.000008	rs756927098	RCV000692095.1	1
c.1406G>A	Chr1(GRCh38):g.25813899G>A	exon 11	substitution	missense	p.Arg469Gln	0.000012	rs779162837	RCV000551007.2	2
c.1446delC	Chr1(GRCh38):g.25813938del	exon 11	deletion	frameshift	p.Leu482Profs*12				4
c.1469G>T	Chr1(GRCh38):g.25813962G>T	exon 11	substitution	missense	p.Trp490Leu				2
c.1574T>G	Chr1(GRCh38):g.25814150T>G	exon 12	substitution	missense	p.Met525Arg	0.000036	rs761631813		1
c.1704_1705del	Chr1(GRCh38):g.25815649_25815650del	exon 13	deletion	frameshift	p.Ser569Hisfs*29				1
c.*1107T>C	Chr1(GRCh38):g.25816825T>C	3'UTR, exon 13	substitution						1
c.1010+2T>G	Chr1(GRCh38):g.25809822T>G	intron	substitution						1
c.1093-1G>T	Chr1(GRCh38):g.25811690G>T	intron	substitution						1
c.1093-41ins	Chr1(GRCh38):g.25811650_25811651insTT	intron	insertion						1
c.1603-2A>G	Chr1(GRCh38):g.25815546A>G	intron	substitution						1
c.404-1G>A	Chr1(GRCh38):g.25805141G>A	intron	substitution						1
c.873-1G>C	Chr1(GRCh38):g.25809682G>C	intron	substitution						2

rsID: Reference SNP cluster ID from dbSNP database. ClinVarID: ID from ClinVar database. N: number of patients carrying the mutation.

Annexe 5: Antibodies for western blot analysis

Primary antibodies

Antigen	Supplier, Reference	Species	Dilution
ASC-1	Abcam, 70627	Rabbit	1 :1000
	Santa Cruz	Mouse	1 :2000
ASCC1	Santa Cruz, sc-160156	Goat	1 :500
CyclinD1	Santa Cruz, sc-450	Mouse	1 :200
	Milipore, DCS-6	Mouse	1 :50
CyclinD3	Santa Cruz, sc-6283	Mouse	1 :1000
p21	Santa Cruz, sc-397	Rabbit	1 :500
Tubulin	Sigma, T5168	Mouse	1 :10000
pRb	BD Pharmingen, G3-245	Mouse	1 :250
MHCe	DSHB, F1.652	Mouse	1 :1000
Halotag	Promega, G9211	Mouse	1 :1000

Secondary antibodies

	Supplier, Reference	Dilution
Goat anti-rabbit HRP conjugate	Thermo Scientific, 31460	1:2500
Goat anti-mouse HRP conjugate	Thermo Scientific, 31430	1:3000
Rabbit anti-goat HRP conjugate	Thermo Scientific, 31402	1:2500

Annexe 6: List of publications

1. Villar-Quiles RN, Catervi F, Cabet E, Juntas-Morales R, Genetti CA, Gidaro T, Koparir A, Yüksel A, Coppens S, Deconinck N, Pierce-Hoffman E, Laporte J, Rendu J, Romero NB, Beggs AH, Servais L, Cossée M, Olivé M, Böhm J, Duband-Goulet I, Ferreiro A. ASC1 is a cell cycle regulator associated with severe and mild forms of myopathy. *Annals of Neurology*. 2020 Feb;87(2):217-232. Doi: 10.1002/ana.25660

2. Villar-Quiles RN, von der Hagen M, Métay C, Gonzalez V, Donkervoort S, Bertini E, Castiglioni C, Chaigne D, Colomer J, Cuadrado ML, de Visser M, Desguerre I, Eymard B, Goemans N, Kaindl A, Lagrue E, Lütschg J, Malfatti E, Mayer M, Merlini L, Orlikowski D, Reuner U, Salih MA, Schlotter-Weigel B, Stoetter M, Straub V, Topaloglu H, Urtizberea JA, van der Kooi A, Wilichowski E, Romero NB, Fardeau M, Bönnemann CG, Estournet B, Richard P, Quijano-Roy S, Schara U, Ferreiro A. SEPN1-related myopathy: towards clinical trial readiness. Spectrum and evolution in 132 cases (*Neurology*, in press)

3. Varone E, Pozzera D, Di Modicaa S, Chernorudskiya A, Nogarab L, Baraldob M, Cinquantad M, Fumagallie S, Villar-Quiles RN, De Simonie MG, Blaauwb B, Ferreiro A, Zito E. SELENON (SEPN1) protects skeletal muscle from saturated fatty acid-induced ER stress and insulin resistance. *Redox biology.* 2019, vol. 24, p. 101176. Doi: 10.1016/j.redox.2019.101176

4. Filipe A, Varone E, Arbogast S, Chernorudskiy A, Pozzer D, Villar-Quiles RN, Dill C, Dudhal S, Fumagalli S, De Simoni M, Giovarelli M, De Palma C, Pinton P, Giorgi C, Clementi E, Missiroli S, Boncompagni S, Zito E, Ferreiro A. SEPN1 is required for normal ER-mitochondrial interaction and regulates mitochondrial bioenergetics (*Cell Death and differentiation*, in press)

ASC-1 Is a Cell Cycle Regulator Associated with Severe and Mild Forms of Myopathy

Rocío N. Villar-Quiles, MD,[1,2] Fabio Catervi, MS,[1] Eva Cabet, PhD,[1] Raul Juntas-Morales, MD,[3] Casie A. Genetti, MS,[4] Teresa Gidaro, MD, PhD,[5] Asuman Koparir, MD,[6] Adnan Yüksel, MD,[6] Sandra Coppens, MD,[7] Nicolas Deconinck, MD, PhD,[7] Emma Pierce-Hoffman, BSc,[8] Xavière Lornage, PhD,[9] Julien Durigneux, MD,[10] Jocelyn Laporte, PhD,[9] John Rendu, PharmD, PhD,[11] Norma B. Romero, MD, PhD,[2,12] Alan H. Beggs, PhD,[4] Laurent Servais, MD, PhD,[5,13] Mireille Cossée, MD,[14] Montse Olivé, MD, PhD,[15] Johann Böhm, PhD,[9] Isabelle Duband-Goulet, PhD,[1] and Ana Ferreiro, MD, PhD[1,2]

Objective: Recently, the ASC-1 complex has been identified as a mechanistic link between amyotrophic lateral sclerosis and spinal muscular atrophy (SMA), and 3 mutations of the ASC-1 gene *TRIP4* have been associated with SMA or congenital myopathy. Our goal was to define ASC-1 neuromuscular function and the phenotypical spectrum associated with *TRIP4* mutations.
Methods: Clinical, molecular, histological, and magnetic resonance imaging studies were made in 5 families with 7 novel *TRIP4* mutations. Fluorescence activated cell sorting and Western blot were performed in patient-derived fibroblasts and muscles and in *Trip4* knocked-down C2C12 cells.
Results: All mutations caused ASC-1 protein depletion. The clinical phenotype was purely myopathic, ranging from lethal neonatal to mild ambulatory adult patients. It included early onset axial and proximal weakness, scoliosis, rigid spine, dysmorphic facies, cutaneous involvement, respiratory failure, and in the older cases, dilated cardiomyopathy. Muscle biopsies showed multiminicores, nemaline rods, cytoplasmic bodies, caps, central nuclei, rimmed fibers, and/or mild endomysial fibrosis. ASC-1 depletion in C2C12 and in patient-derived fibroblasts and muscles caused accelerated

View this article online at wileyonlinelibrary.com. DOI: 10.1002/ana.25660

Received Aug 13, 2019, and in revised form Dec 2, 2019. Accepted for publication Dec 2, 2019.

Address correspondence to Drs Duband-Goulet and Ferreiro, Basic & Translational Myology Laboratory, Unité de Biologie Fonctionnelle et Adaptative, Université Paris Diderot–CNRS, 35, rue Hélène Brion, 75205 Paris cedex 13, France. E-mail: isabelle.duband-goulet@univ-paris-diderot.fr and ana.b.ferreiro@gmail.com

I.D.-G. and A.F. are co–last authors with equal contribution as senior authors.

From the [1]Basic and Translational Myology Laboratory, UMR8251, University of Paris/National Center for Scientific Research, Paris, France; [2]Reference Center for Neuromuscular Disorders, Pitié-Salpêtrière Hospital, APHP, Institute of Myology, Paris, France; [3]Neuromuscular Unit, University Hospital Center Montpellier/EA7402 University of Montpellier, University Institute of Clinical Research, Montpellier, France; [4]Manton Center for Orphan Disease Research, Division of Genetics and Genomics, Boston Children's Hospital, Harvard Medical School, Boston, MA; [5]I-Motion, Institute of Myology, APHP, Paris, France; [6]Department of Molecular Biology and Genetics, Biruni University, Istanbul, Turkey; [7]Department of Pediatric Neurology, Reference Neuromuscular Center, Queen Fabiola Children's University Hospital, Free University of Brussels, Brussels, Belgium; [8]Center for Mendelian Genomics, Broad Institute of Massachusetts Institute of Technology and Harvard, Cambridge, MA; [9]Department of Translational Medicine and Neurogenetics, Institute of Genetics and Molecular and Cellular Biology, National Institute of Health and Medical Research U1258, National Center for Scientific Research UMR7104, University of Strasbourg, Illkirch, France; [10]Department of Neuropediatrics, University Hospital Center Angers, Neuromuscular Diseases Reference Center Antlantique Occitanie Caraïbe, Angers, France; [11]Laboratory of Biochemistry and Molecular Genetics, University Hospital Center Grenoble, Grenoble, France; [12]Neuromuscular Morphology Unit, Institute of Myology, Pitié-Salpêtrière Hospital, Paris, France; [13]Division of Child Neurology, Neuromuscular Diseases Reference Center, Department of Pediatrics, Liège University Hospital and University of Liège, Liège, Belgium; [14]Molecular Genetics Laboratory, University Hospital Center Montpellier/National Institute of Health and Medical Research U827, University Institute of Clinical Research, Montpellier, France; and [15]Neuropathology Unit, Department of Pathology and Neuromuscular Unit, Institute of Biomedical Research of Bellvitge–University Hospital of Bellvitge, Barcelona, Spain

proliferation, altered expression of cell cycle proteins, and/or shortening of the G0/G1 cell cycle phase leading to cell size reduction.

Interpretation: Our results expand the phenotypical and molecular spectrum of *TRIP4*-associated disease to include mild adult forms with or without cardiomyopathy, associate ASC-1 depletion with isolated primary muscle involvement, and establish *TRIP4* as a causative gene for several congenital muscle diseases, including nemaline, core, centronuclear, and cytoplasmic-body myopathies. They also identify ASC-1 as a novel cell cycle regulator with a key role in cell proliferation, and underline transcriptional coregulation defects as a novel pathophysiological mechanism.

ANN NEUROL 2020;87:217–232

Congenital myopathies (CMs) are genetically and clinically heterogeneous inherited disorders. They usually present during the first years of life with delayed motor development, muscular weakness, and hypotonia and have a stable or slowly progressive course. CMs are sometimes associated with cardiac and/or respiratory failure[1–3] and have no specific treatment.[4] More than 20 genes have been associated with CMs,[5,6] most of them encoding proteins involved in (1) skeletal muscle calcium homeostasis,[7] (2) excitation–contraction coupling,[8] (3) membrane remodeling,[9,10] and (4) myofibrillar force generation[11] or thin–thick filament assembly[12] and interactions.[13] However, the genetic defect remains unknown in up to 25% CM patients.

In 2016, we described a form of congenital myopathy caused by recessive mutations in thyroid hormone receptor interactor 4 (*TRIP4*), encoding the transcriptional coactivator ASC-1 (activating signal cointegrator 1), in a large consanguineous family. ASC-1 defines the ASC-1 transcriptional cointegrator complex, together with 3 other subunits (ASCC1, ASCC2, and ASCC3). We termed this novel condition ASC-1 related myopathy (ASC1-RM), thus identifying transcriptional coregulation as a novel CM pathomechanism.[14] Patients presented with severe neonatal hypotonia, potentially lethal respiratory failure, muscle weakness with partial or no ambulation, scoliosis, joint hyperlaxity, and skin abnormalities. Muscle biopsy revealed the as yet unreported association of multiminicores, caps, and dystrophic lesions.

The role of the ASC-1 complex in neuromuscular diseases was confirmed by the simultaneous description of recessive mutations in *TRIP4* (3 families sharing 2 mutations) or in *ASCC1* (1 family)[15] in patients diagnosed with spinal muscular atrophy (SMA) with arthrogryposis multiplex congenita, respiratory distress, and congenital bone fractures. Thereafter, no other patient with *TRIP4* mutations has been described, but 4 additional families with *ASCC1* recessive nonsense or frameshift mutations have recently been reported.[16,17] They showed a similar neonatal phenotype including arthrogryposis, bone fractures, and respiratory failure, but muscle biopsies disclosed myopathic features and were not suggestive of motoneuron involvement.[17]

Transcriptional coregulators are emerging as key modulators of the functions of nuclear receptors and transcription factors.[18] The ASC-1 complex acts as a coactivator through direct binding to transcription factors like AP-1, NF-kappa-B, and serum response factor, involved in cell fate-controlling pathways.[19] ASC-1 is known to interact with basal transcription factors (TBP, TFIIA), transcription integrators (CBP, SRC-1), and nuclear receptors (TR, RXR, ER) in vitro through its highly conserved zinc finger domain.[20] Moreover, ASC-1 contains a conserved C-terminal ASC-1 homology (ASCH) domain with putative RNA-binding activity predicted in silico to coordinate pre-mRNA processing.[21,22] Interestingly, the ASC-1 complex has been recently implicated in amyotrophic lateral sclerosis (ALS) pathogenesis, being proposed as a common link between ALS and SMA.[23] We demonstrated that ASC-1 plays a pivotal role in muscle, its absence leading to defects in human myotube growth.[14] However, the precise ASC-1 function and the phenotypical spectrum associated with *TRIP4* mutations (including motoneuron vs primary muscle involvement) remained largely unknown.

We report here the first series of patients with *TRIP4* mutations, redefine the phenotypical and molecular spectrum of disease, and establish the first phenotype–genotype correlations. We also clarify the disease pathophysiology by revealing an unsuspected function of ASC-1 as a cell cycle regulator.

Materials and Methods

Patients and Biological Samples

Patients were recruited through an international collaboration. We also reassessed evolution of the previously reported ASC1-RM family.[14] Clinical data were systematically retrieved and analyzed retrospectively according to a standardized form. All patients were examined by at least 1 of the authors in specialized neuromuscular departments.

Diagnostic muscle biopsies from 4 patients were processed for standard histological and immunochemical studies and fixed for electron microscopy. Primary fibroblasts from patients and age-paired controls were obtained from skin biopsies or surgically discarded tissues. Muscle tissue was obtained from diagnostic biopsies in 2 patients and from surgically discarded tissue in controls.

Informed consent was obtained from all patients or their guardians in agreement with local ethic committees and with the 1964 Helsinki declaration and its later amendments.

Genotyping

TRIP4 mutations were identified on DNA from peripheral blood samples by exome sequencing or next generation sequencing–based myopathy gene panel, Sanger-confirmed in patients and relatives, and reported according to Human Genome Variation Society recommendations (http://varnomen.hgvs.org).

The Exome Aggregation Consortium (ExAC; https://gnomad.broadinstitute.org/) and gnomAD (http://gnomad.broadinstitute.org/) databases were interrogated to identify previously reported mutations and to determine the frequency of each mutation in the general population. Alamut Visual (Interactive Biosoftware, North Seattle, WA) was used to predict the effect of the variants.

Cell Culture

All cells were grown at 37°C with 5% CO_2. Cells were grown in Dulbecco modified Eagle medium containing GlutaMAX (Gibco, Waltham, MA), fetal calf serum (FCS) 20% and penicillin–streptomycin (P/S) 1% (primary fibroblasts), or FCS 10% and P/S 1% (C2C12).

Transfection: siRNA and Plasmid DNA

C2C12 cells were transfected with *Trip4*-specific siRNAs or scrambled control siRNA (OriGene Technologies, Rockville, MD) 18 hours after seeding according to the manufacturer's instructions using Lipofectamine RNAiMAX (Invitrogen, Carlsbad, CA). The final concentration of siRNAs was 4nM. Maximum downregulation was achieved 48 hours post-transfection.

For rescue experiments, mammalian expression vectors (Promega, Madison, WI) containing the ORF sequence of the human *TRIP4* (pFN21AB7885) or *CELF1* (pFN21AB0039) genes fused with a HaloTag were used. Cells were transfected with siRNAs as described above. A second transfection was performed to overexpress *TRIP4* or *CELF*. Plasmids and Lipofectamine 2000 were mixed in Opti-MEM according to the manufacturer's instructions (Invitrogen).

Cell Proliferation Studies

After seeding at 40,000 cells/well, the number of primary fibroblasts per optical field was counted from 24 to 96 hours on bright-field images. Proliferation of C2C12 cells was analyzed from 24 to 72 hours after transfection.

Cell Size Measurements

C2C12 cells were imaged from 24 to 96 hours postseeding on an Axio Observer A1 inverted microscope (Carl Zeiss, Oberkochen, Germany). Length and width of cells were measured on bright-field images with ImageJ (National Institute of Health, Bethesda, MD).

Fluorescence Activated Cell Sorting Analysis

C2C12 cells were harvested 48 hours after transfection and primary fibroblasts during exponential growth phase. Cells were fixed in 70% ethanol at −20°C overnight and then stained with 50µg/ml propidium iodide, 0.1 or 1% triton, and 100 or 50µg/ml RNAse A for fibroblasts or C2C12 cells, respectively. Analysis was performed using CyAn ADP analyzer (Dako) and FlowJo software (Becton Dickinson, Franklin Lakes, NJ).

Population Doubling Time and Cell Phase Duration

Doubling time was calculated using the website doubling-time.com/compute.php (A. Roth, 2006, Doubling Time Computing) and the formula

$$Doubling\ Time = \frac{duration\ log(10)}{log(Final\ Concentration) - log(Initial\ Concentration)}.$$

The duration of each cell phase was obtained by multiplying each sample doubling time by the percentage of cells in each phase (fluorescence activated cell sorting [FACS]).

Western Blot

Cells were lysed with cold lysis buffer. Cell extracts (20µg) were separated using 10% sodium dodecyl sulfate–polyacrylamide gel electrophoresis gel and transferred on nitrocellulose membranes (Trans Turbo Transfer System; Bio-Rad Laboratories, Hercules, CA), which were blocked and probed with the primary antibody anti–ASC-1 (Abcam, Cambridge, MA), antitubulin (Sigma, St Louis, MO), anti-p21 (Santa Cruz Biotechnology, Santa Cruz, CA), anti–cyclin D3 (Santa Cruz Biotechnology), anti–cyclin D1 (Santa Cruz Biotechnology or Millipore, Billerica, MA), anti-pRb (BD Pharmingen, Franklin Lakes, NJ), anti-MHCe (Developmental Studies Hybridoma Bank, Iowa City, IA), or anti-HaloTag (Promega). Membranes were incubated with the secondary antibodies goat antirabbit horseradish peroxidase (HRP) conjugate (Thermo Fisher Scientific, Waltham, MA) or goat antimouse HRP conjugate (Thermo Fisher Scientific). Signals were detected with enhanced chemiluminescence (ECL, Bio-Rad Laboratories) and quantified using ImageJ software.

Statistical Analyses

Results were expressed as mean ± standard deviation. All data were analyzed with SPSS Statistics version 22.0 (IBM, Armonk, NY). Differences were considered significant if $p < 0.05$.

Results

Clinical Findings: Expanding the Clinical Spectrum

We identified 6 novel patients (2 females and 4 males) from 5 families with *TRIP4* mutations (Table 1). Age at ascertainment ranged from 7 to 63 years. All pedigrees were compatible with autosomal recessive transmission. Consanguinity was confirmed in 3 families (A, C, and E). Patient CIII.7 had 2 siblings deceased during the first year of life due to respiratory distress. Patient DII.2 had a

TABLE 1. Summarized Clinical Findings

	Family; Patient/Gender					
	Family A; III.2/F	**Family B; III.1/M, III.2/F**	**Family C; III.7/M[a]**	**Family D; II.2/M**	**Family E; II.4M**	**Family F,[14] 1 F, 3 M**
TRIP4 pathogenic variant	c.141_142delAT (p.Tyr48fs*3) homozygous	c.534C > G (p. His178Gln) + c.1544_1547delACTG (p.Asp515fs*34)	c.1065delC (p.Ile356fs*6) homozygous	c.55_56insCT (p.Gln19fs*47) + c.1197delA (p.Ser399fs*12)	Homozygous deletion of exons 8 and 9	c.890G > A (p.Trp297*) homozygous
First signs	Hypotonia, DMM	DMM (gait acquisition) in both siblings, Waddling gait and fatigability in III.2	NH, respiratory distress, feeding difficulties	NH, DMM	Difficulty running, poor sports performance (adolescence)	NH, respiratory distress (n = 3), feeding difficulties (n = 3)
Best motor performance	Present age (9 yr): waddling gait, climb stairs, bipodal jump, starts to run	Present age (22 yr, III.1 and 16 yr, III.2): waddling gait, climb stairs	NA	Present age (35 yr): independent ambulation (short distances)	Adulthood: independent ambulation, climb stairs	Supported indoors ambulation in mildest patient until 11 yr
Evolution of motor performance	Improving	Stable	NA	Stable	Stable	WCB before adulthood
Scoliosis	Yes (early childhood)	Yes (early childhood)	No	Yes (early childhood) + arthrodesis at 16 yr	No	Progressive scoliosis and arthrodesis in 3
Rigid spine	No	Yes in III.2	No	Yes	Yes	Yes (n = 2)
Respiratory involvement	Respiratory infections since 7 mo; nocturnal noninvasive ventilation since age 3 yr	Restrictive RF since childhood; latest FVC 60% (III.1, 22 yr) and 52% (III.2, 18 yr); no assisted ventilation	From birth; neonatal respiratory distress needing tracheostomy and ventilation; died from RF at 8 mo	Restrictive RF; nocturnal noninvasive ventilation since 18 yr; latest FVC 35% (35 yr)	Latest FVC 80% (63 y); obstructive sleep apnea syndrome treated by CPAP	From birth (n = 3) and from 2 yr (n = 1); ventilation in the 1st year of life in 3 and from 11 yr in the mildest
Cardiac involvement	No	No	No	No	DCM (LVEF 25%) in the 5th decade	DCM in the 3rd decade (n = 1)
Joint contractures	Yes (Achilles)	No	No	Yes (elbows, Achilles); joint hyperlaxity LL	Yes (elbow, mild)	Yes (n = 2); hyperlaxity (n = 4)
Skin involvement	No	No	Yes (hyperelasticity)	Yes (hyperelasticity, FH)	Yes (xerosis, FH)	Yes (hyperelasticity, xerosis, FH)
Dysmorphic features	Flat face, retrognathia	No	Flat face, prominent venous markings, tapering fingers	Elongated face, low-set ears, retrognathia; flat thorax, pectus excavatum	Flat face, retrognathia; flat thorax, pectus excavatum	Flat face (n = 2), flat thorax (n = 3), funnel thorax (n = 1), pectus excavatum (n = 2), valgus feet (n = 2), high arched palate (n = 1)
Other features	Underweight (<P3), learning and writing difficulties	Right eye keratoconus (III.1), underweight (<P4; III.2)	Severe ophthalmoplegia	Underweight (<P3); myopia	Mild ophthalmoparesis; myopia	LL lipodystrophy (n = 2), learning difficulties (n = 2), language delay (n = 1), testicular ectopia and delayed puberty (n = 1)

[a]Proband BOS1248-1 in the Manton Center for Orphan Disease Research database.

CPAP = continuous positive airway pressure; DCM = dilated cardiomyopathy; DMM = delayed motor milestones; F = female; FH = follicular hyperkeratosis; FVC = forced vital capacity; LL = lower limbs; LVEF = left ventricular ejection fraction; M = male; NA = not applicable; NH = neonatal hypotonia; P3 = centile 3; P4 = centile 4; RF = respiratory failure; WCB = wheelchair-bound.

brother diagnosed with a congenital myopathy with type I fiber uniformity who died at 5 years due to respiratory failure. These 3 affected siblings were not included due to lack of genetic confirmation. We also reassessed the 3 surviving patients from the originally reported family (family F[14]) after 3 years of additional follow-up.

Overall, the clinical phenotype in the novel patients was marked, like in the original family, by early onset proximal and axial weakness, respiratory failure with variable severity, scoliosis, and skin involvement without prominent limb contractures.

None of the patients presented with arthrogryposis or congenital contractures. There were no complications during pregnancy or labor, excepting reduced fetal movements in the most severe patient (CIII.7). First signs appeared before adulthood in all cases.

Patient CIII.7 presented at birth with severe neonatal hypotonia, poor antigravity limb movements, dysmorphic features, feeding difficulties, perinatal asphyxia, and respiratory distress (Fig 1A). He never acquired cephalic control. Two patients (AIII.2 and DII.2) presented with neonatal hypotonia and delayed motor milestones. The 2 siblings from Family B presented with delayed gait acquisition, waddling gait, and fatigability. The mildest patient (EII.4) presented with difficulties running and poor sports performance in adolescence. The last 5 patients acquired independent ambulation, although only 1 did so before the age of 18 months.

In all patients from the 6 families, muscle weakness and amyotrophy was predominantly axial and proximal (3–4/5, Medical Research Council scale), whereas distal limb strength was relatively well preserved. Only 1 patient had marked facial weakness. There was bilateral horizontal ophthalmoparesis in 1 patient and ophthalmoplegia in the most severe case. Ptosis was not observed.

Muscle weakness was stable or slowly progressive. Excepting the 3 patients from the original family (Family F), who never acquired independent ambulation, all the adult patients can walk outdoors without support at ages 23 to 63 years, walking distance being limited by fatigue or dyspnea. Three patients are able to climb stairs with aid. Patient AIII.2, currently 9 years old, is still improving her motor abilities and starting to run.

All the patients who survived beyond childhood, except the mildest (Patient EII.4), had early onset progressive scoliosis, associated with lateral trunk deviation and tilted pelvis in 2 cases (see Fig 1A). This includes the youngest patient of Family F (FIII.1), reassessed after arthrodesis at age 12 years. Scoliosis was associated with spinal rigidity in a total of 5 cases. Thorax deformities (flat thorax and pectus excavatum) were present in 5 patients. Five also had dysmorphic craniofacial features with a similar flat face, along with a large and thick neck appearance.

Respiratory failure was present in 9 of the 10 patients since childhood. The most severe patient suffered neonatal respiratory distress requiring tracheostomy and assisted ventilation. He died at 8 months due to respiratory failure, and so did Patient FII.5 at 16 months. Five patients needed chronic ventilation (nocturnal noninvasive in 3 cases, through a tracheostomy in 2), whereas in the remaining 2 cases only respiratory physiotherapy was prescribed. The mildest patient, currently aged 63 years, has a forced vital capacity of 80% but is treated with continuous positive airway pressure due to sleep apnea/hypopnea syndrome.

No patient had congenital or childhood cardiomyopathy. However, Patient EII.4 developed a severe dilated cardiomyopathy (DCM) in the fifth decade, requiring a preventive automated implantable cardioverter defibrillator. Follow-up of Family F revealed DCM from the beginning of the 3rd decade in Patient FII.2. All the other patients had normal cardiac evaluations at ages 9 to 35 years.

Limb contractures, mild to moderate, were present in 5 patients, mainly affecting Achilles tendon and elbows. Prominent and generalized joint hyperlaxity was observed in 5. Deep tendon reflexes were universally diminished or absent.

Extramuscular involvement included skin abnormalities (hyperelasticity, follicular hyperkeratosis, and xerosis with scratch lesions but without keloids, n = 7) and body composition changes. Three of the novel patients were underweight (<4th percentile), and 1 was overweight with abundant adipose tissue in lower limbs, resembling the female patients from Family F.[14] None of the novel patients had intellectual disability or signs of central nervous system abnormalities.

Creatine kinase level was normal or mildly elevated (<3 × normal) in all patients. Electromyography showed a myopathic pattern without denervation or abnormalities in nerve conduction studies (n = 6) or repetitive stimulation (n = 3).

Muscle magnetic resonance imaging (MRI) of the lower limbs in 2 of the novel patients showed a predominant involvement of the posterior compartment of the thigh, notably of gluteus maximus and adductor longus muscles, with relative preservation of gracilis, sartorius, and semitendinosus muscles (see Fig 1B). This pattern was comparable to that previously observed in Family F.[14]

Histopathological Phenotype: Cores, Cytoplasmic Bodies, Nemaline, Centronuclear, and Cap Lesions

One patient had a quadriceps biopsy in early childhood, reportedly normal, which was not available. Samples from the remaining 4 biopsied patients showed congenital myopathy lesions, including fiber size variability, type 1 fiber predominance (and frequent hypotrophy), and

FIGURE 1: ASC-1–related myopathy phenotypical spectrum. (A) Clinical findings in Patients CIII.7 (a), DII.2 (b–f), and EII.4 (g, h). (a) Congenital presentation with neonatal hypotonia (frog position), poor limb movements, and respiratory distress requiring tracheostomy and assisted ventilation. He had skin lesions, dysmorphic facial features (ie, flat face; not shown), and tapering fingers. (b–f) Patient DII.2, still ambulant at age 35 years. Note severe scoliosis with dorsal lordosis and unbalanced hips (b, d), thoracic deformities (pectus excavatum), and elbow contractures (b) contrasting with prominent joint hyperlaxity (f). Dysmorphic features included large, thick neck, retrognathism, and low-set ears (not shown). (c, e) The skin phenotype was marked by follicular hyperkeratosis, xerosis with scratch lesions, prominent scars (but not keloid), and skin hyperelasticity. (g, h) The mildest patient (EII.4), still ambulant at 63 years, has proximal amyotrophy, pectus excavatum, and dysmorphic facial features (flat face, thick neck, retrognathia). (B) Muscle imaging in 2 patients revealed predominant involvement of posterior thigh compartment with relative preservation of the semitendinosus muscle. (a–c) Lower limb magnetic resonance imaging (MRI) from a mild patient
(Figure legend continues on next page.)

TABLE 2. Main Histological Findings in Skeletal Muscle Biopsies from 5 Patients

Patient	Age at Biopsy	Muscle Sampled	Major Findings
AIII.2	4 yr	Quadriceps	IN, FSV, type1 fiber predominance (95%) and hypotrophy, minimal endomysial fibrosis, whorled fibers, minicores
BIII.1	9 yr	Quadriceps	Reported as normal
CIII.7	2 mo	Quadriceps	IN, FSV, type 1 fiber predominance and hypotrophy, endomysial fibrosis
DII.2	27 yr	Biceps brachii	IN, FSV, type 1 fiber predominance (99%), minicores, rimmed sarcolemma
EII.4	56 yr	2 quadriceps biopsies	IN, FSV, type 1 fiber predominance, lobulated fibers; minicores in 1 biopsy; rods, cytoplasmic bodies, and caps in a second biopsy

FSV = abnormally increased fiber size variation; IN = internalized nuclei.

internalized nuclei, along with other changes in the muscle fiber architecture (Table 2, Fig 2). Three patients had multiminicores, often associated with other forms of sarcomere disorganization (cap lesions, rods and cytoplasmic bodies, whorled fibers). The most severe patient showed fibers with centrally located nuclei interspersed with very small, rounded fibers without fascicular distribution, compatible with centronuclear/myotubular myopathy.

Lobulated fibers and rimmed sarcolemma (intense oxidative rims beneath the sarcolemma; see Fig 2E) were occasionally observed. None of the 4 biopsies disclosed fiber type grouping, angulated fibers, or group atrophy suggestive of denervation.

Genetic Studies: Novel TRIP4 Mutations

Seven previously unreported mutations in the *TRIP4* gene were identified (Fig 3A, B). Transmission was autosomal recessive in all cases. Tested parents from 3 families were healthy heterozygous carriers.

The mutations were distributed along the entire length of the gene. These included the first *TRIP4* missense variant, affecting a highly conserved residue in the zinc finger domain (c.534C > G, p. His178Gln). Two frameshift mutations predicted loss of the ASCH domain (c.1544_1547delACTG, p.Asp515Alafs*34, and homozygous deletion of exons 8 and 9, respectively; see Fig 3C).

Western blot was performed on primary skin fibroblast cultures (Family B) or frozen muscle biopsies (Families D and E) from 4 patients. Family B was compound heterozygous for a missense and a truncating mutation, which led to a reduced level of expression of the full-length protein (10–20% compared to control; see Fig 3D). Frameshift mutations (Family D) or large deletions affecting the C-terminal part of the protein (Family E) led to a total absence of full-length ASC-1 and no detectable truncated form (see Fig 3E).

None of the patients had mutations in other known neuromuscular genes except for the oldest patient (EII.4), in whom exome studies revealed a heterozygous variant of the titin gene (*TTN*; c.6379_6380del, p.Tyr2127Leufs*8), also identified in one of his asymptomatic older sisters whose echocardiography was normal. This variant, predicted to lead to a truncated protein, was absent from ExAC and was not associated with any other *TTN* change (including missense variants) in the patient.

ASC-1 Defects Alter Proliferation of Patient Fibroblasts and Myogenic Cells

When amplifying primary fibroblasts for Western blot, we observed a faster growth of patient cells compared to healthy controls. Thus, we quantified proliferation of skin fibroblasts from Families B (BIII.1 and BIII.2) and F

(BIII.1), still ambulant at age 19 years. Axial T1-weighted images showed mild muscle atrophy and fatty infiltration of glutei, iliopsoas, and posterior thigh muscles with major involvement of adductor longus and relative preservation of gracilis, sartorius, and semitendinosus muscles. Note marked increase in subcutaneous adipose tissue. (d–g) Muscle MRI from Patient EII.4 (aged 56 years) showed the same pattern, including fatty infiltration of paravertebral muscles (d) and the posterior thigh compartment, notably gluteus maximus, adductor longus, and semimembranosus (e, f). Note relative preservation of semitendinosus and gracilis (arrowheads). Leg muscles showed diffuse involvement (g).

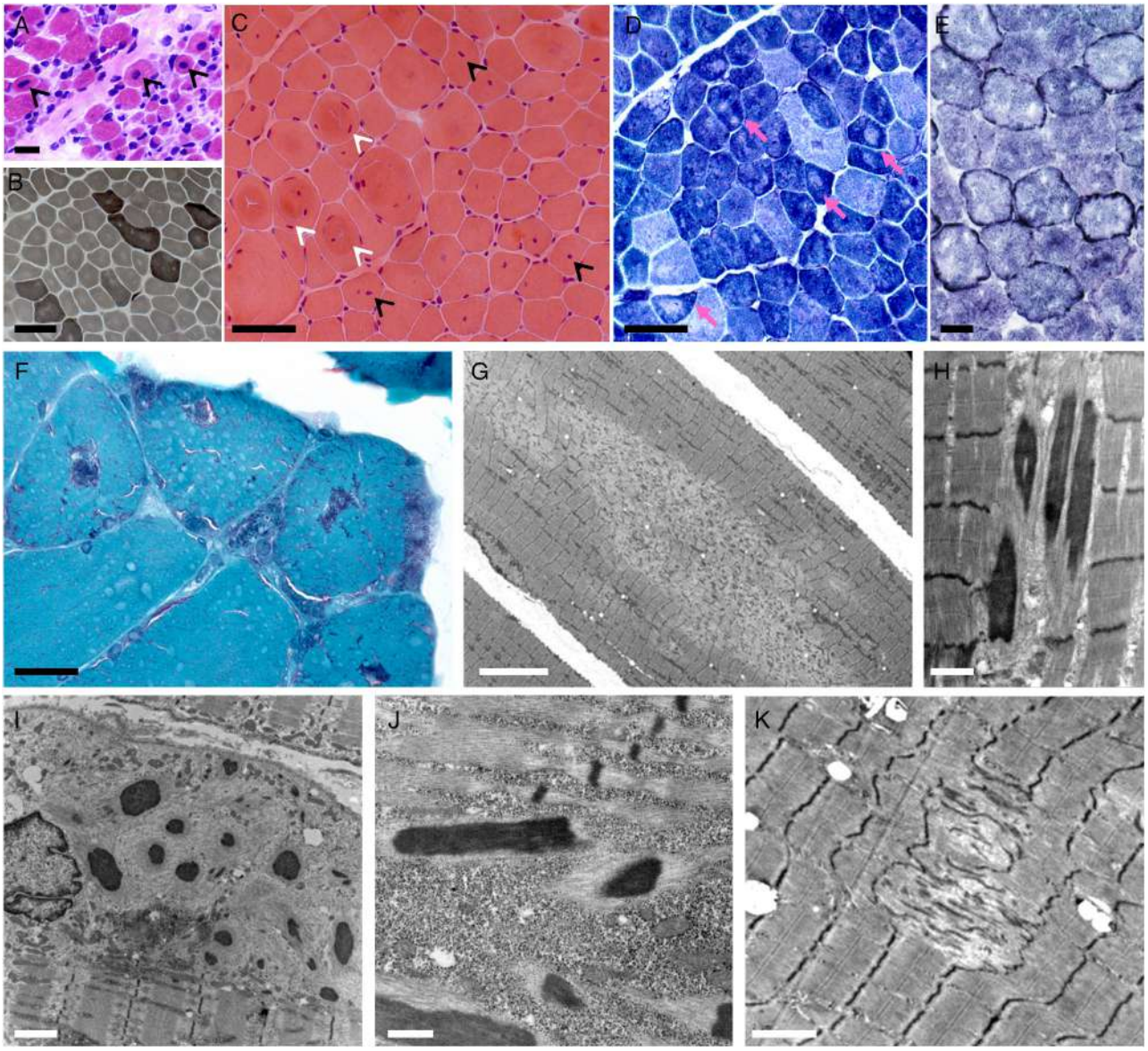

FIGURE 2: Spectrum of histopathological lesions, showing skeletal muscle biopsies from Patients CIII.7 (A), AIII.2 (B–D, G), EII.4 (F, H–J) and DII.2 (E, K). Muscle biopsy from the most severe patient (A) showed mildly increased endomysial connective tissue, a subpopulation of very small fibers, and abundant fibers with apparently normal diameter and centrally located nuclei *(arrowheads)*. In milder patients, dystrophic features were absent and the pattern was more typical of a congenital myopathy, including fiber size variation (B, C), internalized nuclei, often central (C; *black arrowheads*), whorled fibers (C; *white arrowheads*), and type 1 fiber predominance (B). Intense oxidative rims beneath the sarcolemma, compatible with mitochondrial proliferation or mislocalization, were found in 1 patient in nicotinamide adenine dinucleotide–tetrazolium reductase (NADH-TR; E) and also in succinate dehydrogenase and Cox stains (not shown). There were multiple areas lacking oxidative activity (*pink arrows* in D) and showing mitochondrial depletion and sarcomere disorganization on electron microscopy (EM; minicores; G, K). Modified Gomori trichrome revealed purple-stained lesions (F), which corresponded to electron-dense nemaline rods (H, J) on EM. Subsarcolemmal myofibrillar disorganization along with cytoplasmic bodies and/or subsarcolemmal rods were also observed (I). Transversal frozen sections are shown: hematoxylin and eosin (A, C), ATPase pH 9.4 (B), NADH-TR (D, E), modified Gomori trichrome (F), EM (G–K). Scale bars = 25μm (A, B), 50μm (C, D), 25μm (E, F), 10μm (G), 1μm (H), 2μm (I, K), 500nm (J).

(FII.2) versus 4 fibroblast cultures from passage- and age-paired controls (Fig 4). *TRIP4*-mutant fibroblasts showed a significantly higher proliferation rate, with lower mean doubling time than controls, compatible with a shorter cell cycle length (see Fig 4C). This suggested that ASC-1 might be involved in the control of cell cycle progression.

Consistently, FACS studies in nonsynchronous cell cultures showed that, whereas most (>80%) control fibroblasts were in G0/G1 phase, there were significantly fewer patient cells in G0/G1 and more in S and G2 phases (see Fig 4D), indicating a significant increase of cycling cells in ASC-1–depleted cultures. Considering the cell cycle

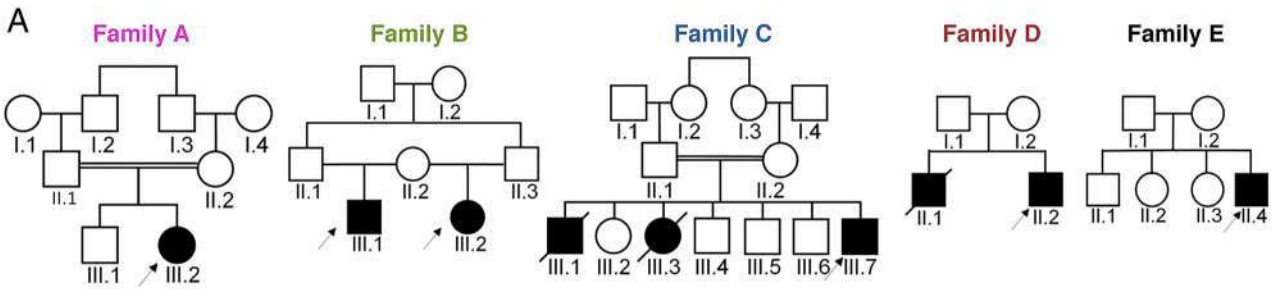

B

Family	Family background	*TRIP4* Exon	cDNA change	Protein change	Variation Type	Predict effect	Allele Frequency (ExAC)	Mutation previously reported?
A	Tunisia	2	c.141_142delAT (homozygous)	p.Tyr48Cysfs*3	Deletion	Frameshift	Not present	Unreported
B	Burundi	4	c.534C>G	p. His178Gln	Substitution	Missense	0.00004942	rs200177653 (dbSNP)
		11	c.1544_1547delACTG	p.Asp515Alafs*34	Deletion	Frameshift	Not present	Unreported
C	Turkey	8	c.1065delC (homozygous)	p.Ile356Leufs*6	Deletion	Frameshift	Not present	Unreported
D	Spain	1	c.55_56insCT	p.Gln19Profs*47	Insertion	Frameshift	Not present	Unreported
		9	c.1197delA	p.Ser399Serfs*12	Deletion	Frameshift	Not present	Unreported
E	France	8+9	Homozygous deletion exons 8 and 9		Deletion	In-frame deletion	Not present	Unreported

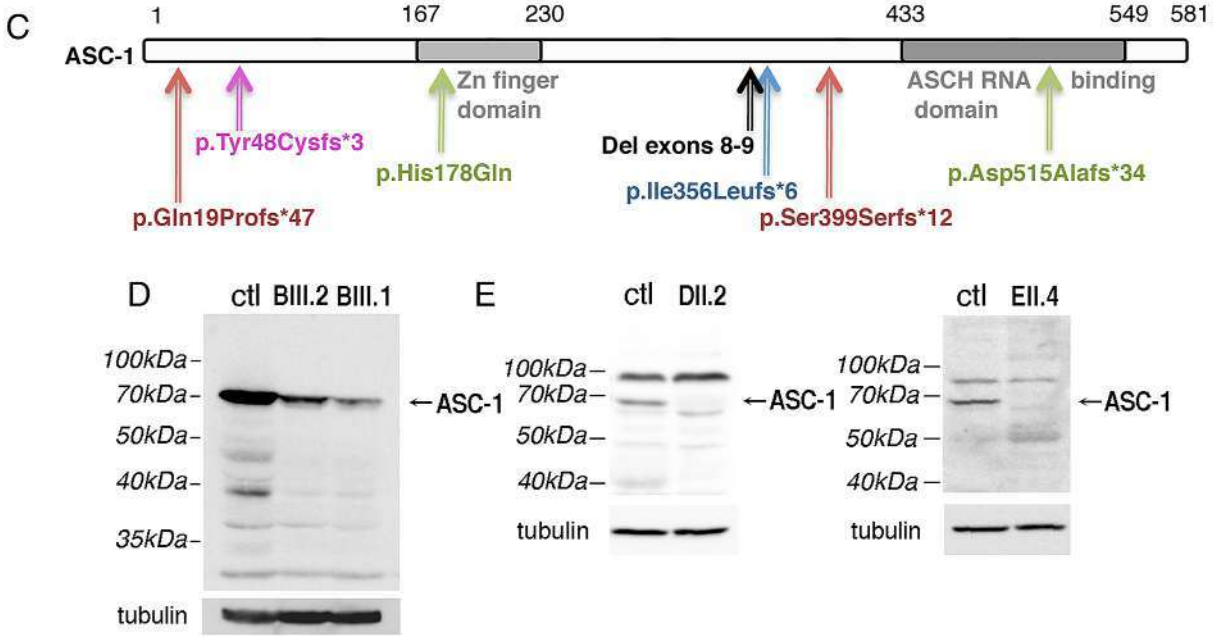

FIGURE 3: ***TRIP4*** **mutations in the novel families. (A) Pedigree of novel families. (B) Summary of the mutations identified. dbSNP = Single Nucleotide Polymorphism Database; ExAC = Exome Aggregation Consortium. (C) Schematic representation of the ASC-1 protein and localization of the patients' mutations. (D, E) ASC-1 expression in patient samples. (D) Low expression of full-length ASC-1** ***(arrow)*** **in fibroblasts from Patients BIII.1 and BIII.2. (E) Full-length ASC-1** ***(arrows)*** **was undetectable in muscle biopsies from Patients DII.2 and EII.4. ctl = control fibroblasts (D), skeletal muscle control (E).**

length, the G0/G1 phase was significantly shortened in patient fibroblasts compared to controls (see Fig 4E), suggesting cell cycle acceleration.

To further clarify the role of ASC-1 in myogenic cells, we used our in vitro *Trip4* knockdown *(Trip4*KD) C2C12 model, comparing cells transfected with an siRNA against *Trip4* (si*Trip4*) to those transfected with a control siRNA (Scbl) or nontransfected (Fig 5). si*Trip4* cells showed a higher proliferation rate, with a shorter doubling time compared to Scbl. Moreover, ASC-1 depleted cells were smaller.

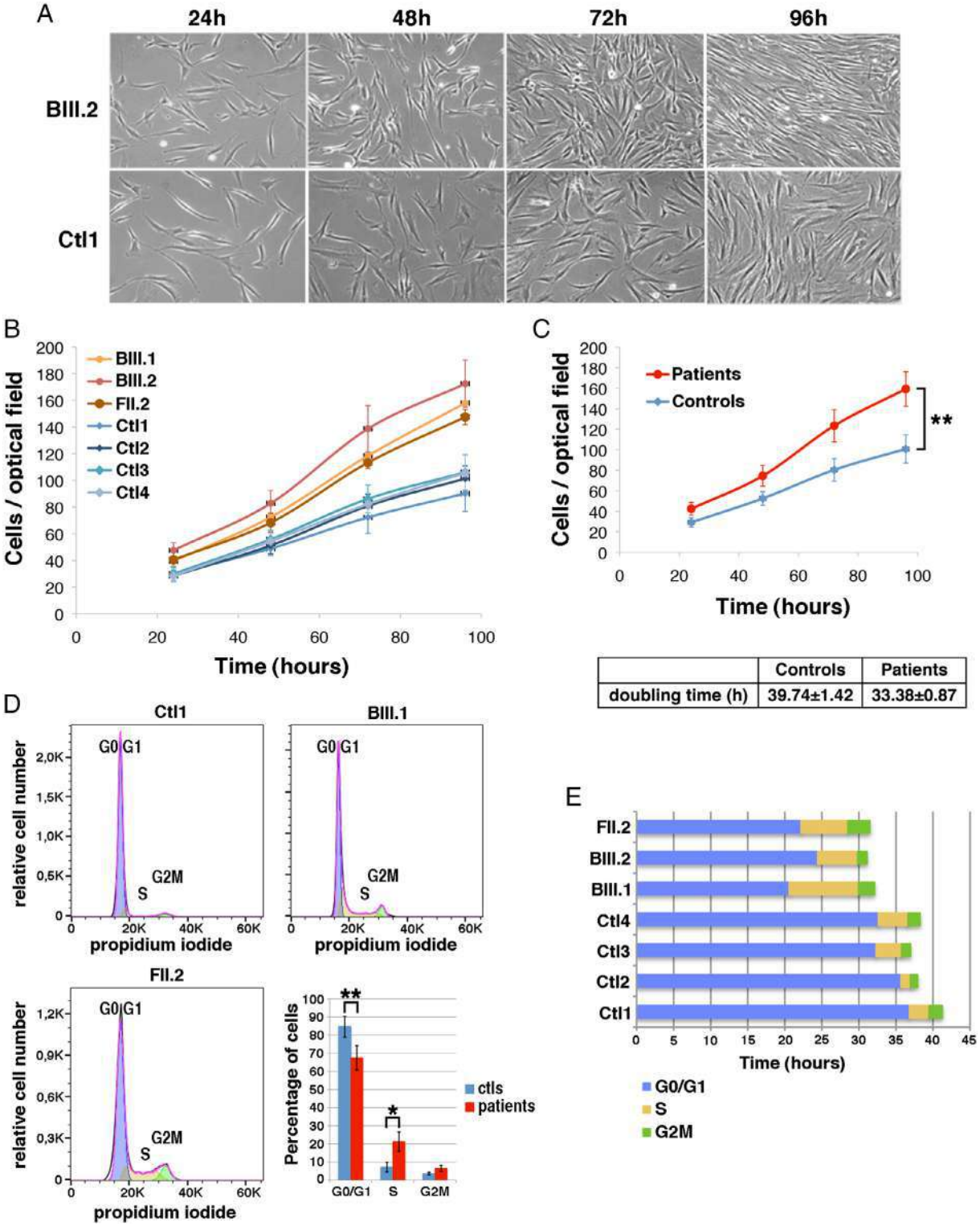

FIGURE 4: Accelerated proliferation and reduced G0/G1 phase of the cell cycle in patient fibroblasts. (A) Bright-field pictures of control (Ctl1) and patient (BIII.2) fibroblast cultures from 24 to 96 hours after seeding. (B) Proliferation curves from 4 control (blue) and 3 patient fibroblast cultures (red). (C) Differences between the proliferation curves from control and patient cells were significant (analysis of variance [ANOVA], 3 *df*, $^{**}p < 0.001$). Mean population doubling time of control and patient cells was calculated for cells in exponential proliferation between 48 and 72 hours. (D) Fluorescence activated cell sorting analysis of cell cycle progression in nonsynchronous proliferative control (Ctl1) or patient (BIII.1; FII.2) fibroblasts. Histogram shows the mean percentage of cells per phase in the 4 control and 3 patient fibroblast samples (ANOVA, 2 *df*, $p < 0.001$; Tukey honestly significant difference: $^{*}p = 0.01$, $^{**}p = 0.002$). (E) The duration of cell cycle phases G0/G1 (blue), S (yellow), and G2M (green) for each sample was determined as the percentage of cells in each phase multiplied by the doubling time corresponding to each sample.

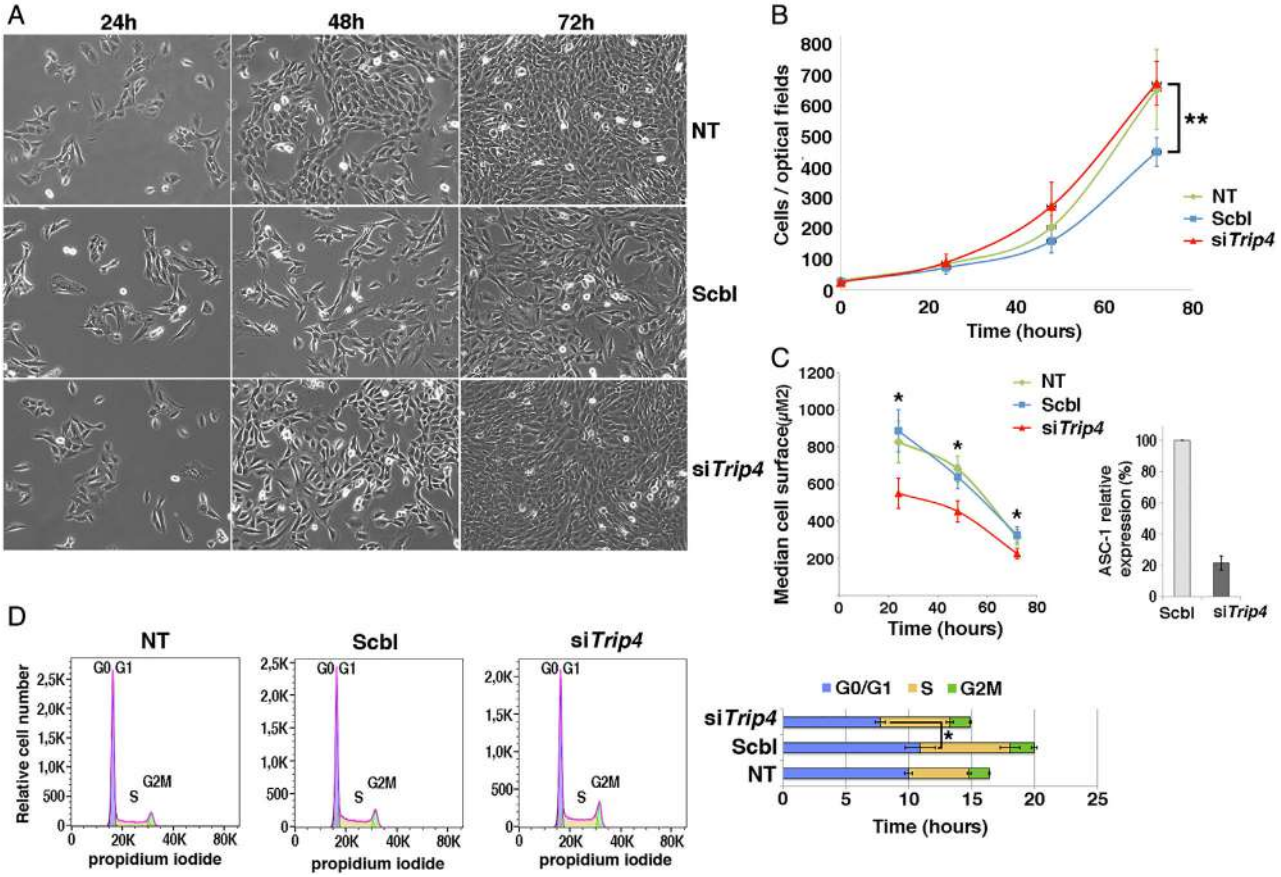

FIGURE 5: Accelerated proliferation and G0/G1 phase reduction and reduced growth in *Trip4*KD myogenic cells. (A) Bright-field pictures of *Trip4*KD C2C12 (si*Trip4*) compared to not treated (NT) or scramble (Scbl) transfected controls from 24 to 72 hours after siRNA transfection. (B) Proliferation curves of si*Trip4*, Scbl, and NT cells. Overall, the proliferation curve of si*Trip4* cells was higher than that from Scbl-transfected controls (analysis of variance [ANOVA], $**p < 0.001$), maintaining values comparable to nontransfected cells. Values are the mean of 4 independent measurements for each time per condition. Mean population doubling time (hours) was calculated for cells in exponential proliferation between 24 and 48 hours after transfection: NT, 16.6 ± 1; Scbl, 20.1 ± 4.4; si*Trip4*, 15.1 ± 1.5. (C) si*Trip4* cells exhibited a smaller cell surface (μm^2) compared to NT or Scbl cells after 24, 48, or 72 hours of culture (Kruskal–Wallis, $*p < 0.05$). A strong reduction (>80%) of ASC-1 in *Trip4*KD cells was observed 48 hours after transfection. This was also observed within 48 hours with 3 independent siRNAs against *Trip4* (data not shown). (D) Fluorescence activated cell sorting analysis of cell cycle in nonsynchronous NT, Scbl, and si*Trip4* cells. Mean cell cycle distributions measured in 3 experiments showed a decrease in the percentage of cells in G0/G1 phase in si*Trip4* condition compared to Scbl and NT (respectively: 51 ± 3.3, 54.3 ± 6.1, 60.1 ± 4.7), an increase in S phase (respectively: 36.4 ± 2.3, 35.6 ± 3.9, 29.1 ± 3.7), and an increase in G2M phase (respectively: 10.8 ± 1.3, 9.64 ± 1.1, 9.74 ± 2.3). The duration of the cell cycle phases (±standard error of the mean) G0/G1 (blue), S (yellow), and G2M (green) was determined as mentioned in Figure 4 (ANOVA, $*p < 0.05$). A parallel increase in the number of cells in S phase in both Scbl and si*Trip4* samples could be explained by the stress induced by transfection.

Consistently, FACS studies confirmed a decrease of cells in G0/G1 phase and a significantly reduced duration of the latter upon ASC-1 depletion. Thus, ASC-1 is involved in cell cycle regulation in both fibroblasts and myogenic cells, its depletion leading to cell cycle acceleration and reduced cell growth due to shortening of the G0/G1 phase.

ASC-1 Depletion Is Associated with Altered Expression and Phosphorylation of Cell Cycle Exit Regulators

Cell cycle arrest is an important step in myogenic differentiation, which involves transitioning from proliferative myoblasts to postmitotic myotubes and muscle fibers. D-type cyclins are regulators of one key G1-phase checkpoint, determining cell cycle arrest or progression into S-phase. Quantification of cyclins D1 and D3 and the cell cycle exit marker p21 in frozen muscle samples from 3 *TRIP4*-mutant patients showed significant cyclin D1 decrease and cyclin D3 increase compared to control (Fig 6A). p21 was significantly reduced in the 2 older patients. Embryonic myosin heavy chain was undetectable, suggesting that the cyclin changes in patient muscles are unlikely to be nonspecifically due to muscle fiber regeneration and probably are directly associated with ASC-1–related cell cycle defects in postmitotic muscles.

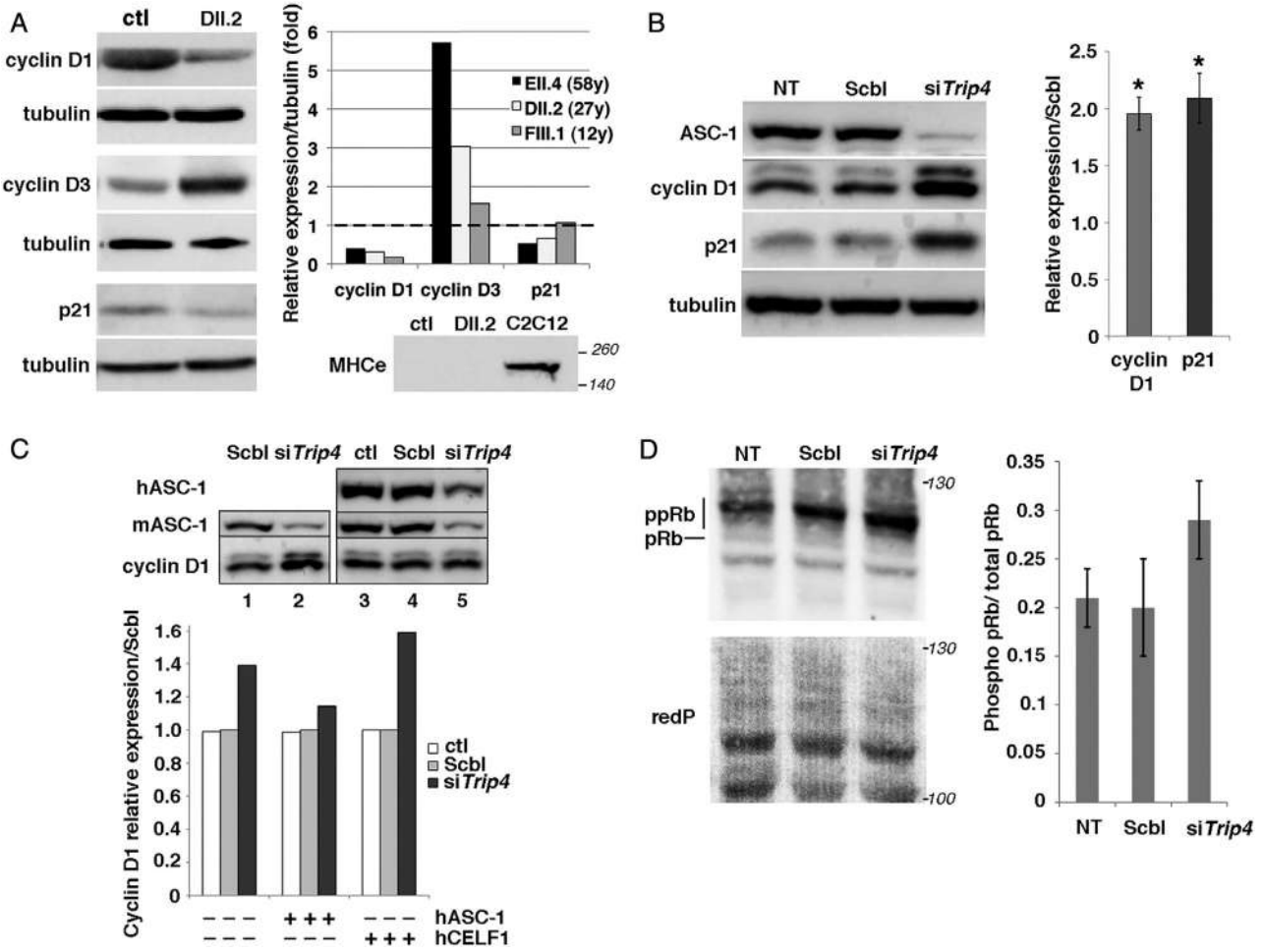

FIGURE 6: Altered expression of cell cycle proteins in patient muscles and in *Trip4*KD myogenic cells. (A) Western blot of lysates from control (ctl) and 3 patient frozen muscles revealed altered expression of cyclins D1 and D3 as well as p21 in Patients DII.2 (left panel), EII.4, and FIII.1 (right panel, control expression normalized to 1, *dashed line*). Absence of embryonic myosin (MHCe) in both Patient DII.2 and control muscle samples excluded that this might be due to active muscle regeneration (including the presence of immature myofibers) in patients (lower panel, C2C12 used as a positive control). (B) Increased cyclin D1 and p21 expression in *Trip4*KD C2C12 with <20% ASC-1 residual expression (data not shown) compared to nontransfected cells (NT) or cells transfected with siRNA control (Scbl; left and right panel, normalized to Scbl transfected cells; Mann–Whitney *U*, *$p < 0.05$). (C) Rescue of the altered levels of cyclin D1 in *Trip4*KD C2C12 by wild-type human ASC-1. Western blot of protein extracts is shown from Scbl (lanes *1* and *4*), si*Trip4* (lanes *2* and *5*), or ctl C2C12 (lane *3*) double-transfected with hASC-1 (lanes *3–5*) 24 hours after endogenous ASC-1 silencing (upper panel). Quantification of the relative expression of cyclin D1 over tubulin (normalized for Scbl) in ctl, Scbl, and si*Trip4* cells in the presence or absence of hASC-1 is shown. A vector expressing hCELF1 was used as a nonspecific control (lower panel). hASC-1 = human ectopic ASC-1; hCELF1 = human ectopic CELF1; mASC-1 = murine endogenous ASC-1. (D) Western blot analysis of retinoblastoma protein (Rb) phosphorylation state in NT, Scbl, and si*Trip4* cells revealed a fast migrating band corresponding to the hypophosphorylated form of Rb (pRb, 110kDa) and slower migrating bands corresponding to hyperphosphorylated forms of Rb (ppRb, 116kDa; left panel). Red ponceau (redP) staining of the membrane showed similar loading in each condition. In all conditions, the hyperphosphorylated forms of Rb were predominant compared to the hypophosphorylated form as expected for cycling cells. Although variability precluded reaching statistical significance, quantification of the ratio ppRb/total pRb for each condition (n = 4) showed an increase by nearly 50% of hyperphosphorylated forms in si*Trip4* cells (right panel).

Analysis of cyclin D1, cyclin D3, and p21 expression during proliferation in *Trip4*KD C2C12 myoblasts confirmed cyclin changes, showing a significant increase in cyclin D1 and p21 (see Fig 6B) without significant changes in cyclin D3 (data not shown). Increased expression of cyclin D1 and p21 in *Trip4*KD was rescued by expression of human wild-type ASC-1 (see Fig 6C and data not shown), confirming that this molecular phenotype is not due to off-target effects of *Trip4* siRNA.

The retinoblastoma protein (pRb) interacts with cyclins and regulates both cell cycle and muscle-specific gene expression through its target E2F. Thus, abnormalities of Rb, whose activity is modulated by cyclin/cyclin-dependent kinase–mediated phosphorylation, might be an

underlying mechanism in ASC1-RM muscle phenotype. We found an increase of the hyperphosphorylated forms of Rb and the hyperphosphorylated/total Rb ratio in *Trip4*KD C2C12 compared to controls (see Fig 6D). This, associated with cyclin D1 changes, could explain the rapid progression of *Trip4*KD cells from G1 to S phase and the myofibrillar abnormalities in patients' muscles, suggesting that ASC-1 is critical for controlling both cell cycle progression and myofibrillogenesis during myogenesis.

Discussion

ASC-1–related disease is emerging as a novel cause of congenital neuromuscular disorders, but its phenotypical spectrum and pathophysiology remained unclear. So far, 3 *TRIP4* mutations have been described in 4 families with a severe neonatal phenotype (1 reported as a CM, the 3 others as SMA).[14,15] We report here 5 additional families with 7 novel *TRIP4* mutations, expanding the phenotypical spectrum beyond lethal congenital forms to mild ambulatory adult patients.

The clinical phenotype in these families is marked by early onset axial and proximal weakness, progressive scoliosis sometimes associated with rigid spine, dysmorphic features, cutaneous involvement, and respiratory failure. No clinical, electromyographic, or histological sign of motor neuron involvement was present. The severity of respiratory involvement correlated with the degree of muscle weakness, unlike in other CMs with minicores (eg, SEPN1-related myopathy[24,25]). The skin phenotype includes skin hyperlaxity, xerosis, and follicular hyperkeratosis. Remarkably, whereas the first patients identified never reached full ambulation, 5 of the novel patients are able to walk without support, being limited mainly by respiratory failure and fatigability. In the mildest case, the first referral signs were noticed in adolescence, and he remains able to climb stairs at 63 years.

Interestingly, dilated cardiomyopathy was detected in 2 patients in the 3rd and 5th decades. We previously showed that *TRIP4* expression is relatively high in murine cardiac muscle.[14] Moreover, neonatal cardiac involvement (cardiomyopathy, atrial septal defect, or patent ductus arteriosus) was reported in 2 SMA families with *TRIP4* mutations.[15] We confirm here that cardiac disease can be part of the *TRIP4*-associated phenotype, and reveal that the absence of pediatric cardiac involvement does not preclude the subsequent development of cardiomyopathy. Therefore, cardiac function should be periodically screened in all *TRIP4*-mutated patients.

Primary myocardial disease is not typical of CM, although it may appear in *TTN*-, *MYH7*-, or *ACTA1*-related myopathies.[1] One of our patients with DCM carries a heterozygous *TTN* truncating variant (TTNtv). Heterozygous TTNtvs are fairly common in the general population (up to 1%)[26–28] and have never been demonstrated to cause congenital skeletal muscle disease by themselves. Congenital titinopathies are autosomal recessive myopathies associated with the combination of either 2 truncating or 1 truncating and 1 missense *TTN* change.[29–31] The TTNtv in our patient is carried by an older sister with normal neurological and cardiological examination, and his muscle MRI is comparable to that in the other ASC1-RM patients. Thus, his skeletal muscle phenotype is most likely explained by the large homozygous *TRIP4* deletion leading to absence of ASC-1. This TTNtv has never been reported in DCM and does not affect the titin domains most commonly associated with cardiomyopathy.[28] However, a potential digenic contribution to his cardiac phenotype cannot be fully excluded at this point. In the other patient with adult onset DCM, linkage and exomic studies excluded recessive pathogenic *TTN* changes.[14]

The spectrum of muscle architectural lesions in ASC1-RM is particularly large. Aside from the multiminicores, internalized nuclei, cap lesions, and mild dystrophic lesions reported,[14] we observed nemaline and cytoplasmic bodies in novel patients. Our findings suggest *TRIP4* as a novel culprit gene for nemaline myopathy, as well as for other forms of congenital muscle disease (including cap disease, core, centronuclear or cytoplasmic-body myopathies, and congenital muscular dystrophy); therefore, we propose that it should be included in the corresponding diagnostic gene panels. Furthermore, we found in one biopsy rimmed fibers comparable to those associated with *ASCC1* mutations.[17] This suggests that *TRIP4* and *ASCC1* are implicated in a common pathophysiological pathway that leads to multiple forms of myofibrillar disarray, and thus to an overlap of different histopathological CM lesions.

Our phenotypical findings can be useful for differential diagnosis. The joint hyperlaxity, mild to moderate joint contractures, spinal rigidity, and skin phenotype observed in some of our patients raise the question of differential diagnosis with collagen VI–related muscular dystrophies,[32] although *TRIP4* mutant patients had no hypertrophic scars. Moreover, minicorelike lesions may occasionally be found in patients with collagen VI–related myopathies.[32,33] Extraocular muscle involvement, previously unreported, may be part of the ASC1-RM spectrum but is typically absent in congenital titinopathies.[31] One of the patients with dilated cardiomyopathy had rigid spine and developed mild elbow contractures with age, features that overlap with Emery Dreifuss muscular dystrophy. However, the conduction defects and marked

contractures typical of the latter were absent in ASC1-RM patients. In addition, muscle MRI in 3 ASC1-RM patients revealed a consistent pattern, with predominant involvement of the adductor longus and posterior thigh compartment and relative preservation of the semitendinosus muscle, sometimes associated with increased subcutaneous adipose tissue.[14] This MRI pattern differed from the typical abnormalities associated with collagen VI defects[32,34] or with other CMs with minicores such as those related to *SEPN1*[35], *RYR1*,[36] or *TTN*,[37] although its specificity requires confirmation by further studies.

This work significantly increases the number of known *TRIP4* mutations, confirms autosomal recessivity, and defines the first genotype–phenotype correlations. The novel mutations include 1 large deletion and 5 frameshift changes predicting a reduction or absence of full-length ASC-1 protein. ASC-1 depletion was confirmed experimentally in 3 families, including 2 patients compound heterozygous for the first identified *TRIP4* missense mutation. Interestingly, ASC-1 was undetectable by Western blot both in our mildest patient and in the first severe cases reported,[14] suggesting other severity modulators. Aditionally, the patients reported as having severe SMA[15] carried *TRIP4* nonsense mutations resulting in exon skipping and upregulation of a shorter isoform containing most ASC-1 functional domains. Although their muscle biopsies showed major reduction of myofiber size compatible with a primary muscle component, our findings suggest that the *TRIP4* mutations leading to ASC-1 protein depletion are associated with a primary striated muscle phenotype, whereas those leading to expression of a truncated protein might be associated with motoneuron disease. A better understanding of the molecular mechanisms of ASC-1–related disease should help to clarify this point.

On this note, we report a pathophysiological pathway associated with ASC-1 defects that contributes to clarify its as yet undefined role and the disease mechanism. Consistently with a muscle and skin phenotype, in the absence of ASC-1, proliferation is accelerated in both fibroblasts and myogenic cells. This increased proliferation is mainly due to a reduction of the G0/G1 phase and is associated with cell size reduction. Shortening of the G1 phase has been associated with cell size and growth reduction in mammalian cells[38,39] and may contribute to explaining the myotube growth defect in ASC-1–depleted patient and C2C12 cells.[14]

This cell cycle phenotype is associated with altered cyclin expression. In C2C12, we found that *Trip4*KD leads to an increase of cyclin D1 and p21, regulators of the G0/G1 phase, and of several downstream targets. Overexpression of D-type cyclins has been shown to shorten the G0/G1 phase.[40] Furthermore, the high levels of p21 and cyclin D1 in the absence of ASC-1 suggest an increased formation of the cyclin D1 and CDK4/6-complex.[41] This complex phosphorylates proteins such as the tumor suppressor pRb,[42] known to control cell cycle. Hypophosphorylated pRb inhibits E2F transcription factors required for S phase entry.[43] In *Trip4*KD cells, we found a consistent tendency toward the reduction of the hypophosphorylated forms of pRb in favor of hyperphosphorylation, which indicates loss of pRb-mediated inhibition of the G0/G1-S transition. Interestingly, pRb activity is also necessary for late muscle development, promoting myofibrillogenesis and muscle cell growth by activating transcription of myogenic and metabolic genes.[44] Defects in this pathway could contribute to explaining the various myofibrillar defects in patients' biopsies. Further experiments are required to corroborate pRb abnormalities and to clarify the latter point.

Cyclin D3 is a critical regulator of the proliferation/differentiation balance of myogenic progenitors in skeletal muscle.[45,46] Under nonpathological conditions, this protein is not expressed in adult muscle fibers, as it is more important for the establishment than the maintenance of terminal myogenic differentiation.[47] Cyclin D3 increase in ASC-1–depleted patients' muscles suggests a dysregulation of its expression that could be attributed to inappropriate activation by MyoD or to improper stabilization by pRb.[45,46] Cyclin D3 is also involved in adipogenesis through its interaction with the nuclear receptor PPARγ.[48] This could be related to the subcutaneous adiposity observed in some patients. In addition, cyclin D1 represses PPARγ and inhibits adipocyte differentiation.[49] Drastically reduced cyclin D1 in postnatal patient muscles might contribute to this adipose phenotype via PPARγ derepression.

In conclusion, our work expands the clinical, histological, and molecular spectrum of ASC1-RM and contributes to disentangling its pathophysiological mechanisms. We propose that *TRIP4* mutations should be considered in any patient with histopathological CM lesions and a noncontractile myopathy, even in adult ambulant patients without clear neonatal signs, particularly if the phenotype includes respiratory insufficiency, joint hyperlaxity, skin abnormalities, or cardiomyopathy. Moreover, we reveal that ASC-1 plays a key role not only in late stages of myogenic differentiation and myotube growth[14] but also as a novel cell cycle regulator in several cell types, controlling cell proliferation via regulation of key cell cycle proteins. This work confirms transcriptional coregulation defects as an emerging mechanism in inherited neuromuscular disease. Based

on the identification of common histopathological lesions in *TRIP4*- and *ASCC1*-mutant patients, we propose the term "ASC-1–related myopathies" to include pathologies associated both with genes and with potential defects of any other protein of the ASC-1 complex, whose relevance in muscle and/or motoneuron pathophysiology is likely to increase in the future.

Acknowledgment

This work was funded by the French Association against Myopathies (20923 and 21267), National Institute of Health and Medical Research, National Center for Scientific Research and University of Paris). R.N.V.-Q. is the recipient of a research grant from the Alfonso Martín Escudero Foundation (Research Fellowship at Universities or Centers Abroad, Convocation 2017). M.O. is supported by the Carlos III Institute of Health through project PI14/00738 (cofunded by European Regional Development Fund). Whole exome sequencing and analysis of Family C were supported by National Institutes of Health (USA) grants UM1HG008900 from the National Human Genome Research Institute, R01HD075802 from the National Institute of Child Health and Human Development, and MDA602235 from the Muscular Dystrophy Association (USA). Sanger confirmation for family C was performed by the Molecular Genetics Core of the Boston Children's Hospital IDDRC funded by National Institutes of Health grant U54HD090255 from the National Institute of Child Health and Human Development.

We thank the patients and their families for their cooperation; Dr M. Iniesto for assistance in statistical analysis; and the ImagoSeine core facility (Mrs Magali Fradet) of the Jacques Monod Institute, which is a member of France BioImaging (ANR-10-INBS-04). Microscopy analyses were performed at the Imaging Plateau facility of the Functional and Adaptive Biology Unit, University of Paris/National Center for Scientific Research, Sorbonne Paris Cité, Paris, France. We thank MYOBANK-AFM (Institute of Myology, BB-0033-00012) and the DNA and Cell Bank (Genethon, Evry, France) for the disposal of biological samples and their contribution to human cell cultures, respectively.

Author Contributions

A.F., I.D.-G., and R.N.V.-Q. conceived and designed this study. Acquisition and analysis of data were performed by R.N.V.-Q., F.C., E.C., R.J.-M., C.A.G., T.G., A.K., A.Y., S.C., N.D., E.P.-H., J.R., N.B.R., A.H.B., L.S., M.C., M.O., X.L., J.L., J.D., J.B., I.D.-G., and A.F. The manuscript was drafted and the figures were prepared by R.N.V.-Q., I.D.-G., and A.F. All authors read and approved the final manuscript.

Potential Conflicts of Interest

Nothing to report.

References

1. North KN, Wang CH, Clarke N, et al. Approach to the diagnosis of congenital myopathies 2017;24:97–116.
2. Schorling D, Kirschner J, Bönnemann C. Congenital muscular dystrophies and myopathies: an overview and update. Neuropediatrics 2017;48:247–261.
3. Bönnemann CG, Wang CH, Quijano-Roy S, et al. Diagnostic approach to the congenital muscular dystrophies. Neuromuscul Disord 2014;24:289–311.
4. Jungbluth H, Ochala J, Treves S, Gautel M. Current and future therapeutic approaches to the congenital myopathies. Semin Cell Dev Biol 2017;64:191–200.
5. Kaplan J-C, Hamroun D. The 2016 version of the gene table of monogenic neuromuscular disorders (nuclear genome). Neuromuscul Disord 2015;25:991–1020.
6. Ravenscroft G, Laing NG, Bönnemann CG. Pathophysiological concepts in the congenital myopathies: blurring the boundaries, sharpening the focus. Brain 2015;138(pt 2):246–268.
7. Treves S, Jungbluth H, Voermans N, et al. Ca 2+ handling abnormalities in early-onset muscle diseases: novel concepts and perspectives. Semin Cell Dev Biol 2017;64:201–212.
8. Horstick EJ, Linsley JW, Dowling JJ, et al. Stac3 is a component of the excitation–contraction coupling machinery and mutated in Native American myopathy. Nat Commun 2013;4:1952.
9. Dowling JJ, Lawlor MW, Dirksen RT. Triadopathies: an emerging class of skeletal muscle diseases. Neurotherapeutics 2014;11: 773–785.
10. Jungbluth H, Gautel M. Pathogenic mechanisms in centronuclear myopathies. Front Aging Neurosci 2014;6:339.
11. Wallgren-Pettersson C, Sewry CA, Nowak KJ, Laing NG. Nemaline myopathies. Semin Pediatr Neurol 2011;18:230–238.
12. Tajsharghi H, Oldfors A. Myosinopathies: pathology and mechanisms. Acta Neuropathol 2013;125:3–18.
13. Jungbluth H, Treves S, Zorzato F, et al. Congenital myopathies: disorders of excitation–contraction coupling and muscle contraction Nat Rev Neurol 2018;14:151.
14. Davignon L, Chauveau C, Julien C, et al. The transcription coactivator ASC-1 is a regulator of skeletal myogenesis, and its deficiency causes a novel form of congenital muscle disease. Hum Mol Genet 2016;25:1559–1573.
15. Knierim E, Hirata H, Wolf NI, et al. Mutations in subunits of the activating signal cointegrator 1 complex are associated with prenatal spinal muscular atrophy and congenital bone fractures. Am J Hum Genet 2016;98:473–489.
16. Oliveira J, Martins M, Pinto Leite R, et al. The new neuromuscular disease related with defects in the ASC-1 complex: report of a second case confirms ASCC1 involvement. Clin Genet 2017;92: 434–439.
17. Böhm J, Malfatti E, Oates E, et al. Novel *ASCC1* mutations causing prenatal-onset muscle weakness with arthrogryposis and congenital bone fractures. J Med Genet 2019;56:617–621.
18. Dasgupta S, Lonard DM, O'Malley BW. Nuclear receptor coactivators: master regulators of human health and disease. Annu Rev Med 2014;65:279–292.

19. Jung D-J, Sung H-S, Goo Y-W, et al. Novel transcription coactivator complex containing activating signal cointegrator 1. Mol Cell Biol 2002;22:5203–5211.

20. Kim HJ, Yi JY, Sung HS, et al. Activating signal cointegrator 1, a novel transcription coactivator of nuclear receptors, and its cytosolic localization under conditions of serum deprivation. Mol Cell Biol 1999;19:6323–6332.

21. Auboeuf D, Hönig A, Berget SM, O'Malley BW. Coordinate regulation of transcription and splicing by steroid receptor coregulators. Science 2002;298:416–419.

22. Iyer LM, Burroughs AM, Aravind L. The ASCH superfamily: novel domains with a fold related to the PUA domain and a potential role in RNA metabolism. Bioinformatics 2006;22:257–263.

23. Chi B, O'Connell JD, Iocolano AD, et al. The neurodegenerative diseases ALS and SMA are linked at the molecular level via the ASC-1 complex. Nucleic Acids Res 2018;46:11939–11951.

24. Ferreiro A, Quijano-Roy S, Pichereau C, et al. Mutations of the selenoprotein N gene, which is implicated in rigid spine muscular dystrophy, cause the classical phenotype of multiminicore disease: reassessing the nosology of early-onset myopathies. Am J Hum Genet 2002;71:739–749.

25. Scoto M, Cirak S, Mein R, et al. SEPN1-related myopathies: clinical course in a large cohort of patients. Neurology 2011;76:2073–2078.

26. Ware JS, Cook SA. Role of titin in cardiomyopathy: from DNA variants to patient stratification. Nat Rev Cardiol 2017;15:241–252.

27. Franaszczyk M, Chmielewski P, Truszkowska G, et al. Titin truncating variants in dilated cardiomyopathy—prevalence and genotype-phenotype correlations. PLoS One 2017;12:e0169007.

28. Schafer S, de Marvao A, Adami E, et al. Titin-truncating variants affect heart function in disease cohorts and the general population. Nat Genet 2017;49:46–53.

29. Savarese M, Maggi L, Vihola A, et al. Interpreting genetic variants in titin in patients with muscle disorders. JAMA Neurol 2018;75:557.

30. Chauveau C, Rowell J, Ferreiro A. A rising titan: TTN review and mutation update. Hum Mutat 2014;35:1046–1059.

31. Oates EC, Jones KJ, Donkervoort S, et al. Congenital titinopathy: comprehensive characterization and pathogenic insights. Ann Neurol 2018;83:1105–1124.

32. Bönnemann CG. The collagen VI-related myopathies: muscle meets its matrix. Nat Rev Neurol 2011;7:379–390.

33. Bönnemann CG. The collagen VI-related myopathies. Handb Clin Neurol 2011;101:81–96.

34. Mercuri E, Lampe A, Allsop J, et al. Muscle MRI in Ullrich congenital muscular dystrophy and Bethlem myopathy. Neuromuscul Disord 2005;15:303–310.

35. Hankiewicz K, Carlier RY, Lazaro L, et al. Whole-body muscle magnetic resonance imaging in SEPN1-related myopathy shows a homogeneous and recognizable pattern. Muscle Nerve 2015;52:728–735.

36. Jungbluth H, Davis MR, Müller C, et al. Magnetic resonance imaging of muscle in congenital myopathies associated with RYR1 mutations. Neuromuscul Disord 2004;14:785–790.

37. Carlier R-Y, Quijano-Roy S. Myoimaging in congenital myopathies. Semin Pediatr Neurol 2019;29:30–43.

38. Jiang W, Kahn SM, Zhou P, et al. Overexpression of cyclin D1 in rat fibroblasts causes abnormalities in growth control, cell cycle progression and gene expression. Oncogene 1993;8:3447–3457.

39. Cadart C, Monnier S, Grilli J, et al. Size control in mammalian cells involves modulation of both growth rate and cell cycle duration. Nat Commun 2018;9:3275.

40. Buttitta LA, Edgar BA. Mechanisms controlling cell cycle exit upon terminal differentiation. Curr Opin Cell Biol 2007;19:697–704.

41. LaBaer J, Garrett MD, Stevenson LF, et al. New functional activities for the p21 family of CDK inhibitors. Genes Dev 1997;11:847–862.

42. Ezhevsky SA, Ho A, Becker-Hapak M, et al. Differential regulation of retinoblastoma tumor suppressor protein by G(1) cyclin-dependent kinase complexes in vivo. Mol Cell Biol 2001;21:4773–4784.

43. Leshem Y, Halevy O. Phosphorylation of pRb is required for HGF-induced muscle cell proliferation and is p27kip1-dependent. J Cell Physiol 2002;191:173–182.

44. Zappia MP, Rogers A, Islam ABMMK, Frolov MV. Rbf activates the myogenic transcriptional program to promote skeletal muscle differentiation. Cell Rep 2019;26:702–719.e6.

45. Cenciarelli C, De Santa F, Puri PL, et al. Critical role played by cyclin D3 in the MyoD-mediated arrest of cell cycle during myoblast differentiation. Mol Cell Biol 1999;19:5203–5217.

46. De Santa F, Albini S, Mezzaroma E, et al. pRb-dependent cyclin D3 protein stabilization is required for myogenic differentiation. Mol Cell Biol 2007;27:7248–7265.

47. Bartkova J, Lukas J, Strauss M, Bartek J. Cyclin D3: requirement for G1/S transition and high abundance in quiescent tissues suggest a dual role in proliferation and differentiation. Oncogene 1998;17:1027–1037.

48. Sarruf DA, Iankova I, Abella A, et al. Cyclin D3 promotes adipogenesis through activation of peroxisome proliferator-activated receptor gamma. Mol Cell Biol 2005;25:9985–9995.

49. Fu M, Rao M, Bouras T, et al. Cyclin D1 inhibits peroxisome proliferator-activated receptor γ-mediated adipogenesis through histone deacetylase recruitment. J Biol Chem 2005;280:16934–16941.

The clinical, histological, and genotypic spectrum of SEPN1-related myopathy: A large case series

Rocio N Villar-Quiles, MD; Maja von der Hagen, MD, PhD; Corinne Métay, MD; Victoria Gonzalez, MD, PhD; Sandra Donkervoort, MD; Enrico Bertini, MD; Claudia Castiglioni, MD; Denys Chaigne, MD; Jaume Colomer, MD, PhD; Maria Luz Cuadrado, MD, PhD; Marianne de Visser, MD, PhD; Isabelle Desguerre, MD; Bruno Eymard, MD, PhD; Nathalie Goemans, MD, PhD; Angela Kaindl, MD, PhD; Emmanuelle Lagrue, MD, PhD; Jürg Lütschg, MD; Edoardo Malfatti, MD, PhD; Michèle Mayer, MD; Luciano Merlini, MD; David Orlikowski, MD, PhD; Ulrike Reuner, MD; Mustafa A Salih, MD; Beate Schlotter-Weigel, MD; Mechthild Stoetter, MD; Volker Straub, MD, PhD; Haluk Topaloglu, MD; J. Andoni Urtizberea, MD; Anneke van der Kooi, MD, PhD; Eckhart Wilichowski, MD; Norma B Romero, MD, PhD; Michel Fardeau, MD, PhD; Carsten G Bönnemann, MD, PhD; Brigitte Estournet, MD, PhD; Pascale Richard, MD, PhD; Susana Quijano-Roy, MD, PhD; Ulrike Schara, MD; Ana Ferreiro, MD, PhD.

Rocio N Villar-Quiles, Basic and Translational Myology Lab, UMR8251, Université de Paris/CNRS, Paris, France; Centre de référence des maladies neuromusculaires Nord-Est-Ile de France, Institut de Myologie, Pitié-Salpêtrière Hospital, AP-HP, Paris, France

Maja von der Hagen, Department of Paediatric Neurology, Medinzinische Fakultät Carl Gustav Carus, Technische Universität Dresden, Dresden, Germany

Corinne Métay, AP-HP, Centre de Génétique Moléculaire et Chromosomique, UF Cardiogénétique et Myogénétique Moléculaire et Cellulaire, GH Pitié-Salpêtrière, Paris, France

Victoria Gonzalez, Basic and Translational Myology Lab, UMR8251, Université de Paris/CNRS, Paris, France; Department of Neurology, University Hospital of Montpellier, France

Sandra Donkervoort, Neuromuscular and Neurogenetic Disorders of Childhood Section, National Institute of Neurological Disorders and Stroke, National Institutes of Health, Bethesda, MD, 20814, USA

Enrico Bertini, Unit of Neuromuscular and Neurodegenerative Disorders, Bambino Gesu' Children's Research Hospital, Rome, Italy

Claudia Castiglioni, Departamento de Neurología Pediátrica, Clínica Las Condes, Santiago, Chile

Denys Chaigne, Paediatrics Department, Hôpital de Hautepierre, Strasbourg, France

Jaume Colomer, Neuromuscular Unit, Neuropaediatrics Department, Institut de Recerca Hospital Universitari Sant Joan de Deu, Barcelona, Spain; Center for the Biomedical Research on Rare Diseases (CIBERER), ISCIII, Spain

Maria Luz Cuadrado, Department of Neurology, Hospital Clínico San Carlos, Instituto de Investigación Sanitaria San Carlos, Madrid, Spain. Department of Medicine, Universidad Complutense de Madrid, Madrid, Spain

Marianne de Visser, Department of Neurology, Amsterdam University Medical Centre, Amsterdam Neuroscience, Amsterdam, The Netherlands.

Isabelle Desguerre, Department of Pediatric Neurology, Necker Enfants Malades Hospital, Paris Descartes University, Paris, France.

Bruno Eymard, Centre de référence des maladies neuromusculaires Nord-Est-Ile de France, Institut de Myologie, Pitié-Salpêtrière Hospital, AP-HP, Paris, France

Nathalie Goemans, Department of Child Neurology, University Hospitals Leuven, Leuven, Belgium

Angela Kaindl, Department of Pediatric Neurology, Center for Chronically Sick Children, Institute of Cell Biology and Neurobiology, Charité - Universitätsmedizin Berlin, Berlin, Germany

Emmanuelle Lagrue, Department of Neuropediatrics, CHRU de Tours, Université François Rabelais de Tours, UMR INSERM U1253, Tours, France

Jürg Lütschg, Department of Neuropediatrics, University children`s hospital of Basel (UKBB), Basel, Switzerland

Edoardo Malfatti, Centre de référence des maladies neuromusculaires Nord/Est/Ile-de-France, Neurology Department, Raymond-Poincaré hospital, AP-HP, Garches, France

Michèle Mayer, Centre de Référence des maladies neuromusculaires Nord/Est/Ile de France, Service de neuropédiatrie, Hôpital Trousseau, Paris, France

Luciano Merlini, Department of Biomedical and Neuromotor Sciences, University of Bologna, Italy

David Orlikowski, Réanimation Médicale, Physiologie- Explorations Fonctionnelles, et Centre d'Investigation Clinique, UMR 1429, Hôpital Raymond Poincaré, Garches, France; INSERM-UMR, 1179, UVSQ, Hôpital Raymond Poincaré, Garches, France

Ulrike Reuner, Department of Neurology, Medizinische Fakultät Carl Gustav Carus Technische Universität Dresden, Dresden, German

Mustafa A Salih, Division of Pediatric Neurology, Department of Pediatrics, College of Medicine, King Saud University, Riyadh, Saudi Arabia

Beate Schlotter-Weigel, FriedrichBaur-Institut, Department of Neurology Ludwig-Maximilians-University of Munich, Germany

Mechthild Stoetter, Department of Pediatric Neurology, University of Tübingen, Germany

Volker Straub, The John Walton Muscular Dystrophy Research Centre, Institute of Genetic Medicine, Newcastle University, Newcastle Hospitals NHS Foundation Trust, United Kingdom

Haluk Topaloglu, Hacettepe University, School of Medicine, Department of Child Neurology, Ankara, Turkey

J. Andoni Urtizberea, Hôpital Marin, Centre de Compétence Neuromusculaire, Hendaye, France

Anneke van der Kooi, Department of Neurology, Amsterdam UMC, University of Amsterdam, Amsterdam Neuroscience, Netherlands

Eckhart Wilichowski, Department of Pediatric Neurology, Georg-August University Goettingen, Germany

Norma B Romero, Centre de référence des maladies neuromusculaires Nord-Est-Ile de France, Institut de Myologie, Pitié-Salpêtrière Hospital, AP-HP, Paris, France, Neuromuscular Morphology Unit, Myology Institute, Pitié-Salpêtrière Hospital, Paris, France

Michel Fardeau, Neuromuscular Morphology Unit, Myology Institute, Pitié-Salpêtrière Hospital, Paris, France

Carsten G Bönnemann, Neuromuscular and Neurogenetic Disorders of Childhood Section, National Institute of Neurological Disorders and Stroke, National Institutes of Health, Bethesda, MD, 20814, USA

Brigitte Estournet, Neuromuscular Unit, Department of Pediatric Neurology, Intensive Care and Rehabilitation, Raymond Poincaré University Hospital, AP-HP, UVSQ Paris Saclay, Garches, France

Pascale Richard, AP-HP, Centre de Génétique Moléculaire et Chromosomique, UF Cardiogénétique et Myogénétique Moléculaire et Cellulaire, GH Pitié-Salpêtrière, Paris, France

Susana Quijano-Roy, Neuromuscular Unit, Department of Pediatric Neurology, Intensive Care and Rehabilitation, Raymond Poincaré University Hospital, AP-HP, UVSQ Paris Saclay, Garches, France

Ulrike Schara, Department of Pediatric Neurology, Developmental Neurology and Social Pediatrics, University of Essen, Germany

Ana Ferreiro, Basic and Translational Myology Lab, UMR8251, Université de Paris/CNRS, Paris, France; Centre de référence des maladies neuromusculaires Nord-Est-Ile de France, Institut de Myologie, Pitié-Salpêtrière Hospital, AP-HP, Paris, France

Corresponding Author:

Ana Ferreiro

35, rue Hélène Brion; Unité de Biologie Fonctionnelle et Adaptative (BFA) CNRS UMR 8251; Université Paris Diderot/Université de Paris Bâtiment Lamark

75205 Paris cedex 13

Phone: + 33 1 57277959, Fax + 33 1 57277953

ana.b.ferreiro@gmail.com

Statistical Analysis was conducted by Dr. Rocio N Villar-Quiles, MD, Basic and Translational Myology Laboratory, Paris

Study Funded by the Institut National de la Santé et la Recherche Médicale (Inserm), the Centre National de la Recherche Scientifique (CNRS), Université de Paris (France) and the German Research Foundation (DFG, SFB1315, FOR3004), the Charité–Universitätsmedizin Berlin (Germany). R.N.V.Q. is the recipient of a research grant from the Alfonso Martín Escudero Foundation (Beca de investigación en universidades o centros en el extranjero, Convocatoria 2017). M. A. S. is supported by Researchers Supporting Project number (RSP-2019/38), King Saud University, Riyadh, Saudi Arabia. The work in C.G. Bönnemann's laboratory is supported by intramural funds from the NIH National Institute of Neurological Disorders and Stroke.

ABSTRACT

Objective: To clarify the prevalence, long-term natural history and severity determinants of SEPN1-related myopathy (SEPN1-RM), we analyzed a large international case series.

Methods: Retrospective clinical, histological and genetic analysis of 132 pediatric and adult patients (2-58 years) followed-up for several decades.

Results: The clinical phenotype was marked by severe axial muscle weakness, spinal rigidity and scoliosis (86.1%, from 8.9±4 years), with relatively-preserved limb strength and previously-unreported ophthalmoparesia in severe cases. All patients developed respiratory failure (from 10.1±6 years), 81.7% requiring ventilation while ambulant. Histopathologically, 79 muscle biopsies showed large variability, partly determined by site of biopsy and age. Multi-minicores were the most common lesion (59.5%), often associated with mild dystrophic features and occasionally with eosinophilic inclusions. Identification of 65 SEPN1 mutations, including 32 novel ones and the first pathogenic CNV, unveiled exon 1 as the main mutational hotspot and revealed the first genotype-phenotype correlations, bi-allelic null mutations being significantly associated with disease severity (p=0.017). SEPN1-RM was more severe and progressive than previously thought, leading to loss of ambulation in 10% cases, systematic functional decline from the end of the third decade and reduced lifespan even in mild cases. The main prognosis determinants were scoliosis/respiratory management, *SEPN1* mutations and body mass abnormalities which correlated with disease severity. Finally, we propose a set of severity criteria, provide quantitative data for outcome identification and establish a need for age stratification.

Conclusion: Our results inform clinical practice, improving diagnosis and management, and represent a major breakthrough for clinical trial readiness in this not-so-rare disease.

Introduction

While recent progress is bringing congenital myopathies to the clinical trial stage, for the forms associated with mutations in the Selenoprotein N gene (*SEPN1 or SELENON*, MIM*606210) clinical trial readiness is lagging behind. *SEPN1* mutations were first associated with rigid spine muscular dystrophy (RSMD1)[1–3] and shortly after with multi-minicore disease[4], congenital fiber type disproportion[5] and desmin-related myopathy with Mallory body-like inclusions[6–9] These four autosomal recessive conditions share so many clinical and molecular features that they are considered the same disorder, which we termed SEPN1-related myopathy (SEPN1-RM)[4].

Selenoprotein N, is an endoplasmic reticulum (ER) glycoprotein containing an EF-hand motif and a predicted catalyric site with putative reductase activity. SEPN1 plays a key role in redox-based calcium homeostasis[10,11] and cell protection against oxidative and ER stress[10,12–14]. These pathways are drug-targetable, and some compounds effectively rescue the SELENON-devoid cell phenotype *ex vivo*[12]. However, SEPN1-RM clinical trial readiness is hindered by the lack of validated biomarkers, the scarcity of quantitative data on its phenotypical spectrum, long-term natural history[4,7,9], disease progression or prognosis determinants. SEPN1-RM is considered to be very slowly progressive, but the impact of age has never been analyzed, and phenotype-genotype correlations are unclear. Finally, while SEPN1-RM is considered an ultra-rare disease, its prevalence is unknown. This global situation complicates patient diagnosis and management and hampers clinical trial implementation.

We report here the largest international SEPN1-RM series, thus informing diagnosis and management and paving the way for clinical trial readiness.

Methods

Patients

We included 132 patients with *SEPN1* mutations identified between 2001 and 2017. Thirty-one were previously reported[3,4,6,9].

Clinical data were analyzed retrospectively according to a standardized form completed by the referent clinicians, except 31 cases from whom only genetic information was available. The frequency of each finding was calculated over the number of patients from whom this data was available.

Standard blood test results were collected from 76 patients, and in 6 serum selenium levels, serum and erythrocyte glutathione peroxidase, lactate, pyruvate, thyroid hormones and carnitine were quantified. Electromyography and brain MRI/CT scan were performed in 24 and 27 patients respectively. Muscle MRIs in 5 patients were reported previously[15].

Skeletal muscle biopsy

We reviewed 79 muscle biopsies (light and electron microscopy) and/or histopathological reports. Muscle biopsy site, known in 43 patients (45 biopsies), was deltoid (n= 22, 48.9%), quadriceps (n=17, 37.8%), biceps brachialis (n=2, 4.3%), gastrocnemius (n=2, 4.3%) or abdominal muscles (n=2, 4.3%).

Genotyping

SEPN1/SELENON was analyzed on genomic DNA from peripheral blood using Sanger sequencing[4] or Next Generation Sequencing-based gene panels [NGS][16]. Variants were reported according to Human Genome Variation Society recommendations (http://varnomen.hgvs.org/) using the complete *SEPN1/SELENON* transcript (NM_020451.2; NP_065184.2). Genome Aggregation

(http://gnomad.broadinstitute.org/) and Clinvar (http://www.ncbi.nlm.nih.gov/clinvar/) databases were interrogated to identify previously-reported mutations and to determine variant frequency in the population. Alamut-Batch-UI v1.11® (Interactive Biosoftware, North Seattle, WA) was used to predict variant impact.

Statistical analysis

Data were analyzed with the SPSS® Statistics version 22.0 (Armonk, NY: IBM Corp.). Results are expressed as mean ± standard deviation. Groups were compared using the Welch's t-test or Mann-Whitney-Wilcoxon test for continuous variables, and Pearson $\chi 2$ test for categorical variables, as appropriate. A 2-sided p value ≤ 0.05 was considered statistically. Kaplan-Meier was used to analyze ventilation-free probability.

Standard Protocol Approvals, Registrations, and Patient Consents

Written informed consent according to local ethical committees in all participating centers was obtained for all patients. Clinical and genetic data were anonymized and entered into a secured database accessible only to the first and last authors.

Data availability

The anonymized raw data supporting our findings are available upon request.

Results

The disease affected similarly females (50.8%) and males (49.2%). Patients were aged 2-58 years at last examination (mean 18.2±11.8 years). Follow-up ranged from 8 months to 25 years.

Consanguinity was confirmed in 30 families and probable in three. Fourteen families reported early deaths of 18 genetically-undiagnosed members (not included) at ages 4-19 years, mainly due to untreated respiratory failure and/or during their sleep. Eight of them showed axial weakness and progressive scoliosis or rigid spine, four had clinical myopathic signs and one had a dystrophic muscle biopsy.

Clinical phenotype

Clinical features are summarized in Table 1.

Onset and first signs: an infantile myopathy, often under-recognized

First signs were noticed before the age of 15 years in all patients, and within the first two years in 84.7% (mean 18.2± 29.8 months).

Delayed motor development was the most common presenting sign (81.4%). Poor head control, the referral abnormality in 57.7% patients was almost systematically retrieved by parents when retrospectively asked. Independent ambulation was acquired by all but one severely affected patient, often (59.3%) before 18 months (mean 17.6± 4.9 months).

Pregnancy information was retrieved in 29 patients. Most were normal, with exceptional pre-term deliveries (n=2), reduced foetal movements (n=3) or intrauterine growth retardation (n=2). Neonatal hypotonia was reported in one third of cases. Other early signs were feeding difficulties and/or failure to thrive (17.5%) and respiratory problems (7.2%). Four patients presented with early-onset scoliosis, hyperlordosis or rigid spine and 16 were referred for unspecified muscular weakness and hypotonia sometimes

associated with abnormal gait, inability to run, difficulty climbing stairs or frequent falls. Arthrogryposis or congenital contractures were absent, excepting congenital torticollis in one patient.

One patient was diagnosed at 31 years, when prolonged bed rest after a stroke (carotid dissection) caused hypercapnic coma, revealing chronic diaphragmatic and respiratory failure. Retrospectively, she reported mild axial and proximal weakness from early childhood.

The axial connection: a recognizable, homogeneous phenotype

All patients shared a remarkably consistent and recognizable phenotype (Fig.1).

In the first decade, patients showed a particular facial appearance, long slender neck, flat retracted thorax, spinal rigidity and axial weakness but preserved ambulation. Most had poor head control, were never able to lift their head from supine, and had to sit up from supine by rolling over and pushing on their arms. However, they were typically able to climb stairs and walk outdoors unsupported, limited mainly by fatigue. Sports performance was usually poor, cervical rigidity preventing some patients from rolling forward.

Amyotrophy involved preferentially neck and trunk muscles (particularly sternocleidomastoid), deltoid, the inner thigh compartment (‘bracket-like thighs’) and distal forearm and leg muscles. Typical facies (Fig.1) was associated with mild to moderate facial weakness, high-arched palate and nasal high-pitched voice. Muscle weakness was severe in neck flexors and in abdominal muscles (0-3, MRC scale), with relatively well-preserved neck extensors. Limb weakness was usually milder and predominantly proximal (MRC 3-4 in scapular girdle, 2-3 in psoas, glutei and adductor muscles). Quadriceps strength was often normal or mildly reduced (MRC 4-5) and

distal weakness was present in the most severe cases. Deep tendon reflexes were invariably diminished or absent.

Rigid spine was present in 87.8%, generally before the age of 10 years (mean 8.1±3.9 years) and reported as early as in the first year. Severe contractures of neck extensors and dorsal paraspinal muscles caused cervico-dorsal rigidity, bending forward remaining possible due to relative preservation of lumbar spine mobility. Loss of dorsal kyphosis and/or dorsal lordosis caused reduced antero-posterior thorax diameter. Pectoralis major and intercostal muscle retractions contributed to thoracic deformities and poor mobility.

The full phenotype usually manifested around puberty, with the development of scoliosis, the detection of respiratory failure, a further drop in weight curves and, in some cases, limb contractures, although all the former appeared earlier in severe cases (Fig.2).

Scoliosis appeared at the mean age of 8.9±4.0 years (10.4 ±3.6 in boys, 7.9±3.9 in girls), was present in 86.1% and in 93.8% of those aged more than 13 years. SEPN1-RM scoliosis is peculiar and recognizable because of dorsal hyperlordosis (leading to scapular pseudo-winging) and important lateral trunk shift contrasting with balanced hips (Fig.1C). Adapted bracing helped delaying surgery until the end of puberty, but did not prevent scoliosis progression. Arthrodesis was performed in 32 post-pubertal patients at ages 10-17 years (mean 13.5±1.9 years). Scoliosis usually remained clinically and radiologically stable after extensive spinal fusion.

Although birth weight was often normal, typically body weight decreased drastically around puberty, leading to loss of subcutaneous adipose tissue and a cachexia-like appearance (Figs.1, 2). Most (72.7%) patients were under the 4th weight percentile, and the mean BMI in adults was 16.9±4.0 (women 16.5±4.3, men 17.4±3.6). Two patients

were overweight and two were obese since childhood; these four patients had severe forms of the disease, with major respiratory failure and early loss of ambulation.

Limb joint contractures, usually mild in children, were reported in 64.4% cases, involving the Achilles tendon (57.4%), hip flexors (50%), elbows (35.2%) or knees (31.5%). Only 9 children showed a more contractile phenotype with severe axial and limb contractures. Finger flexor contractures upon wrist extension or, less often, limitation of mouth opening appeared with age. Distal hyperlaxity was reported in 21 patients and associated with joint contractures in 16 (Fig.3).

Mild limitation of superior vertical eye movements was not uncommon when specifically examined. We identified previously-unreported clear ophthalmoparesis in three severely-affected patients. Oculomotor abnormalities became more obvious with age. Strabismus and mild ptosis were observed in four and six patients, respectively.

Respiratory involvement

Respiratory involvement was strikingly disproportionate to limb weakness, most patients requiring assisted ventilation while ambulant. Both weakness of the respiratory and accessory respiratory muscles and thoracic deformities contributed to respiratory failure. Dorsal spine lordosis and rigidity led to severely reduced thorax anteroposterior diameter, bronchial compression and/or subsequent atelectasis.

Restrictive, hypoxemic and hypercapnic respiratory failure was present in 93% cases (from 10.06±6.10 years). FVC was in most patients between 20-40% of predicted values (36.47±12.31) at last survey (Fig. 4). Diaphragmatic weakness (>10% FVC decrease in supine from baseline sitting position) was reported in 30 patients. Polysomnography detected nocturnal hypoventilation (92.9%) from early ages, even in patients with relatively preserved FVC and no daytime respiratory signs. The three

youngest patients studied had polysomnographic values within normal range at four years but abnormalities requiring ventilation at 5.5 years.

81.9% cases had assisted ventilation, from the mean age of 14.14±7.89 years (3-49 years). Most required nocturnal non-invasive ventilation; 12 had a tracheotomy.

Compressive bracing led to hypercapnic coma in one patient. Four patients developed cor pulmonale and one had isolated increase of right ventricular systolic pressure secondary to respiratory failure. All improved with instauration or adjustment of assisted ventilation.

Other features

One patient with idiopathic cardiomyopathy family history developed dilated cardiomyopathy at 42 years. Fifteen patients developed swallowing difficulties. Gastrointestinal involvement, genitourinary disorders or nonspecific skin abnormalities were reported in a minority of patients. One patient had a cerebral venous thrombosis at age 38. No patient had intellectual disability or CNS involvement.

Ancillary tests

CK levels were normal or mildly elevated (34-453 UI/L, 5 cases≥ 3xN). Two patients had normal in-vitro contracture tests for malignant hyperthermia (MH) susceptibility and none had history of MH. Electromyography disclosed small amplitude, brief, polyphasic action potentials and normal nerve conduction. Brain MRI or CT were normal aside from arachnoid cysts (n=2) or Chiari malformation type 1 (n=1).

A previous review of whole-body MRI, including five patients from this series, revealed a homogeneous and recognizable SEPN1-RM pattern, the most striking feature being the absence or severe atrophy of the semimembranosus muscle[15].

Histopathological phenotype

Multi-minicores were the most recurrent pathologic feature, present in 59.5% biopsies and representing the main lesion in 49.4%, often associated with fiber size variation, type I fiber predominance and relative hypotrophy, internalized nuclei and mild dystrophic features, notably mild increase in endomysial connective tissue (Fig. 5). In 6.3%, minicores were associated with eosinophilic inclusions compatible with Mallory-like bodies, exclusively found in quadriceps. Prominent dystrophic signs were present in 24.1%, either isolated or associated with minicores or 'unspecific changes of internal structure' on oxidative stainings. 25.3% biopsies disclosed non-specific myopathic findings, mainly fiber size variation, type I fiber predominance or internalized nuclei. Rare rimmed vacuoles were found in two patients. Interestingly, patients having non-specific biopsy abnormalities were younger than patients having more specific lesions (8.55±5.3 vs 13.89±11.7 years, 95% Confidence Interval (CI) 1.2-9.5, p= 0.012)

In two patients with biopsies from axial and limb muscles, axial muscles were more severely dystrophic and/or showed larger core lesions than limb muscles, consistently with clinical weakness distribution.

Long-term course and determinants of severity

Excepting one patient who died at 3 years, all acquired independent ambulation and improved motor performance during childhood. After implementation of efficient ventilation and arthrodesis in their teens, most patients remained stable from more than one decade. However, disease progressed steadily from the beginning of the fourth decade of life (Fig.2). Loss of ambulation occurred in 8 patients at ages 8-54 years (median 21.5, IQR 19.75), representing 10% cases for whom follow-up information was available.

Scoliosis and restrictive respiratory failure were often diagnosed simultaneously around the end of the first decade. FVC was <39% in most patients and tended to decrease with age (Fig.4A,C). Analysis of a thoroughly-documented subgroup of 11 patients demonstrated that scoliosis management had a major respiratory impact: spinal fusion led to a dramatic FVC drop in the immediate post-operatory period, with return to preoperative or better values within six months in patients with intensive and regular postsurgical ventilation (Fig.4F). Independently of interventions, we observed marked intra-individual variability in FVC values, with major fluctuations possibly due to fatigue and/or intercurrent infections (Fig.4E).

The main predictive factor of vital prognosis was respiratory failure, 50% of patients needeeding assisted ventilation within the first 13 years (Fig.4D). Six patients deceased at ages 3, 5, 16, 58 and 59, due to respiratory failure (n=2), sudden death (n=2), choking (n=1), or uncharacterized deterioration in a terminal patient (n=1).

To assess potential disease progression determinants, we established the following arbitrary severity criteria: 1) prominent neonatal hypotonia and/or persistent lack of head control; 2) scoliosis and/or respiratory failure before age 10 years; 3) progressive motor disability causing loss of ambulation before adulthood. We identified three phenotypical groups (n=81): ‘severe’ (n=23, 28.4%) when patients presented two or more criteria, ‘moderate’ (n=43, 53.1%) if only one criterion was present and ‘mild’ (n=15, 18.5%) if none was fulfilled.

Mild/moderate patients corresponded to the previously-described classical form of the disease. In severe patients, earlier scoliosis and respiratory failure required assisted ventilation since early childhood. A subgroup of patients with a very severe phenotype showed ophthalmoplegia, rapidly progressive muscular weakness and respiratory failure, loss of ambulation before adulthood and severe tetraparesis in the third decade

of life. Strikingly, these very severe patients showed from childhood subcutaneous adiposity with predominant abdominal distribution. Conversely, most patients with good motor abilities were extremely underweight. In 47 patients with anthropometrical data, we found a significant correlation between body weight and disease severity (p=0.002). Weight gain often led to complaints of poorer functional performance and increased fatigue.

Aging was associated with significant progression even in mild/moderate patients. This series includes nine patients aged ≥ 35 years (35-58 years at last examination). Slow but steady increase of muscle weakness and fatigue from the fourth decade led to reduced gait perimeter and motor performances of upper and lower limbs (Fig. 3). Three mild patients lost ambulation at ages 33, 38 and 54 years; others required a wheelchair for long distances. Swallowing difficulties were not uncommon in older patients and choking caused death in a 59 year-old patient. Another mild patient developed severe tetraparesis, required PEG and ventilation more than 15 hours/day and died at 58 years due to general deterioration. The eldest patient is currently aged 55 years, remains ambulant and leads an active professional life with night-time ventilation, despite aggravation of his difficulties for climbing stairs or getting up from sitting from the end of the third decade. FVC in this age group was severely reduced but remained stable. However, increasing diaphragmatic fatigue led to major orthopnea over the years.

Five adult patients carried pregnancies to term and gave birth by cesarean section. One reported worsening of motor abilities post-pregnancy and another suffered eclampsia with acute pulmonary edema requiring a transient tracheostomy.

Clinical genetics

Transmission was autosomal recessive, without *de novo* mutations, all tested parents being healthy heterozygous carriers. Seventy-two patients were homozygous, and 59 compound heterozygous.

We found 65 variants (32 unreported) of the *SEPN1/SELENON* Reference Coding Sequence (RCS) (Fig.6 and Supplementary Table 1), including missense (n=23, 35.4%), duplications/insertions (n=14, 21.5%), deletions (n=13, 20%) and nonsense mutations (n=8, 12.3%); 29 variants predictedly produced truncated proteins (11 prone to nonsense-mediated decay (NMD)). Four variants leading to loss of the start codon, with subsequent translation and protein absence, were harbored by 29 patients (10 of them complete null). We also report the first *SEPN1* Copy Number Variation (CNV) (c.(872+1_873-1)(1602+1_1603-1)del), a large likely out-of-frame deletion affecting exons 7 to 12.

We found six intronic splicing variants and one homozygous single-point mutation in the *SEPN1* 3′ UTR SECIS (SElenoCystein Insertion Sequence), an untranslated *cis* element necessary for selenocysteine integration. This modification abolishes the binding of SBP2, a central component of the selenocysteine insertion machinery, preventing UGA redefinition and leading to a premature stop codon[17,18].

We observed clustering of mutations in exons 1, 6, 7 and 11 and no mutations in exon 3, spliced in the predominant human transcript[19]. The GC-rich exon 1, a remarkable hotspot, was the most frequently mutated (39.7% patients) and harbored the highest number of variants (28% mutations). The most common variant, identified in 15 families of different origins, was a mutation of the starting codon (c.1A>G) which changes the initiator methionine codon to a valine codon, causing total loss of

translation. We identified founder effects for the mutations c.817G>A (Iran and Turkey), c.943G>A (Northern Europe) and c.713dupA (Western Europe).

Genotype-phenotype correlations

Phenotype–genotype correlations, difficult to establish in a very rare disease due to low numbers of patients carrying the same mutation, were unknown for SEPN1-RM. This series revealed the first correlations between genetic defects and clinical severity, with no correlation between genotype and histopathological findings.

Some exon 1 variants (c.1A>G, c.13_22dup and c.-19_73del92nt) and the exon 6 c.818G>A mutation were most commonly found in patients with a severe phenotype, while other variants such as c.943G>A (exon7), c.1315C>T (exon 10) or c.1446delC (exon 11) were often found in milder cases.

Exon 1 homozygous mutations predicting total loss of translation (c.-19_73del92nt and c.1A>G), carried by the most severe patients in this series, were significantly associated with disease severity (p=0.003). Moreover, homozygous or compound heterozygous patients carrying two variants located in any exon but predicting protein absence (by either loss of the start codon or NMD) exhibited more severe phenotypes (p=0.017).

Finally, only missense mutations were present in the sequence encoding the Selenoprotein N putative catalytic site (SCUG, exon 10)[20]. They were identified in 23 patients (seven homozygous), most with moderate severity.

Conclusion

This study reports the largest SEPN1-RM series and the first one including pediatric and older adult patients followed-up for several decades, furthering our understanding of phenotypical spectrum and natural history. It also allows inferring information about

SEPN1-RM prevalence. Our series includes 63 French patients, identified through the main reference laboratories performing *SELENON*/*SEPN1* screening as part of a national network. We also interrogated the other genetic diagnostic laboratories in France, which have identified 6 additional cases, thus very likely capturing virtually all the diagnosed patients in the country. A total number of 69 cases in France represents an estimated prevalence of 1.03 per million, consistent with a previous study of Congenital Muscular Dystrophies in the UK[21]. This suggests that SEPN1-RM, although rare, is under-recognized. Several reasons might explain this, including the axial predominance of weakness, absence of biomarkers, histopathological variability and gene screen pitfalls.

SEPN1-RM clinical features are homogeneous and distinctive and include a particular facial appearance, long slender neck, flat retracted thorax, severe axial weakness and rigid spine. Indeed, axial muscles (and particularly the diaphragm) are known to be particularly vulnerable to oxidative stress, a known consequence of SEPN1 depletion[12]. Axial weakness and rigidity are generally present from an early age but often overlooked, since they are rarely a cause of spontaneous complaints and contrast with fairly preserved limb strength and ambulation. The suspicion of a muscle disorder is often hindered until the end of the first decade, when scoliosis and restrictive respiratory failure are detected. Interestingly, we show that ophtalmoparesis can be part of the SEPN1-RM phenotype and correlates with disease severity, which can be useful for differential diagnosis (i.e., with titinopathies). The scoliosis pattern and the predominantly cervico-dorsal spinal rigidity in SEPN1-RM were also characteristic and different from the rigid spine in myopathies caused by mutations of *LMNA*[22], *EMD*[23], *FHL1*[24], *COL6*[25], *RYR1*[26], *DNM2*[27], *TTN*[28,29] or *GAA*[30,31]. Finally, the homogeneous and recognizable radiological pattern (axial muscle involvement, severe wasting of

494 sternocleidomastoid muscles and dramatic atrophy of semimembranosus, with relative
495 preservation of the rectus femoris, long adductor and gracilis)[15] can be useful for
496 diagnosis even in very young or mild patients.
497 This series confirms the unusually large SEPN1-RM histological spectrum, and reveals
498 some of its determinants. We found no correlation between the histopathological
499 presentation and clinical severity. Most biopsies were typical of a Congenital
500 Myopathy, showing minicores, type 1 fiber predominance and mild endomysial fibrosis.
501 Moderate dystrophic features or protein aggregates were also found, although the latter
502 typically affect a low percentage of fibers and were found only in quadriceps samples.
503 We revealed a clear-cut discordance between severely dystrophic axial muscles and
504 mildly myopathic limb muscles in the same patient. Thus, the site of biopsy can
505 contribute to explain the histopathological variability. Furthermore, younger ages
506 correlated with less specific biopsy findings. Therefore, muscle biopsy might be best
507 delayed until school-age to increase the diagnostic yield, and could be reserved for cases
508 without a typical phenotype and/or when other tests have been inconclusive.
509 Along these lines, exon 1 emerged as major hotspot for *SEPN1* mutations and is poorly
510 or not covered by NGS panels, probably contributing to underdiagnosis. Our findings
511 confirm that clinical recognition of the SEPN1-RM phenotype is essential and sufficient
512 in most patients for indicating *SEPN1* genetic testing, which should systematically
513 include Sanger-sequencing of exon 1. Moreover, identification of the first *SEPN1* CNV
514 highlights the need to search for large genomic rearrangements, particularly when only
515 one *SEPN1* pathogenic variant has been detected.
516 On another note, most *SEPN1* mutations predicted loss of function, indicating that
517 SEPN1-KO models are relevant for SEPN1-RM studies. Interestingly, all pathogenic

518 variants located around or in the sequence encoding the potential catalytic site (exon 10)
519 were missense changes. The EF-hand domain-encoding sequence showed no mutation.
520
521 This study reveals SEPN1-RM as a more severe and progressive disease than previously
522 thought. While motor abilities were reported to be stable, we found loss of ambulation
523 in 10% of the cases with full follow-up data. Muscle functional performances and
524 respiratory function (particularly diaphragmatic fatigue) declined systematically from
525 the end of the third decade, even in mild cases. Mortality at young age was observed in
526 3 patients and in 18 relatives, most of them never ventilated. But life span was reduced
527 even in two mild cases with optimum respiratory support, the eldest patient being
528 currently 55 years-old.
529 Management of the scoliosis and respiratory failure was a key determinant of prognosis.
530 We previously reported that early non-invasive ventilation may initially stabilize the
531 decline in respiratory muscle strength[32]. Our current data also reveal that scoliosis
532 surgery had a positive impact on the respiratory function but induced a major drop in
533 FVC in the immediate postsurgical period. Intensive or permanent ventilation at this
534 decisive time was critical to restore or even improve FVC pre-surgery values.
535 Other factors associated with disease severity were the type of *SELENON*/*SEPN1* gene
536 defects and previously-unreported body mass abnormalities. Indeed, the analysis of this
537 series allowed us to establish the first phenotype-genotype correlations in SEPN1-RM.
538 Some exon 1 variants were commonly found in patients with a severe phenotype,
539 although the small number of patients harboring each individual variant and the
540 different associated mutations in trans precluded statistical significance. However,
541 biallelic null mutations significantly correlated with higher disease severity.

We also found a significant correlation between body weight and disease severity. We identified a subgroup of patients with increased adiposity since childhood who showed rapid disease progression leading to severe weakness (including non weight-bearing and extraocular muscles) and loss of ambulation before adulthood. This extramuscular phenotype is different from secondary weight gain in a wheelchair-bound patient and could be related to SEPN1-RM pathophysiological mechanisms involving defective mitochondrial bioenergetics and lipid metabolism in muscle[10,12,33,34]. Indeed, we reported that SEPN1 depletion increases susceptibility to insulin resistance and higher toxicity of saturated fatty acids, which triggers chronic ER stress and weakness in skeletal muscle in SEPN1-RM models[33,5]. Thus, high-calorie intake, particularly from a high-fat diet, could trigger or aggravate glucose metabolism abnormalities, oxidative/ER stress and muscle weakness. Consequently, systematic administration of hypercaloric diets/supplements might not be indicated on the bases of low weight alone, unless there are other clear markers of malnutrition.

Our results have significant implications for the identification of outcomes, a keystone for clinical trials. In the last years, significant progress has been achieved in the identification of SEPN1-RM pathophysiological pathways targetable with existing drugs[10,12,33,34]. The antioxidant N-acetylcystein has been identified as an effective treatment *ex vivo*, which led to a small pilot trial (ClinicalTrials.gov Identifier: NCT02505087) whose results are pending. Multicentric, international phase II-III trials require overcoming bottlenecks which are highlighted here. One is the predominantly axial weakness, since there are few validated measures of axial muscle power. We also found an important intra-patient variability in FVC, potentially explained by fatigability of the diaphragm and respiratory muscles, suggesting that FVC is not fully reliable as an outcome measure. Other respiratory function parameters, including pressure values,

should be included in future prospective studies. Another variability factor is heterogeneous orthopedic and respiratory management, particularly around spinal surgery, which has a major functional impact. All the former, together with slow progression until the fourth decade, hinder the choice of outcome measures to evaluate treatment efficacy. We propose straightforward disease severity criteria, thus defining more homogeneous groups, and provide Kaplan-Meier curves quantifying ventilation-free probability to evaluate impact of potential treatments. We also suggest that age stratification could be useful, since limb strength is stable or slowly progressive in younger patients but steadily progressive after the fourth decade.

Homogeneous management recommendations would reduce variability and improve vital prognosis. Based on our data, we recommend systematic sleep studies even in young children and/or in the absence of day-time signs of respiratory failure or major FVC decrease. Non-invasive ventilation should be initiated as soon as respiratory failure or nocturnal hypoventilation are detected, adjusted regularly[35,36] and sustained/intensified post-arthrodesis. Follow-up should include yearly respiratory and cardiac evaluations, given the possibility of pulmonary hypertension or secondary right-ventricle failure. We also recommend yearly spine surveillance, which can be intensified to every six months around the rapid growth spurt in adolescence due to the probability of rapid evolution. Finally, we suggest performing Oral Glucose Tolerance Test, particularly in adolescents and adults, and tailoring BMI control to SEPN1-RM particularities.

This work improves our understanding of SEPN1-RM phenotype and natural history in children and adults. It will hopefully inform clinical practice, contributing to improve diagnosis, management and follow-up and to increase disease awareness and

591 recognition of its phenotypic specificities. Our results also pave the way for the design
592 of prospective natural history studies and clinical trials in the near future.

593

594

Acknowledgments

The authors wish to thank the patients and their families for their cooperation. We especially thank Drs John Rendu (CHU Grenoble), Mireille Cossée (CHU Montpellier), and Valérie Biancalana (IGBMC, Strasbourg), as well as CureCMD, for their valuable contribution to estimations of SEPN1-RM prevalence. We also want to acknowledge Dr Behzad Moghadaszadeh, Dr Pascale Guicheney, Dr Juan Antonio Vargas-Nuñez, Dr JJ Martin, Dr Chantal Ceuterick, Dr Nursel Elçioglu, Dr Annick Labarre-Vila, Dr Wolfram Kress, Dr Louis Viollet and Darith Trin. Finally, we thank Dr Miguel Iniesto (Université Paris Sud) for assistance in statistical analysis.

References

1. Moghadaszadeh B, Desguerre I, Topaloglu H, et al. Identification of a new locus for a peculiar form of congenital muscular dystrophy with early rigidity of the spine, on chromosome 1p35-36. Am J Hum Genet. 1998;62:1439–1445.
2. Lescure A, Gautheret D, Carbon P, Krol A. Novel selenoproteins identified in silico and in vivo by using a conserved RNA structural motif. J Biol Chem. 1999;274:38147–38154.
3. Moghadaszadeh B, Petit N, Jaillard C, et al. Mutations in SEPN1 cause congenital muscular dystrophy with spinal rigidity and restrictive respiratory syndrome. Nat Genet. 2001;29:17–18.
4. Ferreiro A, Quijano-Roy S, Pichereau C, et al. Mutations of the selenoprotein N gene, which is implicated in rigid spine muscular dystrophy, cause the classical phenotype of multiminicore disease: reassessing the nosology of early-onset myopathies. Am J Hum Genet. 2002;71:739–749.
5. Clarke NF, Kidson W, Quijano-Roy S, et al. SEPN1: associated with congenital fiber-type disproportion and insulin resistance. Ann Neurol. 2006;59:546–552.
6. Ferreiro A, Ceuterick-de Groote C, Marks JJ, et al. Desmin-related myopathy

623 with Mallory body-like inclusions is caused by mutations of the selenoprotein N
624 gene. Ann Neurol. 2004;55:676–686.

625 7. Scoto M, Cirak S, Mein R, et al. SEPN1-related myopathies: Clinical course in a
626 large cohort of patients. Neurology. 2011;76:2073–2078.

627 8. Ardissone A, Bragato C, Blasevich F, et al. SEPN1-related myopathy in three
628 patients: novel mutations and diagnostic clues. Eur J Pediatr. 2016;175:1113–
629 1118.

630 9. Schara U, Kress W, Bönnemann CG, et al. The phenotype and long-term follow-
631 up in 11 patients with juvenile selenoprotein N1-related myopathy. Eur J Paediatr
632 Neurol. 2008;12:224–230.

633 10. Arbogast S, Ferreiro A. Selenoproteins and protection against oxidative stress:
634 selenoprotein N as a novel player at the crossroads of redox signaling and
635 calcium homeostasis. Antioxid Redox Signal. 2010;12:893–904.

636 11. Marino M, Stoilova T, Giorgi C, et al. SEPN1, an endoplasmic reticulum-
637 localized selenoprotein linked to skeletal muscle pathology, counteracts
638 hyperoxidation by means of redox-regulating SERCA2 pump activity. Hum Mol
639 Genet. 2015;24:1843–1855.

640 12. Arbogast S, Beuvin M, Fraysse B, Zhou H, Muntoni F, Ferreiro A. Oxidative
641 stress in SEPN1-related myopathy: from pathophysiology to treatment. Ann
642 Neurol. 2009;65:677–686.

643 13. Moulin M, Ferreiro A. Muscle redox disturbances and oxidative stress as
644 pathomechanisms and therapeutic targets in early-onset myopathies. Semin Cell
645 Dev Biol. Elsevier Ltd; 2017;64:213–223.

646 14. Rederstorff M, Castets P, Arbogast S, et al. Increased muscle stress-sensitivity
647 induced by selenoprotein N inactivation in mouse: a mammalian model for
648 SEPN1-related myopathy. Lee S-J, editor. PLoS One. 2011;6:e23094.

649 15. Hankiewicz K, Carlier RY, Lazaro L, et al. Whole-body muscle magnetic
650 resonance imaging in SEPN1-related myopathy shows a homogeneous and
651 recognizable pattern. Muscle and Nerve. 2015;52:728–735.

652 16. Nigro V, Piluso G. Next generation sequencing (NGS) strategies for the genetic

653 testing of myopathies. Acta Myol myopathies cardiomyopathies Off J Mediterr
654 Soc Myol. 2012;31:196–200.

655 17. Lescure A, Rederstorff M, Krol A, Guicheney P, Allamand V. Selenoprotein
656 function and muscle disease. Biochim Biophys Acta - Gen Subj.
657 2009;1790:1569–1574.

658 18. Maiti B, Arbogast S, Allamand V, et al. A mutation in the *SEPN1* selenocysteine
659 redefinition element (SRE) reduces selenocysteine incorporation and leads to
660 *SEPN1* -related myopathy. Hum Mutat. 2009;30:411–416.

661 19. Petit N, Lescure A, Rederstorff M, et al. Selenoprotein N: an endoplasmic
662 reticulum glycoprotein with an early developmental expression pattern. Hum Mol
663 Genet. 2003;12:1045–1053.

664 20. Castets P, Lescure A, Guicheney P, Allamand V. Selenoprotein N in skeletal
665 muscle: From diseases to function. J Mol Med. 2012;90:1095–1107.

666 21. Sframeli M, Sarkozy A, Bertoli M, et al. Congenital muscular dystrophies in the
667 UK population: Clinical and molecular spectrum of a large cohort diagnosed over
668 a 12-year period. Neuromuscul Disord. Elsevier B.V.; 2017;27:793–803.

669 22. Quijano-Roy S, Mbieleu B, Bönnemann CG, et al. De novo *LMNA* mutations
670 cause a new form of congenital muscular dystrophy. Ann Neurol. 2008;64:177–
671 186.

672 23. Kubo S, Tsukahara T, Takemitsu M, et al. Presence of emerinopathy in cases of
673 rigid spine syndrome. Neuromuscul Disord. 1998;8:502–507.

674 24. Shalaby S, Hayashi YK, Goto K, et al. Rigid spine syndrome caused by a novel
675 mutation in four-and-a-half LIM domain 1 gene (FHL1). Neuromuscul Disord.
676 2008;18:959–961.

677 25. Bönnemann CG. The collagen VI-related myopathies. Handb Clin Neurol. 2011.
678 p. 81–96.

679 26. Bharucha-Goebel DX, Santi M, Medne L, et al. Severe congenital RYR1-
680 associated myopathy: The expanding clinicopathologic and genetic spectrum.
681 Neurology. 2013;80:1584–1589.

27. Quijano-Roy S, Avila-Smirnow D, Carlier RY, WB-MRI muscle study group. Whole body muscle MRI protocol: pattern recognition in early onset NM disorders. Neuromuscul Disord. 2012;22 Suppl 2:S68-84.

28. Oates EC, Jones KJ, Donkervoort S, et al. Congenital Titinopathy: Comprehensive characterization and pathogenic insights. Ann Neurol. 2018;83:1105–1124.

29. Chauveau C, Bonnemann CG, Julien C, et al. Recessive TTN truncating mutations define novel forms of core myopathy with heart disease. Hum Mol Genet. 2014;23:980–991.

30. Fadic R, Waclawik AJ, Brooks BR, Lotz BP. The rigid spine syndrome due to acid maltase deficiency. Muscle Nerve. 1997;20:364–366.

31. Laforêt P, Doppler V, Caillaud C, et al. Rigid spine syndrome revealing late-onset Pompe disease. Neuromuscul Disord. 2010;20:128–130.

32. Caggiano S, Khirani S, Dabaj I, et al. Diaphragmatic dysfunction in SEPN1-related myopathy. Neuromuscul Disord. Elsevier B.V.; 2017;27:747–755.

33. Varone E, Pozzer D, Di Modica S, et al. SELENON (SEPN1) protects skeletal muscle from saturated fatty acid-induced ER stress and insulin resistance. Redox Biol. 2019;24:101176.

34. Pozzer D, Varone E, Chernorudskiy A, et al. A maladaptive ER stress response triggers dysfunction in highly active muscles of mice with SELENON loss. Redox Biol. 2019;20:354–366.

35. Wallgren-Pettersson C, Bushby K, Mellies U, Simonds A, ENMC. 117th ENMC workshop: ventilatory support in congenital neuromuscular disorders -- congenital myopathies, congenital muscular dystrophies, congenital myotonic dystrophy and SMA (II) 4-6 April 2003, Naarden, The Netherlands. Neuromuscul Disord. 2004;14:56–69.

36. Wang CH, Bonnemann CG, Rutkowski A, et al. Consensus statement on standard of care for congenital muscular dystrophies. J Child Neurol. 2010;25:1559–1581.

Figure legends

Figure 1. Distinctive clinical signs. **(A) The clinical phenotype in early childhood** was recognizable by predominantly axial weakness, deltoid and inner thigh amyotrophy ('bracket-like thighs') (a,b) and spinal rigidity identifiable upon specific examination (c,d). Axial rigidity was typically more prominent in the cervico-dorsal spine (c, d), with relative or full preservation of lumbar spine flexion (d). **(B) Typical moderate patient at ages 11** (a,b) **and 14 years** (c-e). Often subtle until late childhood, the full phenotype usually became apparent around puberty. Body weight decreased dramatically, leading in some cases to an apparent loss of subcutaneous adipose tissue (lower limbs in c, d) and a cachexia phenotype. Most patients developed scoliosis (e) which required adapted bracing to avoid thorax compression (Garchois brace, c,d). **(C) SEPN1-RM scoliosis is recognizable** due to dorsal lordosis leading to pseudo-scapular winging, prominent lateral trunk deviation with compensatory contralateral neck shift and horizontally aligned hips (a). Severe progression despite bracing often required arthrodesis (moderate patient before (b) and after (c) spinal fusion).

Figure 2. Disease course in typical severe (A), moderate (B) and mild (C) patients. (A): This severe patient presented with neonatal axial muscle weakness, required night-time assisted ventilation since the diagnosis at 6.5 years and showed at that age sternocleidomastoid, deltoid and leg amyotrophy (a,b), antigravity limb strength (e) and ophthalmoparesia with limited upward and horizontal eye movements (c-d). Note the typical SEPN1-RM facial appearance (tubular nose, prominent nasal sella, low-set prominent ears and mild retrognathia, mid-segment hypotrophy (c) and increased trunk

adiposity (a,b). He developed scoliosis from age 7 years (f) which eventually required arthrodesis, lost independent ambulation at 11 years (g) and was wheelchair-bound with severe limb weakness at 16 years (h). **(B):** After spinal fusion and instauration of nocturnal ventilation through a tracheostomy at 15 years (a), this moderate SEPN1-RM patient remained stable until the middle of the fourth decade (b,c), when progressive limb weakness led to a wider base of support, increased hyperlordosis (d,e) and limited upper limb abduction and ambulation. Note reduced anteroposterior thorax diameter, severe diffuse amyotrophy and loss of subcutaneous fatty tissue. **(C):** One of the mildest patients in this series had normal motor development including head control, rigid spine (a) and mild untreated scoliosis (b) and required assisted ventilation only after the age of 35 years. A myopathy was first suspected in the fourth decade due to progression of a previously mild muscle weakness. Continuous progression eventually led to loss of antigravity movements and ambulation and almost permanent ventilation by the age of 57 years (c) and to decease at age 58y.

Figure 3. Hand hyperlaxity and finger flexor contractures. Moderate distal hyperlaxity was common in early childhood (a, 7 year-old patient) and often coexisted with finger flexor contractures visible upon wrist extension. The latter tended to appear from adolescence (b, 16 year-old patient) and became more prominent with age (c, 57 year-old patient).

Figure 4. **Respiratory involvement.** (a) Distribution of FVC (% of predicted values) in 69 cases shows that most patients had FVC <39%, the most frequent range being between 25 and 29%. (b) Respiratory insufficiency (grey line) or scoliosis (black line)

were first detected in most patients around the same age, most commonly between 7 and 10 years. (c) Progression of FVC in 32 patients (ages 4 to 58 years) revealed decrease of FVC with age in years using a logarithmic regression (R_2= 0,16642). Individual values are shown as grey dots. (d) Kaplan-Meier curve showing ventilation-free probability with age. (e) Progression of respiratory involvement in 11 patients, revealing extreme variability between patients with similar disease severity. Note also intra-patient variability in FVC values (arrowheads). (f) Follow-up of respiratory involvement before and after surgical correction of scoliosis in three patients. FVC typically dropped in the postsurgical period (arrows) and then came back to previous or even higher values with correct post-operatory management including ventilation.

Figure 5. Histopathological patterns and different histological severity in axial versus limb muscles. The relative frequency of the different histopathological patterns observed in this series (n=78) is represented in the graph. Foci of **s**arcomere disorganization and mitochondria depletion, spanning only a few sarcomeres on the longitudinal axis of the fiber (minicores), were observed in 60% of the biopsies (Ac-e, Bb,c). **A**: The most common pattern was typical of a **congenital myopathy with minicores** (Multi-minicore disease, MmD), including mild or no endomysial fibrosis (a), type I fiber predominance and relative hypotrophy (dark fibers, b) and multiple lighter zones devoid of SDH or NADH-enzymatic activity (c) corresponding to mitochondria depletion and sarcomere disorganization on EM (minicores) (d,e) **B**: Around 24% of biopsies showed a mild to moderate **congenital muscular dystrophy** pattern, associated with either abundant or scattered/inconspicuous minicores. Note prominent endomysial fibroadiposis but rare necrotic or regenerating fibers (a). **C**: Eosinophilic **inclusions** compatible with Mallory body-like inclusions (arrows, a-c) or **rimmed vacuoles** (arrowheads, d-e) were identified in some samples but typically

involved a small percentage of fibers. Thus, they were easily overlooked unless specifically searched for. **D**: Two muscle samples taken from the same patient at 12 years of age revealed that **histopathological changes were more severe in axial than in limb muscles**, mirroring the clinical situation. Her deltoid muscle (a,b) showed minor myopathic changes, with mild fiber size variation and scattered internalized nuclei and minicores. In contrast, her abdominal muscles revealed major dystrophic changes with muscle fiber loss, fatty-adipose replacement, rimmed-vacuoles (c), rod-like inclusions (e), multi-minicores (d) and also well-delimited cores with a hyperoxidative perilesional rim (similar to those observed in Central Core Disease) (f). Transversal frozen sections stained with hematoxylin-eosin (HE) (A-a; B-a; C-b-d; D-a,c), reduced nicotinamide adenine dinucleotide (NADH) (A-c; B-c; D-b,f), ATPase 4.6 (A-b), Succinate dehydrogenase (SDH) (B-b; D-d), modified Gomori Trichrome (C-a,e; D-e); longitudinal electron microscopy (EM) sections (A-d,e). Scale bars: 50 µm except for A-d,e: 2 µm.

Figure 6. **Schematic representation of the *SEPN1(SELENON)* gene and localization of the identified mutations**. Exons are depicted in light blue and the 3′ UTR SECIS element in orange. Colour code for variants: pink- deletion; green-insertions/duplications; blue-missense; red-nonsense; black-intronic variants affecting splicing; orange-variants affecting SEPN1 3′ UTR SECIS element.

	Number of cases (%)*
Age at first noticed signs (n=98)	
Birth to 6 months	46 (46.94%)
From 6 months to 1 year	25 (25.51%)
From 1 to 2 years	12 (12.24%)
From 2 to 8 years	12 (12.24%)
Older than 8 years	3 (3.06%)
First /Referral signs (n=97)	
Neonatal hypotonia	32 (32.99%)
Delayed motor milestones	79 (81.44%)
Poor head control (head lag)	56 (57.73%)
Delayed gait acquisition	31 (31.96%)
Abnormal gait, inability to run or frequent falls	34 (35.05%)
Non specified weakness/hypotonia	16 (16.49%)
Difficulty feeding/failure to thrive	17 (17.53%)
Early respiratory problems (e.g neonatal respiratory distress, recurrent respiratory infections)	7 (7.22%)
Scoliosis, hyperlordosis or rigid spine	4 (4.12%)
Hypercapnic coma	1 (1.03%)
Muscle weakness distribution (n=80)	
Predominantly axial+proximal	80 (100%)
Significant distal involvement	11 (13.75%)
Facial muscle weakness (n=60)	48 (80%)
High-arched palate (n=58)	36 (62.07%)
High-pitched/nasal voice (n=67)	52 (77.61%)
Mild ptosis (n=79)	6 (7.59%)
Ophthalmoparesis (n=79)	3 (3.79%)
Rigid spine (n=98)	86 (87.75%)
Scoliosis (n=101)	87 (86.14%)
Arthrodesis	32 (36,78%)
Thoracic deformities (n=57)	41 (71.93%)
Flat thorax	18 (31.58%)
Pectus excavatum	15 (26.32%)
Pectus carinatum	1 (1.75%)
Non specified	7 (12.28%)
Respiratory involvement (n=100)	94 (94%)
Not properly evaluated (< 6years)	6 (6%)
Age at detection (n=62)	
0-9 years	29 (46.77%)
10-15 years	27 (43.54%)
> 15 years	6 (9.67%)
FVC(%) (n=69)*	
FVC ≥65%	2 (2.89%)
FVC 50-65%	8 (11.59%)
FVC 30-50%	34 (49.28%)
FVC <30%	25 (36.23%)
Assisted ventilation	77 (81.91%)
Cardiac abnormalities (n=76)*	12 (15.79%)
Cor pulmonale	4 (5.26%)
Increased RV systolic pressure	1 (1.32%)
Mitral valve prolapse	3 (3.95%)
Other valvular abnormalities	3 (3.95%)
Dilated cardiomyopathy	1 (1.32%)
Joint contractures/hyperlaxity (n=87)	56 (64.37%)
Only axial (spinal) contractures	10 (11.49%)
Mild-Moderate axial + limb contractures	37 (42.53%)
Severe axial+upper and lower limbs	9 (10.34%)
Mild distal hyperlaxity	21 (24.14%)
Distal hyperlaxity+Contractures	16 (18.39%)

	Number of cases (%)*
Other clinical features:	
Foot deformities	14
Equinovarus foot	7
Flat feet	7
Hip dysplasia	2
Skin abnormalities	8
Trunk acne	3
Nevus flammeus	2
Follicular hyperkeratosis	1
Facial angyoma	1
Thoracic angyoma	1
Xerosis	1
Strabismus	4
Deglutition problems	15
Genitourinary involvement	6
Gastrointestinal involvement	3
Gastroesophageal reflux	1
Bulbar ulcer	1
Steatorrhoea	1
Mild learning difficulties	3
Dysarthria	3
Congenital torticollis	1
Progression of muscle weakness (n=77)	
Stable/Stationary	45 (58.44%)
Slowly progressive	32 (41.56%)
Rapidly progressive	2 (2.59%)
Wheel-chair bound patients	8
Deaths	6

Table 1. Summarized main clinical features reported by clinicians. Patients of a wide age range (2-56 years) have been included. Younger patients may not have developed all the characteristic features yet. n= Number of patients from whom information about the clinical feature is available. The denominator for percentage calculations was the number of cases with available data for each item (*). FVC: Forced vital capacity. RV: right ventricle

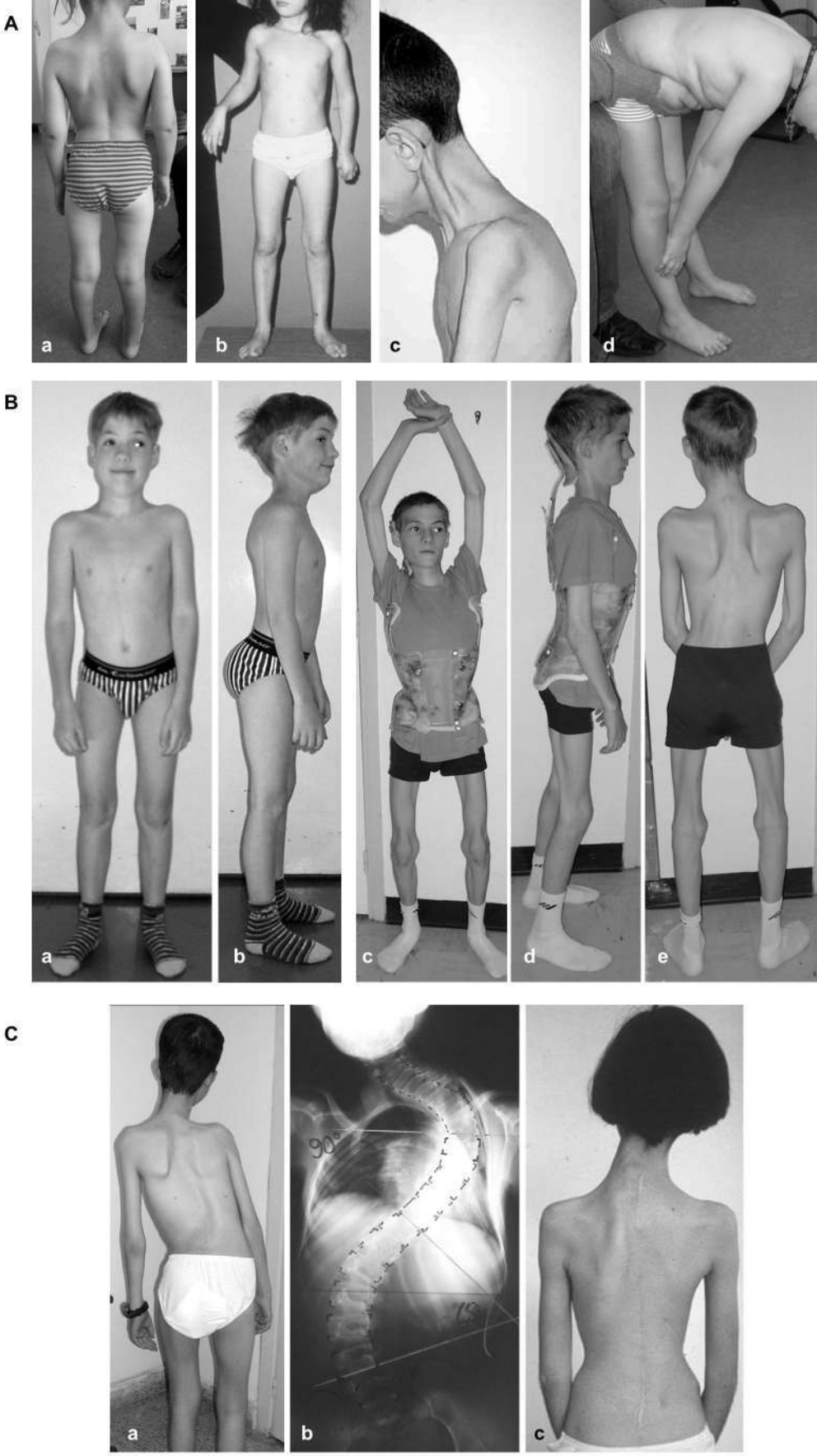
A
a
b
c
d
B
a
b
c
d
e
C
a
b
90°
c

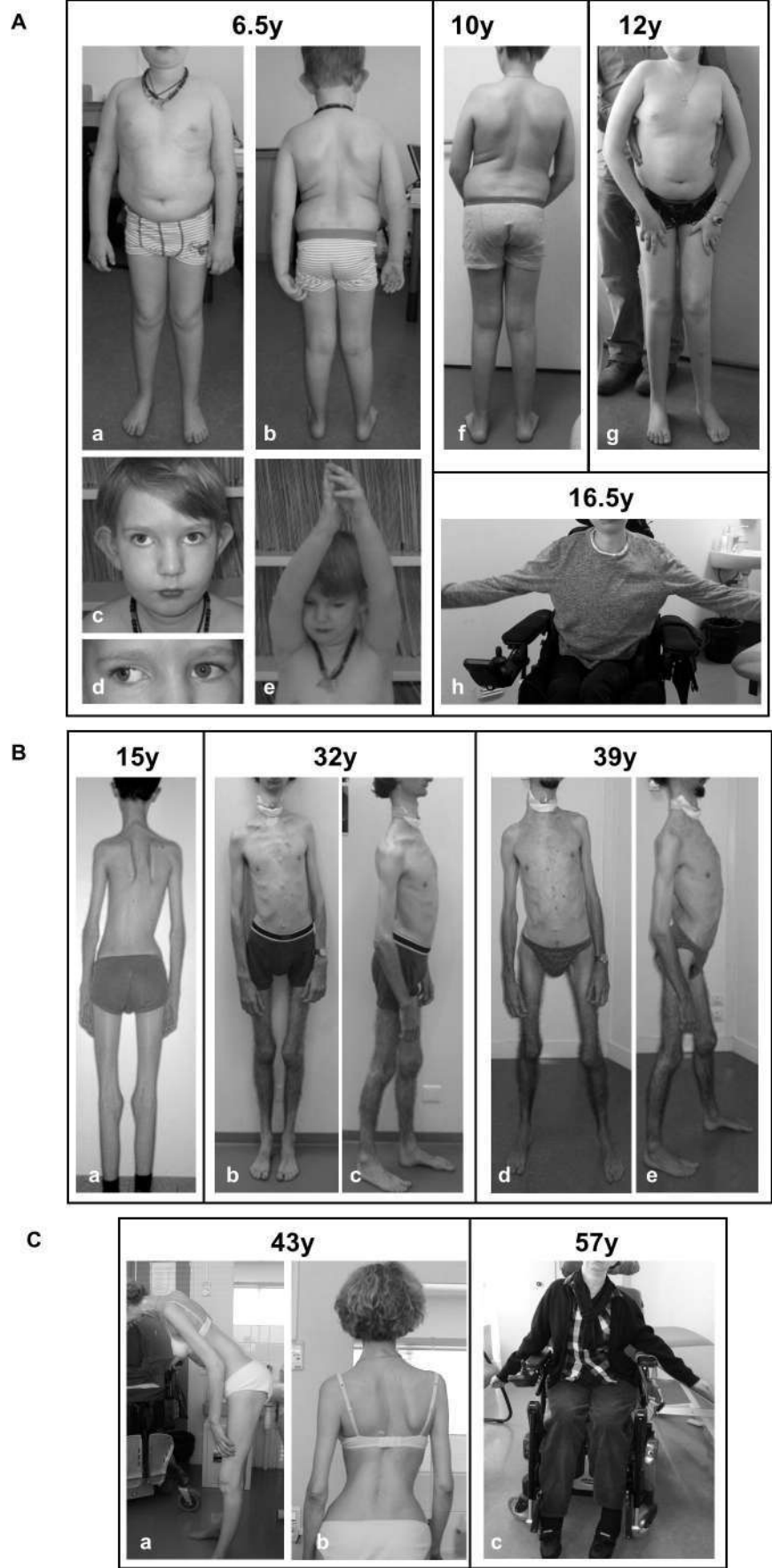
A
6.5y
10y
12y
16.5y
a
b
c
d
e
f
g
h
B
15y
32y
39y
a
b
c
d
e
C
43y
57y
a
b
c

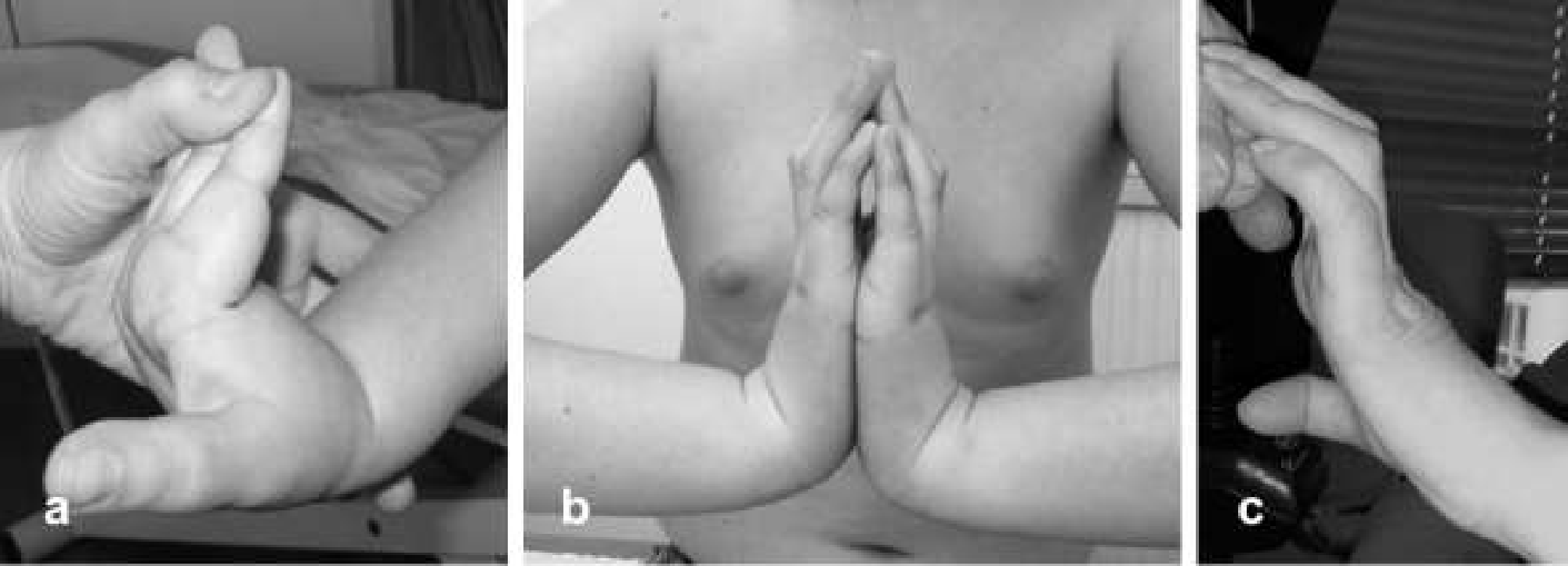
a
b
c

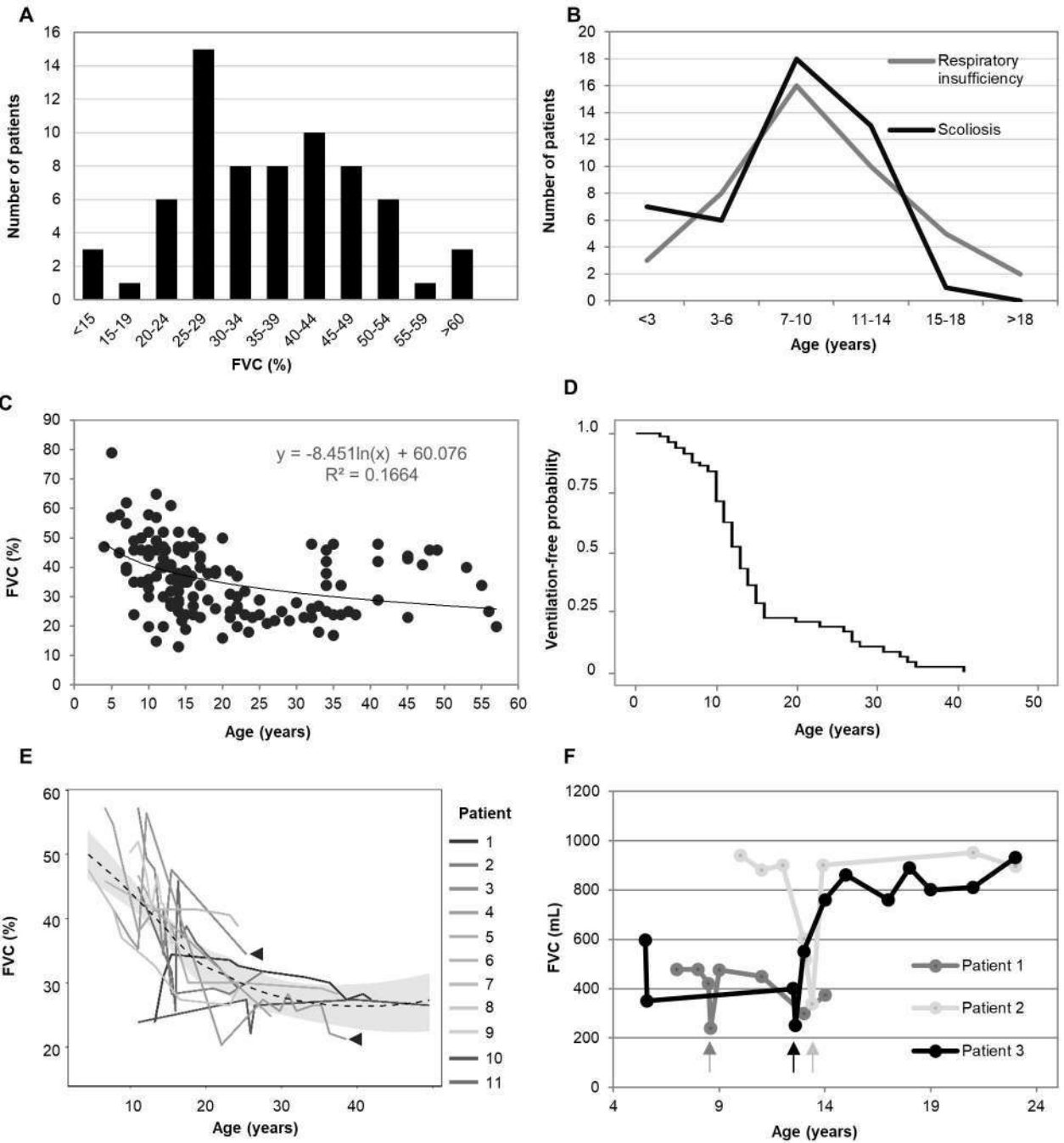
A
Number of patients
FVC (%)
<15
15-19
20-24
25-29
30-34
35-39
40-44
45-49
50-54
55-59
>60
B
Number of patients
Respiratory insufficiency
Scoliosis
<3
3-6
7-10
11-14
15-18
>18
Age (years)
C
y = -8.451ln(x) + 60.076
R² = 0.1664
FVC (%)
Age (years)
D
Ventilation-free probability
Age (years)
E
FVC (%)
Patient
1
2
3
4
5
6
7
8
9
10
11
Age (years)
F
FVC (mL)
Patient 1
Patient 2
Patient 3
Age (years)

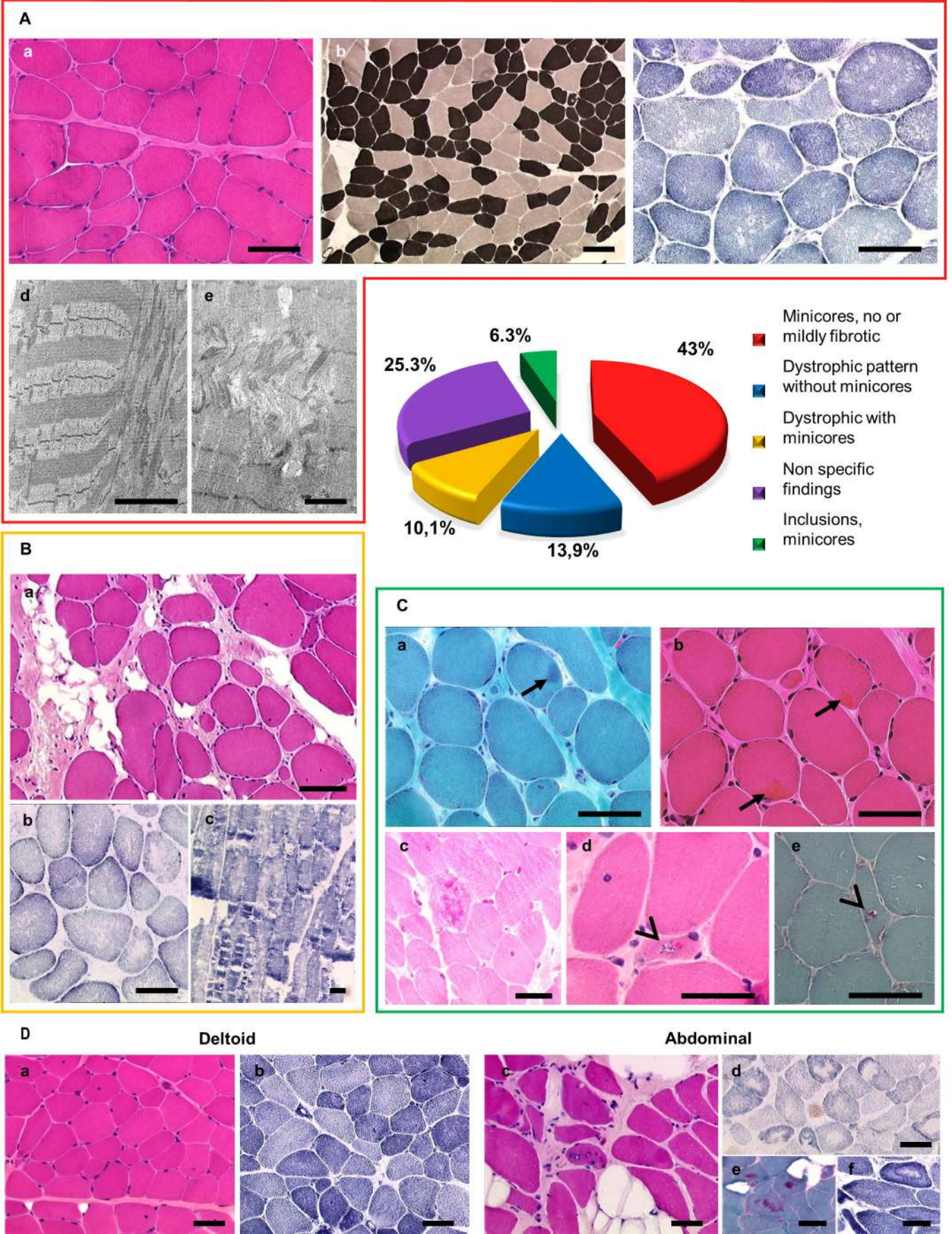
A
a
b
c
d
e
6.3%
43%
25.3%
10,1%
13,9%
Minicores, no or mildly fibrotic
Dystrophic pattern without minicores
Dystrophic with minicores
Non specific findings
Inclusions, minicores
B
a
b
c
C
a
b
c
d
e
D
Deltoid
Abdominal
a
b
c
d
e
f

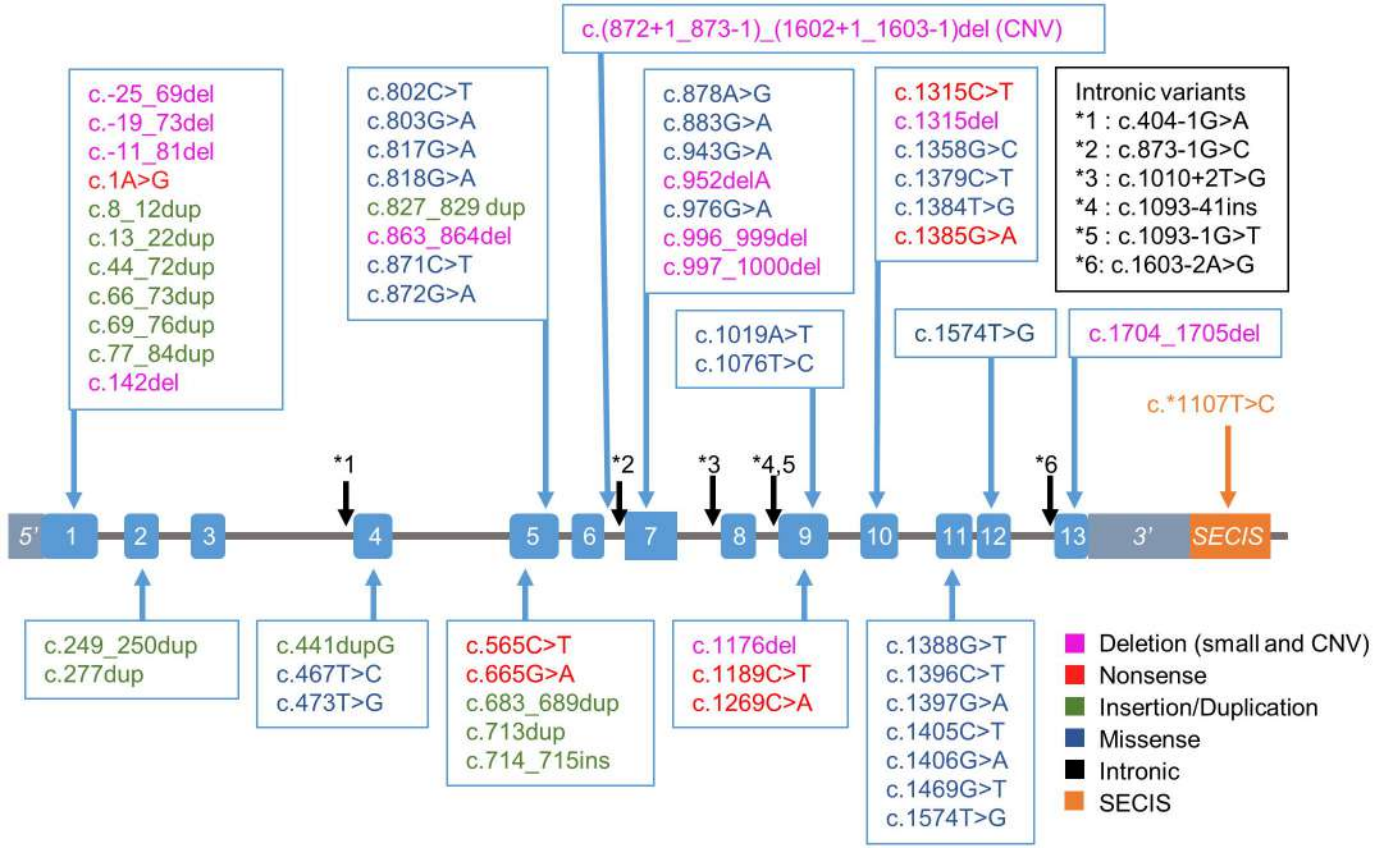
c.(872+1_873-1)_(1602+1_1603-1)del (CNV)
c.-25_69del
c.-19_73del
c.-11_81del
c.1A>G
c.8_12dup
c.13_22dup
c.44_72dup
c.66_73dup
c.69_76dup
c.77_84dup
c.142del
c.802C>T
c.803G>A
c.817G>A
c.818G>A
c.827_829 dup
c.863_864del
c.871C>T
c.872G>A
c.878A>G
c.883G>A
c.943G>A
c.952delA
c.976G>A
c.996_999del
c.997_1000del
c.1315C>T
c.1315del
c.1358G>C
c.1379C>T
c.1384T>G
c.1385G>A
Intronic variants
*1 : c.404-1G>A
*2 : c.873-1G>C
*3 : c.1010+2T>G
*4 : c.1093-41ins
*5 : c.1093-1G>T
*6: c.1603-2A>G
c.1019A>T
c.1076T>C
c.1574T>G
c.1704_1705del
c.*1107T>C
*1
*2
*3
*4,5
*6
5'
1
2
3
4
5
6
7
8
9
10
11
12
13
3'
SECIS
c.249_250dup
c.277dup
c.441dupG
c.467T>C
c.473T>G
c.565C>T
c.665G>A
c.683_689dup
c.713dup
c.714_715ins
c.1176del
c.1189C>T
c.1269C>A
c.1388G>T
c.1396C>T
c.1397G>A
c.1405C>T
c.1406G>A
c.1469G>T
c.1574T>G
Deletion (small and CNV)
Nonsense
Insertion/Duplication
Missense
Intronic
SECIS